A transcriptomic-based drug repositioning approach for the identification of novel muscle-specific therapies for spinal muscular atrophy.

Joseph Matthew Hoolachan

PhD Biomedical Science

March 2022

Keele University

Abstract

Spinal muscular atrophy (SMA) is an autosomal recessive neuromuscular disorder (NMD) caused by depleted survival of motor neuron (SMN) levels and characterised by neuronal degeneration and progressive muscle atrophy. Although three approved SMN-dependent treatments have significantly halted disease progression, they are unfortunately not cures. Thus, additional muscle-specific therapies are most likely also required to synergistically ameliorate symptoms in SMA patients. One useful strategy for the discovery of novel SMA muscle-specific therapies is drug repositioning (or repurposing), as using existing approved pharmacological compounds allows for the development of more cost-effective treatments compared to traditional drug discovery. We have previously investigated drug repositioning in SMA and demonstrated that prednisolone, a synthetic glucocorticoid (GC), improved muscle health and survival in SMA mice. However, the adverse effects associated with chronic GC use limit prednisolone's long-term therapeutic potential in SMA. We thus wanted to discover prednisolone-targeted genes and pathways in SMA skeletal muscle and identify commercially available drugs that similarly modulate these effectors.

We initially performed an RNA sequencing, bioinformatics and drug repositioning database pipeline on muscle from symptomatic post-natal day (P)7 prednisolone-treated and untreated *Smn*$^{-/-}$*;SMN2* SMA mice. These revealed that genes associated with atrophy, metabolism and muscle function pathways were targeted and normalised by prednisolone in SMA skeletal muscle. Furthermore, a total of 223 commercially approved compounds were predicted to similarly target these genes and pathways. We thus selected metformin, a generic anti-hyperglycaemic biguanide and oxandrolone, an anabolic steroid, for further

investigation in SMA, based on their oral bioavailability, safety in infants and previously reported benefits in related conditions.

Metformin was predicted to emulate prednisolone's activity by upregulating *Prkag3* and downregulating *Forkhead box O* (*FoxO*) expression. We indeed confirmed that *Prkag3* was significantly downregulated in muscle from *Smn*$^{-/-}$*;SMN2* and *Smn*$^{2B/-}$ SMA mice. Furthermore, *in vitro* experiments in C2C12 myoblast-like cells suggest that the dysregulation of metformin's molecular targets are SMN-independent and linked to atrophy. However, metformin treatment in both C2C12 cells and *Smn*$^{2B/-}$ SMA mice (200 mg/kg/day) did not improve disease progression. Furthermore, a higher dose of metformin (400 mg/kg/day) significantly exacerbated disease progression in *Smn*$^{2B/-}$ SMA mice, which were most likely due to mitochondrial marker dysfunction in the spinal cord. On the other hand, oxandrolone was predicted to upregulate the expression of the *androgen receptor* (*Ar*) and its downstream components. However, analyses in both C2C12 cells and muscle from *Smn*$^{-/-}$*;SMN2* and *Smn*$^{2B/-}$ SMA mice revealed that most of the predicted oxandrolone targets were in fact not dysregulated. Still, oxandrolone treatment rescued canonical atrophy in C2C12 myotubes and slightly improved survival in *Smn*$^{2B/-}$ SMA mice (4 mg/kg/day).

Taken together, our *in vitro* and *in vivo* experiments revealed that metformin and oxandrolone did not successfully emulate prednisolone's activity in SMA, suggesting that our *in silico* approach requires refinement for a better prediction of valid drug candidates. Nevertheless, our discovery of prednisolone-targeted pathways and extensive list of drug candidates supports the usefulness of a transcriptomic-based drug repositioning strategy, and that with alterations, it can be quite beneficial for future therapeutic endeavours in SMA.

Acknowledgments

There are many people and organisations I would like to acknowledge, whose support, tutorage and contribution helped me throughout my PhD. Although I cannot name all, I still like to give my thanks to everyone.

First off, a great many of thanks goes towards my principal supervisor Dr Melissa Bowerman (School of Medicine, Keele University), who not only provided me this life changing opportunity, but throughout has been a pillar of guidance and pastoral support. She is an amazing role model for early career researchers, and I am grateful for all I have learned from her. Additional appreciation goes towards my co-supervisor Dr Daniel Tonge (School of Life Sciences, Keele University) for supervising and tutoring me in bioinformatics in the early phases of my project.

There are also many current and former colleagues in the Bowerman group who I would like to acknowledge. Firstly, Emma Sutton (Final year PhD Biomedical science student, Keele University) as she has been an amazing friend, scientist and supportive colleague both in lab and outside of it. Other colleagues I would like to thank are Magnus Okoh (Final year medical student, Keele University) and Özge Çetin (First year PhD Biomedical science student, Keele University) who have aided me at various stages of my project. In addition, I appreciate all the technical support from technicians across Huxley Life Science building, Keele Medical School and the Biomedical Sciences Unit (BSU).

Scientific research is a collaborative endeavour and there many researchers outside of Keele University who I would like to thank for their contribution towards my project. These include Professor Peter Claus, Dr Lisa Walter and the bioinformatics team at Hannover Medical School for their role in the RNA

sequencing prior to my project starting. Furthermore, many thank goes to Dr Stephanie Duguez at Ulster University for providing type 3 SMA and control patient myoblast samples.

Outside of colleague support, this project would not have been possible without the generous financial contributions made by Keele School of Medicine and SMA Angels charity, in which I am eternally grateful. Other organisations I give thanks to are CureSMA, SMA Europe and Biochemical Society UK for providing me the wonderful opportunities of presenting my research at national and international conferences.

On a personal note, I would like to give my appreciation to family and friends back home. Firstly, my parents Susan Lorraine and Martin Alfred Hoolachan who have been a constant pillar of support. Outside of my parents, I like to acknowledge my siblings Thomas Henry Hoolachan and Ashley Morgan Luter alongside her family of Adam Luter and their children Joshua, Esme and Jacob Luter. My pets throughout my life Sandy, Spud, Zeus, Fudge and Sooty. Also, to my friends Ryan Shreeve, Robert Perry, Paul Kinsella, Adam Filkins, Chris Barton, Tom Bulger, Jacob Harris and Joel and Zoe Walker, thank you for always being there. Finally, I would just like to add a blessing called a Shehecheyanu which can be recited for joyous occasions, such as this.

בָּרוּךְ אַתָּה יְיָ אֱלֹהֵינוּ מֶלֶךְ הָעוֹלָם, שֶׁהֶחֱיָנוּ וְקִיְּמָנוּ
וְהִגִּיעָנוּ לַזְּמַן הַזֶּה.

Baruch atah, Adonai Eloheinu, Melech haolam, shehecheyanu, v'kiy'manu, v'higiyanu laz'man hazeh.

Contents

List of Figures

List of Tables

List of Abbreviations

3β-HSD	3β- hydroxysteroid dehydrogenase
ACh	Acetylcholine
AChR	Acetylcholine receptor
Act2R	Activin receptor type 2
AD	Alzheimer's disease
Akap6	A-kinase anchor protein 6
ALS	Amyotrophic lateral sclerosis
AMPK	AMP-activated protein kinase
Ar	Androgen receptor
ARE	Androgen response element
ARX-2	Actin-related protein 2
AS160	Akt substrate of 160 kDa
ASO	Anti-sense oligonucleotide
BAM	Binary alignment map
BAT	Brown adipose tissue
BBB	Blood-brain-barrier
BCAA	Branched chain amino acid
BCL	Binary base call

BED12	Browser extensible data 12
BMI	Body mass index
BP	Base pair
BPM	Beats per minute
BrDU	Bromodeoxyuridine
BRET	Bioluminescence resonance energy transfer
BSU	Biomedical Sciences Unit
CBS1	Cystathionine β-synthetase 1
CD36	Cluster of differentiation
CDS	Coding domain sequences
cDNA	Complementary DNA
CMC	Carboxymethylcellulose
CMD	Congenital myotonic dystrophy
CMT1A	Charcot-Marie Tooth disease type 1A
CNS	Central nervous system
CNV	Copy number variation
Comt	Catechol-O-methyltransferase
COX2	Cyclooxygenase-2
Cry	Cryptochrome
D	Differentiation day

DDIT4	DNA Damage Inducible Transcript 4
DEG	Differentially expressed gene
DGE	Differential gene expression
DGIdb	Drug Gene Interaction database
dH_2O	Distilled H_2O
DHT	Dihydrotestosterone
DM	Diabetes mellitus
DMD	Duchenne muscular dystrophy
DMEM	Dulbecco's Modified Eagle's Media
Dok5	Docking protein 5
FBS	Foetal bovine serum
FoxO	Forkhead box O
E	Embryonic day
ECG	Electrocardiogram
EDL	Extensor digitorum longus
Ednrb	Endothelin receptor type B
EGFR	Epidermal growth factor receptor
EMA	European Medicines Agency
Erα	Oestrogen receptor alpha
Ers1	Oestrogen receptor 1

ESC	Embryonic stem cells
ESRRA	Oestrogen related receptor alpha
FA	Fatty acid
FABP	Fatty acid binding protein
FATP1	Fatty acid transport protein 1
FC	Fold change
FDA	Food and Drug Administration
FDR	False discovery rate
FL-	Full length-
FMI	Fatty mass index
GC	Glucocorticoid
GR	Glucocorticoid receptor
GLM	General linearized model
GO	Gene Ontology
GSK-3β	Glycogen synthase kinase 3 beta
GUI	Graphical user interface
HDACi	Histone deacetylase inhibitors
HFD	High fat diet
HIV	Human immunodeficiency virus
Hk2	Hexokinase-2

hnRNPs	Heterogeneous nuclear ribonucleoproteins
HRP	Horseradish peroxidase
HS	Horse serum
IBM	Inclusion body myositis
ICD	International Classification of Diseases
IGF-1	Insulin-like growth factor 1
Igfals	Insulin-like growth factor binding protein, acid labile subunit
Igfbp5	Insulin-like growth factor binding protein 5
Il6ra	Interleukin-6 receptor, alpha
iPSC	Induced pluripotent stem cells
IR	Insulin receptor
IRS-1	Insulin receptor substrate 1
ISS-N1	Intronic splicing silencer N1
KD	Knockdown
Klf15	Krüppel-like factor 15
KO	Knockout
LC-FA	Long chain fatty acid
LCHAD	Long-chain 3-hydroxyacul-CoA dehydrogenase
LDH	Lactate dehydrogenase assay
LGMD	Limb girdle muscular dystrophy

lncRNA	Long non-coding RNA
LOF	Loss-of-function
Lrp4	Low density lipoprotein receptor related protein 4
MD1	Myotonic dystrophy type 1
MD2	Myotonic dystrophy type 2
MEP	Maximum expiratory pressure
MG	Myasthenia gravis
MHC	Myosin heavy chain
MLCP	Myosin light chain phosphatase
MoR	Median of Ratios
MPB	Muscle protein breakdown
MPS	Muscle protein synthesis
MRF	Myogenic regulatory factor
MtDNA	Mitochondrial DNA
MTT	3-(4,5-dimethylthiazol-2-yl)-2,5-diphenyl-2H-tetrazolium bromide
MuRF1	Muscle RING-finger protein-1
MuSK	Muscle specific kinase
MYBBP1A	Myb-binding protein 1a
Myf5	Myogenic factor 5
Myf6	Myogenic factor 6

MyoD	Myoblast determination protein 1
MyoG	Myogenin
NAFLD	Non-alcoholic fatty liver disease
Ndufs1	NADH-ubiquinone oxidoreductase 75 kDa subunit, mitochondrial
NGS	Next generation sequencing
NMD	Neuromuscular disorder
NMJ	Neuromuscular junction
NRF	Nuclear respiratory factor
ns-SARM	Non-steroidal selective androgen receptor modulator
ORA	Overrepresentation analysis
P(N)	Post-natal day
PBS	Phosphate buffered saline
PCR	Polymerase chain reaction
PDK1	Phosphoinositide-dependent kinase 1
Per	Period
PGC1-α	Peroxisome proliferator-activated receptor gamma coactivator 1-α
PI3K	Phosphoinositide 3-kinase
Pink1	PTEN-induced kinase 1
PIP_3	Phosphatidylinositol (3,4,5)-triphosphate
PPAR	Peroxisome-activator receptor

Pre-RNA	Pre-messenger RNA
PTM	Post-translational modification
qPCR	quantitative PCR
R&D	Research and development
RNA-Seq	RNA sequencing
RNP	Ribonucleoprotein
ROCK	Rho-associated kinase
RPKM	Reads per kilobase per million mapped reads
rRNA	Ribosomal RNA
RSEM	RNA-Seq by Expectation Maximisation
RT	Reverse transcription
Ryr1	Ryanodine receptor 1
SARM	Selective androgen receptor modulator
SBMA	Spinal and bulbar muscular atrophy
scAAV	Self-complementary adeno-associated virus
SCHAD	Short-chain 3-hydroxyacyl-CoA dehydrogenase
SCI	Spinal cord injury
SF2/ASF	Splicing factor 2/alternative splicing factor
siRNA	Small interfering RNA
SMA	Spinal muscular atrophy

snRNA	Small nuclear RNA
snoRNP	Small nucleolar RNP
SMN	Survival of motor neuron
sncRNA	Small non-coding RNA
T1DM	Type 1 diabetes mellitus
T2DM	Type 2 diabetes mellitus
TA	*Tibialis anterior*
TES	Transcriptional end site
TFAM	Transcription factor A, mitochondrial
TMM	Trimmed mean of M values
tRNA	Transfer RNA
TSS	Transcriptional start site
TTFLs	Transcription-translation feedback loops
WAT	White adipose tissue
UBA1	Ubiquitin-like-modifier-activating enzyme 1
UTR	Untranslatable regions

List of Publications and Presentations

Publications

1. Meijboom KE, Volpato V, Monzon-Sandoval J, **Hoolachan JM**, Hammond SM, Abdendroth F, de Jong OG, Hazell G, Ahlskog N, Wood MJA, Webber C, and Bowerman M. Combining multi-omics and drug perturbation profiles to identify muscle-specific treatments for spinal muscular atrophy. **JCI Insight**. DOI: 10.1172/jci.insight.149446. (2021).
2. **Hoolachan JM**, Sutton ER, and Bowerman M. Teaching an old drug new tricks: repositioning strategies for spinal muscular atrophy. **Future Neurology**. DOI: 10.2217/fnl-2019-0006 (2019).

Conferences

1. **Hoolachan, JM.** "A transcriptomic-based drug repurposing strategy for the identification of new SMN-independent skeletal muscle treatments for spinal muscular atrophy". 45th FEBS Congress: *Bioinformatics and computational biology P-06.5-14,* online event (2021). (POSTER)
2. **Hoolachan, JM.** "A transcriptomic-based drug repurposing strategy for the identification of new SMN-independent skeletal muscle treatments for spinal muscular atrophy". 20th FEBS Young Scientists' Forum: *Bioinformatics and computational biology P-06.5-14,* online event (2021). (POSTER)
3. **Hoolachan, JM.** "Transcriptomics-based drug repositioning predicts metformin as a potential SMN-independent therapy for spinal muscular

atrophy". CureSMA 25th SMA Researcher Meeting: *Drug POC/Translational therapies*, online event (2021). (POSTER)

4. **Hoolachan, JM**. "Transcriptomics-based drug repositioning predicts metformin as a potential SMN-independent therapy for spinal muscular atrophy". UK Neuromuscular Translational Research Conference 2021: Category A. Motor nerve disorders, online event (2021). (POSTER)
5. **Hoolachan, JM**. "Opening Presentation for the 2020 UK SMA Research Conference". 2020 UK SMA Research Conference, online event (2020).
6. **Hoolachan, JM.** "A transcriptomic-based drug repurposing strategy for the identification of new SMN-independent skeletal muscle treatments for spinal muscular atrophy", SMA Europe 2nd International Scientific Congress on Spinal Muscular Atrophy: *Session 1 – Emerging treatments & novel approaches in therapy, poster session P6,* Evry, France (2020). (POSTER)
7. **Hoolachan, JM**. "A transcriptomic-based drug repurposing strategy for the identification of new SMN-independent skeletal muscle treatments for spinal muscular atrophy", SMA Europe 2nd International Scientific Congress on Spinal Muscular Atrophy: *Session 1 – Emerging treatments & novel approaches in therapy*, Evry, France (2020).
8. **Hoolachan, JM**. "A transcriptomic-based drug repurposing strategy for the identification of new SMN-independent skeletal muscle treatments for spinal muscular atrophy", Drug Repurposing – Biochemical Society: *Drug repurposing across organisms (OC002)*, IET Birmingham: Austin Court, Birmingham, UK (2019).

9. **Hoolachan, JM**. “Identification of new muscle-specific targets in SMA”, CureSMA 23rd SMA Researcher Meeting: *Identification of Candidate Therapeutic Targets and Disease Modifiers,* Disneyland, Anaheim, California (2019).
10. **Hoolachan, JM**, Sutton ER, Walter LM, Claus P, Tonge DP, Bowerman M. **“**The benefits of computer analysis to develop new treatments for neuromuscular disorders”, ISTM Early Careers Symposium, North Staffordshire Medical Institute, Stoke-on-Trent, UK (2019). (POSTER)
11. **Hoolachan, JM**. “Defining the benefits of prednisolone in SMA muscle”, UK SMA Research Day, Keele University, UK (2019).

Chapter 1.

Introduction

1.1. Spinal muscular atrophy (SMA)

1.1.1. Clinical features

Spinal muscular atrophy (SMA) is an autosomal recessive genetic neuromuscular disorder (NMD) with heterogeneous clinical manifestations characterised mainly by alpha motor neuron degeneration in the anterior horn of the lower spinal cord [1]. Consequently, the resulting denervation causes skeletal muscle atrophy and weakness in the proximal regions that progressively spreads to distal and torso regions [1–3]. Clinically, SMA can be separated into 5 different types that are defined by age of onset, lifespan and severity [4,5] (Table 1.1).

Table 1.1. Clinical classifications of spinal muscular atrophy (SMA).

Type	Age of Onset	Cases	Life Expectancy	Main Clinical Features
0 (Prenatal-onset SMA)	Prenatal	< 5%	Stillborn to < 6 months	Widespread motor function loss Hypotonia
1 (Werdnig-Hoffman disease)	< 6 months	50 – 60%	< 2 years	Inability to sit upright Respiratory muscle weakness
2 (Dubowitz disease)	6 – 18 months	20 – 30%	Adulthood	Inability to walk Progressive muscle weakness and motor dysfunction
3 (Kugelberg-Welander disease)	> 18 months	10 – 20%	Normal	Assisted walking Tremors Progressive mild muscle weakness
4 (Adult-onset SMA)	Adulthood	< 5%	Normal	Restricted motor abilities Progressive mild muscle weakness

Type 0 (prenatal-onset SMA) is the rarest and most severe form occurring *in utero* and where onset of muscle weakness and hypotonia limits life expectancy to under 6 months [5,6] (Table 1.1). Type 1 SMA (Werdnig-Hoffman disease) is the most common form, which accounts for > 50% of cases [7]. Disease onset usually arises within the first 6 months after birth, prior to the developmental stage of sitting upright [8]. As a result patients usually display hypotonia, flaccid paralysis

and absence of head control [8] (Table 1.1). If left untreated, the life expectancy of type 1 patients is < 2 years, with mortality linked to severe respiratory complications from weakened diaphragm and intercostal muscles [8,9] (Table 1.1). The second most common form is type 2 SMA (Dubowitz disease), which manifests around 6-18 months of age, when an infant has reached the ability to sit upright unassisted but not walk independently [10] (Table 1.1). Although life expectancy for type 2 SMA patients is higher (around 40 – 60 years), if left untreated their symptoms worsen with mechanical ventilation required in later life [11,12]. Type 3 SMA (Kugelberg-Welander disease) accounts for 10-20% of cases and usually develops at > 18 months [13]. Although type 3 SMA patients have a normal life expectancy and reach the independent walking stage, disease progression can hinder their motor abilities and muscle function in later life [11,14]. Finally, type 4 SMA (adult-onset SMA) is a rare form that usually manifests in adulthood, leaving patients with a normal life expectancy albeit with mild neuromuscular pathologies, which has often led to this type being misdiagnosed [15] (Table 1.1).

1.1.2. Genetics

Traditionally SMA was thought to be the second most common autosomal recessive disorder that affects pan-ethnic populations at incidence rates of 1 in 6000 – 10,000, alongside carrier frequencies of 1 in 40 – 60 [16–18]. However, as of 2020, recent evidence suggests SMA might actually be less common with a lower incidence rate of 1 in 28,137, based on newborn screenings in New York, although this estimation remains to be similarly observed in different population groups [19].

The genetic cause for SMA in 96% of cases is the loss-of-function (LOF) in the *survival of motor neuron 1* (*SMN1*) gene located in the telomeric 5q13 chromosome region [20,21]. Around 95% of *SMN1*-linked SMA patients possess a homozygous deletion of *SMN1* exon 7 or the whole gene [22,23], whilst the remaining individuals are defined as compound heterozygotes as they carry a deletion in one *SMN1* allele and a LOF intragenic mutations on the other [23,24]. Although 98% of *SMN1* mutations originate from autosomal inheritance from heterozygous carrier parents [25,26], the remaining 2% of SMA cases can arise from *de novo SMN1* mutations [25,27]. Although most species possess a single homolog of the *SMN* gene [28], humans are interestingly unique as their genome possesses a 500 kb inverted duplication, leading to the generation of an *SMN2* gene within the centromeric 5q13 locus [29]. Both *SMN1* and *SMN2* share a high homology, with only 5 single nucleotide point mutations distinguishing them [21,30,31]. The 840C>T point mutation in the heptameric splicing factor 2/alternative splicing factor (SF2/ASF) motif in exon 7 plays a detrimental role in *SMN2* as it weakens the upstream 3' splice site and prevents SF2/ASF-mediated splicing [31–35]. This in

turn promotes a protein expression ratio of 90% truncated and non-functional SMN (SMNΔ7): 10% functional full length-SMN (FL-SMN) [31–35] (Figure 1.1).

Although *SMN2* plays a redundant role in healthy individuals with a functional *SMN1* gene (Figure 1.1.a), it has nevertheless remained conserved in the human genome and is an important genetic modifier in SMA (Figure 1.1.b) [28,29]. Indeed, homozygous *Smn* knockout (KO) mice with a total absence of FL-Smn are embryonic lethal [36,37]. However, the transgenic expression of the human *SMN2* in the KO mice prevented *in utero* death [38], highlighting that low levels of FL-SMN (around 10-20%) are sufficient to allow survival, albeit at the cost of developing neuromuscular pathologies. Interestingly, inclusion of additional *SMN2* transgenes into *Smn*-KO mice correlated with milder pathologies, with 8 *SMN2* copies rescuing the SMA phenotype [39,40]. These results suggest that a minimum threshold of FL-SMN expression is required for a healthy phenotype [39,40]. Similarly, this accounts for most of the clinical heterogeneity in SMA as *SMN2* copy number inversely correlates with disease severity (i.e., increased *SMN2* copy number confers milder SMA types) [41–43] (Table 1.1, Figure 1.1.c).

Although the aetiology of *SMN2* copy number variation (CNV) is still under investigation, it is thought that both gene duplication and conversion play important roles [44,45]. Certain examples include type 2 SMA patients possessing heterozygous *SMN1*-to-*SMN2* conversion (3 *SMN2* copies) and type 3 and 4 SMA patients harbouring homozygous *SMN1*-to-*SMN2* conversions (>4 *SMN2* copies) [44,45].

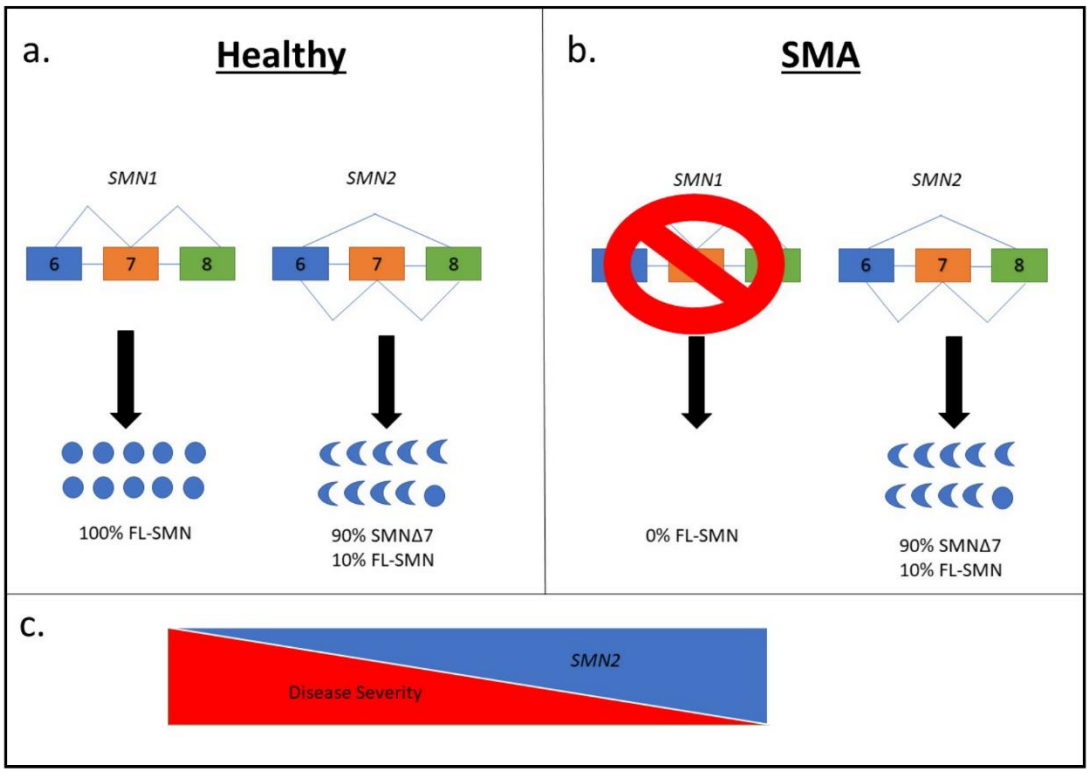

Figure 1.1. *SMN1* and *SMN2* expression in healthy and SMA patients.
a. In healthy individuals, the *survival of motor neuron 1* (*SMN1*) gene expresses 100% full length (FL) SMN protein, whilst each copy of the *SMN2* gene only expresses 10% FL-SMN protein and 90% truncated non-functional SMN (SMNΔ7) that lacks exon 7 due to alternative splicing.
b. In SMA patients, the LOF of *SMN1* prevents expression of FL-SMN from the *SMN1* gene, with patients compensated by the 10% of FL-SMN expressed by each *SMN2* copy number their genome possesses.
c. *SMN2* copy number variation inversely correlates with disease severity.

1.1.3. SMA Mouse Models

The homology of the *SMN1* gene in various species has been useful for the development of pre-clinical models that characterise the molecular, cellular, physiological, and anatomical pathologies in SMA. Model organisms for SMA include zebrafish (*Danio rerio*) [46], *Drosophila melanogaster* [47], *Xenopus tropicalis* [48] and *Caenorhabditis elegans* [49]. However, the most commonly used model are mice (*Mus musculus*).

As previously discussed in section 1.1.2, initial studies in mice revealed that complete *Smn* KO caused embryonic lethality due to their possession of only one *Smn* gene copy [37]. Nevertheless, over the last two decades, viable SMA mice have been developed that manifest a spectrum of mild to severe SMA pathologies (Table 1.2). Two well-used models for severe SMA, reminiscent of infantile-onset (type 0 and 1), are the Taiwanese *Smn$^{-/-}$;SMN2(2Hung)$^{+/+}$* (or *Smn$^{-/-}$;SMN2*) [38], the *Smn$^{-/-}$;SMN2$^{+/+}$* [40] and the *Smn$^{-/-}$;SMN2$^{+/+}$;SMNΔ7* [50] (or *SMNΔ7*) models (Table 1.2).

Developed first, the Taiwanese *Smn$^{-/-}$;SMN2* mouse model expresses two copies of human *SMN2* transgene in an endogenous *Smn* null background (by KO of exon 7), resulting in 15% FL-SMN expression [38]. Its life expectancy is around 10-14 days with symptomatic onset at post-natal day (P)5 [38] (Table 1.2). Interestingly, the first study on Taiwanese *Smn$^{-/-}$;SMN2* SMA mice presented limited data, which did not fully characterise the suitability of this model for SMA [38]. Alas, subsequent research has helped to reduce this limitation with emerging evidence of neuronal degeneration [51], neuromuscular junction (NMJ) denervation

[52] and muscle pathologies [53] being validated in Taiwanese *Smn*$^{-/-}$;*SMN2* SMA mice.

On the other hand, the *SMNΔ7* mice were generated by the addition of a human *SMNΔ7* gene into the previously established severe *Smn*$^{-/-}$;*SMN2*$^{+/+}$ SMA mouse model, which differed from the severe Taiwanese *Smn*$^{-/-}$;*SMN2* SMA mice via a different endogenous *Smn* null genotype of exon 2 KO instead of exon 7 [38,40,50] (Table 1.2.). Additionally, both the *Smn*$^{-/-}$;*SMN2*$^{+/+}$ [40] and *SMNΔ7* [50] SMA mice are useful severe SMA models in terms of disease characterisation, as more published data is available on its neuronal, NMJ and muscle pathologies [2,54–56] compared to Taiwanese *Smn*$^{-/-}$;*SMN2* SMA mice [38]. However, the severity of *Smn*$^{-/-}$;*SMN2*$^{+/+}$ SMA mice restricts its life expectancy to 5 days [40], making the less severe *SMNΔ7* model a useful alternative due to its higher natural life expectancy of around 2 weeks [50] (Table 1.2.).

Although severe SMA mice have been useful in SMA research, they have certain limitations such as not modelling later onset type 2-4 SMA and preventing investigations into the long-term effects of SMA pathogenesis due to their shortened lifespan [38,40,50]. To overcome these limitations, SMA mice with milder pathologies were developed (Table 1.2). A commonly used mild SMA model is the intermediate *Smn*$^{2B/-}$ mouse, which does not possess a human *SMN2* transgene [57,58] (Table 1.2.). Instead, one *Smn* allele (*Smn*^{2B}) is endogenously mutated to prevent exon 7 splicing [58], whilst the other allele is KO (*Smn*$^{-}$) [37], which results in an endogenous 15% FL-Smn expression and milder disease manifestation [57] (Table 1.2.). Furthermore, the Smn$^{2B/-}$ SMA mice were characterised with neuromuscular pathologies of gradual axonal degeneration, NMJ and muscle pathologies that have also been observed in severe SMA mice

[40,50,57]. The average lifespan of *Smn*$^{2B/-}$ mice is around 21-30 days, although this variability is dependent on the genetic background of the mouse strain i.e. C57BL/6 or FVB [57,59] (Table 1.2.).

In recent years, additional mild SMA mouse models have been developed with greater lifespans than the previously mentioned SMA mice [60,61] (Table 1.2.). Importantly, these mild models are advantageous to establish clearer distinctions between pre-symptomatic and symptomatic stages during disease progression. Overall, the various SMA mouse models have been important in helping us gain a greater understanding of both disease pathology and treatment efficacy in SMA.

Table 1.2. Commonly used SMA mouse models.

Severity	Model (Genotype)	Lifespan	Main Clinical Features	Year Developed	References
Lethal	*Smn*$^{-/-}$	Embryonic lethal	Embryonic lethal.	1996	Schrank *et al* (1997) [37]
Severe	Taiwanese *Smn*$^{-/-}$*;SMN2*	10 – 14 days	Severe neuromuscular defects with symptomatic onset at P5	2000	Hsieh-Li *et al* (2000) [38]
	Smn$^{-/-}$*;SMN2*$^{+/+}$	5 days	40% motor neuron loss at P5 with severe neuromuscular defects.	2000	Monani *et al* (2000) [40]
	SMNΔ7 Smn$^{-/-}$*;SMN2*$^{+/+}$*; SMNΔ7*	14 days	Severe neuromuscular defects	2005	Lee *et al* (2005) [50]
Mild	Intermediate *Smn*$^{2B/-}$	21 – 30 days	Mild neuromuscular defects, Progressive weight loss from P15, Metabolic defects	2012	Bowerman *et al* (2012) [57]
	Smn$^{c/c}$	Near normal	Mild neuromuscular defects, Cardiac abnormalities, Tail necrosis	2012	Osborne *et al* (2012) [60]
	Smn$^{2B/-}$*;SMN2*$^{+/-}$	1 – 2 years	Mild neuromuscular defects that are more prominent in males.	2020	Deguise *et al* (2020) [61]

1.1.4. Ubiquitous SMN functions

The human FL-SMN protein is 38 kDa and composed of 294 amino acids with high sequence conservation across vertebrate species [62–65]. It is comprised of the N-terminal basic-lysine rich region, central Tudor domain and C-terminal proline-rich and YG domains [64–72]. When expressed, the FL-SMN protein is known to self-oligomerise through interactions between the N-terminal (exon 2b) and C-terminal domains (exon 6), which is supported by evidence that SMA-causing point mutations in these sites can impair self-oligomerisation [73,74]. Furthermore, improper self-oligomerisation contributes to the instability of the truncated SMNΔ7 protein [73,74]. Indeed, exon 7 loss in SMN results in a frameshift mutation that create a four amino acid length EMLA motif in exon 8, which exposes the SCF^{Slmb} degron [73–75]. This degron exposure leads to the recruitment of proteasomes such as lysosomal proteases and calpains that enhances protein degradation [73–75].

In mammals, SMN is ubiquitously expressed in the nucleus and cytosol of cells [76–80] . The SMN protein itself is associated with 8 additional proteins (Gemins 2-8 and Unrip) to form a large core SMN-complex that localises in the nucleus as Gemini of coiled bodies (Gems) and in the cytosol as U bodies [79,81–84] (Figure 1.2). The earliest functional studies discovered that the core SMN complex associates with exported small nuclear (sn)RNAs and Sm core proteins, required for the later stages of sn-ribonucleoprotein (snRNP) assembly [79,82,85–89]. Subsequent studies have since supported the importance of SMN's housekeeping role in snRNP biogenesis as well as major (U2-dependent) and minor (U-12 dependent) mRNA splicing [83,90–92] (Figure 1.2).

Indeed, transcriptome analyses of Smn-depleted murine motor neuron-like NSC-34 cells [93] as well as neuronal and muscle tissue from the severe Taiwanese *Smn*$^{-/-}$*;SMN2* SMA mice [94] revealed a pattern of elevated U-12 dependent intron retention, suggesting that aberrant splicing plays a role in SMA pathogenesis.

Although SMN forms a core complex with the Gemins and Unrip proteins [79,81–84], the SMN protein itself has a vast interactome of additional protein partners, which creates transient SMN complexes with ubiquitous and/or tissue-specific functions that differ to snRNP assembly and splicing regulation [95–97]. Although research is still active on discovering these novel protein partners, certain examples have been identified such as myb-binding protein 1a (MYBBP1A) [96] and profilin-2 [98] to name just a few.

In terms of SMN roles outside of snRNP biogenesis and pre-mRNA splicing, subsequent studies have identified further RNA housekeeping functions such as transcription [99], small nucleolar RNPs (snoRNPs)-dependent post-transcriptional modification of non-coding RNAs [100], telomerase activity [101], 3’ end histone mRNA modification [102] and RNA trafficking [103] (Figure 1.2).

In addition to RNA metabolism, novel ubiquitous SMN functions have also been associated with DNA recombination and repair [99,104–107] as well as protein homeostasis [108] (translation [109], autophagy [110,111] and ubiquitination [112–115]) (Figure 1.2). Furthermore, SMN harbours cell-specific roles with one example being its ability to govern signalling pathways linked to actin remodelling via Rho-associated kinase (ROCK) activity [69,116,117] in neuronal cells, thus regulating functions such as intracellular trafficking [118] and endocytosis [119].

Although these are only a few examples, research into SMN function(s) is still an ongoing endeavour. In SMA, this research is of vital importance for understanding the variable temporal- and tissue-specific effects of SMN depletion as well as for the development of therapies.

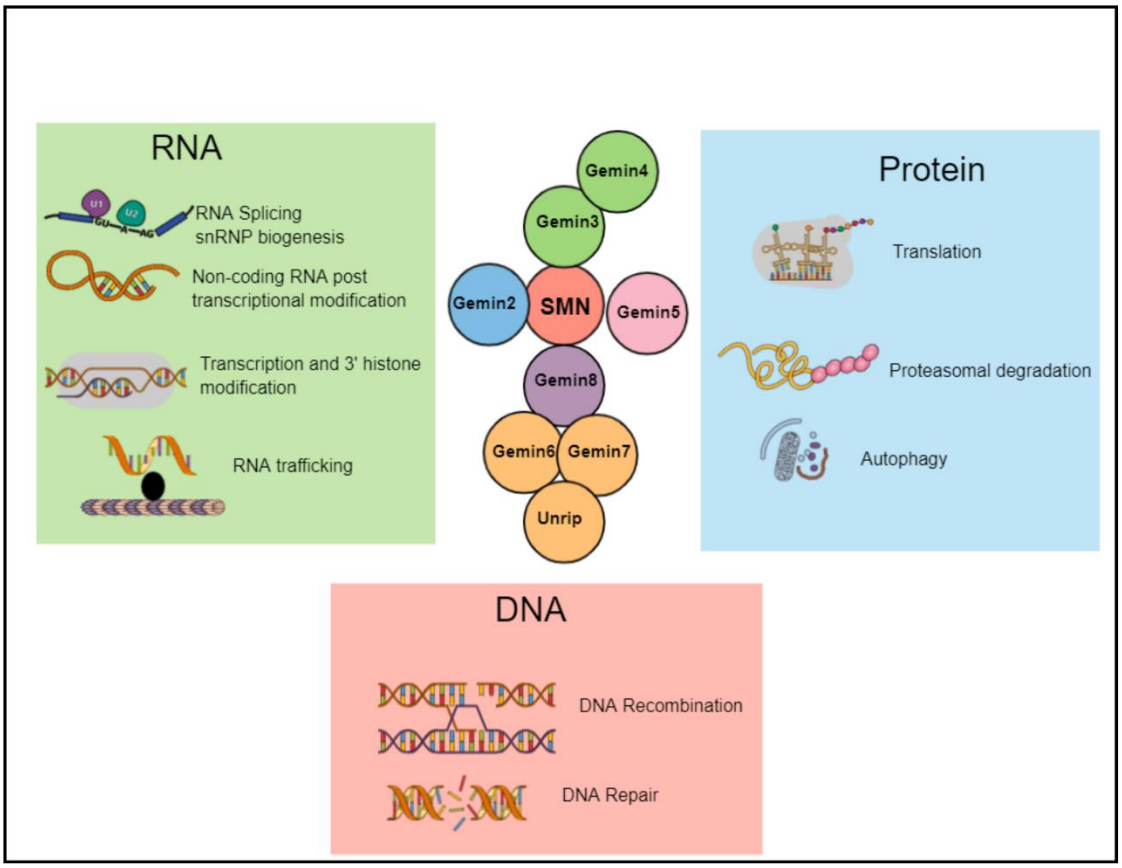

Figure 1.2. Ubiquitous housekeeping roles for SMN.
SMN complex is in the centre (SMN, Gemins2-8 and Unrip). RNA regulatory roles for SMN (green box) include snRNP biogenesis, RNA splicing, non-coding RNA post-transcriptional modification, transcription, 3' histone modification and RNA trafficking. Protein regulatory roles for SMN (blue box) include translation, proteasomal degradation and autophagy. DNA regulatory roles for SMN (orange/peach box) include DNA recombination and repair. Figure was created on Mind the Graph.

1.2. Neuronal pathologies in SMA

Although SMN is ubiquitously expressed [77], the motor neurons are particularly susceptible to SMN depletion, which results in alpha-motor neuron degeneration in the anterior horn of the spinal cord [1]. Expression studies aimed at understanding this susceptibility in neurons have uncovered a variety of key findings. One is that a high SMN threshold is required to govern normal neuronal development and function, as evidenced by the consistently high SMN levels in the central nervous system (CNS) and the presence of an axonal-specific isoform termed axonal-SMN [76,77,120]. Another key finding is that motor neurons are more sensitive to *SMN1* LOF due to the limited genetic modifier ability of *SMN2* in this tissue, as *SMN2* expression analyses in type 1 SMA foetuses revealed that FL-SMN protein levels expressed from this gene are greater in peripheral non-neuronal tissues compared to the spinal cord [121].

More in depth analyses have shown that SMN is abundantly localised within the axonal and growth cone regions of motor neurons, in association with Gemin proteins [122,123] (Figure 1.3). This led to subsequent investigations into the role of SMN in actin dynamics, since axons and growth cones are rich actin-cytoskeletal structures that have vital roles in functional processes such as axonal extension, neurite outgrowth, synaptic development and vesicle release [124–126] (Figure 1.3). In fact, these neuronal features have been demonstrated to be defective in patient-derived SMA spinal cord biopsies, induced pluripotent stem cell (iPSC)-derived neurons, *in vivo* models and SMN-depleted immortalised cell lines, suggesting that dysfunctional actin dynamics may play a contributory pathogenic role in SMA motor neuron degeneration [118,123,127–129].

One specific role for SMN in actin dynamics is the trafficking of β-actin mRNA via heterogeneous nuclear ribonucleoproteins (hnRNPs) [118,130,131], which is important for axon guidance, extension and synaptogenesis [124,132] (Figure 1.3). Interestingly, Smn deficiency in motor neurons of severe *Smn*$^{-/-}$;*SMN2*$^{+/+}$ SMA mice and immortalised PC12 rat neuronal cells show reduced β-actin mRNA localisation in axonal and growth cone regions, resulting in impaired neurite outgrowth that is reversed upon Smn overexpression in differentiating PC12 cells [118,127].

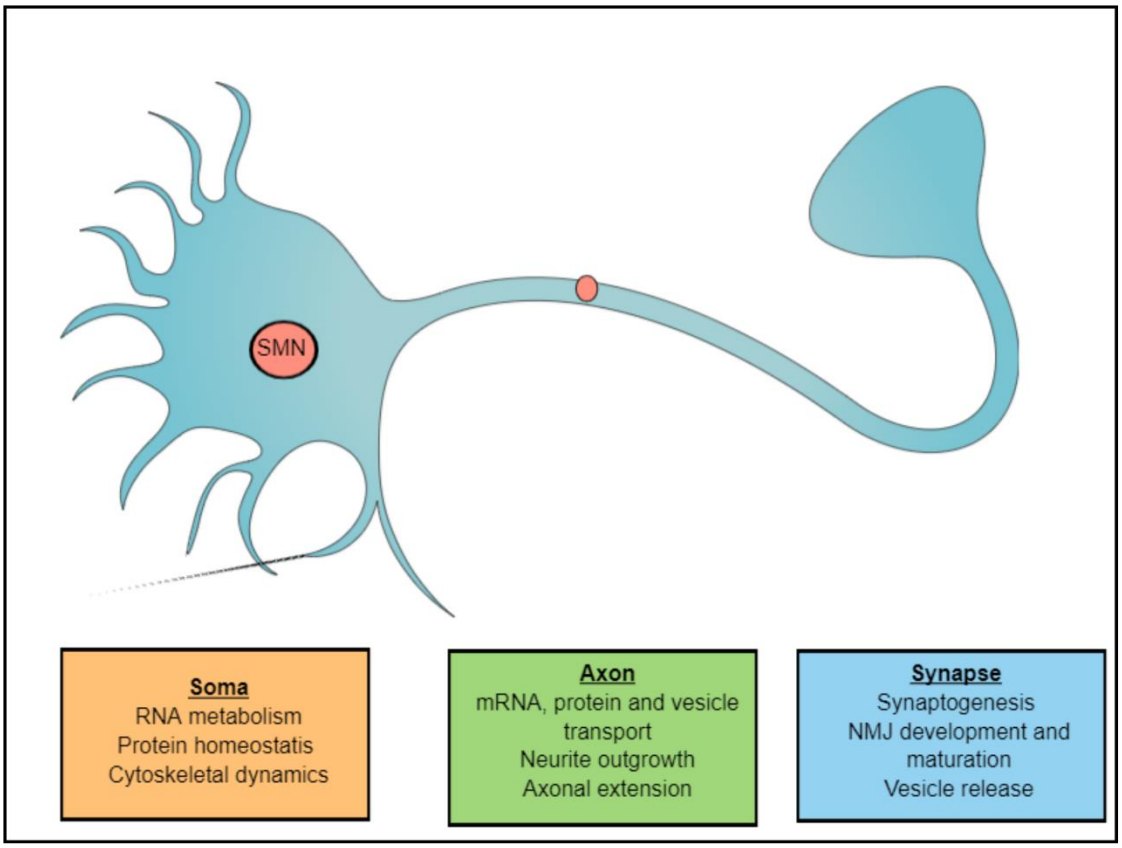

Figure 1.3. Functional roles of SMN in the motor neuron.
SMN protein (red circle) is localised in the soma and axonal regions of the motor neuron. SMN plays key functional roles in different motor neuron regions. In the soma, it is important for RNA and protein homeostasis and cytoskeletal dynamics. In the axon, it is transported along the actin cytoskeleton and regulates mRNA, protein and vesicle trafficking. SMN also plays an important role in neurite outgrowth. In the synapse, SMN plays an important role in neuromuscular junction (NMJ) development and function. The figure and textual references are adapted from Ojala *et al* (2021) In search of a cure: The development of therapeutics to alter the progression of spinal muscular atrophy. *Brain Sciences*, 11, 194. Figure was created on Mind the Graph.

Alongside actin transport, SMN is also thought to transduce actin signalling pathways [133]. One such example is the interactive binding of the SMN polyprotein motif to profilin-2a [69,116,134]. This in turn prevents ROCK-dependent profilin-2a phosphorylation, allowing for the phosphorylation of cofilin and myosin light chain phosphatase (MLCP) instead, which enables normal actin dynamics [116,134,135]. However, Smn depletion in PC12 cells suggests that the loss of SMN allows for ROCK to competitively hyper-phosphorylate and activate profilin-2a, which leaves cofilin and MLCP hypo-phosphorylated, leading to an imbalance in actin remodelling and to impaired neurite outgrowth [116,136]. Similarly, profilin-2a and RhoA/ROCK signalling have recently been validated as regulators of actin rod assembly, which is defective upon Smn depletion in the murine motor neuron-like NSC-34 cell line [137]. Furthermore, *in vivo* studies have also reported increased RhoA/ROCK activity in symptomatic intermediate *Smn*$^{2B/-}$ SMA mice, which was attenuated independently of Smn restoration via treatment with ROCK inhibitors Y-27632 and fasudil, highlighting the importance of the pathway in SMA neuronal pathology [117,138].

Interestingly, genes involved in actin remodelling also act as genetic modifiers of SMA. Indeed, linkage analysis of an asymptomatic SMA patient with the same genotype as their affected sibling, identified that the asymptomatic individual had elevated mRNA and protein levels of plastin-3, an actin-binding protein [139,140]. The notion of plastin-3 being a positive genetic modifier of SMA is further supported by evidence in *Smn*$^{2B/-}$ SMA mice that demonstrated a concomitant plastin-3 decrease and profilin-2a elevation in neuronal tissue prior to symptomatic onset [98]. Furthermore, plastin-3 overexpression improved the lifespan, motor function and NMJ activity of *SMNΔ7* SMA mice [141,142].

Although actin dysregulation is an interesting pathological mechanism, it is not solely responsible for motor neuron degeneration in SMA. Indeed, established, and ongoing research have identified a multitude of dysfunctional mechanisms and pathways that contribute to motor neuron degeneration upon SMN depletion. These include autophagy [111], pro-apoptotic elevations of Caspase-3 [111,143,144], alongside mitochondrial depletion, impaired mitochondrial biogenesis and oxidative phosphorylation [129,145,146].

Alongside intrinsic motor neuron dysfunctions, effects on other CNS cells have also been reported in SMA models. One example is astrocytes, which serve as primary support cells for the CNS [147]. Indeed, both SMA patient iPSC-derived neurons and *SMNΔ7* SMA spinal cords display morphological and functional alterations in astrocytes, which in turn prevents stimulation of neurite outgrowth [148,149].

Collectively, the evidence provided thus far presents the neuronal pathologies in SMA as complex multi-factorial mechanisms that govern canonical roles in the CNS.

1.3. Peripheral pathologies in SMA

The notion of SMA being solely a motor neuron disease has been reconsidered in recent years, with emerging evidence from independent studies suggesting it may be a systemic multi-organ disease (Figure 1.4). Indeed, investigations reporting pathologies in peripheral tissues alongside established evidence of SMN being ubiquitously expressed have helped support this notion [77,150,151].

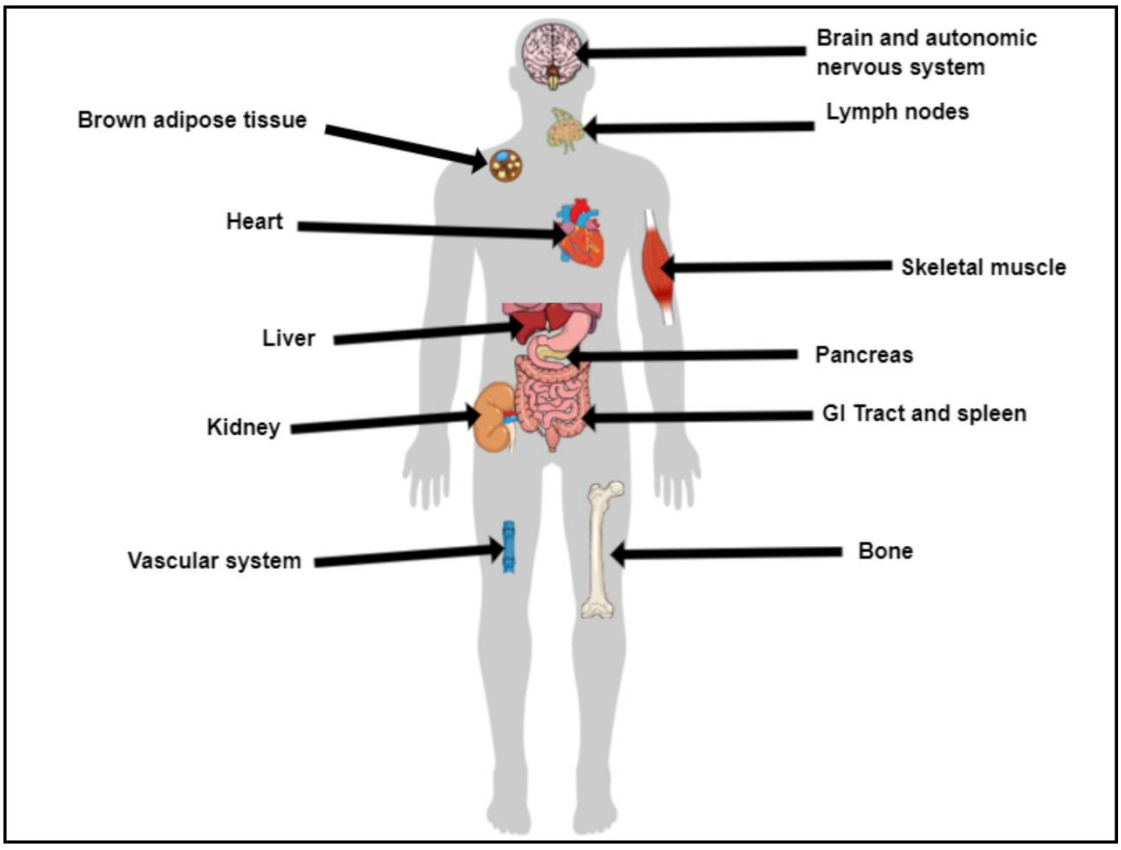

Figure 1.4. SMA is a systemic disease that affects multiple organs.
Figure was created on Mind the Graph.

1.3.1 Developmental and functional dysfunction in SMA skeletal muscle.

Traditionally, it can be assumed that denervation-induced muscle atrophy via alpha-motor neuron degeneration and NMJ defects is the main contribution of muscle loss and weakness in SMA [2,152–154]. However, this idea had been challenged in recent years with emerging evidence that different SMA mouse models have naturally smaller body sizes and thus smaller muscles compared to healthy mice [38,40,50,57]. Furthermore, deletion of atrophy-promoting genes *atrogin-1* and *Muscle RING Finger 1* (*MuRF1*) in severe *SMNΔ7* SMA mice failed to improve weight or survival phenotypes [155]. Thus, we need to evaluate and take into consideration the extent that innate muscle dysfunctions outside of denervation-induced atrophy contributes to SMA disease phenotype.

Although, one study argued that intrinsic SMN depletion does not impact skeletal muscle (e.g. muscle-specific *Smn*-KO *SMNΔ7* mice do not display muscle defects) [156], multiple studies across pre-symptomatic models, patient biopsies and muscle cell lines have presented contradictory evidence of pathologies in SMA skeletal muscle, which are independent of neuronal degeneration [54,55,157–160]. Indeed, muscle cells derived from human type 1 SMA embryonic stem cells (ESCs) demonstrated impaired myogenic development, function and metabolism, independent of motor neuron innervation [161]. Furthermore, *MyoD-iCre SMN2*$^{+/-}$*; SmnF7*$^{/-}$ (or *MyoD-iCre*) SMA mice, which only had 25% FL-Smn expression in skeletal muscle instead of systemic FL-Smn depletion presented pathological similarities akin to intermediate *Smn*$^{2B/-}$ SMA mice such as survival, progressive weight loss, NMJ activity and muscle fibre size [162].

Thus, although SMN activity and levels have critical importance in motor neurons (see section 1.2), its intrinsic depletion can still have a direct impact on muscle development and function that contributes to the manifestation of SMA pathologies.

1.3.1.1. SMA and skeletal muscle development.

Myogenesis is the formation of skeletal muscle and is split into primary and secondary phases, which are regulated in a spatial and temporal manner by muscle specific master regulatory transcription factors called myogenic regulatory factors (MRFs) [163,164] (Figure 1.5). Of note, most myogenic developmental timelines have been based on mouse studies [165,166] (Figure 1.5)

The primary phase begins with the upregulation of the MRFs myogenic factor 5 (Myf5), myogenic factor 6 (Myf6 or Mrf4) and myoblast determination protein 1 (MyoD) in a temporal pattern that converts $Pax3^+$ myogenic precursors into myoblasts [167–171] (Figure 1.5). These myoblasts then terminally differentiate into single mononucleated myocytes via Myogenin (MyoG) and fuse together to form multi-nucleated primary myofibers [172–175] (Figure 1.5). Eventually, the primary phase culminates with the generation of multinucleated type 1 slow myofibers that express slow- and embryonic-specific myosin heavy chains (MHCs) like Myh3 and Myh7 [176,177] (Figure 1.5).

The secondary phase involves the fusion of $Pax7^+$ myogenic precursors to the primary myofiber scaffold via MyoD and Myogenin upregulation [170,178–180] (Figure 1.5). Throughout the secondary phase, type-2 fast myofibers begin to emerge, which is evidenced by the expression of the fast MHC isoforms Myh2, Myh4 and

Myh1 [163,181] (Figure 1.5). A subset of these Pax^{7+} cells then form a quiescent pool of satellite cells, which are important for muscle growth, regeneration and repair [182–186] (Figure 1.5). Briefly, MyoD upregulation and Pax7 downregulation converts most of these satellite cells into proliferating myoblasts, whilst a small pool undergo self-renewal for stock replenishment in the basal lamina [187–192].

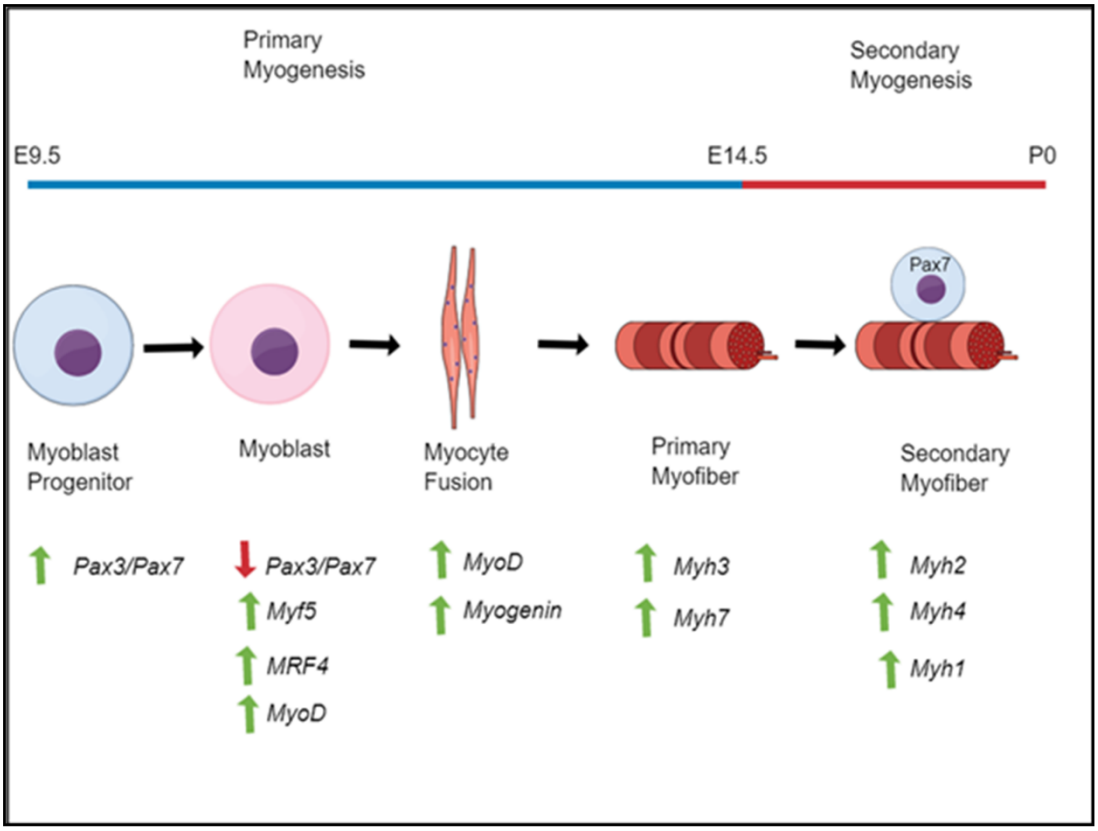

Figure 1.5. Timeline of murine skeletal myogenesis.
From left to right the developmental timeline for myogenesis encompasses primary phase from embryonic days (E) 9.5-14.5 (blue line) and secondary phase from E14.5 to post-natal day (P) 0 (red line). Primary phase begins with $Pax3^{+}$ myoblast progenitors, which are converted into myoblasts through upregulation of myogenic regulatory factors (MRF) Myf5, MRF4 and MyoD alongside Pax3/7 downregulation. These mononucleated myoblasts are directed to terminally differentiate into myocytes through MyoD and Myogenin. Myogenin becomes important later on to mediate myocyte fusion to form multinucleated myofibers. At E14.5, primary phase ends with the formation of type-1 primary myofibers, which express embryonic and type 1 myosin heavy chain (MHC) isoforms: Myh3 and Myh7. Secondary myogenesis begins around E14.5 and lasts until birth through fusion of $Pax7^{+}$ myogenic precursors onto a primary myofiber scaffold and each other through MRF direction. Throughout secondary myogenesis, type 2 skeletal myofibers form, which express fast MHC isoforms: Myh2, Myh4 and Myh1. Upregulated gene expression represented with green arrows. Downregulated gene expression represented with red arrows. Figure was created on Mind the Graph.

In SMA, one or more pathological features such as reduced myotube size, centralised nuclei, fusion defects and premature differentiation of satellite cells have been reported across pre-symptomatic SMA mice, patient and foetal muscle biopsies and *Smn*-depleted C2C12 myoblast-like cells, which could be attributed to delayed myogenesis [54,55,157–160]. One such intrinsic defect reported in early and later stages of SMA muscle development is delayed myogenesis. Indeed, myogenic cell lines generated from type 1 SMA human ESCs revealed a greater expression of pre-myogenic marker Pax3 and a lower expression of MyoD and Myogenin compared to healthy controls, reminiscent of myogenic precursors [161]. Furthermore, these SMA myogenic precursor-like myoblasts were unable to properly differentiate *in vitro,* as evidenced by a consistent downregulation of *Myogenin* mRNA and MYH1/2/4/6 isoforms [161]. Similarly, *in vivo* investigations of *tibialis anterior* (TA) and cranial muscle biopsies from pre-symptomatic neonatal severe (*Smn*$^{-/-}$;*SMN2*$^{+/+}$ and *SMNΔ7*) and intermediate *Smn*$^{2B/-}$ SMA mice also revealed reduced expression of Pax7, MyoD and Myogenin, suggesting that intrinsic SMN depletion delays early myogenesis in both pre- and neo-natal SMA muscle [54]. Interestingly, the longer life expectancy of *Smn*$^{2B/-}$ SMA mice, compared to its severe counterparts (*Smn*$^{-/-}$;*SMN2*$^{+/+}$ and *SMNΔ7*), was advantageous in revealing a significant increase of Pax7, MyoD and Myogenin levels in the older P21 muscle [54], suggesting a delay in muscle development and maturation of SMA muscle. In addition, type 1-3 SMA muscle biopsies also presented similar features such as increased expression of MRFs (MyoD, Myogenin and MRF4), prenatal MHC isoforms and intermediate filaments that are commonly associated with immature muscle fibres (desmin and vimentin [193]) [157,158,194], further supporting a delayed myogenesis in SMA muscle.

In addition to embryonic muscle development, features of impaired muscle differentiation are also observed in satellite cells [160]. While there was no significant difference in satellite cell pools between Extensor digitorum longus (EDL), TA and soleus muscles from P2 *Smn*$^{-/-}$;*SMN2*$^{+/+}$ SMA and control mice, myofiber analyses revealed a higher proportion of cells co-expressing Pax7 and MyoD in SMA muscles [160]. Furthermore, *in vitro* differentiation of satellite cells isolated from SMA mice resulted in an earlier expression of Myogenin and MHC isoforms in centrally-located nuclei of myotubes, suggesting that SMA satellite cells contribute to immature muscle fibres by premature differentiation [160].

One proposed theory for how SMN impacts myogenesis is its regulation of cellular fusion processes like cell migration, alignment and cell-to-cell contact [195]. Indeed, slow migratory movements were observed in H2K-SMA myoblasts, as evidenced by disorganised actin cytoskeleton and persistent presence of talin and vinculin markers at the cell surface [195,196], which are cytoskeletal proteins that typically undergo cycles of assembly and disassembly to promote cell migration [197–199]. Furthermore, restoration of Smn levels improved cell migration, supporting the functional role of SMN in this regulatory pathway [195].

Based on the multitude of evidence highlighting SMN's intrinsic roles in myogenesis, multiple models reflecting its function have been proposed. The direct model suggests that SMN directly interacts and modulates the activity of molecular effectors of myogenesis. The indirect model proposes that reduced SMN levels contributes to increased alternative splicing and risk of DNA damage in genes critical for myogenesis, as DNA damage was evident in pre-symptomatic SMA skeletal muscle prior to damage in motor neurons [106,107]. Alternatively, both direct and indirect models could co-exist to explain SMN's

role(s) in muscle development. In spite of the remaining knowledge gaps, the evidence for impaired myogenesis as an early disease marker in SMA highlights the importance of directly treating skeletal muscle in this disease as early as possible.

1.3.1.2. SMA and skeletal muscle contraction.

Mature myofiber contraction is a tandem-controlled process where mechanical force is mediated by contractile myofibrils composed of sarcomere subunits [200]. Sarcomeres display a striped and organised pattern of sliding thin actin and thick myosin filaments with each individual subunit defined by the Z-disc borders [200,201] (Figure 1.6). Z-discs are cross-links predominantly composed of α-actinin, which interlock adjacent sarcomeres and anchor the actin filaments across the sarcomeres [201–204]. In addition to stability and contraction, the Z-disc is also important for mechano-sensation and signalling linked to mechano-transduction and hypertrophy [203].

In SMA, muscle fatigue is a pathological hallmark that can be associated with weakened contractile force [55]. Indeed, *ex vivo* contractility experiments with TA muscles from pre-symptomatic P2 *Smn*$^{-/-}$;*SMN2*$^{+/+}$ and P9 *Smn*$^{2B/-}$ SMA mice revealed weakened twitch and maximum peak tectonic force at 200 Hz stimulation compared to healthy animals [55]. Furthermore, the increased unstimulated force generated by the *Smn*$^{-/-}$;*SMN2*$^{+/+}$ TA muscle indicated that these mice were unable to efficiently recover from muscle fatigue [55]. Additionally, evidence of weakened contractile force being linked to muscle-specific intrinsic

SMN depletion is observed from the reduced peak specific force in soleus muscle from *MyoD-iCre* SMA mice with muscle-specific FL-Smn depletion [162].

From an indirect perspective, one possibility for SMN depletions contribution to muscle fatigue and weakened contractility is that the increased alternative splicing and DNA damage in pre-symptomatic skeletal muscle could affect genes important for the sarcomere and contraction [106,107]. SMA muscle development studies indeed support this indirect model as the delayed MHC isoform expression observed in pre-symptomatic SMA mice and human ESC-derived type 1 SMA myoblasts creates an immature contractile apparatus that would consequently generate less force than in age-matched controls [55,161]. In addition, reduced expression of calcium regulatory proteins such as ryanodine receptor 1 (Ryr1) and SERCA1a, which are important for excitation-contraction coupling further supports SMN's indirect contribution to weaker contraction in SMA muscle [55,205,206].

However, evidence of a direct SMN model in muscle contraction first emerged when analysis of *Drosophila melanogaster* [207] and mouse myofibrils [207,208] revealed SMN co-localisation at the sarcomeric Z-disc through an α-actinin interaction. Interestingly, further analysis in the mouse myofibrils revealed the presence of core SMN complex partners (Gemins 2-8 and Unrip) [79,82,83] and the absence of spliceosomal Sm-class snRNP components [87,88,208], suggesting that sarcomeric core SMN complex functions are unrelated to its ubiquitous spliceosomal counterpart [79,81,84,85,208]. Although these earlier studies did not conclude the exact functional role of SMN in the sarcomere [207,208], a recent study comparing age-matched human control and type 1 SMA quadricep biopsies revealed that sarcomeric SMN associates with the Z-disc only in SMA muscle [209].

On the other hand, sarcomeric SMN in healthy muscle normally localises to the actin-positive I band (non-overlapping actin) [200] and titin-positive M band, which cross links titin and myosin via the myomesin complex for sarcomere stability [209,210]. Furthermore, the mislocalisation of sarcomeric SMN in type 1 SMA muscle was associated with dysregulation of the sarcomeres actin cytoskeleton and focal damage in co-existing hypertrophic and atrophic myofibers [209], suggesting that SMN plays an important role in the stability of the sarcomeres architecture and function.

With functional differences between spliceosomal [79,81,84,85] and sarcomeric SMN complexes [207–209], protein partners of the latter were discovered that helps build a theoretical model for its unique and direct involvement in muscle contraction. Indeed, the control human muscle biopsies presented co-localisation of profilin-2 in spatial proximity of SMN in the sarcomere [209]. Interestingly, prior studies that confirmed profilin-2 and SMN's direct interactive role in actin dynamics (see section 1.2) suggests the possibility that SMN depletion in SMA muscle results in the dysregulation of the sarcomeres actin cytoskeleton via hyperphosphorylation of profilin-2 by ROCK [116,136,137] (Figure 1.6). Although ROCK was not analysed in the control and type 1 SMA muscle biopsies [209], previous evidence that ROCK inhibition via Fasudil [138] and Y-27632 [117] treatment improved skeletal muscle morphology in *Smn*$^{2B/-}$ SMA mice, supports the possibility of its involvement in our model. However, further studies are needed to corroborate if this is the case.

Another interactive partner discovered for sarcomeric SMN was calpain, a Ca^{2+} signalling-dependent protease with around 17 different isoforms that are involved in a variety of processes in skeletal muscle including apoptosis, synaptic plasticity, cell motility and myoblast fusion [211–216]. Interestingly, in mouse

myofibrils both *in vivo* and *in vitro* experiments revealed that calpain cleaved sarcomeric SMN [208], supporting previous evidence of increased cleaved SMN C-terminal residues by calpain activity [217]. Although the authors could not conclude which calpain isoform interacted with sarcomeric SMN and its role in contraction [208], one theory could be that calpain cleaves SMN at the Z-disc as a counteractive feedback mechanism to minimise sarcomere instability (Figure 1.6). Although further studies are needed to investigate the role of calpains in the sarcomere of SMA muscle, parallel observations of sarcomere instability and weakened muscle contractions in diseases characterised by LOF mutations in the calpain-3 isoform such as limb-girdle muscular dystrophy type 2 A (LGMD2A) [218–220] and various titinopathies [221–223], suggest this isoform could be a promising candidate.

Despite the gap in functional knowledge, the overwhelming evidence of reduced contractile force in SMA skeletal muscle, aberrant expression of MHC isoforms and intracellular Ca^{2+} activity showcase reduced muscle contraction as a contributory factor in SMA muscle fatigue. Furthermore, the impact of SMN depletion on expression of contractile components and the presence of a distinct sarcomere SMN complex linked to sarcomere stability suggests SMN plays both a direct and indirect role in muscle contraction.

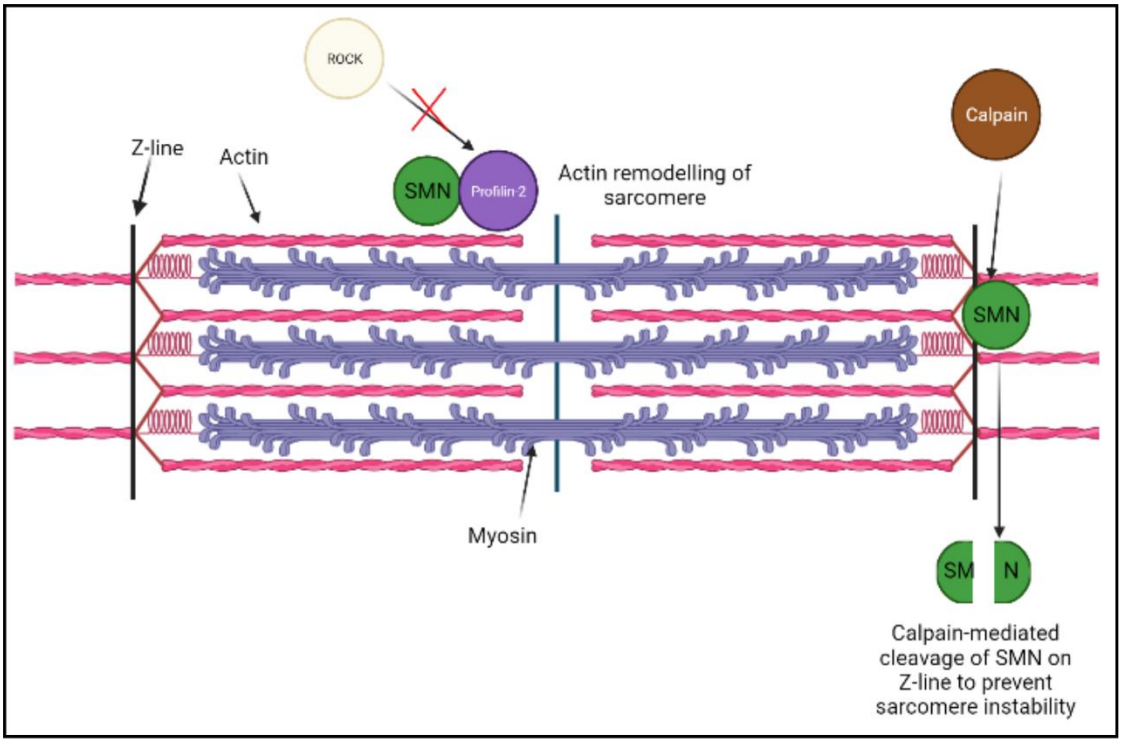

Figure 1.6. Proposed functional role of sarcomeric SMN complex in skeletal muscle
The sarcomere is composed of thick myosin (purple lines) and thin actin (red lines) filaments. The Z-disc (black line) is bound to actin on the peripheries of the sarcomere. Sarcomeric SMN (green circle) is present on thin actin filment interacting with Profilin-2 (purple circle) to competitively prevent ROCK (yellow circle) hyper-phosphorylation for proposed role in actin regulation of sarcomere. Calpain (brown circle) cleaves any sarcomeric SMN that has accumulated on the Z-line to prevent sarcomere instability. Figure was created on BioRender.com.

1.3.2. SMA and neuromuscular junction (NMJ) pathologies.

The NMJ is a specialised synaptic region comprised of the pre-synaptic motor neuron and post-synaptic motor endplates of myofibers that facilitates contraction via acetylcholine (ACh) and ACh receptor (AChR) interaction [224]. In mice, the NMJ develops around embryonic day (E)12-13 through formation of plaque-like motor endplate structures that express slow conducting AChR γ-isoforms that are imperfectly aligned with a myriad of motor neuron synaptic bulbs that extend axons to cover more regions than needed [225–231]. The critical step for NMJ development occurs during post-natal maturation in the first 3 weeks [230], where endplates undergo perforations and invaginations to form pretzel-like structures and the immature γ-isoforms are replaced with adult AChR ε-isoforms that align to the motor neuron synaptic bulbs [232–236]. In the pre-synaptic region, the motor neurons that are outcompeted in the polyneuronal cluster for motor unit innervation are progressively segregated and eventually pruned [231,237] by mechanisms of axonal degeneration [238], shredding [239] and/or retraction [240–242]. In the end, a mature motor unit is composed of muscle fibres governed by the axonal arbor of one motor neuron [230].

In terms of pre-synaptic NMJ pathologies in SMA, these can be associated with the previously described roles of SMN in the motor neuron (see section 1.2.) Early pre-synaptic NMJ defects [243–245] that arise in SMA include Schwann cell dysregulation [246,247], impaired voltage-gated ion channels [248] and polyneuronal innervation [249] (the NMJ before synaptic pruning [231,237]). However, one hallmark feature that progressively worsens is neurofilament accumulation [250]. Normally, in a healthy motor neuron, 10 nm intermediate filaments abundant in the axon are transported along the cytoskeleton for various functions such as development,

maintenance and nerve activity [251,252]. However, in SMN-depleted motor neurons, neurofilaments instead accumulate around the neuronal endplate regions [250,253,254], which may be potentially due to the reduced β-actin transport [118,127], although this has yet to be proven. Throughout disease progression, this accumulation increases, resulting in further exacerbation of impaired NMJ maturation and function [2,250,253,255,255,256].

In addition to the pre-synaptic region, post-synaptic NMJ abnormalities include aberrant AChR γ-isoform expression, immature motor endplate morphology and impaired AChR clustering [255,257]. Motor endplate shrinkage has also been reported across several SMA mouse models [55,258], although this could be attributed to the smaller myofiber size brought about by defects in myogenesis and MRF regulation, as previously described in section 1.3.1.1. Although studies across mouse embryos with impaired neuronal development, symptomatic SMA mice and iPSC-derived SMA motor neurons co-cultured with C2C12 myotubes suggest that impaired AChR clustering is denervation dependent [255,259–262], a case can also be made for intrinsic muscle involvement. Indeed, primary cultures from type 1 SMA embryonic skeletal muscle cells displayed reduced expression of nicotinic AChR, independent of interaction with motor neurons [263]. Furthermore, neurofilament accumulation was increased in the NMJs of triceps, gastrocnemius and intercostal muscles from muscle-specific FL-*Smn* knockdown (KD) *MyoD-iCre* SMA mice, independent of motor neuron degeneration, suggesting that muscle-specific intrinsic SMN depletion can influence both pre- and post-synaptic NMJ pathologies in SMA [162].

One important contributor to NMJ formation is the agrin-muscle specific kinase-low density lipoprotein receptor related protein 4 (agrin-MuSK-Lrp4) pathway [264–

[267]. Interestingly, agrin is mis-spliced and downregulated in both motor neurons and quadriceps of SMA mice [268–270]. In addition, exogenous agrin upregulation via NT-1654 (agrin agent) treatment in SMA mice improved myofiber size and NMJ activity, suggesting that agrin is a contributory effector to SMA NMJ pathologies [268–270]. Downstream of agrin, MuSK dysregulation has also been reported in SMA and MuSK activation via an agonist antibody significantly improved NMJ innervation and synaptic efficacy in the splenius muscle of *SMNΔ7* mice [271]. MuSK dysregulation has also been linked to other muscle-wasting conditions such as amyotrophic lateral sclerosis (ALS) and MuSK-myasthenia gravis (MuSK-MG) [272–274]. These studies thus highlight SMN-independent pathways that can contribute to aberrant NMJ pathology in SMA.

Despite NMJ defects being observed in most SMA muscle, the vulnerability to synaptic loss and NMJ denervation is selective [2,256]. Although studies in both *Smn*$^{-/-}$*;SMN2*$^{+/+}$ [256] and *SMNΔ7* SMA [2,256] mice have aimed to better understand this selectivity, they highlighted that no single neuronal (fast vs denervated synapse, neurofilament accumulation) or muscular (fast vs slow twitch) factor was the main cause [2]. Instead, they concluded that a combination of neuronal and muscular risk factors are possibly involved in the vulnerability of NMJ denervation [2,256], supporting the idea of taking both pre- and post-synaptic NMJ defects into consideration.

Although NMJ defects are a pathological hallmark feature of SMA, how SMN deficiency directly impacts NMJ development and function remains unclear. Low SMN levels could contribute to mis-splicing of genes important for NMJ development and function as was demonstrated with agrin [93,270]. However, an important caveat of previous studies is that human and murine NMJs are

morphological distinct [275,276]. Nevertheless, the presence of NMJ defects still exists in pre-clinical models and patients, highlighting its importance in SMA pathology.

1.3.3. SMA and metabolic dysfunctions in skeletal muscle and non-neuromuscular tissue.

In a healthy individual, skeletal muscle accounts for 40% of human body mass and its functional requirements for movement, posture and organ system support are associated with a high metabolic demand [277–280]. In addition, the plasticity of skeletal muscle as it adapts rapidly to external factors such as diet, exercise and age requires rapid and efficient regulation of metabolic pathways to produce the required energy [281,282]. For example, resting tissue consumes up to 30% of energy (ATP), while exercised muscle consumes nearly 100% [281,282]. Three of the major macromolecular metabolic pathways important for skeletal muscle function regulate glucose, fatty acids (FAs) and proteins.

1.3.3.1. Glucose metabolism

Skeletal muscle is a primary site for whole-body glucose regulation [283]. Normally, glucose uptake is pre-dominantly mediated by insulin stimulation in skeletal muscle via its binding to the sarcolemma expressed insulin receptor (IR)-α subunit, which induces a conformational change and auto-phosphorylation of the tyrosine residue in the IR-β subunit [284–286]. The following downstream signalling cascade of IR substrate 1 (IRS-1)/phosphoinositide 3-kinase (PI3K)/phosphatidylinositol (3,4,5)-triphosphate (PIP_3)/phosphoinositide-dependent kinase 1 (PDK1)/Akt/Akt substrate of 160 kDa (AS160) is then activated [287–294]. This results in the translocation of vesicles containing GLUT4 to the sarcolemma and insulin-stimulated exocytosis, which enables glucose influx into the myocyte [294–297]. In conditions of high energy requirements the intra-

myocellular glucose is then phosphorylated by hexokinase-2 (Hk2) for glycolysis [298].

A common metabolic disease characterised by reduced glucose uptake and insulin resistance is diabetes mellitus (DM) [299,300], however in recent years, studies have found similar glucose regulatory pathologies in SMA. Indeed, type 1-3 SMA patients display hypo- and hyper-glycaemia in fasted states [301–303], glucose intolerance [301], hyperleptinaemia [304], and insulin resistance [305]. In addition, case studies have reported the co-existence of pre-diabetes [303], type 1 DM (T1DM) [306] and ketoacidosis [307–309] in SMA patients. Similarly, pre-clinical studies also characterised pathologies such as hyperglycaemia, hyperglucagonaemia and glucose intolerance in *Smn*$^{2B/-}$ SMA mice, which suggests that dysfunctional glucose metabolism and insulin activity are features in SMA [301,310].

Normally within DM skeletal muscle, these glucose metabolic aberrations are characterised by insulin resistance, diminished peripheral glucose uptake and reduced glycolysis [299,300]. Similarly, the mRNA levels for glucose uptake and metabolism markers *HK2* [311] and *GLUT4* [295,296] were also downregulated in type 1 SMA iliopsoas muscles and TA muscle from *Smn*$^{2B/-}$ SMA mice [312], highlighting a pathological overlap in skeletal muscle glucose defects between SMA and DM.

Although insulin resistance and aberrant glucose metabolism can be secondary consequences of progressive muscle wasting [313,314], one study suggested that intrinsic SMN depletion could also play an active role [161]. Indeed, ESC-derived type 1 SMA myoblasts that were not subjected to denervation-induced muscle wasting displayed impairments in glycolysis and oxidative phosphorylation [161].

However, we cannot rule out exacerbation from progressive muscle wasting in SMA [315,316] since skeletal muscle insulin resistance and aberrant peripheral glucose uptake are also reported in related NMDs and myopathies like Duchenne muscular dystrophy (DMD) [317,318], myotonic dystrophy type 1 and 2 (MD1 and MD2) [319–321] and ALS [322,323].

Outside of skeletal muscle, another organ critical for whole body glucose metabolism is the pancreas [324]. This importance is best characterised in T1DM patients who develop insulin resistance by insufficient insulin production from pancreatic β-islet cells [325]. Interestingly, both SMA and T1DM share pathological pancreatic morphologies. Pancreatic biopsies from type 1 SMA patients and *Smn*$^{2B/-}$ mice displayed reduced insulin-producing β-islet cells and increased glucagon-producing α-islet cells in pre-symptomatic stages, which is reminiscent of the pancreatic pathophysiology in T1DM [301]. Furthermore, non-SMA *Smn*$^{+/-}$ mice (reminiscent of SMA carriers) with only 50% FL-Smn expression, were also found to have a pre-disposed risk of developing glucose metabolism and pancreatic defects in later life compared to wild type counterparts [310], suggesting that the SMN protein plays a crucial role in pancreatic development and function.

Altogether, these findings suggest a systemic dysfunction in glucose metabolism in SMA that shares similarities to other metabolic and muscle-wasting diseases.

1.3.3.2. Fatty acid (FA) metabolism

In a fasted state, FAs serve as another source for ATP production in skeletal muscle [326]. Normally, long-chain FAs(LC-FAs) are either taken up via passive diffusion across the sarcolemma or actively transported by FA binding protein (FABP), FA transport protein 1 (FATP1) and cluster of differentiation 36 (CD36) complex [327,328]. Once inside the myocyte, LC-FAs are converted into fatty acyl-CoA by Acyl-coenzyme A synthetase [329,330], followed by the acyl-CoA either serving as a substrate for lipid synthesis [331] or being converted into acyl-carnitine and transported into the mitochondrial matrix for β-oxidation via carnitine palmitoyltransferase 1 (CPT1) [332,333]. Aberrations in skeletal muscle FA metabolism are commonly observed in metabolic disorders, including diminished FA oxidation [334,335] and intramyocellular lipid accumulation [336,337], which ultimately can simultaneously exacerbate insulin resistance and impact glucose uptake (see section 1.3.3.1.).

Interestingly, case studies that span decades have reported FA metabolism aberrations across type 1-3 SMA patients that include elevated circulating short- and medium-chain FAs, carnitine deficiencies, dyslipidaemia, and dicarboxylic aciduria [303,338–340]. Furthermore, rigorous body composition analyses via the fatty mass index (FMI) method reported elevated adipose to lean muscle ratio in type 1-3 SMA patients, despite them being normal or underweight on a body mass index (BMI) scale [341]. In depth analysis of skeletal muscle biopsies from 5 patients diagnosed with type 1-3 SMA further supported FA metabolic dysfunctions as they showed reduced activity of enzymes important for FA β-oxidation (long-chain 3-hydroxyacyl-CoA dehydrogenase (LCHAD), short-chain 3-hydroxyacyl-CoA dehydrogenase (SCHAD), 3-ketothiolase) [342], whilst another

independent study reported reduced expression of acyl-CoA dehydrogenase [339]. Similar findings were also reported in the skeletal muscle of *Smn*$^{2B/-}$ SMA mice, where polymerase chain reaction (PCR) arrays revealed a dysregulation in FA metabolism genes [343]. Interestingly, a comparison between age-matched patients with a non-SMA neurodegenerative condition and type 1-3 SMA patients in a fasted state showed elevated levels of dodecanoic acid, a saturated 12-carbon chain medium-chain FA, specifically in the latter group, suggesting that juvenile FA impairments may be SMA-specific [340,344,345].

Outside of the muscular system, the liver plays a central role in FA metabolism and its dysfunction can lead to the development of non-alcoholic fatty liver disease (NAFLD) due to triglyceride over-accumulation [346,347]. Although NAFLD is commonly associated with obesity and metabolic disorders [347], hepatic fatty deposits reminiscent of the NAFLD phenotype have also been reported in both SMA patients and *Smn*$^{2B/-}$ mice [343]. Importantly, SMN restoration in *Smn*$^{2B/-}$ mice rescued this pathology, highlighting the role of SMN in both the liver and FA metabolism [348]. Additional studies provide support for the vital role of SMN in the liver. Indeed, one study specifically depleted FL-SMN levels in the liver of wild type C57BL/6J mice [349]. Remarkably, the liver-specific FL-SMN depletion led to late embryonic lethality caused by hepatic atrophy, dysfunction, iron overload and impaired regeneration [349]. In addition, the liver of pre-symptomatic *Smn*$^{-/-}$*;SMN2* SMA pups display reduced levels of *Insulin-like growth factor binding protein, acid labile subunit* (*Igfals)*, which encodes a serum protein important for the stabilisation of insulin-like growth factor 1 (Igf-1) [350,351]. With IGF-1 being vital for normal growth development and metabolism [352,353] and reports of reduced serum

IGF-1 levels in SMA patients [354], these studies support a crucial role for SMN in liver development and function [350].

Another non-neuromuscular site for FA metabolism is brown adipose tissue (BAT), which plays a functional thermogenesis role in infants to prevent hypothermia [355]. Recent investigations have revealed that BAT also show SMA-related abnormalities [356], although research is still ongoing to better understand the molecular mechanisms behind these abnormalities (Bowerman *et al*, *unpublished*).

Altogether, these findings across body composition, serum, skeletal muscle, liver and BAT highlight aberrant FA metabolism as a key pathology in SMA.

1.3.3.3. Protein metabolism

Protein metabolism is essential for regulation of skeletal muscle size with approximately 80% of muscle's dry weight being protein based [357]. Muscle size is modulated by anabolic pathways that promote protein synthesis and contribute to muscle hypertrophy and catabolic pathways that promote the breakdown of intramyocellular proteins that contribute to muscle atrophy [358]. Given that progressive muscle atrophy is a pathological hallmark of SMA [2,152–154], numerous studies have aimed to understand the pathways involved, not only to discover therapeutic targets, but also to explain the different severities across the SMA spectrum.

One study utilised a biased microarray approach to investigate if the canonical muscle growth IGF-1/PI3K/Akt regulatory pathway is dysfunctional in skeletal muscle biopsies of type 1 and 3 SMA patients [359,360]. Normally, IGF-1 signalling

leads to the activated mTOR kinase in the mTORC1 complex being phosphorylated and activated by Akt, which in turn activates via phosphorylation the downstream effectors S6K1 and 4E-BP1, ultimately promoting muscle growth [360–362]. Akt also represses Forkhead-box O (FOXO) transcription factors, which promote expression of auto-phagosomal and proteasomal degradation effectors that promote muscle atrophy [360,363–365]. In the above study, type 1 SMA muscle biopsies displayed consistent FOXO activation, indicative of progressive atrophy, whilst type 3 SMA muscle biopsies showed FOXO downregulation and mTOR upregulation, suggesting a co-existence of atrophic and hypertrophic muscle fibres that could account for the difference in muscle pathology between the different SMA types [359].

A latter study on severe *Smn*$^{-/-}$;*SMN2*$^{+/+}$ and milder *Smn*$^{2B/-}$ SMA mice further supported the idea of severity-dependent impairment of atrophy pathways [56]. Although atrophy in both models involved proteasomal degradation, as indicated by increased expression of E3-ubiquitin ligase atrogenes *atrogin-1* and *MuRF1* and increased presence of ubiquitinated proteins, the muscles from *Smn*$^{2B/-}$ SMA mice also specifically displayed increased autophagosomal protein breakdown [56]. Electron microscopy analyses confirmed this by demonstrating a marked increase of autophagic vacuoles in the TA muscle from *Smn*$^{2B/-}$ SMA mice [56]. Contrary to the previous study that presented *FOXO* overexpression in severe type 1 muscle only [359], this study reported it only in the milder *Smn*$^{2B/-}$ SMA mice, which may be attributed to the dual conserved roles of these transcription factors in activating genes involved in both proteasomal and autophagosomal degradation pathways [56,363,366]. However, the authors noted that the lack of *FoxO*

overexpression in the severe *Smn*$^{-/-}$;*SMN2*$^{+/+}$ SMA mice could be due to their shorter lifespan and may in fact become elevated if they lived longer [56].

With protein metabolism being an important factor in maintaining skeletal muscle health, further studies have investigated additional targets that regulate protein synthesis, proteasomal and auto-phagosomal pathways. One recent example is the glucocorticoid (GC)/ Krüppel-like factor 15 (Klf15)/branched chain amino acid (BCAA) pathway [53]. Klf15 is a Klf transcription factor involved in amino acid, lipid and glucose metabolism, that when activated can promote BCAA catabolism to decrease mTORC1 activity [367–370]. In addition, Klf15 can also transactivate atrogin-1 and MuRF1, creating a state of elevated atrophy [371]. In both *Smn*$^{-/-}$*;SMN2* and *Smn*$^{2B/-}$ SMA mice, a pattern of reduced *Klf15* expression in pre-symptomatic stages and elevated levels in post-symptomatic stages is observed, supporting this pathway's potential role in promoting muscle atrophy [53]. The evidence provided so far therefore highlights that protein metabolism plays a key role in regulating the severity of denervation-induced skeletal muscle atrophy across different SMA types.

1.3.3.4. Metabolism and circadian rhythms.

Despite the evidence of metabolic defects across muscular and non-neuromuscular tissues in SMA, the actual mechanism(s) of how intrinsic SMN depletion confers these dysfunctions remains ambiguous. One recent idea proposes that circadian pathways are a link between SMN depletion and metabolic defects in SMA.

Normally, the circadian rhythm is an autonomous system that controls molecular and physiological functions including metabolism over a 24-hour period within cells and tissues [372,373]. A major factor in synchronising its oscillatory pattern is the environmental diurnal light and dark phases over 24 hours [374], which influences sleep patterns, although other factors can include diet and temperature to name a few [372,373].

Circadian rhythmicity involves core transcription-translation feedback loops (TTFLs) composed of transcriptional activators CLOCK and BMAL1 [375], which promote the expression of repressor proteins period-1 (Per1), 2 and 3 and cryptochrome (Cry1) and 2, thus establishing a negative-feedback loop mechanism [376,377]. Importantly, intrinsic circadian oscillatory gene patterns govern metabolic and tissue-specific functions such as in skeletal muscle [378], adipose tissue [379], pancreas [380] and liver [381]. Furthermore, dysregulations within the reciprocal relationship between circadian rhythm and metabolism have been suggested to contribute to metabolic diseases [372,373].

In the case of SMA, both metabolic (see section 1.3.3.1-3) and circadian defects (e.g. abnormal sleep pattern influenced by light-dark exposure [382,383]) have been reported. Thus, one study aimed to evaluate if circadian dysregulation could contribute to SMA pathology. Interestingly, they identified aberrant expression of circadian rhythm core clock (*Clock*, *Bmal1*, *Cry1*/2 and *Per1/2*) and clock output (*Nr1d1* and *Dbp*) genes across skeletal muscle (TA), spinal cord, liver, heart, white adipose tissue (WAT) and BAT in *Smn*$^{-/-}$*;SMN2* SMA mice [356,384,385]. Furthermore, observations of the *Smn* gene revealed an age and tissue-dependent diurnal expression pattern suggesting a possible relationship between SMN activity, circadian rhythm and metabolic homeostasis [356].

Although this study has set the groundwork for establishing a link between SMN depletion, metabolic defects, and circadian rhythm in SMA, future studies are needed to increase our understanding of this model.

1.3.3.5. Mitochondrial biogenesis and function.

Mitochondria are often referred to as the “cell powerhouse” as they utilise glucose and FA molecules as fuel sources for energy (ATP) production [386]. In skeletal muscle, the abundance of mitochondria defines the fibre type and hence function, with oxidative slow-twitch type 1 and fast-twitch type 2a fibres containing more mitochondria than glycolytic fast-twitch type 2b muscle fibres [387].

Several studies in SMA have reported dysfunctional mitochondrial activity in neuronal and peripheral tissues [145,146,388–394]. In skeletal muscle, defects in mitochondrial biogenesis and functions have been reported in biopsies from both type 1-3 SMA patients and SMA mice [388–393]. These include aberrant morphology, increased mitochondrial swelling, reduced aerobic capacity, reduced dynamics, cytochrome-c oxidase deficiency, lower activity of electron transport chain complexes 1, 2 and 3 and reduced mitochondrial DNA (mtDNA) levels [129,388–393,395]. These pathologies can be attributed to the dysregulation of upstream molecular targets that normally govern mitochondrial biogenesis and function such as *peroxisome proliferator-activated receptor gamma coactivator 1-α* (*PGC1-α*), a master regulator of mitochondrial biogenesis [388,389,393]. Normally, PGC1-α targets downstream effectors *nuclear respiratory factor 1* (*NRF1*) and *NRF2*, which regulate the expression of genes that encode mitochondrial electron transport chain components and mtDNA transcription regulators [396–401].

Interestingly, *PGC1-α, NRF1*, *NRF2*, and *transcription factor A, mitochondrial* (*TFAM*) are downregulated in skeletal muscle of *Smn*$^{2B/-}$ SMA mice and muscle biopsies from SMA patients [388,389,393].

Furthermore, exercise studies in *Smn*$^{2B/-}$ SMA mice suggest that PGC1-α may also regulate SMN transcription via the AMP-activated protein kinase (AMPK)-p38- PGC1-α pathway, which may provide a link between intrinsic SMN depletion and mitochondrial activity [389]. Additional studies have also postulated potential functional roles for the SMN protein in mitochondrial regulation, which include mitochondrial trafficking via colocalisation with actin-related protein 2 (ARX-2) [394,402], mRNA trafficking of mitochondrial fusion proteins such as *Mitofusin2* via colocalisation with HuD [394,403,404] as well as regulating mitochondrial biogenesis and mitophagy via SMN-dependent Wnt/beta-catenin and UBA1-mediated pathways [114,394,394,405,406].

Thus, through these mechanisms SMN depletion could contribute to the mitochondrial pathologies observed in SMA skeletal muscle [388–393]. Although further research is required to understand the role of SMN in mitochondrial activity and how its depletion leads to the reported defects.

1.3.4. Cardiovascular system

Outside of the neuromuscular system, emerging research suggests that low SMN levels can contribute to cardiac pathologies. A systematic review that searched literature related to cardiac pathologies or abnormalities in type 1-3 SMA patients, identified an association between structural cardiac defects and severe SMA [407]. Indeed, type 1 SMA patients with a single *SMN2* gene copy frequently showed structural cardiac defects in the atrial septum, cardiac outflow tract, patent ductus arteriosus and ventricular septum regions that aligned with electrocardiogram (ECG) abnormalities such as bradycardias (heart rate less than 40 beats per minute (BPM)) [407]. Furthermore, congenital heart defects were also reported in type 0 SMA patients, which helped reinforce the link between structural cardiac abnormalities and severe SMA [408]. Although, structural cardiac abnormalities are not commonly associated with milder forms of SMA (type 2 and 3), patients have reported ECG baseline tremors (type 2: 100% and type 3: 54%) [407]. In addition, a minority of these patients also displayed cardiac defects such as impaired impulse initiation, and atrial and ventricular enlargement to name a few [407].

Investigations in severe SMA mice (*Smn*$^{-/-}$*;SMN2*$^{+/+}$ and *SMNΔ7*) have also reported structural and functional cardiac defects, including bradycardia, cardiac remodelling, ventricular and atrial defects, alongside reduced cardiac output, heart rate and stroke volume [409–413]. Interestingly, these were reported in both pre-symptomatic and symptomatic stages and improved after Smn restoration, indicating that SMN depletion plays an important role in cardiac development and function [412,413].

Although the role of SMN in cardiomyocytes is partially elusive, the SMN complex has been demonstrated to interact with α-actinin at the Z-disc in cardiac myofibrils [208], which are important for functional contraction, hypertrophy and mechano-transduction of the heart [414,415]. Furthermore, SMN depletion could indirectly impact the function of cardiomyocytes through downstream targets such as ubiquitin-like-modifier-activating enzyme 1 (UBA1), a ubiquitin protein involved in proteasomal degradation that is possibly mechanistically linked to the Lamin A/C protein [114,416]. Encoded by the *LMNA* gene, Lamin A/C governs nuclear stability, chromatin structure and gene expression and when dysregulated contributes to certain cardiomyopathies [417,418]. In SMA, Lamin A/C elevation has been inversely linked with decreased UBA1 expression in cardiac tissue, which is thought to contribute to impaired cardiac function and fibrosis via cardiomyocyte remodelling and impaired cytoskeletal contractile apparatus [416]. In addition, one case study reported a case of SMA with cardiac disease caused by a novel nonsense mutation (1057C>T) in the *LMNA* gene, further supporting its role in SMA cardiac pathology [419].

In addition to the cardiac muscle, vascular pathologies have also been reported in SMA such as vascular depletion [420,421], hypo-vascularity [420,421], poor perfusion [422], and capillary density reduction [423], highlighting the cardiovascular system as an important target of SMN depletion.

1.3.5. Respiratory system

Respiratory complications and diminished oxygen uptake are usually the common form of mortality in untreated type 1-2 SMA, which can be attributed to the weakened diaphragm and intercostal skeletal muscles [8,9,395]. However, lung biopsies from *Smn*$^{-/-}$*;SMN2* SMA mice showed dark red discolouration indicative of intrinsic pulmonary infarction due to a higher proportion of blood clots [424]. Nevertheless, this was only one study in SMA mice and further research is therefore needed to better understand the role of SMN in the lungs.

1.3.6. Immune system

Intriguingly, discoveries in SMA mice have identified defects in lymphoid organs involved in immunity [425–428]. The spleen, which participates in blood filtration and the immune response [429], displays abnormalities across mild to severe SMA mice (*Smn*$^{2B/-}$*, SMNΔ7* and *Smn*$^{-/-}$*;SMN2*) [426–428]. Morphologically, these mice had a reduced spleen size and weight compared to their respective healthy counterparts, in both pre-symptomatic and symptomatic stages [426]. Although decreased proliferation and elevated apoptosis in late symptomatic stages was thought as the main contributor to the reduced spleen size in *Smn*$^{-/-}$*;SMN2* SMA mice [428], it is still unclear what is responsible for its reduced size in other models [425]. In addition, the red pulp region, which is important for blood filtration, displayed decreased distribution and composition alongside increased megakaryocyte presence in the spleen of SMA mice [426,428,429]. On the other hand, the white pulp region, which is important for lymphocyte storage, was nearly absent, whilst B-lymphocyte concentration was increased, thus presenting

evidence for dysfunctional immunity [426–429]. Although these studies were only performed in pre-clinical models, preliminary analysis of biopsies from infantile type 1 SMA patients also confirmed the presence of spleen abnormalities [428].

Conversely, the thymus, a primary lymphoid organ important for adaptive immunity, did not display gross morphological abnormalities [427,430]. However, in-depth histological investigation in the thymus from *Smn*$^{-/-}$*;SMN2* and *Smn*$^{2B/-}$ SMA mice revealed cortex thinning, increased apoptotic activity and abnormal T-cell development at late symptomatic stages, which also can exacerbate immune dysfunction since the thymus is important for T-cell maturation [427,430].

Despite the evidence of lymphatic organ abnormalities and immune dysfunction, as evidenced by heightened neuroinflammation and pathogenic pulmonary susceptibility in SMA patients, how SMN contributes to the immune system is still unclear [425,431]. However, higher expression of Smn in the spleen and thymus in comparison to the CNS in *Smn*$^{2B/-}$ SMA mice suggests that this protein's role is vitally important in these tissues [427]. As above, restoration of SMN expression in *Smn*$^{-/-}$*;SMN2* and *Smn*$^{2B/-}$ mice rescued spleen abnormalities [426,427], suggesting that the SMN protein plays a crucial role in the immune system.

1.3.7. Other organs and tissues affected in SMA

Although only a few non-neuromuscular peripheral systems have been described herein, SMN depletion has also contributed to pathologies in other organs and systems. These include the skeletal system, with reported impaired bone development and low mineral density, which was recently associated with intrinsic abnormalities in cell division and cartilage remodelling [432,433]. Another affected organ is the kidney as renal pathologies have been reported in both *Smn*$^{-/-}$*;SMN2* mice and type 1 SMA patients [434,435]. Furthermore, sex-specific Smn-dependent differences have also been identified, with impaired testis development and low fertility occurring with mild *Smn*$^{C/C}$ SMA mice [105].

Overall, the selected examples of non-neuronal pathologies (Figure 1.4) show the importance of viewing SMA as a systemic disease and highlight the ubiquitous role that SMN plays in development. Furthermore, it also supports the need to take non-neuromuscular organs into consideration when treating SMA.

1.4. Treatment strategies in SMA.

1.4.1. SMN-dependent therapies

Prior to 2016, the only available therapy options for SMA patients were palliative care for complications stemming from progressive muscle loss, motor dysfunction and weakened respiratory functions [436–438]. Being a monogenic disorder with an identified gene target, several investigations into SMA treatment options focused on restoring FL-SMN protein levels to combat progressive motor neuron degeneration and peripheral pathologies [439,440]. These therapies, which are classed as SMN-dependent have since marked a new era in the SMA therapeutic field, with three of these treatments now clinically approved by the Food and Drug Administration (FDA) and European Medicines Agency (EMA) (Figure 1.7).

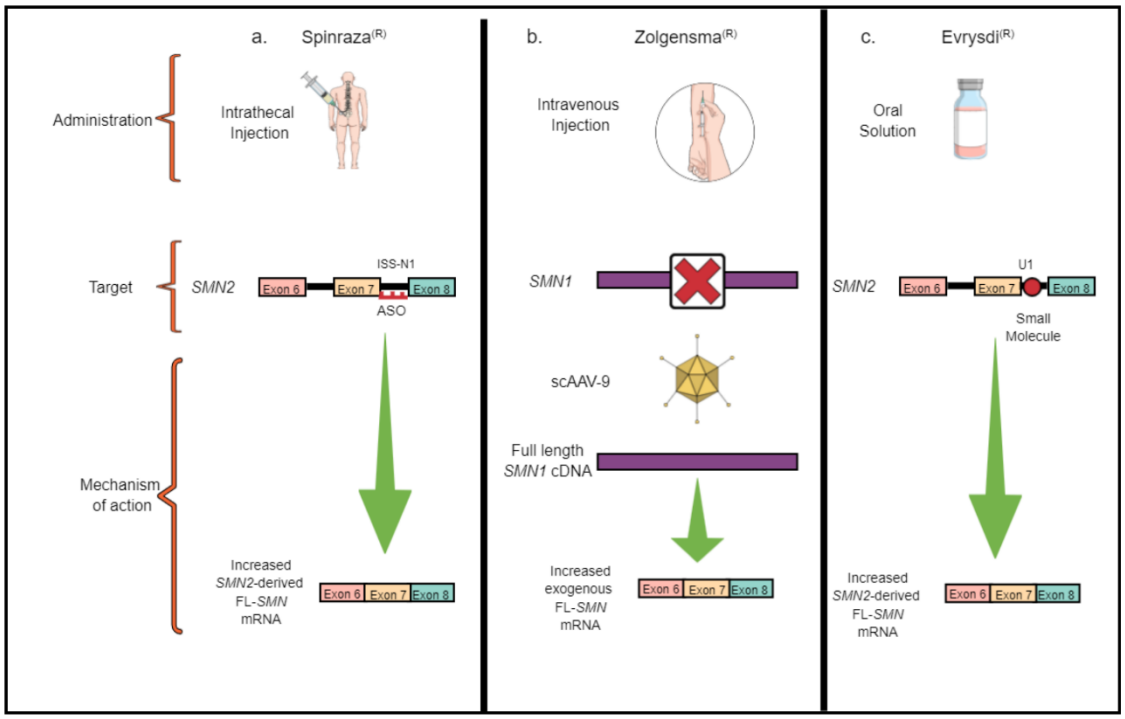

Figure 1.7. Mechanisms of action of SMN-dependent therapies for SMA.

a. Spinraza(R): A 22-nucleotide length antisense oligonucleotide (ASO) that is intrathecally injected into SMA patients and binds to the intronic splicing silencer N1 (ISS-N1) region between exon 7 and 8 in *SMN2* to promote exon 7 inclusion and increase expression of full length (FL)-*SMN* mRNA transcripts.

b. Zolgensma(R): A self-complementary adeno-associated virus 9 (sc-AAV9) that contains a FL-*SMN1* complementary DNA (cDNA) that is intravenously injected into SMA patients to exogenously restore the intrinsic *SMN1* LOF.

c. Evrysdi(R): A small molecule that is orally administered to SMA patients to enhance U1 pre-mRNA associated exon 7 inclusion in *SMN2*, which promotes expression of FL-*SMN* mRNA transcripts.

The figure and textual references are adapted from Ojala *et al* (2021) In search of a cure: The development of therapeutics to alter the progression of spinal muscular atrophy. *Brain Sciences*, 11, 194. Figure was created on Mind the Graph.

1.4.1.1. Spinraza®

As previously described in section 1.1.2., humans are fortunate that *SMN2* CNV enables a minor compensatory production of FL-SMN albeit with a reduced efficiency (10% FL-SMN: 90% SMNΔ7) [31,32,35]. This ability of the *SMN2* gene to modify SMA severity [41] (Table 1.1), laid the groundwork for an SMN-dependent treatment strategy aimed at modulating *SMN2* splicing to promote expression of endogenous FL-SMN levels, thus compensating for the absent production in LOF *SMN1* alleles [31,32,35,40,441].

Initial preclinical screenings in SMA mice possessing transgenic *SMN2* genes (*Smn$^{-/-}$, hSMN2$^{+/+}$, SMNΔ7$^{+/+}$* & *Smn$^{-/-}$;SMN2*) supported a therapeutic *SMN2* targeting mechanism by anti-sense oligonucleotides (ASOs) [350,441–445], which are synthetic single-stranded oligodeoxynucleotide sequences that hybridise to target RNA, affecting transcriptional and translational regulation [446]. Indeed, the ASO that targeted *SMN2* intronic splicing silencer N1 (ISS-N1) was eventually developed into Spinraza® (or Nusinersen) as it increased FL-SMN expression and improved survival and disease phenotype in SMA mice [350,441–445] (Figure 1.7.a). Designed as a 2'O-methoxyethyl backbone ASO with a complementary 22-nt ISS-N1 motif sequence [447,448], Spinraza's® > 400 Da size prevents its ability to pass through the blood-brain-barrier (BBB) [449,450]. Thus, neuronal delivery of Spinraza® in SMA patients requires single intrathecal injections (12 mg/5 ml recommended dosage) [451–453] (Figure 1.7.a). Based on results from open-label phase 1 trials in type 2-3 SMA patients [452] (ClinicalTrials.gov ID: NCT01494701) and phase 2 open-label, escalating dose trials in infantile-onset type 1 SMA patients [451] (ClinicalTrials.gov ID: NCT01839656) the first three initial doses are

delivered at 14-day intervals, followed by a 4th 30 days after [453]. Subsequent maintenance doses are then administered for every 4 months [453].

Thus far, phase 3 clinical trials for Spinraza® have been undertaken in type 1 SMA patients (Age: <7 months, non-respiratory support, *SMN2* CNV: 2, ENDEAR (ClinicalTrials.gov ID: NCT02193074) [454]) and later onset type 2 and 3 SMA patients (Age: 2 – 14 years, *SMN2* CNV: 3-5, and no history of serious hospitalisation, CHERISH (ClinicalTrials.gov ID: NCT02292537) [455]). Although a 47% survival rate was reported in type 1 infants [454], both studies reported significant functional improvements with 51% of surviving type 1 patients achieving the developmental milestone of sitting upright [454] and 57% of type 2-3 patients improving their motor function score [455]. Currently, two ongoing clinical trials are focusing on pre-symptomatic (NURTURE, ClinicalTrials.gov ID: NCT02386553) and adult SMA patients (SAS, ClinicalTrials.gov ID: NCT03709784), with NURTURE interim results reporting that developmental milestones have been reached by treated SMA patients [456]. However, the SAS clinical trial has reported reductions in general strength and motor function in treated SMA adult patients, suggesting that optimised doses for different treatment durations and ages may be required [457].

Although Spinraza's® approval marked a new era in SMA, its use is not without challenges and limitations. Firstly, intrathecal administration is an invasive procedure that requires trained staff, equipment and anaesthetics, thus creating a burden for younger patients alongside access difficulties for those from lower socio-economic backgrounds [458,459]. In addition, intrathecal administration can be even more difficult in cases of scoliosis, which commonly occur in SMA patients [460–462]. Another issue is that intrathecal administration limits systemic distribution

to peripheral tissues, which impacts Spinraza's® efficacy via poor BBB penetrance as pre-clinical studies have shown that systemic SMN restoration greatly improved survival and disease phenotype in SMA mice compared to SMN restoration in the CNS alone [350]. Finally, the annual treatment costs of around $750,000 could potentially limit accessibility to patients from lower socio-economic backgrounds and create approval restrictions across various countries [459].

1.4.1.2. Zolgensma®

In 2018, the second SMN-dependent therapy approved was Zolgensma® (or Onasemnogene abeparvovec-xioi or AVXS-101), a one-time intravenously administered gene replacement therapy that consists of a self-complementary adeno-associated virus serotype 9 (scAAV-9) vector, which contains a human FL-*SMN*1 complementary DNA (cDNA) sequence expressed by a chicken β-actin promoter that exogenously restores FL-SMN levels [463–466] (Figure 1.7.b). A natural advantage of Zolgensma® is scAAV9's ability to cross the BBB, which allows for less invasive injection methods (intravenous) that can systemically reach neuronal and peripheral tissues [467]. This was supported by pre-clinical studies reporting that SMA mice receiving intravenous injections of scAAV9-*SMN1* displayed improved survival and motor function as well as attenuated neuromuscular pathologies, which was associated with the increased SMN levels in both neuronal and peripheral tissues [464,468,469] (Figure 1.7.b).

As a result of the pre-clinical success, an initial phase 1 clinical trial was conducted in 15 type 1 SMA patients (START, ClinicalTrials.gov ID:

NCT02122952) who received either low ($6.7x10^{13}$ vg per kg of body weight) or high doses ($2.0x10^{14}$ vg per kg of bodyweight) of Zolgensma® [470]. Two years post-treatment, a 100% survival rate was reported, whereby 11 patients achieved the ability to sit unassisted and 2 patients walked independently [463,470,471]. Furthermore, a pattern emerged showing that earlier treatment (< 3 months old) was associated with a more rapid achievement of motor milestones [471]. START phase 1 patients have now been transferred to a follow up study aimed at evaluating the long-term efficacy of Zolgensma® (15 years post-treatment, ClinicalTrials.gov ID: NCT03421977). As of 2021, a published 5-year follow up study reported no regression in improved motor function abilities, no deaths and no requirements for permanent mechanical ventilation [472].

Based on this initial success, further Zolgensma® clinical trials have now started, including an open-label, single-arm phase 3 trial (STR1VE) in both the US (ClinicalTrials.gov ID: NCT03306277) and Europe (ClinicalTrials.gov ID: NCT03461289), with interim results showing a 90.9% survival rate without permanent ventilation at 18 months of age and 59.1% of patients reaching independent milestones [473,474]. Furthermore, an open-label, single-arm phase 3 trial termed SPR1NT (ClinicalTrials.gov ID: NCT03505099) is focusing on pre-symptomatic SMA infants (< 6 weeks age and 2-4 *SMN2* CNV), with interim results similar to those reported in parallel studies (START and STR1VE) [475]. With Zolgensma® being only clinically approved for type 1 SMA patients, a new study has begun in type 2 SMA patients (STRONG, ClinicalTrials.gov ID: NCT03381729), which uses intrathecal injections instead of intravenous. However, as of 2021, the STRONG clinical trial has been put on hold due to unpublished pre-clinical findings by Avexis that identified the development of

inflammation and sometimes neurodegeneration in the dorsal root ganglia of primate models intrathecally administered with Zolgensma [476].

Despite the preliminary success observed in type 1 SMA patients, limitations of Zolgensma® have also been identified. From an experimental design point of view, START, STR1VE and SPR1NT focused on a small sample size and reported Zolgensma® as only being effective in type 1 SMA patients who received treatment at earlier symptomatic timepoints [463,470,471,473–475]. Thus, with a small cohort treated at earlier disease stages, it is too early to conclude Zolgensma's® efficacy at later time-point administration or in elder patients, such as those with type 2-4 SMA. Moreover, the short timeline of 5 years (so far) for the evaluation of Zolgensma® treatment in type 1 SMA patients creates uncertainty around this therapy's long-term effects. Already, short-term adverse effects have been reported such as serious liver complications that required GC treatment to attenuate elevated serum aminotransferase levels and thrombotic microangiopathy [470,477,477,478]. Furthermore, the 5 year follow up START study has reported long-term side effects such as acute respiratory failure independent of weakened diaphragmatic and intercostal muscle in 62% of treated patients [472]. In addition, a more recent pre-clinical study provides evidence suggesting that long-term scAAV9-mediated SMN overexpression counterintuitively exacerbates motor dysfunction via the formation of toxic gain-of-function (GOF) protein aggregates that promote neurodegeneration, neuroinflammation and widespread transcriptome splicing dysregulations [479]. There is also potential uncertainty of long-term efficacy with the risks of anti-AAV antibodies rejecting the treatment [480]. Finally, although Zolgensma® is a single-dose treatment, as of 2021 it is still the

world's most expensive drug, limiting its availability for patients from lower socioeconomic backgrounds and regulatory bodies in different countries [481].

1.4.1.3. Evrysdi®

The most recently approved SMN-dependent therapy (2020) was Evrysdi® (Risdiplam), which belongs to a class of pyrido-pyrimidinone small molecules that modulate alternative splicing of *SMN2* to promote FL-SMN expression [482–484] (Figure 1.7.c). Compared to Spinraza® and Zolgensma®, Evrysdi® holds a dual advantage of oral bioavailability and BBB penetrability, providing a non-invasive treatment option that can be administered daily in patients and allows for systemic distribution to elevate FL-SMN levels in neuronal and peripheral tissues [482–484] (Figure 1.7.c).

The development of Evrysdi® began with the preliminary success of pyridopyrimidine compounds that promoted FL-*SMN2* expression in SMA fibroblasts and iPSCs and improved survival and disease phenotypes in *SMNΔ7* SMA mice [485]. However, initial phase clinical 1 trials for the first pyridopyrimidine derivative RG7800 (MOONFISH, ClinicalTrials.gov ID: NCT02240355) was terminated due to pre-clinical reports of genotoxic adverse effects in cynomolgus monkeys and *SMNΔ7* SMA mice [485–488]. Instead, Roche developed Evrysdi®, which improved systemic FL-*SMN2* expression and reduced genotoxic risks in *SMNΔ7* SMA mice compared to its predecessor [484,488].

Later on, phase 1 clinical trials (ClinicalTrials.gov ID: NCT02633709) in healthy males supported the evidence for increased FL-*SMN2* expression and no adverse risks [489]. Subsequent, phase 2/3 clinical trials in symptomatic type 1

(FIREFISH, ClinicalTrials.gov ID: NCT02913482) [490,491] and type 2-3 SMA patients (SUNFISH, ClinicalTrials.gov ID: NCT02908685) [492,493] have so far been promising. Indeed, type 1 patients that received doses of 0.2 mg/kg/day demonstrated improved motor function, the ability to independently sit upright and survival rates of 85% [490,491].

Similarly, the type 2 and 3 patients displayed improved motor function 24 months after initial treatment [492,493]. In addition to these two studies, another ongoing clinical trial is JEWELFISH (ClinicalTrials.gov ID: NCT03032172), which aims to evaluate Evrysdi® in type 1-3 SMA patients previously enrolled in MOONFISH or previously treated with Spinraza® and Zolgensma®. Furthermore, a new study currently in recruitment (RAINBOWFISH, ClinicalTrials.gov ID: NCT03779334) aims to evaluate the efficacy of Evrysdi® in pre-symptomatic type 1 SMA patients aged up to 6 weeks.

Although, the therapeutic potential of Evrysdi® is promising, there are certain challenges that still need to be addressed. From a pharmacodynamics perspective, the exact mechanism of how Evrysdi® promotes *SMN2* exon 7 inclusion is still not yet fully understood [483]. Mechanistic studies with the precursory SMN-C3 pyridopyrimidine analog have associated recruitment of splicing factors FUBP1 and KHSRP to the central AC-rich motif in exon 7 as a mechanism for exon 7 inclusion [494] (Figure 1.7.c). However, considering the structural modifications in Evrysdi®, the mechanism of action could be different [483,488]. Importantly, higher concentrations of the drug have produced off-target splicing events in the *STRN3*, *FOXM1*, *APLP2*, *MADD* and *SLC25A17* genes suggesting a common splicing factor [483,488].

Another consideration with Evrysdi® is that long-term suitability has yet to be fully investigated and adverse effects have already been reported in patients, including fever, joint pain, urinary tract infections, upper respiratory tract infections and pneumonia [483]. Finally, although Evrysdi® is marketed at $340,000 per annum (based on 20 kg patients), making it a less expensive option than its competitors Spinraza® and Zolgensma®, it still comes at a high price that could limit its access [495].

1.4.2. Current skeletal muscle specific SMN-independent therapies for combinatorial treatments

1.4.2.1. Combinatorial therapies for SMA.

Despite the significant lifesaving effects of Spinraza®, Zolgensma® or Evrysdi®, (see section 1.4.1), these SMN-dependent therapies are unfortunately not a cure. Indeed, although pre-clinical and clinical studies have demonstrated significantly reduced disease severities and death rates, none have reported a 100% efficacy rate [441,451,454,456,463,464,470,475,488–490,493], with maximal therapeutic benefits associated with earlier intervention in pre-symptomatic and symptomatic onset stages [496,497]. In the absence of new-born screening, this creates issues for older type 1 and 2 SMA patients who have surpassed these stages and for type 3 and 4 patients who usually receive a diagnosis after symptomatic onset [8,10,13–15,498–500].

Furthermore, for treated SMA patients, these are unprecedented times as the delay in disease onset and/or progression has allowed them to surpass their natural disease progression and for type 1 patients, their life expectancy [8,14], allowing for an uncharted era where novel or incompletely rescued pathologies may begin to manifest. Thus, a combinatorial therapeutic approach that uses established primary SMN-dependent therapies alongside secondary SMN-independent therapies that target tissue-specific pathologies could synergistically benefit SMA patients [501].

Although motor neurons are a suitable target for both SMN-dependent and -independent therapies, peripheral tissue targets are also required, as pre-clinical studies have highlighted that systemic treatments had a greater therapeutic

impact than CNS treatments alone [77,350]. A major non-neuronal target for consideration is skeletal muscle as atrophy and muscle fatigability are hallmarks of SMA [1,3,55]. In addition, we have previously discussed the numerous skeletal muscle defects detected in SMA patients and pre-clinical models (*in vivo* and *in vitro*) that are attributed to both intrinsic SMN depletion and/or denervation and overlap with non-related NMDs and myopathic disorders such as ALS, MG and DMD (see section 1.3).

Thus, skeletal muscle-specific treatments would be a great addition to synergistically improve skeletal muscle pathologies in SMA. Indeed, there are ongoing clinical trials for evaluating the effectiveness of two novel skeletal muscle treatments in SMA (Figure 1.8).

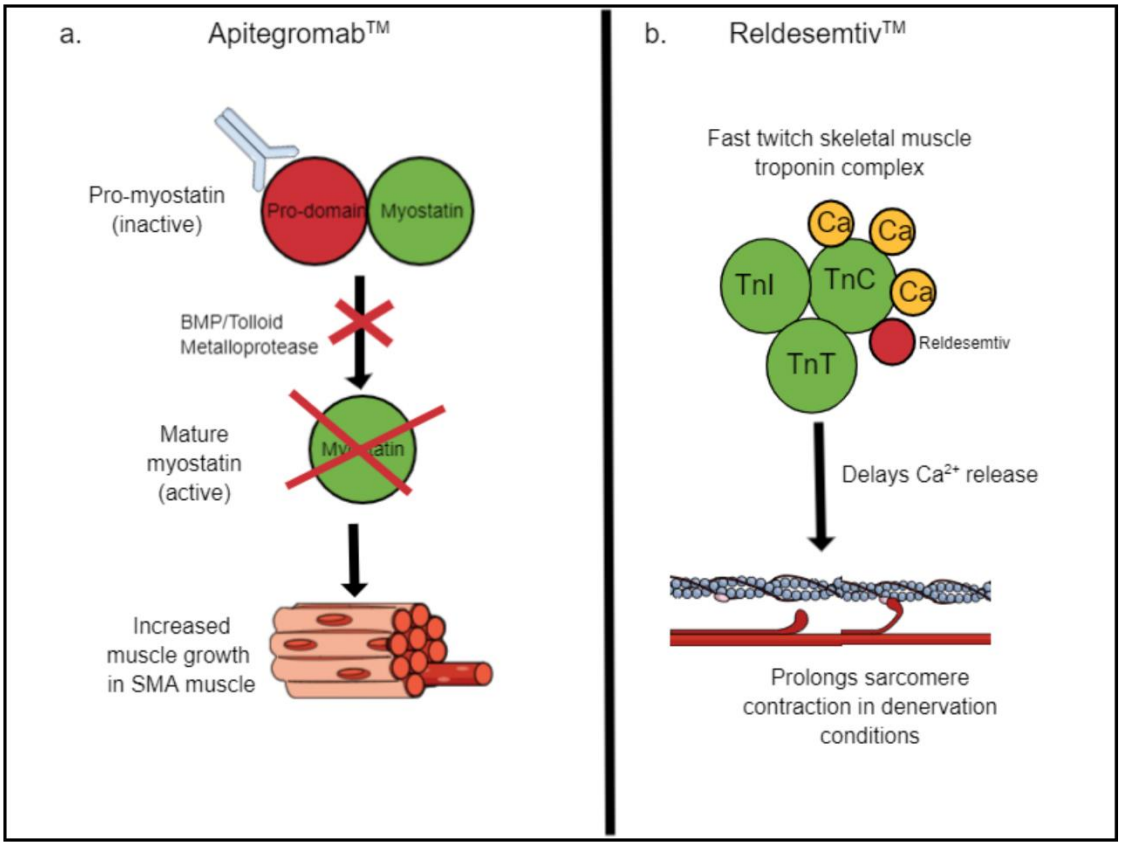

Figure 1.8. Mechanisms of action of Apitegromab™ and Reldesemtiv™ in SMA skeletal muscle.
a. Apitegromab™ is an anti-pro-myostatin antibody that prevents pro-domain cleavage by BMP/Tolloid metalloproteases in pro-myostatin to prevent activation of mature myostatin. The reduced myostatin activity in SMA skeletal muscle allows for increased muscle growth.
b. Reldesemtiv™ binds to troponin C (TnC) of the troponin complex (TnI, TnC, TnT) in fast-twitch skeletal muscle to delay the rate of Ca^{2+} release (yellow circles). This delay prolongs the troponin complexes' activity to increase sarcomere contraction in denervated skeletal muscle, which reduces muscle fatigue in SMA.
Figure was created on Mind the Graph.

1.4.2.2. Apitegromab™ (SRK-015)

Apitegromab™ (SRK-015) is a novel monoclonal anti-myostatin antibody developed by Scholar Rock, which has been designed to improve muscle strength and growth in SMA patients as a complementary SMN-independent therapy [502–504] (Figure 1.8.a). Myostatin is a myokine member of the TGFβ superfamily, which plays a critical role in the negative regulation of skeletal muscle mass [504–506]. Myostatin is initially secreted as a full length inactive pro-myostatin precursor that undergoes two subsequent proteolytic cleavage steps, first by a proprotein convertase, second by BMP/tolloid metalloprotease, producing the active mature myostatin [507–510]. The active myostatin binds to the activin receptor type 2 B (Act2RB) or (Act2RA) and activates ALK4 and 5, resulting in phosphorylation of cytosolic Smad2 and 3, which recruits Smad4 to form the Smad2/3/4 complex, a transcription factor that translocates to the nucleus and promotes expression of atrophy-related genes and downregulation of muscle maintenance components [507,511–517]. Furthermore, active myostatin/activin dephosphorylates the Akt-FoxO pathway, promoting upregulation of ubiquitin-proteasome activity [514,515].

The suitability of myostatin as a therapeutic target in muscle-wasting conditions is evidenced by its upregulation in skeletal muscle of individuals with cachexia [514,518], sepsis [519], DMD [520], LGMD [521,522], ALS [523,524], sarcopenia [525,526], and DM [527]. Furthermore, its complete inactivation seems to confer little adverse effects based on examples of animals and humans born with myostatin LOF mutations that displayed excessive hypertrophic growth with minimal medical complications [528–530].

Previous pre-clinical studies of myostatin inhibition in SMA [531–533] and other muscle-wasting conditions [534–536] have revealed limitations of non-negligible off-target effects as the active myostatin and its downstream components share high homology with other TGFβ members [536–538]. Apitegromab™ was developed to overcome this limitation as it binds to the pro-domain of pro-myostatin and inhibits BMP/tolloid metalloprotease proteolysis [502,503] (Figure 1.8.a). The low homology of the pro-domain to other TGFβ proteins thus minimises off-target effects [502,539–541]. Indeed, the pre-clinical safety assessments reported that Apitegromab™ did not exhibit any adverse effects previously observed with other myostatin inhibitors [542]. However, in terms of treatment efficacy it was found that Apitegromab™ alone did not improve muscle phenotype in *SMNΔ7* SMA mice [502]. Instead, combination with SMN-dependent therapies was required to achieve improved muscle growth [502]. This was later attributed to the discovery that endogenous myostatin levels were actually lower in untreated SMA patients and counterintuitively were only elevated after SMN replacement [502,543]. Thus, Apitegromab™ must rely on SMN replacement therapy for maximal efficacy (Figure 1.8.a).

Currently, Apitegromab™ is being evaluated in a phase 2 clinical trial (TOPAZ, ClinicalTrials.gov ID: NCT03921528) in type 2 and 3 SMA patients, whereby it is delivered via intravenous injections every 4 weeks, following a successful phase 1 study in healthy young males receiving up to 30 mg/kg doses [544]. Although finalised results will not be published until 2023, the interim TOPAZ results report no adverse effects in all patients and those in the higher dose tier display greater functional improvements after 6 months of treatment [545].

1.4.2.3. Reldesemtiv™ (CK-2127107)

Another SMN-independent skeletal muscle therapy currently in clinical trials is Reldesemtiv™ (CK-2127107), a fast-skeletal muscle troponin activator (FSTA) [546,547] (Figure 1.8.b). In striated muscle, the sarcomeric-associated troponin complex is necessary for sarcomere contraction [548–550]. However, in skeletal muscle, troponin complex isoforms are fibre type specific to cope with the different metabolic, energy and innervation requirements for contraction [551–556].

In fast-twitch skeletal muscle, troponin subunits C (*TNNC2*), T (*TNNT3*) and I (*TNNI2*) are bound to tropomyosin within the thin actin filaments of the sarcomere [553–559]. The troponin complex then regulates contraction through the binding of Ca^{2+} to the 4 Ca^{2+} binding sites of troponin C, which induces a conformational change that facilitates actin-myosin binding [550,556,560–567]. Normally, this activity is dependent upon motor neuron activity as contractile force is proportional to innervation intensity [567]. However, in SMA, the denervation of muscle and reported reduced expression of Ca^{2+}-releasing receptors limit troponin activity and as a result, weaken the contractile force and endurance of fast-twitch skeletal muscles [55,260,568].

To compensate for lower intracellular Ca^{2+} levels across various NMDs, FSTAs were designed to specifically delay the rate of Ca^{2+} release from troponin C and promote maximum sarcomere contractions, as evidenced by muscle strength improvements in ALS and MG murine models after treatment [569–571] (Figure 1.8.b). Reldesemtiv™ on the other hand, was originally assessed in rat models for heart failure [546]. However, reports of improved endurance and contraction in plantaris and soleus muscles supported its potential repositioning in NMDs like

SMA [546]. When Reldesemtiv™ was evaluated in phase 1 clinical trials, the safety, tolerability and increased contractile force in healthy young and elderly adult volunteers [547] led to approval for a phase 2 trial in SMA type 2-4 patients (ClinicalTrials.gov ID: NCT02644668). In 2021, the finalised results were published and demonstrated that both 150 and 450 mg doses improved maximum expiratory pressure (MEP) in SMA patients, suggesting improved respiratory function from the contractile diaphragm and intercostal muscles [572]. Furthermore, the 450 mg treatment alone significantly improved the 6-minute walking distance performance, supporting its promising potential for improving endurance and approval for a phase 3 trial [572].

Although, both Apitegromab™ and Reldesemtiv™ are still in ongoing clinical trials, their preliminary results are promising and highlight the exciting endeavour of combining SMN-dependent therapies with skeletal muscle treatments. However, the fact that there have been limited clinical trials for skeletal muscle treatments in SMA indicate that future directions should be focused on identifying additional muscle treatments and targets.

1.4.3. Drug repositioning for the development of combinatorial treatments for SMA.

1.4.3.1. Drug repositioning

The overt reliance of traditional drug discovery in rare diseases like SMA can often leave gaps in treatment availability. Typically, the traditional drug discovery timeline starts with compound identification, followed by pre-clinical studies and ends with clinical approval and marketing, which can last up to 20 years [573,574]. Although schemes like the Orphan Drug Act (USA) and Orphan Drug Designation Programme (Europe) have reduced the drug development timeline and costs for novel rare disease treatments [575–577], there are still limitations to traditional drug discovery. The main one being that this approach comes with a high likelihood of failure, with the probability of success only being around 2-14% [578–580]. In the SMA field, such reported failures were R06885247 (ClinicalTrials.gov ID: NCT02240355), an oral small molecule *SMN2* modulator, and Olesoxime (TRO19622), a cholesterol-oxime that preserves mitochondrial function to maintain motor neuron integrity [581] ((ClinicalTrials.gov ID: NCT01302600) [582] (ClinicalTrials.gov ID: NCT02628743) [583]). Furthermore, the high research and development (R&D) costs of around $12 billion and laborious work associated with traditional drug discovery can often lead to approved treatments being expensively marketed [573,584–586]. Indeed, the pricing of the approved SMN-dependent treatments reflect this as the estimated costs are between $340,000 to $1.8 million depending on the drug type administered [495]. Importantly, the development of novel non-regulated complementary SMN-independent treatments would elevate these costs, further exacerbating the accessibility issues discussed earlier (see section 1.4.1).

To overcome these limitations, an alternative approach is drug repositioning (or repurposing), a strategy aimed at finding new therapeutic roles for existing pharmacological compounds [587]. Drug repositioning provides numerous advantages over traditional discovery that can be beneficial for novel SMA treatments [586,588,589]. A primary benefit is that repositioned pharmacological compounds often have readily available data obtained from pre-clinical and phase 1 studies that include pharmacological activity, toxicity, clinical efficacy, dosage requirements and adverse effects [586,590]. With 90% of traditional drug discovery failures being linked to phase 1 clinical trials, repositioned compounds can often be allowed to skip this stage and directly enter phase 2 trials instead [579,591,592]. Not only does this reduce the development timeline to 3-12 years, it also minimises the R&D and clinical trial costs by 50-60% [586,590,593]. Consequently, in SMA, this could open up opportunities for more cost-effective treatment options.

1.4.3.2. Drug repositioning for SMN-dependent therapies

The pan-ethnic incidence rates of SMA highlights the presence of this disorder across various countries of differing socio-economic background [16–18]. Consequently, this can limit the availability of Spinraza®, Zolgensma®, and Evrysdi® treatments to all patients. However, both, *in vitro* and *in vivo* chemical screens of generic compounds have serendipitously revealed repositioned candidates with the ability to modulate *SMN2* splicing to promote FL-SMN expression [588].

One class of drugs associated with elevated FL-SMN levels are histone deacetylase inhibitors (HDACi) [594]. Compared to the splicing modulation observed with Spinraza® and Evrysdi®, HDACi promote enhanced *SMN2* transcription and exon 7 inclusion by relaxing and opening the euchromatin structure around acetylated histones that facilitates the recruitment of transcriptional machinery [595,596]. Indeed, *in vitro* studies of HDACi including sodium butyrate [597], sodium phenylbutyrate [598], valproic acid [599–601], suberoylanilide hydroxamic acid [602] and trichostatin A [603], confirmed increased FL-*SMN2* levels following exposure to the drugs. Furthermore, studies of HDACi in SMA mice showed improved neuromuscular phenotype and median survival [51,599,602–606].

Nevertheless, the clinical trial history of HDACi in SMA presents a different story. Both sodium phenylbutyrate [607] and valproic acid [608–612] reported no clinical benefits, no significant upregulation of FL-*SMN2* and adverse side-effects. As a result, planned phase 2/3 clinical trials NPTUNE01 (ClinicalTrials.gov ID: NCT00439569) and NPTUNE02 (ClinicalTrials.gov ID: NCT00439218) were eventually cancelled. Despite these failures, there are renewed interests in HDACi as complementary therapies alongside Spinraza®, since dual treatment synergistically enhanced transcription of *SMN2* exon 7 inclusion in SMA fibroblasts and improved disease phenotypes in SMA mice [501,613].

Another clinically-approved drug linked with increased FL-*SMN2* expression is celecoxib, a non-steroidal, anti-inflammatory cyclooxygenase-2 (COX-2) inhibitor that is primarily used to treat rheumatoid- and osteo-arthritis [614]. Pre-clinical studies demonstrated that celecoxib increased and stabilised FL-*SMN2* mRNA levels via p38 pathway activation, which resulted in improved neuromuscular

phenotype and significantly extended the median survival in *SMNΔ7* SMA mice [615]. Furthermore, the BBB penetrability and oral bioavailability of celecoxib allowed for systemic distribution [615]. Despite these pre-clinical benefits, an approved phase 2, open-label, dose-respondent (40, 80 and 160 mcg/kg) trial (ClinicalTrials.gov ID: NCT02876094) in type 2 and 3 SMA patients was eventually terminated as of 2020 for yet to be revealed reasons. Although these drug repositioning studies have so far proved unsuccessful on the SMN-dependent treatment front, further chemical screens have the potential to identify a myriad of different generic compounds that could help promote and stabilise FL-*SMN2* levels.

1.4.3.3. Drug repositioning for SMN-independent skeletal muscle therapies

The absence of approved SMN-independent skeletal muscle therapies in SMA emphasises the need for their swift discovery and approval. Even though Apitegromab™ and Reldesemtiv™ are showing progress in phase 2 clinical trials [545,572], the high R&D costs and traditional drug discovery routes may lead to elevated prices [586], widening the accessibility gap for SMA patients. Although drug repositioning clinical trials aimed at targeting skeletal muscle pathologies specifically in SMA patients are scarce [588,589], evidence of their use in NMDs and myopathies with related pathologies support their potential for SMA treatment [589]. Unfortunately, most research supporting drug repositioning for novel SMA skeletal muscle treatments remains at the pre-clinical level [589].

One example is tideglusib, a small heterocyclic thiadiazolidine based non-ATP competitive inhibitor of glycogen synthase kinase 3 beta (GSK-3β), which failed

to improve cognitive impairments in a phase 2 clinical trial for Alzheimer's disease (AD) patients (ClinicalTrials.gov ID: NCT01350362) [616–618]. Although initially investigated in neuronal tissue, the ubiquitous function of GSK-3β in cell proliferation and survival alongside its negative regulation of MRF activity and muscle hypertrophy, highlight its therapeutic potential in skeletal muscle [619–622]. Indeed, studies in murine C2C12 myoblasts and C57BL/6 muscle atrophy mouse models confirmed increased myotube formation and muscle growth following GSK-3β inhibition [621–623]. Furthermore, a phase 2 clinical trial in congenital MD (CMD) (ClinicalTrials.gov ID: NCT03692312) demonstrated neuromuscular improvements in patients, thus highlighting its potential for SMA [624].

In addition, observation of beneficial effects from drugs in other myopathic conditions could also provide ideal candidates for SMA [589]. One such example is the synthetic GC prednisolone, which is usually used to treat the inflammatory pathologies in DMD [625–627]. Commonly, chronic or daily GC usage has been associated with increased risks of myopathic development as evidenced by its clinical history [628,629] and studies in muscle of the *Mdx* mouse model for DMD [630,631]. However, short term or intermittent GC treatment in DMD patients [629,632–634], *Mdx* mice [630,635] and LGMD mice [636] had the opposite effect with reported benefits of improved muscle force, increased muscle endurance, sarcolemma repair and decreasing presence of centrally-nucleated myofibers. Furthermore, molecular analysis identified that intermittent GC treatment increased GC-Klf15 activity compared to chronic regimens, which resulted in the activation of ergogenic gene programs not associated with atrophy in muscle [630,635]. These benefits in muscle health from intermittent GC treatment led to prednisolone's investigation in SMA, where survival, weight and neuromuscular phenotypes

were improved in both severe *Smn*$^{-/-}$;*SMN2* and milder *Smn*$^{2B-}$ SMA mice [53]. Although the GC-Klf15-BCAA was a prime prednisolone target in SMA muscle, subsequent investigations with transgenic SMA mice that specifically over-expressed *Klf15* in skeletal muscle showed synergistic benefits, suggesting that non-*Klf15* pathways also contribute to prednisolone's efficacy [53]. With only 7% of GC-regulated genes linked to Klf15 [635], this leaves a large number of potential molecular effectors that were targeted by prednisolone to improve muscle health in SMA [53]. Although prednisolone has not been directly investigated in SMA clinical trials, it is interestingly being used to treat the hepatic side effects reported in SMA patients treated with Zolgensma® [470].

However, one limitation of prednisolone treatment in SMA is that the above studies are examples of short-term treatment and thus, the long-term effects are unknown [53]. We know from prednisolone's clinical history that long-term GC use is associated with adverse myopathic effects [628,629,637] and in the case of SMA, this would be detrimental for muscle improvements. Thus, we would need to consider investigating in further detail the molecular effects that prednisolone has on SMA skeletal muscle and the non-Klf15 pathways it targeted [53]. Not only would this help us develop a better understanding of prednisolone's activity in SMA muscle, but it could also lead to the discovery of repositioned drug candidates that could emulate or synergistically improve prednisolone's impact in SMA muscle, albeit with no long-term adverse risks.

1.5. Aim and objectives

Aim

To identify the genes and pathways targeted by prednisolone in SMA skeletal muscle and investigate if any orally-based clinical compounds can be repositioned to emulate prednisolone's benefits without the adverse effects of long-term GC use.

Objectives

1. Perform transcriptomic analyses on skeletal muscle from prednisolone-treated and untreated *Smn$^{-/-}$;SMN2* SMA and *Smn$^{+/-}$;SMN2* healthy mice to identify the differentially expressed genes (DEGs) targeted by prednisolone treatment.
2. Identify specific upstream regulators and pathways (KEGG and Gene Ontology (GO)) linked to the DEGs targeted by prednisolone in SMA skeletal muscle.
3. Identify orally bioavailable pharmacological compounds predicted to emulate prednisolone's activity in SMA skeletal muscle.
4. Validate predicted drug targets in SMA patient myoblasts and skeletal muscle from severe *Smn$^{-/-}$;SMN2* and milder *Smn$^{2B/-}$* SMA mice.
5. Evaluate *in vitro* effects of *Smn* depletion, canonical atrophy and drug treatment on predicted molecular targets and morphology in murine C2C12 myoblasts and myotubes.
6. Evaluate *in vivo* effects of predicted drug treatments on survival, weight and motor function in *Smn$^{2B/-}$* SMA mice.

7. Investigate the effects of predicted drug treatments on molecular targets and pathological markers in the skeletal muscle, spinal cord and non-neuromuscular tissue of *Smn*$^{2B/-}$ SMA mice.

Chapter 2.

General Methods.

2.1. Bioinformatics Experiments

2.1.1. Biological sample preparation

Total RNA was extracted from the triceps of symptomatic P7 untreated and prednisolone-treated (5 mg/kg every 2 days, starting at P0, gavage) Taiwanese *Smn*$^{-/-}$*;SMN2* (FVB/N background, FVB·Cg-Smn1tm1HungTg(SMN2)2Hung/J) SMA mice and *Smn*$^{+/-}$*;SMN2* healthy control littermates (n=3 for all except prednisolone-treated *Smn*$^{+/-}$*;SMN2* healthy mice, which is n=2) (Table 2.1) (Prednisolone treatment and dissection of the Taiwanese *Smn*$^{-/-}$*;SMN2* SMA and *Smn*$^{+/-}$*;SMN2* healthy control mice was performed by Dr Melissa Bowerman).

For each sample, 500 ng of total RNA was inputted for mRNA enrichment through NEBNext® Poly(A) mRNA Magnetic Isolation Module' (E7490L: New England Biolabs) and converted into cDNA libraries using NEBNext® Ultra Directional RNA Library Prep Kit for Illumina (E7420L; New England Biolabs). These cDNA libraries underwent further purification using 1x Agencourt® AMPure® XP Beads (#A63881; Beckman Coulter, Inc.). The cDNA libraries obtained a single indexed bar code using 'NEBNext Multiplex Oligos for Illumina – Set 1 (Index Primer 1-11), which were then amplified in 10 cycles of final PCR. Through library generation the fragment length distribution was monitored using Bioanalyzer high sensitivity DNA assay (5067-4626; Aligent Technologies) and quantified with Qubit® dsDNA HS Assay Kit (Q32854; ThermoFisher Scientific). The eleven individual barcoded library samples (Table 2.1) were pooled into equal molar amounts, denatured with NaOH and diluted to 1.5 pM concentration. The denatured library strands were then loaded onto a High Output Flowcell for 75 base pair (bp) single reads (#FC-404-2005; Illumina) and ran in a NextSeq

550 sequencer (Illumina). The raw binary base call (BCL) files generated by the NextSeq550 were converted to a FASTQ format using bcl2fastq conversion software v2.20.0.422 (Illumina) (All of the library sequence preparation and Illumina NextSeq 550 sequencing was performed at Hannover Medical School in collaboration with Professor Peter Claus and Dr Lisa Walter).

Table 2.1. Sample identification for each mouse that underwent RNA extractions of skeletal muscle (Triceps).

Untreated *Smn*$^{+/-}$;*SMN2* mice	**Untreated *Smn*$^{-/-}$;*SMN2* mice**	**Prednisolone-treated *Smn*$^{-/-}$;*SMN2* mice**	**Prednisolone-treated *Smn*$^{+/-}$;*SMN2* mice**
N0597	N0600	N0603	N0605
N0598	N0601	N0604	N0607
N0599	N0602	N0606	

2.1.2. Single read quality processing

The 75 bp raw single read FastQ files for all 11 samples (Table 2.1) were uploaded onto Galaxy [638,639] (usegalaxy.org), a free web server workflow system that uses a graphical user interface (GUI) to perform computational biology and bioinformatics analyses on multi-omics and biological datasets [638,639]. In addition, Galaxy has built-in genomes and biological references for a variety of commonly used model organisms including *Mus musculus* [638,639]. Initially, the FastQ files were assessed by FastQC [640] v0.72+galaxy1 to quality control check and summarise: basic statistics, per base sequence quality, per sequence quality scores, per base sequence content, per sequence GC content, per base N content, sequence length distribution, sequence duplication levels, overrepresented sequences and adapter content. Based on the report findings, the FastQ files underwent trimming of bases with < 20 Phred scores across an average of 4 bases using Trimmomatic [641] v0.36.5, which is specifically designed

for Illumina generated reads. A further ILLUMINACLIP step was also performed on Trimmomatic [641] v0.36.5 to remove any identifiable TruSeq2 single-ended adapters. Additionally, an in-built Galaxy FASTX-toolkit of Trim sequences [642] v1.0.2 was used to trim base sequences where difference in ACTG nucleotide composition was > 10%. The results of these quality control operations were confirmed through FastQC [640] v0.72+galaxy1 again.

2.1.3. Single read mapping

The post-processed single reads were aligned to an in-built *Mus musculus* mm10 (UCSC) genome through HISAT2 [643] v2.1.0, which uses whole genome index for read alignment and local FM index for alignment extension to accurately map sequences. Initially, HISAT2 [643] v2.1.0 was performed at default parameters. This setting allowed the Infer Experiment v2.6.4.1 function of RSeQC [644] in Galaxy to determine whether the reads in binary alignment map (BAM) files correspond to forward transcripts or reverse complements. To do this a reference UCSC *Mus musculus* mm10 browser extensible data 12 (BED12) file was required as it defined sense (forward) or antisense (reverse) identities to aligned strands. Confirmation of strand identity was visualised through MultiQC [645] v1.6. We then performed HISAT2 [643] v2.1.0 alignment again with the only change being the specify strand information set at *-reverse*. Distribution of the reads against the *Mus musculus* mm10 genome structure was constructed by the *read_distribution.py* function of RSeQC [644] through use of sample (Table 2.1) BAM files and the UCSC *Mus musculus* mm10 BED12 reference. Graphical confirmation of strand distribution was visualised through MultiQC [645] v1.6.

2.1.4. Differential gene expression analysis

We used FeatureCounts [646] v1.6.3+galaxy2 to quantify the number of reads in each sample's BAM file that uniquely aligned to known genes using a Galaxy built-in Entrez *Mus musculus* mm10 gene transfer format (GTF). In FeatureCounts [646] v1.6.3+galaxy2 strand specification was set at *-reverse*, and known gene identifier was set at *-exon level* to name genes based on Entrez ID. The proportion of raw counts assigned to known genes was visualised through MultiQC [645] v1.6.

The raw counts then underwent DGE analyses through DESeq2 [647] v2.11.40.2 on Galaxy. The design formula used to model signs of variance was based on condition (SMA or healthy controls) and treatment (untreated or prednisolone-treated). DESeq2 [647] internally normalised the raw count data through Median of Ratios (MoR) method. Firstly, a geometric mean for each gene is calculated across all the samples, which is then used to divide the raw count of their respective genes to create a ratio [647]. The median of the ratios in a sample is classed as the size factor, this in turn normalises the genes raw counts for each sample [647]. Shrinkage estimations of these normalised counts are then implemented to distinguish between biological and technical variations, which minimises dispersions and high variability amongst lowly expressed genes [647,648]. These shrunken normalised counts are then fit into a negative-binomial general linearized model (GLM) to calculate the log2 transformation of DEG fold changes (FC) based on count distributions [647]. These DEGs are then calculated for significance $p < 0.05$ using the Wald-test [647]. Furthermore, *post-hoc* Benjamini-Hochberg test can minimise false positive DEGs through false discovery rate (FDR) (or *p*-adj) <0.05 [647]. With this DESeq2 [647] v2.11.40.2 platform, three

separate analyses were performed with log2(FC) measurements of DEGs based on the first group highlighted in bold:

1. **Untreated *Smn$^{-/-}$;SMN2* SMA mice** vs untreated *Smn$^{+/-}$;SMN2* healthy mice.
2. **Prednisolone-treated *Smn$^{-/-}$;SMN2* SMA mice** vs untreated *Smn$^{-/-}$;SMN2* SMA mice.
3. **Prednisolone-treated *Smn$^{-/-}$;SMN2* SMA mice** vs untreated *Smn$^{-/-}$;SMN2* SMA and *Smn$^{+/-}$;SMN2* healthy mice.

Graphical outputs were produced to show principal component analysis (PCA), sample-to-sample distance, dispersion estimates, histogram of *p* values, and MA plot. Statistical data outputs included the base mean, log2(FC), standard error, Wald-stats, *p* value and FDR (Benjamini-Hochberg). Furthermore, DESeq2 [647] v2.11.40.2 produced a normalised counts file for each Entrez gene ID across the samples in each analysis. Although DESeq2 [647] automatically uses Cooks distance to internally removes outliers, we still validated any additional outliers through a Grubbs test [649] using the normalised count data for a small number of genes within individual experimental cohorts. The final list of significant Entrez gene ID results were filtered based on log2(FC) >0.6 and FDR <0.05. The Entrez gene ID's were then translated to official *Mus musculus* gene names and symbols through AnnotatemyID [638,639,650] v3.7.0 on Galaxy. The log2(FC) values of significant DEGs were uploaded onto Volcano Plot v0.0.3 on Galaxy [638,639] for graphical visualisation of up- and down-regulated genes. In addition, the normalised counts file of prednisolone-treated *Smn$^{-/-}$;SMN2* SMA mice vs untreated *Smn$^{-/-}$;SMN2* SMA and *Smn$^{+/-}$;SMN2* healthy mice was ran in

Heatmap2 v2.2.1+galaxy1 with the data log2 transformed and scaled by *row - scale genes*.

2.1.5 Pathway analysis

Pathway analysis of the prednisolone-treated *Smn$^{-/-}$;SMN2* vs untreated *Smn$^{-/-}$;SMN2* mice was performed with iPathwayGuide [651–654] (Advaita) with default criteria of log2(FC) >0.6 and FDR <0.05 for DEGs. Designed as an online GUI software, iPathwayGuide calculated KEGG [655] pathways through impact analysis and Gene Ontology (GO) [656,657] through overrepresentation analysis (ORA) [658] (KEGG v1910 Release 90.0+/05-29, May 19; GODb v1910 2019-Apr 26). In addition, iPathwayGuide predicted upstream regulators (STRING v11.0, Jan 19th, 2019) and disease similarities (KEGG v1910 Release 90.0+/05-29, May 19). Identification of drug candidates that targeted the iPathwayGuide KEGG pathways was performed through an in-built KEGG drugs database. Identification of drug candidates that target predicted upstream regulators was done with the Drug Gene Interaction database (DGIdb [659]) v3.0. Identified drugs were catalogued to determine efficacy, bioavailability, current use in diseases and conditions, molecular targets and regulatory status using various drug databases (KEGG [655], Inxight: Drugs [660], British National Formulary: National Institute for Health and Care Excellence (BNF: NICE [661]), DrugBank [662,663], clue.io cMap L1000 platform [664]).

2.2. *In vitro* experiments

2.2.1. Maintenance and differentiation of murine C2C12 myoblast-like cells.

All cell culture experiments were performed within a Class 2 Biological Safety Cabinet (NUAIRE^{TM}). The immortalised murine cell line used was the C2C12 myoblasts [665,666] (ATCC, USA). These C2C12 myoblasts were thawed out of liquid nitrogen (LN_2) storage and resurrected in a T-75 cell culture flask (Fisher Scientific) containing growth media, comprised of high glucose (4.5 g/L) and L-glutamine (0.6 g/L) Dulbecco's Modified Eagle's Media (DMEM) (Lonza), 10% foetal bovine serum (FBS) (Gibco) and 1% Penicillin-Streptomycin (10,000 U/ml) (Lonza). The resurrected C2C12 myoblasts were stored in an incubator with humid 37^{o}C and 5% CO_2 conditions (Heracell 150i CO_2 incubator, ThermoScientific).

After initial resurrection, when C2C12 myoblasts were >60% confluent they were transferred into a T-175 cell culture flask (Fisher Scientific) with 20 ml of growth media. From passage number 2 till 20, the C2C12 myoblasts underwent subsequent passages when they reached >60% confluence. Cell passage involved the removal of growth media, followed by a phosphate buffered saline (PBS) (Lonza) wash and exposure to 5 – 7ml of 1X TrpLE Express Enzyme (Gibco) for 5 minutes in 37^{o}C and 5% CO_2 incubator for trypsin-mediated cell detachment. The detached C2C12 myoblasts were centrifuged at 500 RPM for 2 minutes and resuspended in 4 ml of growth media. A 1:4 cell suspension dilution at 1 ml volume was then aliquoted into a fresh T-175 flask with 20 ml growth media for storage in 37^{o}C and 5% CO_2 incubator. C2C12 myoblasts were checked for confluency everyday with a fresh media change every 48 hours until

>60% confluency was reached. For *in vitro* experiments, 30 µl of the 4 ml C2C12 myoblast cell suspension was seeded into each well of 6-well cell culture plates (Fisher Scientific) that contained 2 ml of growth media. For 12-well cell culture plates (Fisher Scientific) with 1 ml growth media per well, 20 µl of the 4 ml C2C12 myoblast cell suspension was seeded into each well. The *in vitro* treatments of C2C12 myoblasts did not begin until they reached 50-60% confluency.

For differentiation, C2C12 myoblasts at an approximate confluence of 50-60% in 6- and/or 12-well cell culture plates were exposed to differentiation media comprised of high glucose (4.5 g/L) and L-glutamine (0.6 g/L) DMEM, 2% horse serum (HS) (Gibco), 1% Penicillin-Streptomycin (10,000 U/ml) and 0.1% insulin (1 µg/ml) (Sigma) for 2-8 days with storage in humid 37^{o}C and 5% CO_2 incubator and media replacement every 48 hours.

2.2.2. Primary type 3 SMA and age-matched control deltoid myoblasts

Age-matched control and type 3 SMA primary human myoblasts cultured from deltoid muscle biopsies were generously provided by Dr Stephanie Duguez (University of Ulster) (Table 2.2).

Table 2.2. Control and type 3 SMA myoblasts from deltoid muscle biopsies.

Sample	Condition	Skeletal muscle type	Age	Gender
SD1052C25D	Control	Deltoid	25	Male
SD1049C22D	Control	Deltoid	22	Male
GO729C52D	Control	Deltoid	52	Female
GO780C47D	Control	Deltoid	47	Female
GO837C59D	Control	Deltoid	59	Male
GO812SMA30D	Type 3 SMA	Deltoid	30	Male
G0878SMA27D	Type 3 SMA	Deltoid	27	Male
GO949SMA66D	Type 3 SMA	Deltoid	66	Male
GO750SMA53D	Type 3 SMA	Deltoid	53	Female
GO751SMA48D	Type 3 SMA	Deltoid	48	Male

2.2.3. Small interfering (si)RNA-mediated *Smn* knockdown

A *Smn* small interfering RNA (siRNA) (Duplex name: mm.RiSmn1.13.1) was used to induce *Smn* KD. In addition, a scrambled siRNA (scrambled DsiRNA, #51-01-19-08) (Integrated DNA technologies) was used as a negative control. The *Smn* and scrambled siRNAs were separately aliquoted into an siRNA-lipofectamine complex (Lipofectamine® RNAiMAX Reagent, Life Technologies), following manufacturer's procedure. Proliferating C2C12 myoblasts were transfected for 48 hours, whilst transfection reagents were replaced every 48 hours in each well containing differentiating C2C12 cells. *Smn* depletion was confirmed via quantitative polymerase chain reaction (qPCR) (See chapter 4, figures 4.7.a-b).

2.2.4. Serum-starvation-induced canonical muscle atrophy

Serum starvation is a validated method of inducing atrophy in immortalised C2C12 myotubes [667,668]. Differentiated C2C12 cells were incubated in serum-free high glucose (4.5 g/L) and L-glutamine (0.6 g/L) DMEM with 1% Penicillin-Streptomycin (10,000 U/ml) for 24 hours. The atrophied C2C12 cells were confirmed by atrogene upregulation (*Atrogin-1* and *MuRF-1*) via qPCR and muscle wasting morphology under 10x magnification (Motic AE31E).

2.3. *In vivo* experiments

2.3.1. Animals used

All breeding mice were from C57BL/6 background [669]. The two initial breeding lines used were *Smn*$^{2B/2B}$ [57] (Professor Rashmi Kothary (University of Ottawa) to Dr Lyndsay Murray (University of Edinburgh) to Professor Matthew Wood (University of Oxford) to Charles River for rederivation) and *Smn*$^{+/-}$ [670] (B6.Cg-Smn1/J, stock #007963, Jackson labs). *Smn*$^{2B/-}$ SMA mice and healthy *Smn*$^{2B/+}$ littermates were generated from breeding *Smn*$^{2B/2B}$ and *Smn*$^{+/-}$ parents. All live animal procedures were performed in the Biomedical Sciences Unit (BSU) after authorisation and approval by the Keele University ethics committee and UK Home Office (project licence: P99AB3B95, personal licence: IA54D3EC1) under the Animals Scientific Procedures Act (1986).

2.3.2. Genotyping

Genotyping involved initial DNA extraction from ear clips (*Smn*$^{+/-}$ and *Smn*$^{2B/2B}$) or tail clips (*Smn*$^{2B/-}$) using PCRBIO Rapid Extract PCR kit (PCR Biosystems). The genotyping of *Smn*$^{+/-}$ and *Smn*$^{2B/-}$ involved master mix reagent of: 2x PCRBIO Taq mix (PCRBIO Taq DNA polymerase, 6 mM $MgCl_2$, 2 mM dNTPs and red dye) (PCR Biosystems), 400 nM *Smn* oIMR7031-4 primers (Table 2.3) and PCR-Grade Water. The following programme used in ^{3}Prime thermocycler (Techne) involved: an initial denaturation at 94^{o}C for 5 minutes, followed by 10 cycles of 94^{o}C for 20 seconds, 65^{o}C for 15 seconds (0.5^{o}C decrease every cycle) and 68^{o}C for 10 seconds. This was later followed by 28 cycles of 94^{o}C for 15

seconds, 60ºC for 15 seconds, and 72ºC for 10 seconds. The reaction ended with final stage of 72ºC for 3 minutes.

The PCR for *Smn*$^{2B/2B}$ mice used the same genotyping master mix with 400 nM *Smn*^{2B} primers instead (Table 2.3). Genotyping involved a ^{3}Prime thermocycler (Techne) programme: initial denaturation at 94ºC for 3 minutes, followed by 35 cycles of 94ºC for 45 seconds, 58ºC for 45 seconds and 72ºC for 45 seconds. The reaction ended with a final stage at 72ºC for 5 minutes.

Confirmation of genotypes in both methods was observed via 1.2% agarose gel electrophoresis in 10,000X Gel Red (BIOTIUM) for 70 minutes at 100 V (NanoPAC-300P, Clever Scientific) followed by band size UV visualisation using ChemiDoc MP Imaging System (BioRad) (Figure 2.1).

Table 2.3. Primers used for C57BL/6 mouse genotyping

Genes	Mouse Genotypes	Forward Primers (5' – 3')	Reverse Primers (5' – 3')
Smn^{-} (oIMR7031)	WT, *Smn*$^{+/-}$, *Smn*$^{2B/-}$	GAA CTA GAA GAC AGG TGG AG	N/A
Smn^{-} (oIMR7032)	WT, *Smn*$^{+/-}$, *Smn*$^{2B/-}$	N/A	GTC TGT CCT AGC TTC CTC ACT G
Smn^{+} (oIMR7033)	WT, *Smn*$^{+/-}$, *Smn*$^{2B/-}$	TGG GAG TCC ATC CAT CCT AAG TC	N/A
Smn^{+} (oIMR7034)	WT, *Smn*$^{+/-}$, *Smn*$^{2B/-}$	N/A	GCT AAG AAA ATG ACA ATT GCA CAT TTG
Smn2B	*Smn*$^{2B/2B}$	AAC TCC GGG TCC TTC CT	TTT GGC AGA CTT TAG CAG GGC

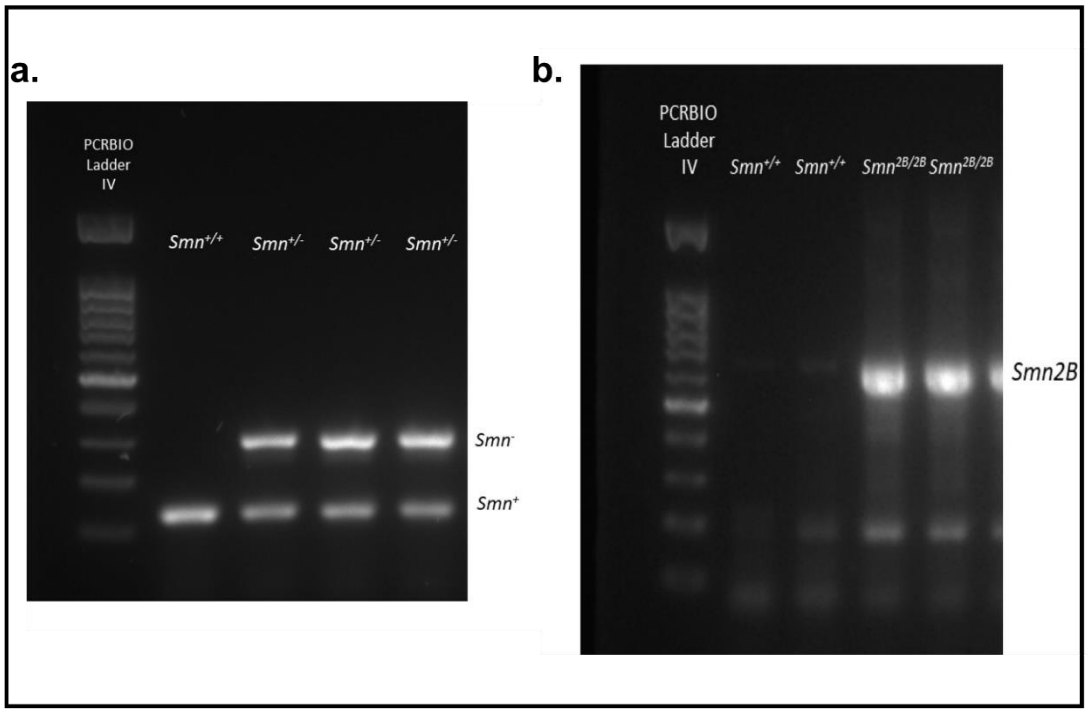

Figure 2.1. Genotyping of *Smn*$^{2B/2B}$ and *Smn*$^{+/-}$ mice.

a. Genotype screening of *Smn*$^{+}$ (oIMR7033 and oIMR7034) and *Smn*$^{-}$ (oIMR7031 and oIMR7032) primer sets that was used in PCR amplification to generate amplicon products from *Smn*$^{+/+}$ and *Smn*$^{+/-}$ samples. Amplicon products were size separated by 65 minute electrophoresis on 1.2% agarose gel alongside PCRBIO Ladder IV reference. The amplicon products were size separated resulting in 308 bp size for *Smn*$^{-}$ and 143 bp for *Smn*$^{+}$ primers. The *Smn*$^{+/-}$ genotype was confirmed by heterozygous band products.

b. Genotype screening of *Smn2B* primer set that was used in PCR amplification to generate amplicon products from *Smn*$^{+/+}$ and *Smn*$^{2B/2B}$ samples. Amplicon products were size separated by 60 minute electrophoresis on 1.2% agarose gel alongside PCRBIO Ladder IV reference. The *Smn2B* amplicon band size is 519 bp and the higher intensity is associated with the *Smn*$^{2B/2B}$ genotype.

Images were developed under UV visualisation on ChemiDoc MP Imaging System (BioRad).

2.3.3. Phenotypic analysis on live animals.

Phenotypic analyses included measurements of bodyweight and righting reflex (up to 30 seconds), which is the ability for a pup to independently reorientate itself back into the upright position [671]. These neuromuscular phenotypes were measured every day from P0 to respective humane endpoints. Day of death was determined when animals reached the humane endpoint as defined in our Home Office Project Licence (P99AB3B95): hindlimb paralysis or immobility or inability to right (greater than 30 seconds) or up to 20% body weight loss. They were culled via Schedule 1 or approved non-Schedule 1 methods.

2.3.4. Animal Tissue Harvest

Culling method was dependent on the age of the mice: decapitation for pups < P10 and Schedule 1 methods for animals > P10. Harvested skeletal muscle (both *Triceps brachii* and TA), spinal cord and liver were placed in cryovials for immediate flash freezing in liquid nitrogen (LN_2), followed by long term storage in -80^{o}C freezer. In addition, RNA samples from the triceps of P7 untreated *Smn$^{-/-}$;SMN2* SMA and *Smn$^{+/-}$;SMN2* healthy mice were generously provided by Professor Peter Claus and Dr Lisa Walter (Hannover Medical School).

2.4. Gene Expression Analysis

2.4.1. Tissue Lysis and RNA Extraction

C2C12 cells cultured in each well of 6- or 12-well cell culture plates were lysed in 350 µl of β-mercaptoethanol/RLT solution (1:100 dilution) (Bioline) for 5 minutes before RNA spin-column extraction was performed with ISOLATE II RNA Mini Kit following the manufacturers protocol. Age matched control and type 3 SMA primary human myoblasts were extracted using Trizol-chloroform combined with spin column (Qiagen) following a set published protocol [672]. Tissue samples required homogenisation in 350 µl of β-mercaptoethanol/RLT solution (1:100 dilution) in 2 ml Eppendorf tube with 7 mm stainless steel ball (Qiagen) in Tissue Lyser LT (Qiagen) set a 60 oscillations/second for 2 minutes followed by centrifugation at >10,000 RCF (MSE Sanyo Hawk 15/05) for 1 minute. RNA extractions from skeletal muscle tissues were then performed with RNeasy Fibrous Tissue Kit (Qiagen) and non-muscular tissue was extracted with ISOLATE II RNA Mini Kit (Bioline) as per manufacturers protocol. RNA concentrations (ng/µl) were measured with the Nanodrop 1000 spectrophotometer (ThermoScientific) against a reference RNase-free water control.

2.4.2. Reverse Transcription

Reverse transcription (RT) to generate cDNA required a final 15 µl volume of sample RNA and RNase-free water per 200 µl PCR tube to achieve total RNA concentrations ranging from 200 – 1000 ng. Additionally, a reagent mix comprised of 4 µl 5x cDNA synthesis (mix anchored oligo(dT), random hexamers,

15 mM MgCl2, 5 mM dNTPs) (PCR Biosystems), and 1 µl 20x RTase (PCR Biosystems) were used to finalise 20 µl volume per RT sample. The RT reactions then ran for 30 minutes at 42^{o}C followed by a denaturation step of 85^{o}C for 10 minutes in a ^{3}Prime thermocycler (Techne). The cDNA samples were then diluted 1:5 with 80 µl PCR-grade water.

2.4.3. Quantitative PCR (qPCR)

A total of 2 µl diluted cDNA was aliquoted into each well of a 96-well qPCR plate composed of 10 µl 2x PCRBIO Sygreen Blue Mix Hi-ROX (PCR Biosystems), 0.8 µl 10 µM forward primer, 0.8 µl 10 µM reverse primer (Integrated DNA Technologies) (Tables 2.4-5) and 6.4 µl PCR-grade water for total 20 µl volume per well. The qPCR reactions were performed in the StepOnePlus™ Real-Time PCR System (ThermoFisher Scientific) with the following programme: initial denaturation at 95^{o}C for 2 minutes followed by 40 cycles of 95^{o}C for 5 seconds and 60^{o}C for 30 seconds and ending with melt curve stage of 95^{o}C for 15 seconds, 60^{o}C for 1 minute and 95^{o}C for 15 seconds. The qPCR data was analysed using the StepOne Software v2.3 (ThermoFisher Scientific) with relative gene expression quantified using the Pfaffl method [673] with *PolJ* (murine) and *POL2RA* (human) housekeeping genes (Table 2.4-5). Primer efficiency for the Pfaffl method was calculated using LinRegPCR V11.0.

Table 2.4. Murine primers used for qPCR.

Genes	Forward Primers (5' – 3')	Reverse Primers (5' – 3')
PolJ	ACC ACA CTC TGG GGA ACA TC	CTC GCT GAT GAG GTC TGT GA
Smn	TGC TCC GTG GAC CTC ATT TCT T	TGG CTT TCC TGG TCC TAA TCC TGA
Atrogin-1	TCA AAG GCC TCA CGA TCA CC	CCT CAA TGA CGT ATC CCC CG
MuRF-1	GAG AAC CTG GAG AAG CAG CT	CCG CGG TTG GTC CAG TAG
Prkag3	GGT CAT CTT TGA CAC GTT	AGA GGA GCT GCC CTC ACA C
FoxO1	CTA CGA GTG GAT GGT GAA GAG C	CCA GTT CCT TCA TTC TGC ACT CG
FoxO3	GGA AGG GAG GAG GAG GAA TG	CTC GGC TCC TTC CCT TCA G
FoxO4	CAA GAA GAA GCC GTC TGT CC	CTG ACG GTG CTA GCA TTT GA
FoxO6	AGA GCG CCC CGG ACA AGA GA	GCC GAA TGG AGT TCT TCC AGC C
Ar	TAC CAG CTC ACC AAG CTC CT	GAT GGG CTT GAC TTT CCC AG
MyoG	GTG TAA GAG GAA GTC TGT GTC GG	GCT CAA TGT ACT GGA TGG CG
Igfbp5	AAG AGC TAC GGC GAG CAA ACC A	GCT CGG AAA TGC GAG TGT GCT T
Akap6	AAG GAA CGA GCG CCG AGA AAC A	TGC TGG CAC AAC CTC AGA ATG G
Dok5	CGT TAT GGA CGA GAC ACC ACG T	GAG TGG ACC TTC TGG TAG ATG G
Ddit4	CCT GCG CGT TTG CTC ATG CC	GGC CGC ACG GCT CAC TGT AT
Hk2	GAA GGG GCT AGG AGC TAC CA	CTC GGA GCA CAC GGA AGT T
Glut4	GAC GGA CAC TCC ATC TGT TG	CAT AGC TCA TGG CTG GAA CC
Pgc1-α	TGG AGT GAC ATA GAG TGT GCT GC	CTC AAA TAT GTT CGC AGG CTC A
Nrf1	CAG CAC CTT TGG AGA ATG TG	CCT GGG TCA TTT TGT CCA CA
Tfam	CAA GTC AGC TGA TGG GTA TGG	TTT CCC TGA GCC GAA TCA TCC
Nfdus1	GTG GAT GCT GAA GCC TTA GTA GC	GGA ACG TAA GTC TGT ACC AGC TC

Table 2.5. Human primers used for qPCR

Genes	Forward Primers (5' – 3')	Reverse Primers (5' – 3')
POL2RA	CAA CGC ACA CAT CCA GAA CG	TCC TTG ACT CCC TCC ACC AC
PRKAG3	TGC TTC AAG CCT CTG GTC TCC A	GGA ACT TGA GCA GGC GTT TGT G
FOXO1	AAG AGC GTG CCC TAC TTC AA	CTG TTG TTG TCC ATG GAT GC
FOXO3	GAA CGT GGG GAA CTT CAC TGG TGC TA	GGT CTG CTT TGC CCA CTT CCC CTT
AR	CCT GGC TTC CGC AAC TTA CAC	GGA CTT GTG CAT GCG GTA CTCA
MYOG	CGC AGT GCC ATC CAG TAC A	CGT GAG CAG ATG ATC CCC T
DOK5	GAG CAG ACG CCT CGG GAT TTA TCA G	CCTC CCT GCC TCA AAA GTG AAC CAC
DDIT4	GGA TGG GGT GTC GTT GCC CG	GGC AGC TCT TGC CCT GCT CC

2.5. Statistical Analyses

Statistical analyses were carried out using the most up-to-date GraphPad PRISM software. Prior to any analyses, outliers were identified with the Grubb's test (GraphPad) and subsequently removed. Appropriate statistical tests used include unpaired t-test, one-way analysis of variance (ANOVA), and two-way ANOVA. Each post-hoc analyses used is noted in the respective figure legend. Kaplan-Meier survival curves required a log-rank test. Statistical significance was considered at $p < 0.05$, described in graphs as *$p < 0.05$, **$p < 0.01$, ***$p < 0.001$, ****$p < 0.0001$.

Chapter 3.

In silico drug repositioning approach to identify commercially available compounds that mimic prednisolone activity in SMA skeletal muscle as new potential SMN-independent therapies.

3.1. Introduction

In chapter 1, we discussed the published findings that prednisolone treatment (5 mg/kg every 2 days, starting at P0, gavage) in both severe *Smn*$^{-/-}$;*SMN2* and milder *Smn*$^{2B/-}$ SMA mice improved survival and muscle health [53]. Although, prednisolone's activity in SMA muscle was linked to the activation of the GC-Klf15-BCAA pathway, it's treatment in SMA mice with skeletal muscle-specific *Klf15* overexpression revealed synergistic benefits [53]. Interestingly, our evidence of these synergistic benefits in SMA muscle alongside independent reports of Klf15 contributing to only a small number of GC-regulated genes, suggests that a large number of prednisolone molecular targets that improve SMA muscle health are unknown [53,635].

To identify molecular targets based on gene expression profiles, low throughput analysis techniques such as qPCR and northern blot would not be extensive enough to cover the range of potential candidates [674]. Instead, high throughput methods such as microarray-hybridisation [675] or RNA sequencing [676,677] (RNA-Seq) are preferable. Although both techniques can quantify the expression profiles of many genes simultaneously, RNA-Seq has several advantages over microarray-hybridisation that make it a more suitable method. Firstly, RNA-Seq can cover the entire transcriptome in a single run [676], whilst microarray requires multiple runs, making it a more laborious process [675,678]. Secondly, microarray-hybridisation is biased in its approach as probes for known genes are required [675,679]. On the other hand, RNA-Seq does not require specific gene probes, making it less biased and allowing for in depth discovery and expression quantification for known and novel transcripts [680,681]. Thirdly, RNA-Seq is better for analysing both coding [682] (pre-messenger RNA (pre-RNA) and mRNA) and

non-coding transcripts [683] (ribosomal RNA (rRNA), transfer RNA (tRNA), small non-coding RNA (sncRNA) and long non-coding RNA (lncRNA)).

RNA-Seq is a multi-tier pipeline [681,684] (Figure 3.1) that begins with the specific preparation and sequencing of cDNA libraries from RNA extracts, dependent on factors such as rRNA removal or polyA+ selection to increase sequence coverage and on the next generation sequencing (NGS) platform used [685,686], which in most cases is Illumina [686–688]. Once sequenced, these RNA-Seq reads are initially quality assessed through various tools such as FastQC [640] and HTQC [689] and modified to minimise any anomalies that can arise from the multiple stages of cDNA library preparation [681,684]. The reads that have passed the quality check are then mapped to their genomic locations in their appropriate model organism through specialised alignment tools [690,691] such as TopHat [692], HISAT2 [643] and STAR [693] that can locate exon-intron junctions and polyA tails to take into consideration spliced transcripts [681,691,694]. After alignment, the reads can either be constructed into a *de novo* transcriptome through Cufflinks [695] and StringTie [696] or can bypass this stage to count the read number aligned to known genes through HTSeq-counts [697] or FeatureCounts [646]. However, both processes [646,697] require specific model organisms GTF or general feature format (GFF) [698] that are accessible from various genomic databases such as UCSC [699], Entrez [700], and Ensembl [701] for gene identity.

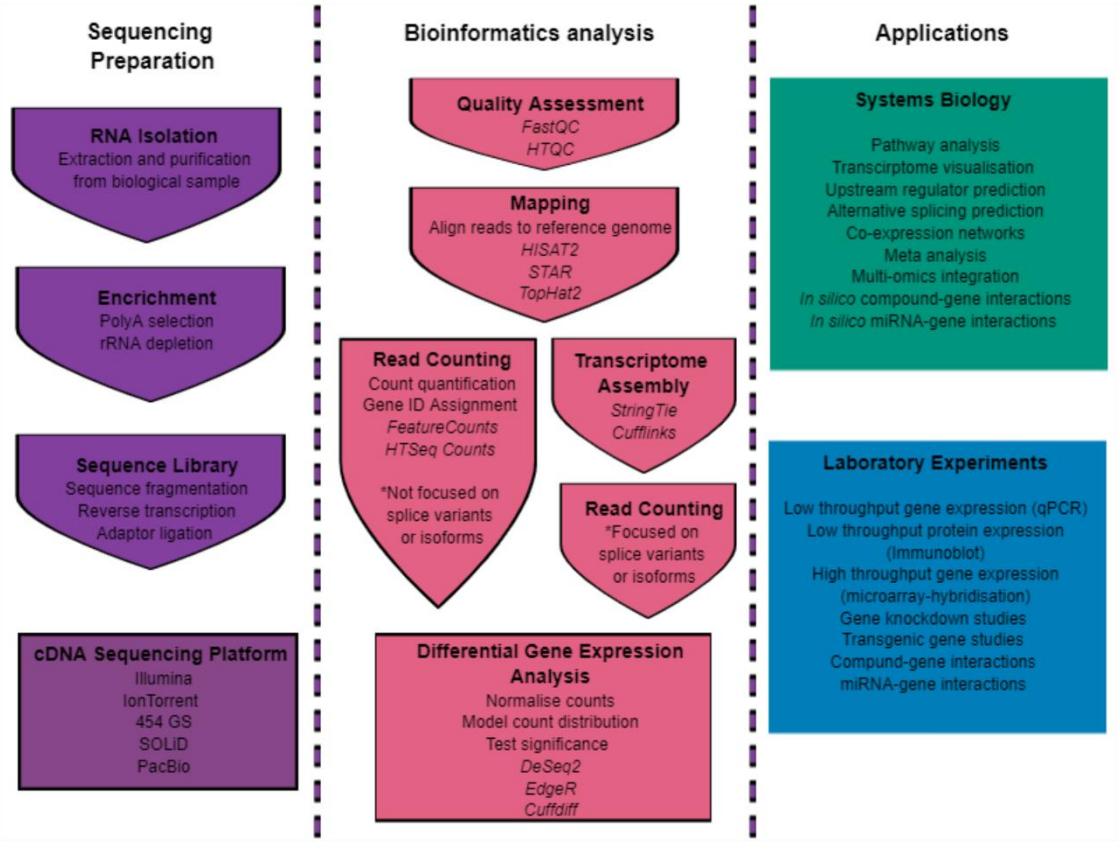

Figure 3.1. RNA sequencing (RNA-Seq) pipeline.
The sequencing preparation (purple) and bioinformatics analysis (pink) columns cover the linear workflow from RNA extraction to differential gene expression analysis. The applications column covers the applications of RNA-Seq data, which includes systems biology (green) and laboratory experiments (blue) to address biological questions.
Figure was created on Mind the Graph.

An important quality step prior to differential gene expression (DGE) analysis is normalisation of the raw count reads by factors like sequencing depth for gene expression comparisons between samples, gene length for gene expression comparisons within the same sample and RNA composition for improved accuracy [702]. These steps improve DGE analysis by minimising the influence of individual differences within each cohort. Certain methods include reads per kilobase per million mapped reads (RPKM) [703], RNA-Seq by Expectation Maximisation (RSEM) [704], Trimmed mean of M values (TMM) [705,706], and MoR [647,707]. These normalised counts are then analysed through various DGE tools

such as CuffDiff [695], DESeq2 [647] and EdgeR [705] that use an algorithm of probability-based count distributions [708] (Poisson [709] or negative binomial [710]) and statistical significance calculations [711] to predict DEGs. To narrow down the biological patterns hidden within the high volume of DEGs identified by RNA-Seq, the data is usually grouped and categorised into pathways using various tools and databases [712], the most common example being ORA [658] for GO database [656,657,713].

The combination of transcriptomics followed by pathway analysis has been previously successful in SMA studies involving patients [714,715], animal models [94,716,717] and specific tissue types [94,714,718], where it has proven useful for the discovery of dysregulated pathways [718] and identifying potential biomarkers [714]. Another benefit of transcriptomics in biomedical research is its application to drug repositioning, a strategy, as discussed above (see section 1.4.3.1.), aimed at finding new therapeutic roles for existing pharmacological compounds [587]. Traditional clinical or *in vivo* and *in vitro* wet lab methods of drug repositioning are sometimes limiting as they usually rely on compound availability [719] and observing phenotypic attenuation before determining suitability [720]. However, *in silico* techniques counteract these limitations as the incorporation of computationally predicted targets with publicly available drug databases significantly expands the list of potential available candidates [721]. Furthermore, selection of pharmacological compounds from a list of predicted drug candidates helps to narrow down the drugs to be further evaluated to a select few, which can prove to be cost-effective in validation experiments in cellular and animal models [721]. We recently demonstrated the validity of this *in silico* approach in SMA in a study where we predicted that harmine, a naturally occurring alkaloid from the

Peganum harmala plant, could target muscle pathologies in SMA, which we validated in relevant cellular and animal models [716].

In this chapter, we used an RNA-Seq approach to investigate the effect of prednisolone on the transcriptomic profile of skeletal muscle of SMA mice. This strategy revealed that prednisolone normalised the expression of a large number of genes in SMA muscle towards healthy levels. These genes were associated with pathways involved in skeletal muscle metabolism, regulation, and function. Furthermore, the use of various drug databases allowed the discovery of available compounds that are predicted to emulate these effects. This chapter highlights the advantages of *in silico* drug repositioning for identifying novel SMN-independent therapies with the potential of improving muscle health in SMA.

3.2. Results

3.2.1. Quality control analysis, alignment and read count estimation minimises risks of skewed data sets for differential gene expression analysis.

To investigate the gene transcripts modulated by prednisolone in skeletal muscle of P7 *Smn*$^{-/-}$*;SMN2* SMA mice, we first had to evaluate for potential data anomalies and genomic alignment accuracy. Initial quality assessment of raw reads is a vital step before genomic alignment as the multi-stage process of RNA-Seq from RNA extraction to NGS presents potential risks during sample preparation [681,684]. These include contamination, low RNA-yields, RNA degradation, PCR artefacts, presence of non-coding RNA (for polyA+ selection experiments), adapter retention and sequencing error [681,684,722–724]. If kept, these factors can skew DGE analysis and produce false results [723]. We thus used FastQC [640] to initially quality assess the data for such anomalies and identified that the raw 75 bp single reads (Figure 3.2.a) across the 11 samples (Table 2.1) contained an aberrant nucleotide composition > 10% in the first 12 bp positions (Figure 3.2.b), and Illumina adapter overrepresentation (Table 3.1).

Table 3.1. Presence of TruSeq2 single-ended adapters in raw 75 bp RNA-Seq reads.

Adapter	Samples
TruSeq Adapter, Index 1 (100% over 50bp)	N0597
TruSeq Adapter, Index 2 (100% over 50bp)	N0598
TruSeq Adapter, Index 3 (100% over 50bp)	N0599
TruSeq Adapter, Index 4 (100% over 50bp)	N0601
TruSeq Adapter, Index 5 (100% over 50bp)	N0600
TruSeq Adapter, Index 6 (100% over 50bp)	N0602
TruSeq Adapter, Index 7 (100% over 50bp)	N0603
TruSeq Adapter, Index 8 (100% over 50bp)	N0604
TruSeq Adapter, Index 9 (100% over 50bp)	N0606
TruSeq Adapter, Index 10 (100% over 50bp)	N0605
TruSeq Adapter, Index 11 (100% over 50bp)	N0607

Although anomalies such as aberrant nucleotide profiles (Figure 3.2.b) at the start of reads are not unexpected [724], they are still worthy of correction to improve alignment reliability [644]. Thus, these aberrations were corrected by Trimmomatic [641] and FAST-X Trim sequences [642], as evidenced across the modified 63 bp single strand reads (Figure 3.3.a), which displayed a stabilised nucleotide composition < 10% (Figure 3.3.b) and absence of Illumina adapters. Although the modified single reads were 12 bp shorter, previous literature has shown that sizes > 50 bp can still produce reliable alignments [725]. Furthermore, these modifications had little effect on the overall sequence quality, with a mean Phred score of 35 consistent in pre- and post-processed reads (Figure 3.4). In addition, duplicated reads (Figure 3.5) were not modified in this case as computationally it is difficult to distinguish PCR duplicates from natural duplicates and thus removal would have risked worsening the FDR in DGE analysis [726,727].

a.

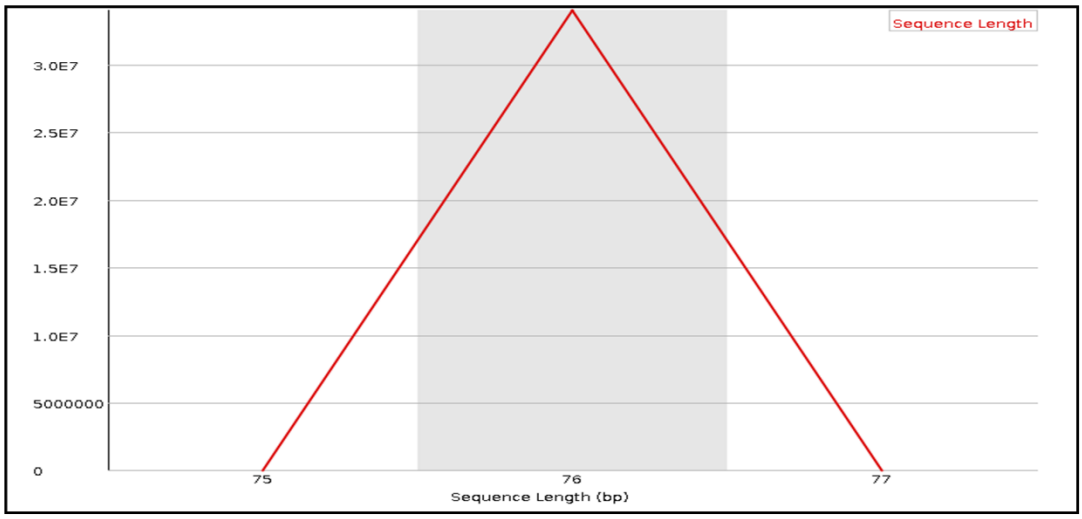

b.

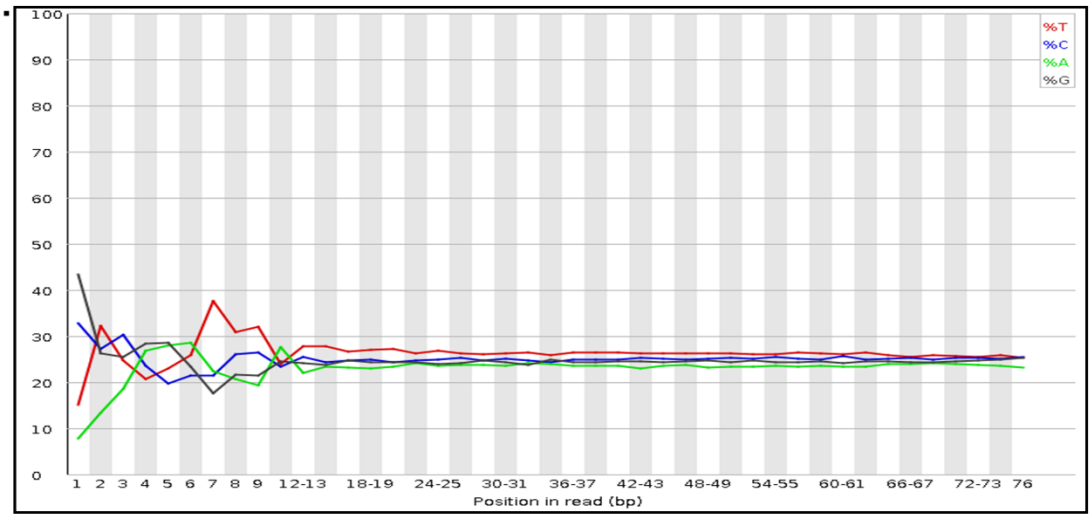

Figure 3.2. Sequence length and base content of raw single-end RNA-Seq reads.
a. Sequence length distribution report calculates the number of reads (y axis) that fall within a certain sequence length (bp) (x axis).
b. Per base sequence content reports plots the percentage of nucleotide guanine (red), adenine (blue), thymine (green) and cytosine (black) within each base position (x axis) of the sequence files. Graphs were generated by FastQC v0.72+galaxy 1.

a.

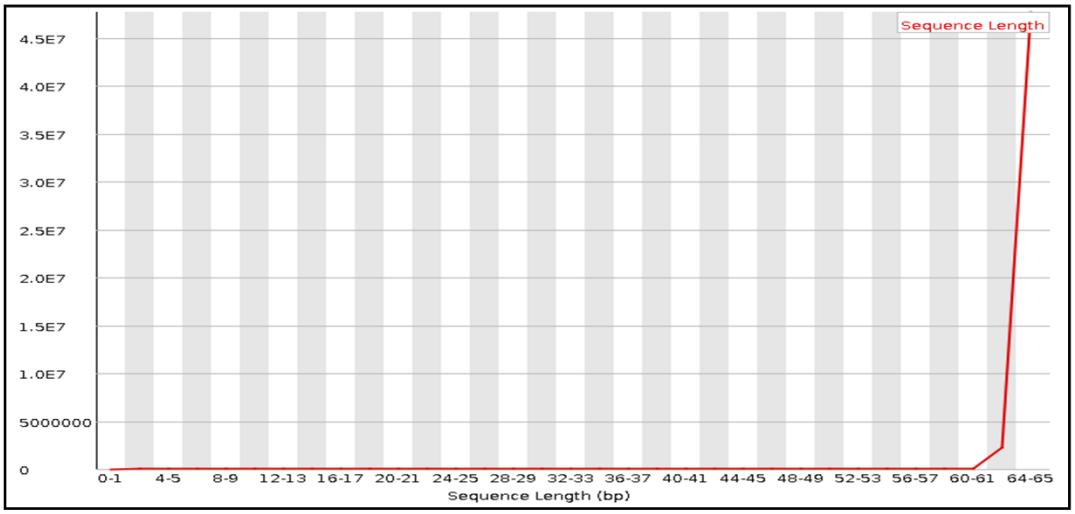

b.

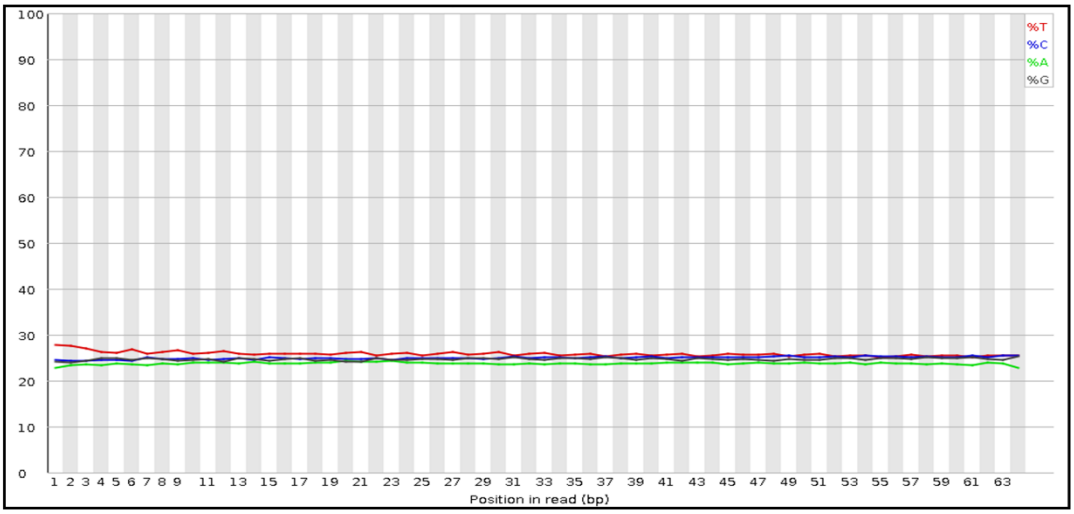

Figure 3.3. Sequence length and base content of Trimmomatic and FAST-X processed single-end RNA-Seq reads.
a. Sequence length distribution report calculates the number of reads (y axis) that fall within a certain sequence length (bp) (x axis).
b. Per base sequence content reports plots the percentage of nucleotide guanine (red), adenine (blue), thymine (green) and cytosine (black) within each base position (x axis) of the sequence files. Graphs were generated by FastQC v0.72+galaxy 1.

a.

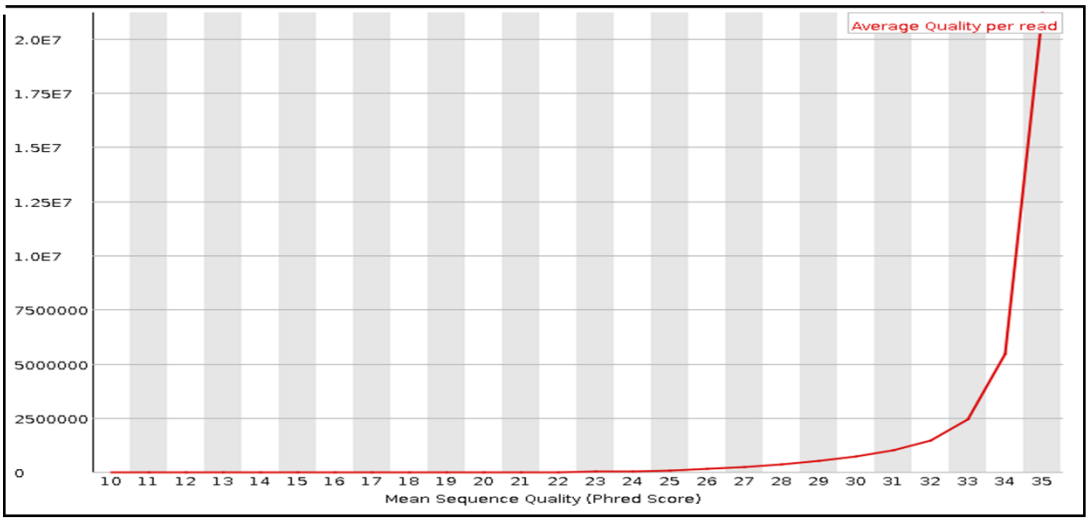

b.

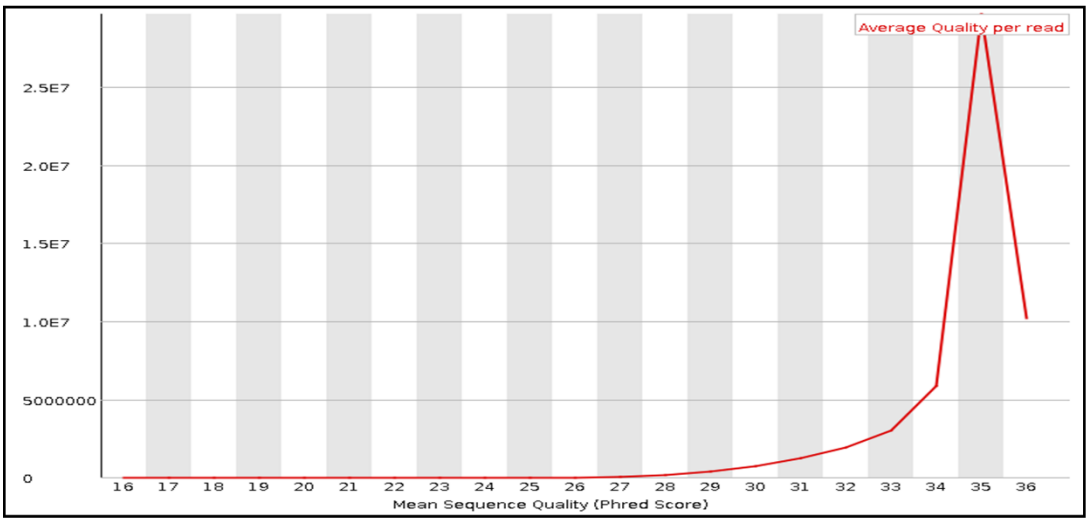

Figure 3.4. Sequence quality of single-end RNA-Seq reads.
Comparison of sequence quality between **a.** raw 75 bp and **b.** processed 63 bp single-end reads.
Per sequence quality score report compares the phred score (x axis) against the number of reads (y axis). Average quality per read box positions the average phred score. Graphs were generated by FastQC v0.72+galaxy 1.

a.

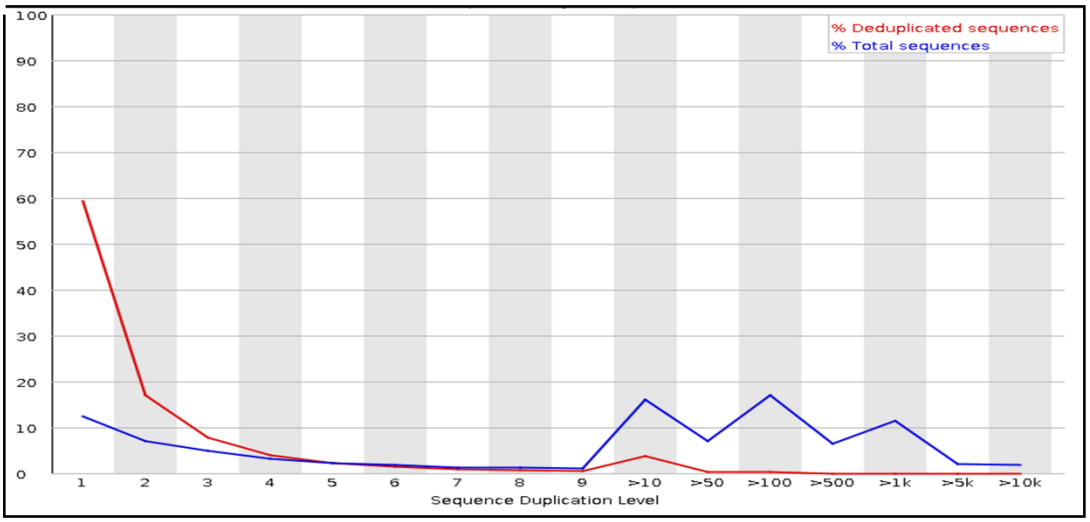

b.

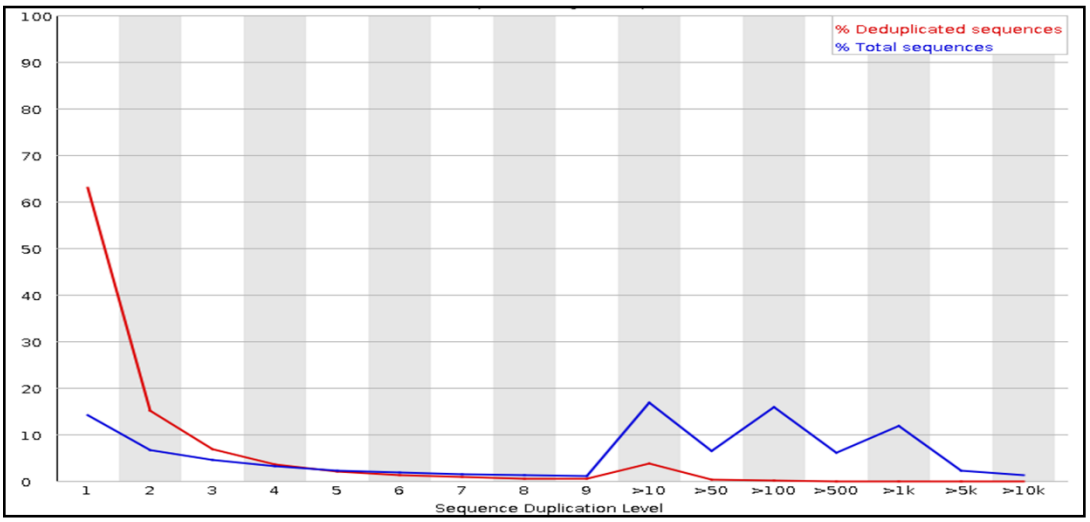

Figure 3.5. Duplication levels of single-end RNA-Seq reads.
Comparison of sequence duplication between **a.** raw 75 bp and **b.** processed 63 bp single-end reads. Sequence duplication levels report from FastQC calculates sequence duplication levels (x axis) for a percentage of reads (y axis) of the total sequences (blue) and deduplicated sequences (red). Graphs were generated by FastQC v0.72+galaxy 1.

The confirmation of read correction from the quality assessments allowed for alignment against the UCSC *Mus musculus* mm10 reference genome through HISAT2 [643] v2.1.0. This tool uses a whole genome index for read alignment and local FM index for alignment extension to accurately map sequences with a reduced run time and memory requirement compared to other programs [643,728] such as TopHat2 [692] and STAR [693]. With the wet-lab sequencing performed at a separate facility (in collaboration with Professor Peter Claus and Dr Lisa Walter, Hannover Medical School), we first had to determine if the reads were aligned to the genomic forward or reverse strand. Preliminary alignment through the *-unstranded* read setting was initially used to decipher if the sequence reads were in the forward or reverse direction. Analysis of these preliminary alignments through RSeQC [644] determined a dominant reverse strand pattern of up to 90% (Figure 3.6.a). With a reverse strand alignment pattern known, the single reads for each sample were again mapped using HISAT2 [643] v2.1.0 with alignment set at *-reverse* strand. Through these altered parameters, we identified an average of 80.8% single-end reads that were uniquely mapped to the UCSC *Mus musculus* mm10 genome across the 11 samples (Figure 3.6.b).

a.

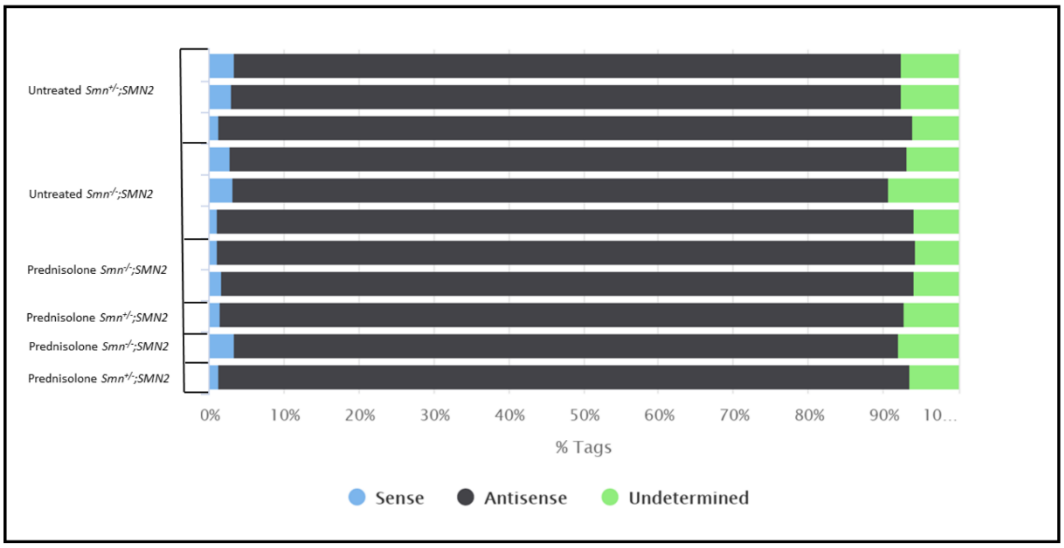

b.

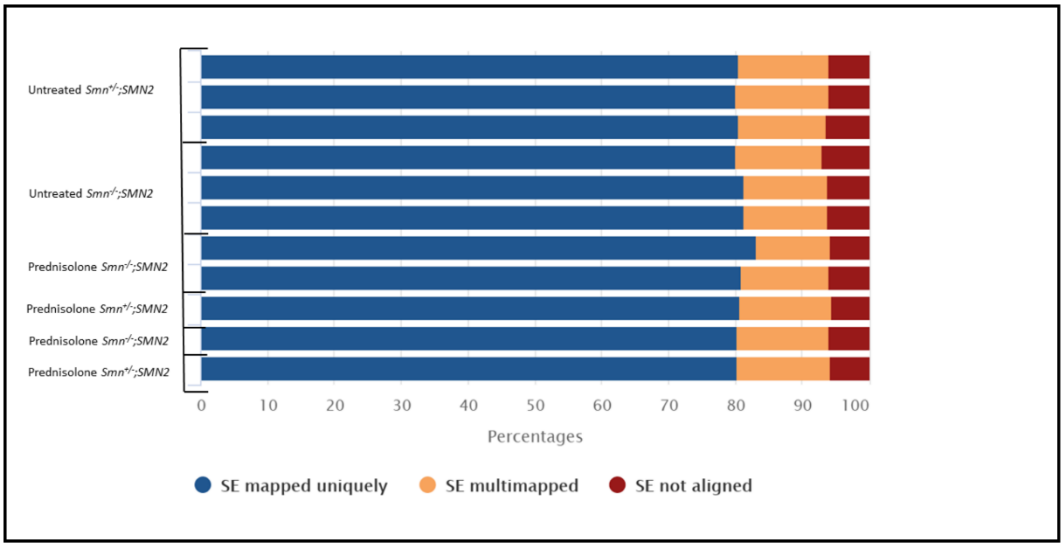

Figure 3.6. Single-end read alignments of sample groups to mm10 *Mus musculus* genome. Alignment software used for the single-end reads was HISAT2 v2.1.0. **a.** Percentage of forward (sense, blue), reverse (antisense, black) and undetermined (green) single-end strands aligned to the UCSC mm10 *Mus musculus* genome. Strands measured through RSeQC function of Infer experiment v2.6.4.1. **b.** Percentage alignment score for the anti-sense single strand reads against UCSC mm10 *Mus musculus* genome. Alignment scores were separated into three categories: mapped uniquely (blue), multi mapped (orange), and not aligned (red). Graphs were generated by MultiQC v1.6.

We next wanted to determine the read distribution of the alignments across the mm10 genome structure to identify the proportion that fall within post-spliced mRNA transcript regions (exons, 5' untranslatable regions (UTR) and 3' UTR). To do this, the *read_distribution.py* function in RSeQC [644] assigned the HISAT2 aligned BAM files to an mm10 BED12 reference file. On average, 90.37% of the aligned reads were matched to a post-spliced mRNA structure with 66.35% of these in coding domain regions, 9.45% in 5' UTR and 24.20% in 3' UTR (Figure 3.7.a). Furthermore, we identified that 2.97% of total read distributions aligned to intronic regions, which could be associated with pre-spliced mRNA samples and alternatively spliced mRNA with intron retention (Figure 3.7.a).

As we wanted to focus on the identification of known genes instead of novel transcripts, we omitted the use of StringTie [696] for transcript construction and instead used FeatureCounts [646] v1.6.3+galaxy2 to summarise the genes aligned with our single reads. Using the exons of Entrez *Mus musculus* mm10 GTF as reference, we identified that 60.55% of reads were aligned to known genes (Figure 3.7.b), which was similar to the 66.35% of coding domains in the HISAT2 read distribution (Figure 3.7.a). Furthermore, FeatureCounts quantified the total counts of known gene reads, which averaged around 32 million across the 11 samples (Table 3.2). Overall, the quality assessments, read alignments and count distributions conducted allowed for quantifiable data that minimises the risks of false results and that are appropriate for further DGE analysis to address our experimental question.

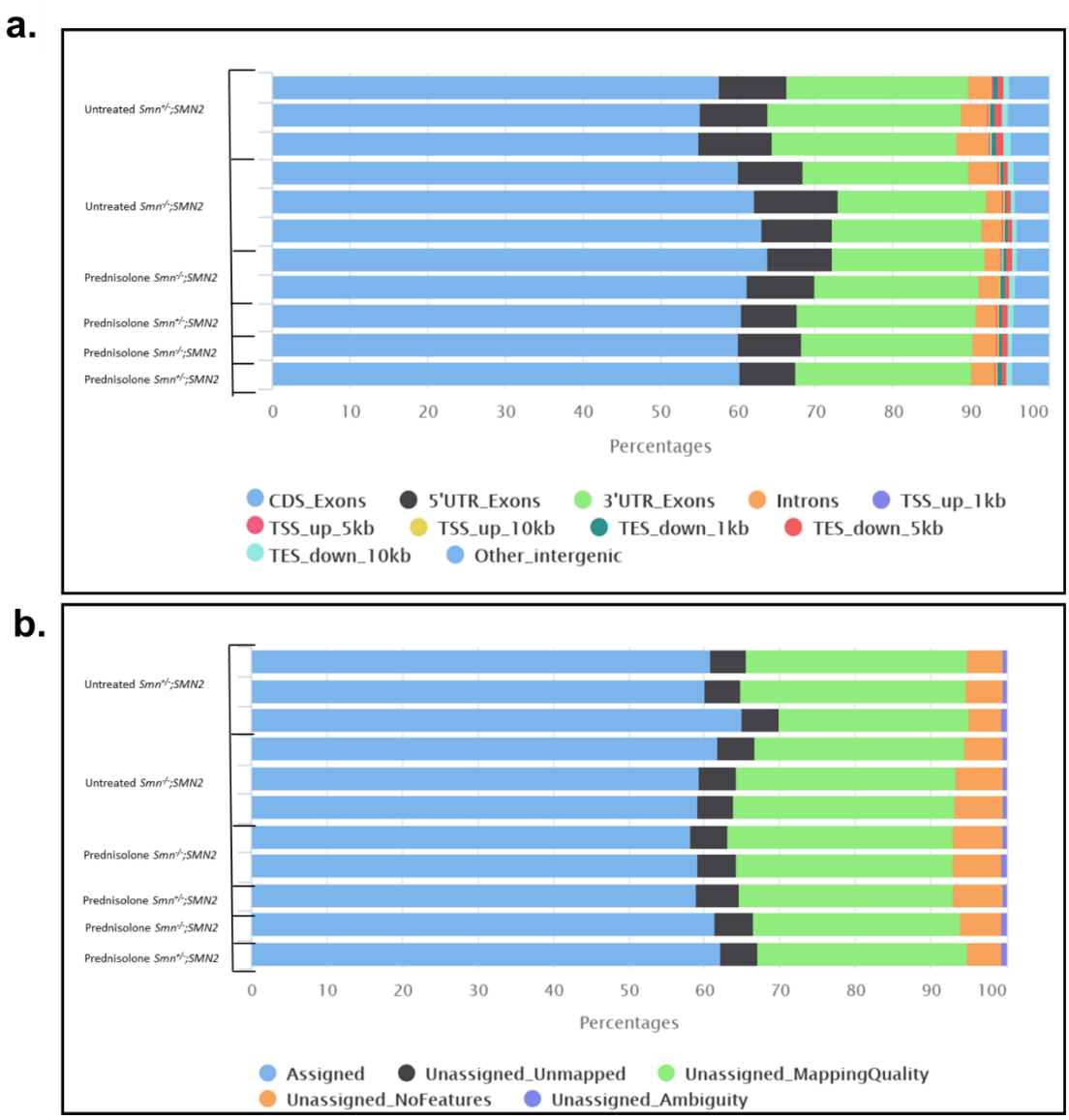

Figure 3.7. Genomic features and read count distribution of aligned single-end reads to mm10 *Mus musculus* genome.
Alignment software used for the single-end reads was HISAT2 v2.1.0.
a. Distribution of single strand mapped reads across UCSC mm10 *Mus musculus* genome. Genomic features include coding sequence (CDS)_exons (blue), 5'untranslatable region (UTR)_exons (black), 3'UTR_exons (green), introns (orange), transcriptional start site (TSS)_up_1kb (purple), TSS_up_5kb (pink), TSS_up_10kb (yellow), transcriptional end site (TES)_down_1kb (jade), TES_down_5kb (red), TES_down_10kb (light blue) and other intergenic regions (blue). Read distribution was measured by read_distribution.py function of RSeQC.
b. Count distribution was analysed by FeatureCounts v1.6.3+galaxy2 using a built-in mm10 *Mus musculus* Entrez gene annotation file (GTF). Read counts were summarised by percentages of assigned (blue), Unassigned_Unmapped (black), Unassigned_Mapping Quality (green), Unassigned_NoFeatures (orange) and Unassigned_Ambiguity (purple). Graphs were generated by MultiQC v1.6.

Table 3.2. Proportion of reads assigned to known genes in the Entrez Mus musculus mm10 genome through FeatureCounts.

Sample name	Percentage reads assigned (%)	Number of reads assigned (Million)
N0597	60.90%	20.8
N0598	60.20%	24.7
N0599	65.00%	30.6
N0600	61.80%	29
N0601	59.30%	36.6
N0602	59.10%	38.9
N0603	58.20%	36.3
N0604	59.10%	25.7
N0605	58.90%	37.6
N0606	61.50%	42.4
N0607	62.10%	28.9
Average	60.55%	31.95

3.2.2. Differential gene expression analysis

3.2.2.1 Genes related to atrophy, metabolism and function are dysregulated in untreated SMA triceps muscle.

We first set out to compare the transcriptomic patterns between SMA and healthy triceps in order to identify tissue-specific genes that are affected by the disease. For DGE analysis, we used a negative-binomial GLM, due to the data being count based and the sample mean and variance not being equal [710]. DESeq2 [647] v2.11.40.2 was selected as the DGE tool as its internal MoR normalisation method corrects for RNA composition and library size biases between samples (Table 3.2) and its focus on sequencing depth and RNA composition makes it suitable for gene count comparison between samples [50]. Furthermore, DESeq2 [647] v2.11.40.2 performs two separate shrinkage-dispersion stages to filter low counts and higher dispersions and is able to analyse study designs with multiple biological factors [647], which in our case was condition (healthy or SMA) and treatment (prednisolone or untreated).

Initially, we quality assessed the data to determine the degree of influence that "condition" had between untreated *Smn*$^{-/-}$*;SMN2* SMA and *Smn*$^{+/-}$*;SMN2* healthy mice. Through PCA, we identified stronger variation (PC1: 82%) between *Smn*$^{+/-}$*;SMN2* healthy (red) and *Smn*$^{-/-}$*;SMN2* SMA (blue) mice, which suggests that the "condition" i.e., healthy and SMA skeletal muscle highly influenced DGE variation (Figure 3.8.a). Another quality control measure that we analysed was dispersion estimations. Dispersions play an important role in RNA-Seq data as they can over- and under-estimate read count distribution, which can result in false positives or undetected known genes [729]. Within these conditions, the estimated

genes followed a similar dispersion shrinkage pattern to the fitted line from 1e+00 to 1e-02 when the mean of normalised counts increased (Figure 3.8.b), which indicated that a high proportion of known genes will have their FDR <0.05. Furthermore, the MA scatter plots displayed a higher proportion of DEGs (red) compared to non-DEGs (black) in untreated *Smn*$^{-/-}$*;SMN2* SMA mice (Figure 3.8.c). However, MA plots do not take significant (*p* <0.05) DEGs into account. Instead, a histogram of *p*-values from 0 to 1 showed a higher frequency of DEGs around *p* <0.05 (Figure 3.8.d) suggesting that most of the genes identified in the MA plot (Figure 3.8.c) were significant. Nevertheless, we wanted to filter significance based on FDR <0.05 and Log2(FC) >0.6 to minimise false results and low expressed genes. Through these filters, a total of 4144 DEGs were identified, with 2102 upregulated and 2042 downregulated in untreated *Smn*$^{-/-}$*;SMN2* SMA mice relative to untreated *Smn*$^{+/-}$*;SMN2* healthy mice (Figure 3.8.e).

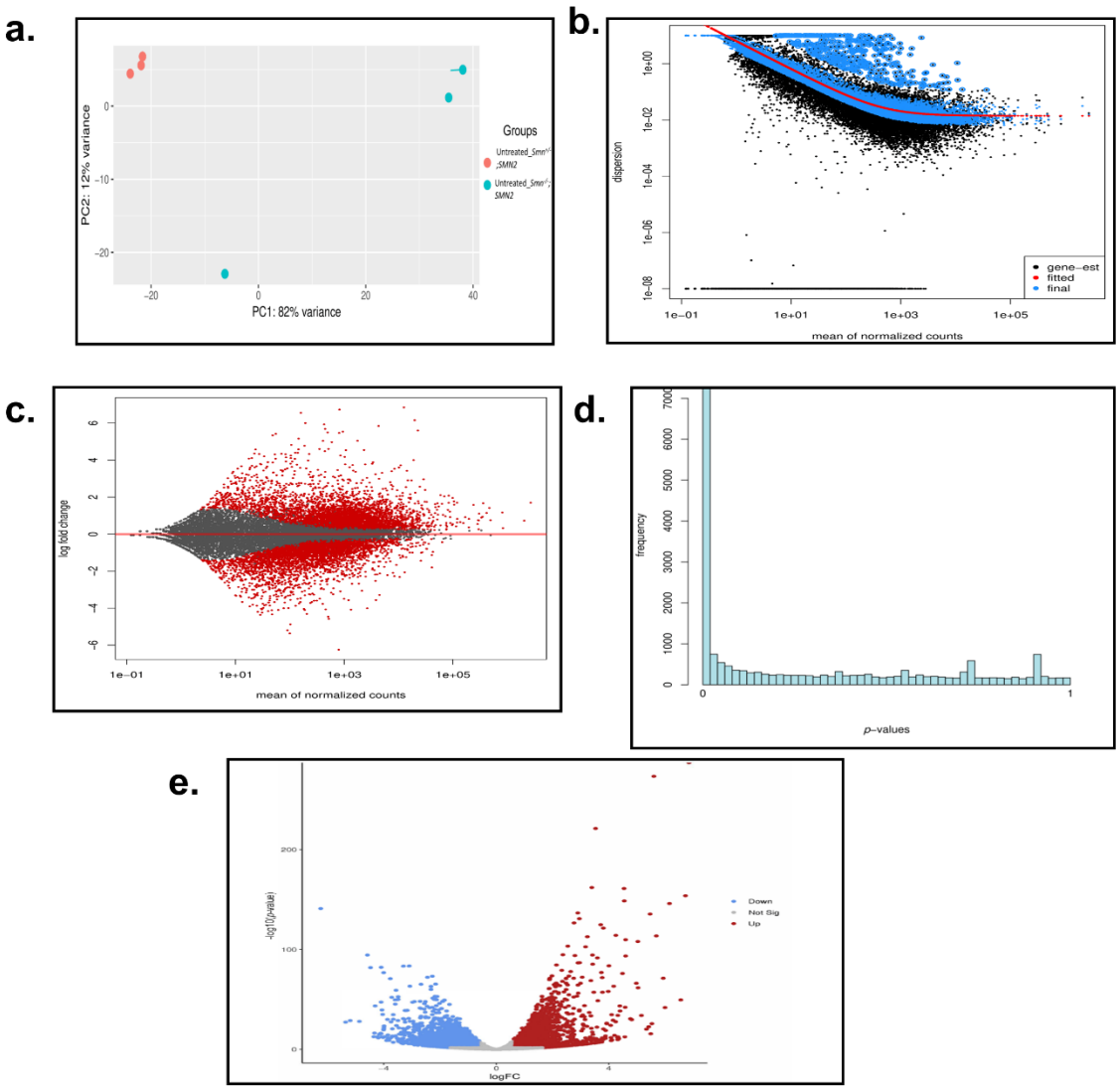

Figure 3.8. Differential gene expression analysis in skeletal muscle (Triceps) between untreated *Smn*$^{+/-}$*;SMN2* healthy and *Smn*$^{-/-}$*;SMN2* SMA mice.

DGE analysis was performed through DESeq2 v2.11.40.2 with the study design set to "condition".

a. PCA between untreated *Smn*$^{+/-}$*;SMN2* healthy (orange, n=3) and *Smn*$^{-/-}$*;SMN2* SMA mice (turquoise, n=3). **b.** Shrinkage estimation of dispersion. Maximum likelihood estimates (MLE) for the dispersion (y-axis) and mean expression level (x-axis) plotted for each gene (black). These genes are further plotted against a fitted MLE model (red), which predicts the final dispersion estimates (blue). **c.** MA plot for visual representation of the average normalised counts across all samples (x-axis) against the log2 fold change of normalised counts (y-axis) for each gene (black). Genes with adjusted *p* value below the default threshold of 0.1 are shown in red. **d.** Histogram plot for the frequency of genes (y-axis) that fall within a certain *p* value threshold for significance between 0 and 1 (x-axis). **e.** Volcano plot for the visualisation of significant upregulated (red) and downregulated (blue) genes based on parameters of *p* <0.05 (y-axis) and log fold change >0.6 (x-axis). Non-significant genes are highlighted in grey. Graph was generated by DeEeq2 v2.11.40.2.

Focusing on the top 20 up- and down-regulated DEGs in untreated *Smn*$^{-/-}$*;SMN2* SMA mice (Table 3.3), we observed that a certain number of those upregulated are well described pro-markers of muscle atrophy associated with metabolic, starvation or induced muscle-wasting (*Mt1* [730,731] and *Mt2* [730,731]), chronic-GC induced atrophy (*Fkbp5* [368] and *Serpina3n* [732]) as well as denervation (e.g. spinal cord injury (SCI), immobilisation and NMD) (*Fbxo32* [359,731,733–735] and *Arrdc2* [736,737]).

Furthermore, *Grem2* [738] was downregulated, which could potentially impact SMA muscle size as one previously described role for this gene is the antagonistic modulation of myostatin, a negative regulator of skeletal muscle growth [505,738] (Table 3.3). In addition to atrophy, certain DEGs displayed similar patterns to those observed in metabolic diseases, especially in cases of impaired glucose metabolism and insulin resistance (e.g. *Fkbp5* [739]). Genes linked to regulatory skeletal muscle functions and processes such as myoblast proliferation (e.g. *Aldh1a1* [740]), fast MHC protein synthesis (e.g. *Peg10* [741]) and mitochondrial regulation (e.g. *Apln* [742]) were also dysregulated (Table 3.3). Although these are only a few examples from the 4144 identified DEGs, they strongly indicate that genes associated with muscle size, metabolism, and function are dysregulated in SMA muscle.

Table 3.3. Top 20 significant up- and down-regulated genes in the skeletal muscle (Triceps) from untreated Smn$^{-/-}$;SMN2 SMA mice vs untreated Smn$^{+/-}$;SMN2 healthy mice

Upregulated		**Downregulated**	
Gene	**Log2(FC)**	**Gene**	**Log2(FC)**
Mt2	6.849	*Prnd*	-6.244
Fam46b	6.728	*Tmem72*	-5.362
Gm11827	6.555	*Pimreg*	-5.197
Mt1	6.154	*Pbk*	-4.873
E230001N04Rik	6.000	*Apln*	-4.579
Ankrd55	5.929	*Peg10*	-4.463
Fkbp5	5.842	*Bard1*	-4.362
Angptl7	5.685	*Melk*	-4.335
Fbxo32	5.600	*Pclaf*	-4.312
Klk1b26	5.537	*Neil3*	-4.239
Krtap16-3	5.492	*Ska3*	-4.200
Arrdc2	5.465	*Cenph*	-4.160
Gck	5.417	*Bub1*	-4.114
LOC100862287	5.337	*Cenpf*	-4.100
Nell2	5.159	*Btbd17*	-4.099
Aldh1a1	5.039	*A930003A15Rik*	-4.081
1700011I03Rik	5.038	*Chrna4*	-4.072
Serpina3n	4.968	*Grem2*	-4.068
Prima1	4.822	*Slc17a7*	-4.044
E030003E18Rik	4.774	*Sapcd2*	-4.027

3.2.2.2 Prednisolone decreases the expression of genes associated with atrophy and pathology and increases the expression of ergogenic genes in SMA triceps muscle

We next wanted to determine the impact of prednisolone on the dysregulated genes in muscle of *Smn*$^{-/-}$*;SMN2* SMA mice. In this case, the variable factor was "treatment" (prednisolone or untreated) with SMA pathology as the fixed factor. Initial quality assessment identified anomalies with the dataset. Firstly, the PCA displayed similar variances between groups (PC1: 48%) and within groups (PC2: 36%) alongside a skewed cluster pattern, suggesting that intragroup variances influenced the transcriptomic pattern (Figure 3.9.a). Secondly, there was a reduced dispersion shrinkage slightly above 1e-02 (Figure 3.9.b), implying an increased risk of false results. Thirdly, the MA and histogram plots displayed both a lower proportion of DEGs and significant (p <0.05) frequencies (Figures 3.9.c-d), which altogether indicates the presence of an outlier. A Grubbs test was performed across the normalised read counts, which identified prednisolone-treated *Smn*$^{-/-}$*;SMN2* SMA mouse sample N0603 as the outlier.

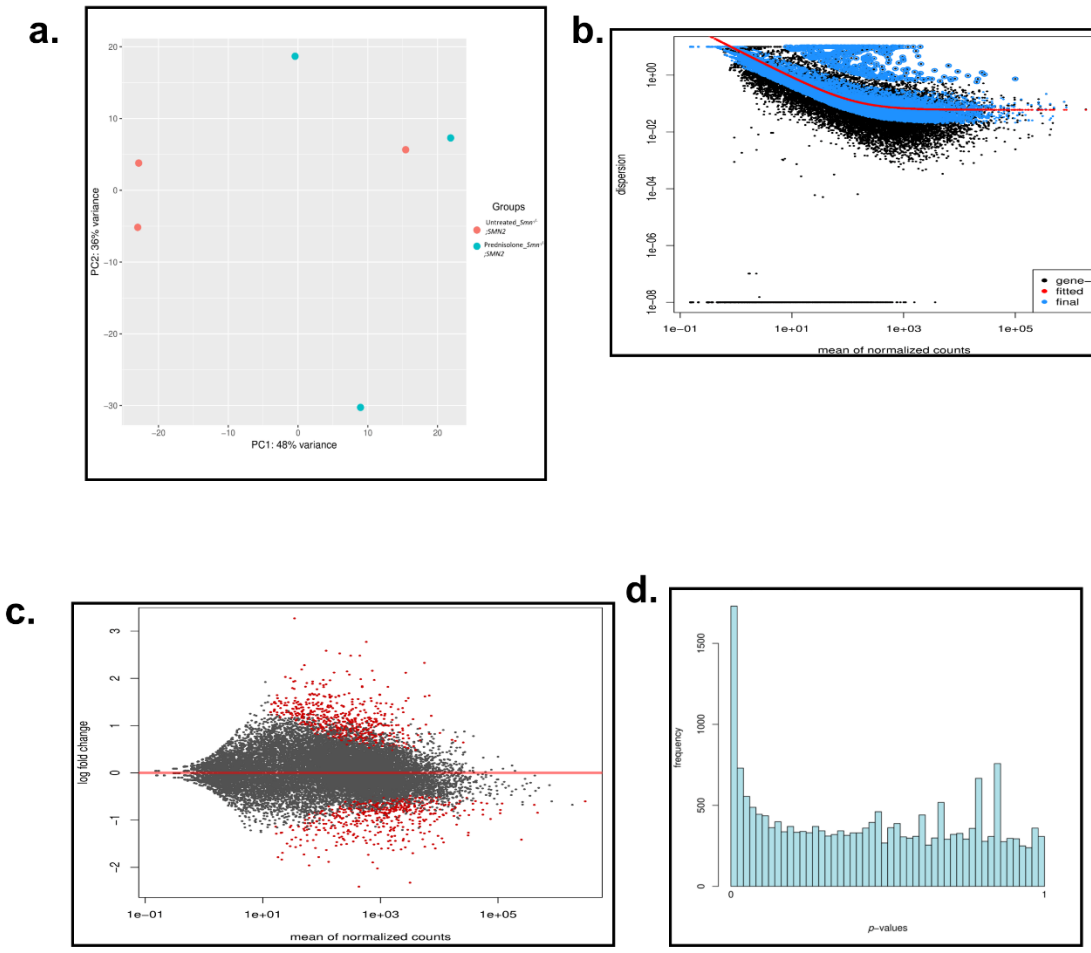

Figure 3.9. Outlier presence in skeletal muscle (Triceps) from prednisolone-treated *Smn*$^{-/-}$;*SMN2* SMA mice when compared against untreated *Smn*$^{-/-}$;*SMN2* SMA mice in differential gene expression analysis.
DGE analysis was performed through DESeq2 v2.11.40.2 with the study design set to "treatment". **a.** PCA between prednisolone-treated *Smn*$^{-/-}$;*SMN2* SMA mice (turquoise, n=3) and untreated *Smn*$^{-/-}$;*SMN2* SMA mice (orange, n=3). **b.** Shrinkage estimation of dispersion. Maximum likelihood estimates (MLE) for the dispersion (y-axis) and mean expression level (x-axis) plotted for each gene (black). These genes are further plotted against a fitted MLE model (red), which predicts the final dispersion estimates (blue). **c.** MA plot for visual representation of the average normalised counts across all samples (x-axis) against the log2 fold change of normalised counts (y-axis) for each gene (black). Genes with adjusted *p* values below the default threshold of 0.1 are shown in red. **d.** Histogram plot for the frequency of genes (y-axis) that fall within a certain *p* value threshold for significance between 0 and 1 (x-axis). Graph was generated by DESeq2 v2.11.40.2.

Although removal of N0603 in the prednisolone-treated *Smn*$^{-/-}$*;SMN2* SMA group leaves a smaller sample size (N=2) and reduces replicability, the removal was necessary as inclusion of the outlier produced 250 DEGs (Log2(FC) >0.6, FDR <0.05). A risk of using 250 DEGs for subsequent pathway analysis is that it would result in a low output of significant pathways (p <0.05) and drug candidates. Despite the N=2 sample size for the prednisolone-treated *Smn*$^{-/-}$*;SMN2* SMA mice, previous evidence has shown DESeq2 is a useful tool for low replicate RNA-Seq [743] and thus this group can still be compared against untreated *Smn*$^{-/-}$*;SMN2* SMA mice (N=3). This modified experimental design produced higher intergroup variances (PC1: 68%) compared to sample group (PC2: 20%) with distinct clusters between prednisolone-treated and untreated *Smn*$^{-/-}$*;SMN2* SMA mice (Figure 3.10.a). Furthermore, quality assessments identified increased dispersion shrinkages (Figure 3.10.b) and a higher proportion of DEGs alongside higher significant (p <0.05) frequencies (Figures 3.10.c-d). These led to a total of 3056 DEGs (Log2(FC) >0.6, FDR<0.05) with 1486 upregulated and 1570 downregulated in prednisolone-treated *Smn*$^{-/-}$*;SMN2* SMA mice relative to their untreated counterpart (Figure 3.10.e), whereby the top 20 up- and down-regulated genes are listed in Table 3.4.

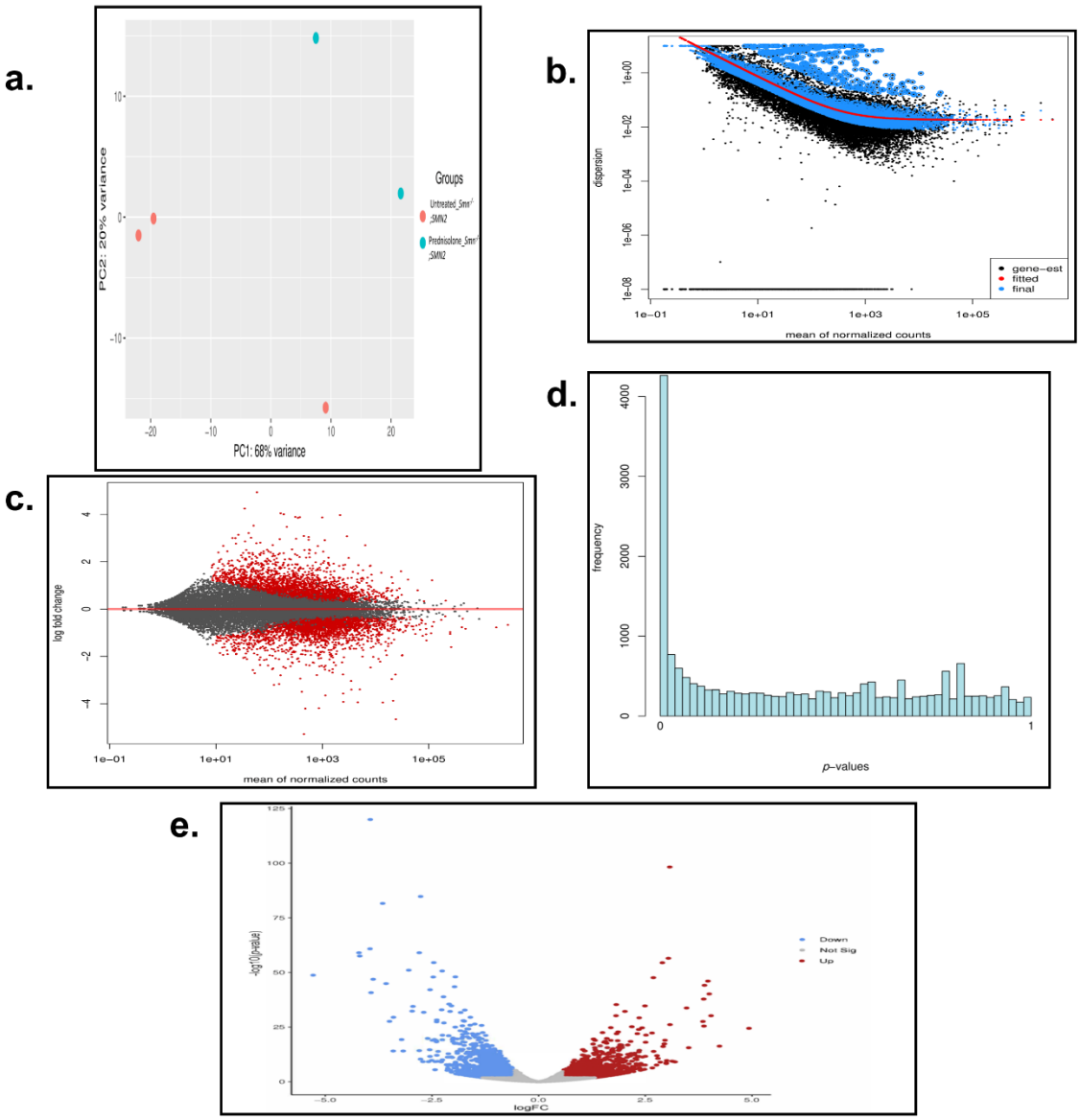

Figure 3.10. Differential gene expression analysis in skeletal muscle (Triceps) between prednisolone-treated and untreated *Smn*$^{-/-}$;*SMN2* SMA mice.
DGE analysis was performed through DESeq2 v2.11.40.2 with the study design set to "treatment". **a.** PCA between prednisolone-treated *Smn*$^{-/-}$;*SMN2* SMA (turquoise, n=2) and untreated *Smn*$^{-/-}$;*SMN2* SMA mice (orange, n=3). **b.** Shrinkage estimation of dispersion. Maximum likelihood estimates (MLE) for the dispersion (y-axis) and mean expression level (x-axis) plotted for each gene (black). These genes are further plotted against a fitted MLE model (red), which predicts the final dispersion estimates (blue). **c.** MA plot for visual representation of the average normalised counts across all samples (x-axis) against the log2 fold change of normalised counts (y-axis) for each gene (black). Genes with adjusted *p* values below the default threshold of 0.1 are shown in red. **d.** Histogram plot for the frequency of genes (y-axis) that fall within a certain *p* value threshold for significance between 0 and 1 (x-axis). **e.** Volcano plot for the visualisation of significant upregulated (red) and downregulated (blue) genes based on parameters of $p < 0.05$ (y-axis) and log fold change >0.6 (x-axis). Non-significant genes are highlighted in grey. Graph was generated by DESeq2 v2.11.40.2.

Table 3.4. Top 20 significant up- and down-regulated genes in the skeletal muscle (Triceps) from prednisolone-treated Smn$^{-/-}$;SMN2 SMA mice vs untreated Smn$^{-/-}$;SMN2 SMA mice.

Upregulated		**Downregulated**	
Gene	**Log2(FC)**	**Gene**	**Log2(FC)**
Orm3	4.935	***Ankrd55***	-5.281
Igha	4.243	***Angptl7***	-4.203
Slc17a7	4.046	***Arrdc2***	-4.185
Kcng4	4.004	***Mt2***	-3.946
Ky	3.970	***Fkbp5***	-3.939
Hdhd3	3.893	*8430408G22Rik*	-3.920
Grem2	3.881	***Mt1***	-3.875
A930003A15Rik	3.871	*Il6ra*	-3.648
Orm1	3.853	*Acot1*	-3.569
F830016B08Rik	3.524	*BB123696*	-3.491
Peg10	3.470	*Ddit4*	-3.402
Lep	3.207	*Igfn1*	-3.396
Best3	3.136	*Tmem252*	-3.205
Tnfaip2	3.085	*Slc10a6*	-3.166
Tfrc	3.075	*Cebpd*	-3.039
Map2k6	3.042	*Trim63*	-2.960
Ttbk1	3.010	*Hif3a*	-2.938
Orm2	2.999	*Hmgcs2*	-2.798
Tmem72	2.998	*Arhgap26*	-2.789
Fam212b	2.969	*Pdk4*	-2.765

*Genes highlighted in bold represent targets that were previously regulated in opposite pattern in Table 3.3 for untreated *Smn$^{-/-}$;SMN2* SMA mice.

Interestingly, prednisolone-treatment significantly downregulated the expression of atrogenes found to be upregulated in untreated SMA muscle (e.g. *Mt1* [730], *Mt2* [730], *Arrdc2* [736,737], *Fkbp5* [368]) (Tables 3.3-4). Additionally, genes related to atrophy were also identified as being significantly decreased by prednisolone (e.g. *Pdk4* [744], *Il6ra* [745–747], *Ddit4* [748,749], *Trim63* [734,735,750,751]) (Table 2.5). Conversely, *Grem2* [738], the antagonistic modulator of myostatin was significantly upregulated in prednisolone-treated muscle, supporting muscle health improvements at the transcriptional level (Table 3.4).

Prednisolone treatment also resulted in the upregulation of genes important for skeletal muscle contraction (e.g. *Peg10* [741]) and endurance (e.g. *Orm1* [752]) and the downregulation of negative regulators such as *Igfn1* [753], which impedes myosin-binding protein C synthesis in denervated fast- and slow-type skeletal muscle [753] (Table 3.4). Furthermore, prednisolone-treated SMA muscle displayed opposite expression patterns for genes that are dysregulated in muscle-wasting conditions such as myofibrillar myopathy (e.g. *Ky* [754,755]) and MG (e.g. *Cebpd* [756]), further supporting muscle health improvements (Table 3.4). Similarly, prednisolone-treatment in SMA muscle also restored the expression patterns of protein (e.g. *Ddit4* [757–759]), glucose (e.g. *Fkbp5* [739], *Hif3a* [760], *Pdk4* [761–763]) and FA (e.g. *Acot1* [764,765]) metabolism genes to levels previously observed in healthy muscle, suggesting an improvement in muscle metabolism. Genes whose activity are linked to inflammation and immune response (e.g. *Orm3* [766,767], *Il6ra* [768–770]) were also found to be downregulated upon prednisolone treatment, which could be attributed to the anti-inflammatory properties of GC drugs [625,626] (Table 3.4).

Although we observed that prednisolone inversed the expression pattern of a subset of the top 40 (20 upregulated and 20 downregulated) DEGs in the muscle

of untreated *Smn$^{-/-}$;SMN2* SMA mice (Tables 3.3-4), the extent to which prednisolone normalised the transcriptomic profile in SMA muscle was still unclear. A further DESeq2 analysis was thus conducted that implemented both "condition" and "treatment" as variable factors. Higher intergroup variability (PC1: 72%) was observed, with prednisolone-treated *Smn$^{-/-}$;SMN2* SMA, untreated *Smn$^{-/-}$;SMN2* SMA and untreated *Smn$^{+/-}$;SMN2* healthy mice separating into distinct clusters (Figure 3.11.a). Furthermore, the prednisolone-treated *Smn$^{-/-}$;SMN2* SMA mice were clustered in the middle of the other two groups (Figure 3.11.a). Based on the total of 1361 genes that overlapped between untreated *Smn$^{-/-}$;SMN2* SMA mice, untreated *Smn$^{+/-}$;SMN2* healthy mice and prednisolone-treated *Smn$^{-/-}$;SMN2* SMA mice (Figure 3.11.b), heatmap analysis showed that prednisolone treatment normalised the expression of a subset of genes in SMA skeletal muscle to levels similarly observed in untreated *Smn$^{+/-}$;SMN2* healthy mice (Figure 3.11.c).

Overall, we have shown that there is a predicted dysregulation in the transcriptomic pattern of genes linked to size, metabolism, and function in SMA skeletal muscle that is attenuated upon prednisolone treatment. Furthermore, we identified perturbations in transcripts linked to the anti-inflammatory and immune response of prednisolone treatment. Importantly, we have observed that prednisolone normalises the transcriptomic profile of a subset of genes in SMA skeletal muscle towards that of healthy controls.

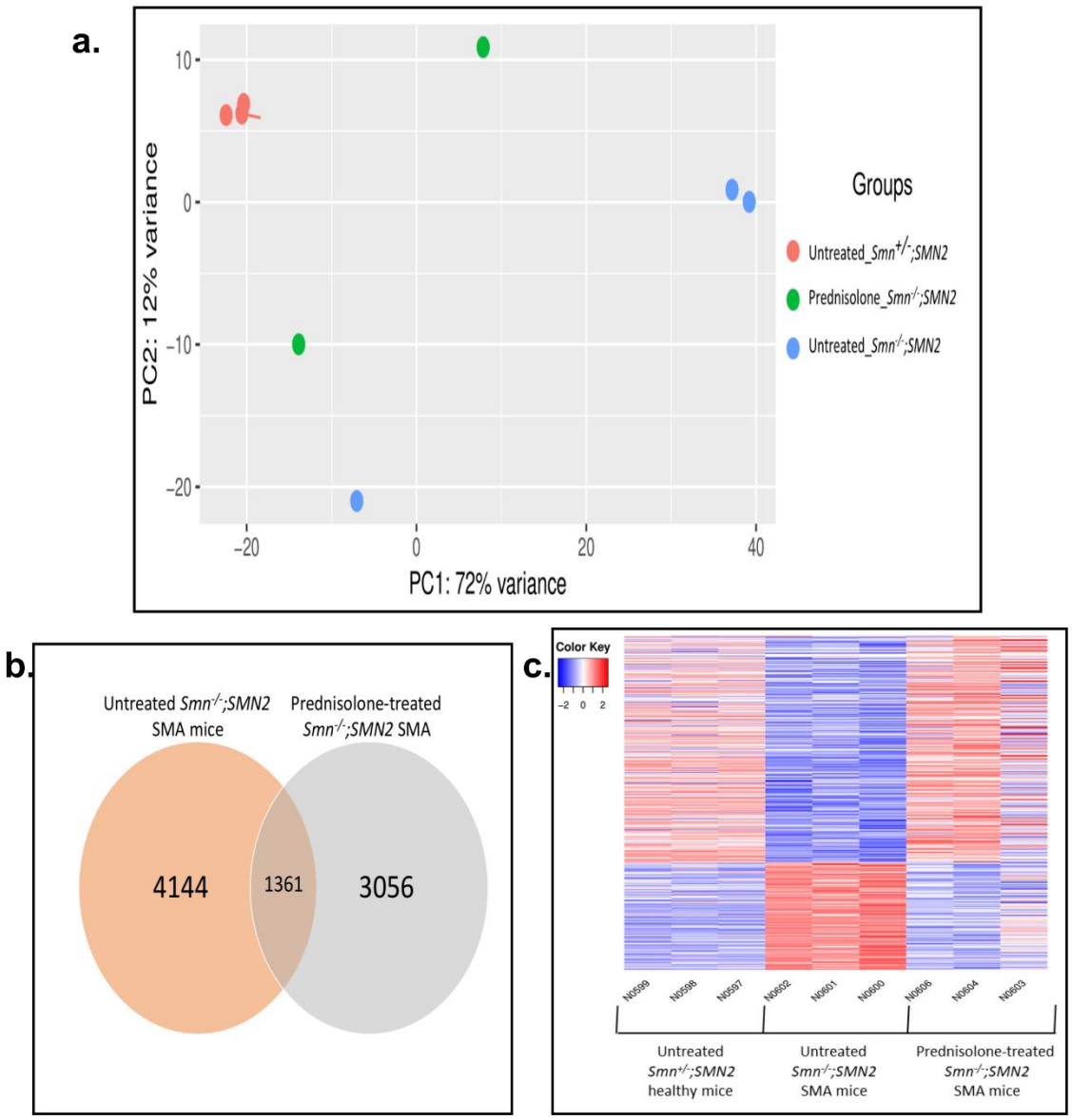

Figure 3.11. Prednisolone-treatment in *Smn$^{-/-}$;SMN2* SMA mice normalises the transcriptomic profile of specific genes in skeletal muscle (Triceps) to levels observed in untreated *Smn$^{+/-}$;SMN2* healthy mice.
DGE analysis was performed through DESeq2 v2.11.40.2 with the study design set to "condition" and "treatment". **a.** PCA between untreated *Smn$^{+/-}$;SMN2* healthy mice (red, n=3), untreated *Smn$^{-/-}$;SMN2* (blue, n=3) and prednisolone-treated *Smn$^{-/-}$;SMN2* SMA mice (green, n=2). PCA graph was generated by DESeq2 v2.11.40.2. **b.** Venn diagram for the total number of significantly regulated genes (Log2FC >0.6 or -0.6; FDR <0.05) in untreated *Smn$^{-/-}$;SMN2*SMA mice (orange circle), prednisolone-treated *Smn$^{-/-}$;SMN2* SMA mice (grey circle) and the overlap of specific genes significantly regulated in untreated *Smn$^{-/-}$;SMN2* SMA mice that is targeted by prednisolone. **c.** Heatmap visualisation for significant differentially expressed specific genes (Log2FC >0.6; FDR <0.05) between untreated *Smn$^{+/-}$;SMN2* healthy mice (left), untreated *Smn$^{-/-}$;SMN2* SMA mice (centre), and prednisolone-treated *Smn$^{-/-}$;SMN2* SMA mice (right). Upregulated genes highlighted in red and downregulated genes highlighted in blue. Heatmap was generated by Heatmap2 v2.2.1+galaxy1.

3.2.3. Pathway analysis

3.2.3.1. Impact analysis predicts that prednisolone treatment in *Smn$^{-/-}$;SMN2* SMA mice targets skeletal muscle size, metabolic and regulatory pathways.

We next wanted to identify the biological pathways associated with the DEGs in prednisolone treated SMA muscle. Pathway analysis was performed with iPathwayGuide [651–654], a GUI software, which implements a novel technique called impact analysis. A third-generation tool, impact analysis utilises a combination of enrichment (over-representation of DEGs and their perturbations) and topology (gene position and pathway structure) to identify significant perturbed pathways catalogued in the KEGG database [651–653]. Based on the 3056 significant DEGs (Log2(FC) >0.6, FDR: <0.05) between prednisolone-treated *Smn$^{-/-}$;SMN2* vs untreated *Smn$^{-/-}$;SMN2* SMA mice, a total of 28 significant KEGG pathways (p <0.05) were identified, 23 of which were calculated by impact analysis (Table 3.5). Similar to the top DEG lists (Tables 3.3-4), the pathways influenced by prednisolone were associated with skeletal muscle metabolism (e.g. HIF-1 signalling [771], Pentose and glucuronate interconversions [772], 2-Oxocarboxylic acid metabolism [773], Apelin signalling [742], Mannose type O-glycan biosynthesis [774] and Peroxisome-activator receptor (PPAR) signalling [775]) and regulatory processes (e.g. FoxO signalling [363] and circadian rhythm [776–778]) (Table 3.5). Furthermore, some of these pathways have previously been reported as being dysregulated in various SMA models and patients (e.g. FoxO signalling [56], longevity regulating pathway [53,56,389,767,779–783], p53 signalling [779,780], AMPK signalling [389,781,782], mitophagy [388,784], circadian rhythm [356], PPAR signalling [389], autophagy – animal [56,389]) (Table 3.5). On the other hand, we also identified pathways associated with non-NMDs such as AD and various cancers (Table

3.5). Although in these examples, the DEGs overlap with conserved pathways such as mitochondrial dysregulation in AD [785] and mTOR signalling in cancer [786]. Overall, impact analysis has predicted that prednisolone treatment attenuates SMA skeletal muscle pathology by targeting pathways linked to size, metabolism, and regulatory function. Importantly, some of these key pathways targeted are also reported as dysregulated in SMA.

Table 3.5. Top significant KEGG pathways identified through impact analysis that are targeted by prednisolone in the skeletal muscle (Triceps) from prednisolone-treated Smn$^{-/-}$;SMN2 SMA mice.

KEGG ID	Pathway name	#Genes (DE/All)	*p* value
04066	HIF-1 signalling pathway	30/91	0.001
05214	Glioma	25/71	0.002
04213	Longevity regulating pathway - multiple species	24/57	0.003
04068	FoxO signalling pathway	41/116	0.003
04713	Circadian entrainment	23/73	0.004
04211	Longevity regulating pathway	30/83	0.004
04115	p53 signalling pathway	25/67	0.006
00040	Pentose and glucuronate interconversions*	8/15	0.007
05010	Alzheimer disease	19/158	0.008
04152	AMPK signalling pathway	37/110	0.008
04080	Neuroactive ligand-receptor interaction	23/118	0.011
05418	Fluid shear stress and atherosclerosis	38/125	0.013
05223	Non-small cell lung cancer	22/64	0.014
05034	Alcoholism	25/104	0.014
04744	Phototransduction	4/9	0.015
05215	Prostate cancer*	28/88	0.016
04137	Mitophagy - animal	22/61	0.018
04659	Th17 cell differentiation	18/72	0.024
03030	DNA replication*	13/35	0.026
05031	Amphetamine addiction	13/49	0.028
05200	Pathways in cancer*	110/434	0.031
04710	Circadian rhythm	12/29	0.033
01210	2-Oxocarboxylic acid metabolism*	7/16	0.039
04140	Autophagy - animal	36/123	0.041
04372	Apelin signalling pathway	34/121	0.045
05226	Gastric cancer	36/123	0.048
00515	Mannose type O-glycan biosynthesis*	8/20	0.048
03320	PPAR signalling pathway	20/56	0.048

*Over-representation only

3.2.3.2. Overrepresentation analysis predicts that prednisolone treatment in *Smn*$^{-/-}$*;SMN2* SMA mice targets skeletal muscle mass, metabolic and regulatory pathways.

We decided to validate the prediction by impact analysis that prednisolone targets skeletal muscle mass, metabolic and regulatory function pathways in *Smn*$^{-/-}$*;SMN2* SMA mice with the commonly used ORA [658], which predicts pathways in the GO database [656,657,713] based on the significant enrichment of DEGs through a hypergeometric model (Fishers exact test) [658,787]. Although ORA lacks the detailed pathway topology of impact analysis [651–653], its ability to categorise enriched DEG groups in certain pathways still makes it a useful validation tool [658]. To overcome the limitation in classical ORA of assumptions that genes annotated to certain pathways will also be also associated with their upstream counterparts, we implemented weight pruning, which assigned a weight score to each gene in a GO term based on their scores in neighbouring GO terms [788–790]. The main advantage of this is that it minimised the risk of false positives [788–790]. For ORA of the 3056 DEGs significantly modulated by prednisolone in SMA muscle, we focused on the enrichment of >5 genes in pathways related to the three GO term tiers of: biological processes, molecular functions, and cell components. In biological processes, 131 significant GO term pathways (>5 DEGs, p <0.05) were identified that overlapped with those previously observed in impact analysis such as circadian rhythm, autophagy, longevity (starvation response) and PPAR signalling (Tables 3.5-6). Furthermore, metabolic pathways related to glucose and FA metabolism were also identified (Table 3.6), alongside skeletal muscle processes related to myotube differentiation and sarcomere thin filament assembly (Table 3.6). The lower GO term tiers of molecular function and

cell components also identified pathways related to glucose (e.g. glucose transport [791] and insulin receptor binding [792]) and FA (e.g. cholesterol transport [793,794]) metabolism (Table 3.7). In addition, processes related to skeletal muscle mass (e.g. MAP kinase phosphatase activity [795]), regulation (e.g. Protein tyrosine/serine/threonine phosphatase activity [796]) and contraction [797] (e.g. M band [210] and Z disc [203]) were also identified (Tables 3.7-8). Across these three tiers, we see that similar to impact analysis, ORA predicts that prednisolone treatment in *Smn*$^{-/-}$*;SMN2* SMA mice targets pathways related to skeletal muscle mass, metabolism, and regulation.

Table 3.6. Top 25 significant GO biological process terms with weight pruning and >5 DGE components that are targeted by prednisolone in the skeletal muscle (Triceps) from prednisolone-treated $Smn^{-/-}$;SMN2 SMA mice.

GO ID	GO Name	#Genes (DE/All)	*p* value (Weight)
GO:0000055	ribosomal large subunit export from nucleus	8/8	0.0000054
GO:0010830	regulation of myotube differentiation	25/53	0.000088
GO:0034504	protein localization to nucleus	81/247	0.00011
GO:0046320	regulation of fatty acid oxidation	17/32	0.00028
GO:0048662	negative regulation of smooth muscle cell proliferation	20/44	0.00045
GO:0031062	positive regulation of histone methylation	17/35	0.00046
GO:0046854	phosphatidylinositol phosphorylation	17/36	0.0007
GO:0016239	positive regulation of macroautophagy	26/64	0.00113
GO:0000083	regulation of transcription involved in G1/S transition of mitotic cell cycle	8/12	0.00113
GO:0042594	response to starvation	49/148	0.00114
GO:0031398	positive regulation of protein ubiquitination	36/101	0.00115
GO:0090073	positive regulation of protein homodimerization activity	7/10	0.00157
GO:0048671	negative regulation of collateral sprouting	6/8	0.00208
GO:0007050	cell cycle arrest	40/121	0.00319
GO:1990830	cellular response to leukaemia inhibitory factor	37/110	0.00321
GO:1901215	negative regulation of neuron death	60/198	0.00378
GO:0007623	circadian rhythm	50/160	0.00378
GO:0061635	regulation of protein complex stability	6/9	0.00508
GO:0033137	negative regulation of peptidyl-serine phosphorylation	12/26	0.00533
GO:0032088	negative regulation of NF-kappaB transcription factor activity	22/59	0.00537
GO:0006094	gluconeogenesis	23/63	0.00604
GO:0001937	negative regulation of endothelial cell proliferation	15/36	0.00629
GO:0010715	regulation of extracellular matrix disassembly	7/12	0.00681
GO:0030240	skeletal muscle thin filament assembly	7/12	0.00681
GO:0035358	regulation of peroxisome proliferator activated receptor signalling pathway	7/12	0.00681

Table 3.7. Top 25 significant GO molecular function terms with weight pruning and >5 DGE components that are targeted by prednisolone in the skeletal muscle (Triceps) from prednisolone-treated $Smn^{-/-}$;SMN2 SMA mice.

GO ID	GO Name	#Genes (DE/All)	*p* value (Weight)
GO:0042802	identical protein binding	388/1498	0.000091
GO:0042826	histone deacetylase binding	37/107	0.0019
GO:0002151	G-quadruplex RNA binding	6/8	0.0021
GO:0034046	poly(G) binding	6/8	0.0021
GO:0008138	protein tyrosine/serine/threonine phosphatase activity	16/36	0.0023
GO:0016279	protein-lysine N-methyltransferase activity	21/53	0.0029
GO:0005355	glucose transmembrane transporter activity	7/11	0.0035
GO:0005179	hormone activity	16/38	0.0044
GO:0033549	MAP kinase phosphatase activity	7/12	0.0069
GO:1904047	S-adenosyl-L-methionine binding	5/7	0.0073
GO:0005251	delayed rectifier potassium channel activity	9/18	0.0083
GO:0019900	kinase binding	180/693	0.0084
GO:0035064	methylated histone binding	20/54	0.0086
GO:0043560	insulin receptor substrate binding	6/10	0.0105
GO:0043995	histone acetyltransferase activity (H4-K5 specific)	6/10	0.0105
GO:0043996	histone acetyltransferase activity (H4-K8 specific)	6/10	0.0105
GO:0046972	histone acetyltransferase activity (H4-K16 specific)	6/10	0.0105
GO:0008179	adenylate cyclase binding	7/13	0.0121
GO:0017127	cholesterol transporter activity	7/13	0.0121
GO:0005158	insulin receptor binding	10/22	0.0124
GO:0008270	zinc ion binding	141/540	0.0124
GO:0001968	fibronectin binding	12/29	0.0151
GO:0004303	estradiol 17-beta-dehydrogenase activity	5/8	0.0159
GO:0030235	nitric-oxide synthase regulator activity	5/8	0.0159
GO:0000980	RNA polymerase II distal enhancer sequence-specific DNA binding	25/75	0.0159

Table 3.8. Top 17 significant GO cell components terms with weight pruning and >5 DGE components that are targeted by prednisolone in the skeletal muscle (Triceps) from prednisolone-treated $Smn^{-/-}$;SMN2 SMA mice.

GO ID	GO Name	#Genes (DE/All)	*p* value (Weight)
GO:0031430	M band	13/21	0.000083
GO:0016363	nuclear matrix	29/82	0.0033
GO:0030018	Z disc	38/117	0.0047
GO:0008076	voltage-gated potassium channel complex	18/46	0.0058
GO:0005852	eukaryotic translation initiation factor 3 complex	8/15	0.0073
GO:0005730	nucleolus	191/748	0.0079
GO:0005801	cis-Golgi network	17/45	0.0107
GO:0005776	autophagosome	22/64	0.0139
GO:0043204	perikaryon	29/91	0.0164
GO:0044305	calyx of Held	9/20	0.0174
GO:0005615	extracellular space	223/881	0.0175
GO:0031932	TORC2 complex	6/12	0.0291
GO:0034045	phagophore assembly site membrane	6/12	0.0291
GO:0098982	GABA-ergic synapse	19/57	0.0295
GO:0101031	chaperone complex	8/19	0.0375
GO:0005783	endoplasmic reticulum	323/1343	0.0447
GO:0099524	postsynaptic cytosol	9/23	0.0453

3.2.3.3. DEGs targeted by prednisolone in SMA skeletal muscle are predicted to be associated with myopathies, neuromuscular and metabolic disorders.

An alternative dataset to gain further insight into the DEGs and pathways targeted by prednisolone in the skeletal muscle of *Smn*$^{-/-}$*;SMN2* SMA mice is the International Classification of Diseases (ICD) database. The iPathwayGuide used ORA [658] to annotate the 3056 DEGs significantly upregulated and downregulated in prednisolone-treated SMA muscle to diseases in the KEGG [655] ICD database, 10th revision (ICD-10) [798]. The DEGs were linked to 39 diseases (p <0.05), the majority of which are categorised into the following disease groups: “Congenital malformations, deformations, and chromosomal abnormalities” (dark blue), “diseases of the nervous system” (light blue), “Endocrine, nutritional, and metabolic diseases” (dark orange) and “neoplasms” (light orange) (Figure 3.12). Furthermore, most of the significant “diseases of the nervous system” terms are related to NMD and myopathies (Table 3.9). Interestingly, the muscular, metabolic and neuromuscular ICD conditions share similar pathways and patterns to those identified by impact (Table 3.5) and ORA (Tables 3.6-8) such as skeletal muscle metabolism, growth and regulation. Thus, this analysis provides evidence of an overlap between dysregulated pathways in SMA and additional muscle wasting, metabolic and neurodegenerative disorders, and conditions.

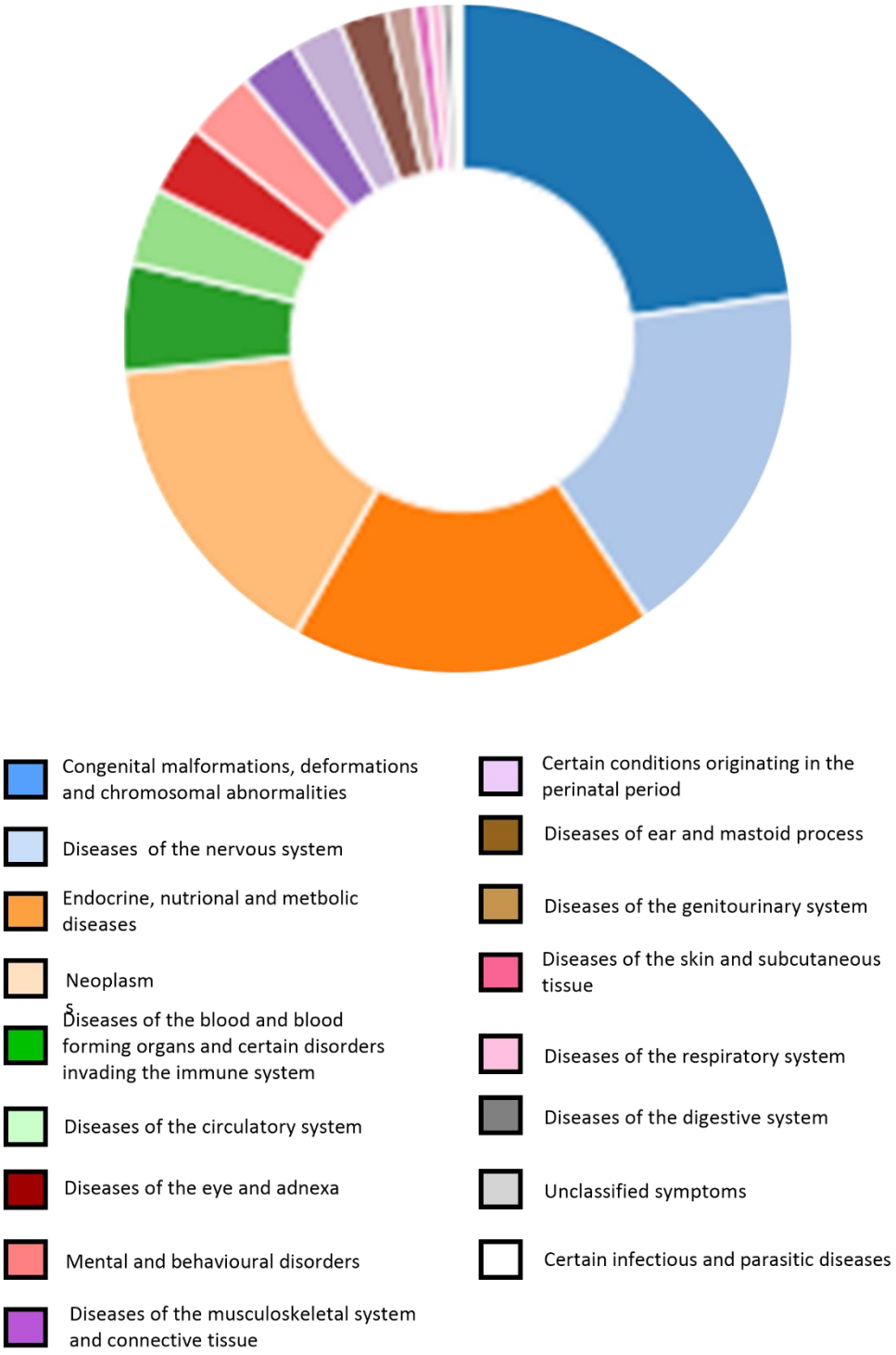

Figure 3.12. Predicted target genes of prednisolone in *Smn$^{-/-}$;SMN2* SMA mice are linked to related myopathies, neuromuscular and metabolic diseases.
A pie chart representation of diseases that are linked to the differentially expressed genes (Log2(FC) >0.6, FDR <0.05) targeted by prednisolone in prednisolone-treated *Smn$^{-/-}$;SMN2* SMA mice. Each coloured region of the pie chart represents a general disease category that falls under the International Classification of Diseases, 10th revision (ICD-10), which are highlighted in coloured keys.
Graph is an edited version of interactive figure generated in iPathwayGuide.

Table 3.9. Top 25 significant identified diseases from the KEGG database that the DEG identified in the skeletal muscle (Triceps) from prednisolone-treated $Smn^{-/-}$;SMN2 SMA mice are annotated towards.

KEGG ID	Disease Name	ICD-10 Disease Category	#Genes (DE/All)	*p* value
H00698	Nemaline myopathy	Diseases of the nervous system	8/14	0.004
H00720	Long QT syndrome	Diseases of the circulatory system	9/17	0.004
H00030	Cervical cancer	Neoplasms	5/7	0.007
H01225	D-2-hydroxyglutaric aciduria	Endocrine, nutritional, and metabolic diseases	3/3	0.010
H01370	SHORT syndrome	Congenital malformations, deformations, and chromosomal abnormalities	3/3	0.010
H01592	Medullary thyroid cancer	Neoplasms	3/3	0.010
H01193	Familial tumoral calcinosis	Diseases of the musculoskeletal system and connective tissue	7/13	0.011
H00058	Amyotrophic lateral sclerosis (ALS); Lou Gehrig disease	Diseases of the nervous system	12/29	0.013
H00055	Laryngeal cancer	Neoplasms	4/6	0.022
H00593	Limb-girdle muscular dystrophy	Diseases of the nervous system	13/35	0.026
H00120	Muscular dystrophy-dystroglycanopathy type A	Diseases of the nervous system	7/15	0.027
H02307	Muscular dystrophy-dystroglycanopathy	Diseases of the nervous system	7/15	0.027
H00529	Cranioectodermal dysplasia	Congenital malformations, deformations, and chromosomal abnormalities	3/4	0.034
H00910	Hirschsprung disease	Congenital malformations, deformations, and chromosomal abnormalities	3/4	0.034
H00916	Congenital central hypoventilation syndrome	Diseases of the nervous system	3/4	0.034
H02031	Inclusion body myopathy with Paget disease of bone and frontotemporal dementia	Diseases of the nervous system	3/4	0.034
H00020	Colorectal cancer	Neoplasms	11/30	0.042
H00014	Non-small cell lung cancer	Neoplasms	4/7	0.043
H00016	Oral cancer	Neoplasms	4/7	0.043
H00017	Esophageal cancer	Neoplasms	4/7	0.043
H01019	Catecholaminergic polymorphic ventricular tachycardia	Diseases of the circulatory system	4/7	0.043
H01613	Follicular lymphoma	Neoplasms	4/7	0.043

H00022	Bladder cancer	Neoplasms	5/10	0.044
H01959	Muscular dystrophy-dystroglycanopathy type C	Diseases of the nervous system	5/10	0.044
H00425	Lysosomal cysteine protease deficiencies	Congenital malformations, deformations, and chromosomal abnormalities	2/2	0.046

*International Classification of Diseases, 10th Edition (ICD-10)

3.2.4. Clinically approved drugs primarily used to treat muscle wasting, metabolic and inflammatory disorders are predicted to mimic the pharmacological activity of prednisolone in SMA muscle.

Our bioinformatics analyses suggest that the benefits of prednisolone in the skeletal muscle of *Smn*$^{-/-}$*;SMN2* SMA mice [53] are due to modulation of metabolic, regulatory and growth pathways (Tables 3.5-8). However, chronic administration of prednisolone compared to intermittent use risks the activation of GC-associated atrophy pathways which promote muscle wasting [628,630,637,749], indicating that this is not suitable as a long-term therapy in SMA [628,799–801]. We therefore set out to identify approved non-GC pharmacological compounds currently used to treat other disorders as a way to potentially target the same genes and pathways as prednisolone in SMA muscle, without increasing the risk of GC-associated muscle atrophy [628,630,637,749]. Predictively, this would allow for repositioned compounds that mimic the positive benefits of short-term prednisolone treatment in SMA muscle, whilst avoiding the adverse long-term GC-associated muscle wasting side effects [628,799–801].

The first approach relied on the integration of the KEGG pathway and drug databases in iPathwayGuide that annotates certain compounds to their respective protein targets in each pathway [654]. We thus analysed the KEGG drug candidates listed in iPathwayGuide that targeted the significant pathways (Table 3.5), which revealed a total of 6320 compounds, which we filtered further to generate a useable and valuable list of potential drugs. Firstly, we focused on compounds that targeted >4 significant pathways (Table 3.5), which left 2210 potential candidates. Secondly, we catalogued each drug in terms of efficacy, target(s), bioavailability, primary disease usage and regulatory status based on

up-to-date information from various databases (KEGG [655], Inxight: Drugs [660], BNF: NICE [661], DrugBank [662,663], clue.io cMap L1000 platform [664]). This allowed us to omit drugs primarily designed for cancer treatment as these often promote muscle wasting [802] and thus left us with 136 candidates, 58 of which targeted proteins encoded by the DEGs modulated by prednisolone (Table 3.10). The majority of these drugs were linked to metabolic (55), neuromuscular and neurodegenerative (17) and autoimmune and inflammatory (12) disorders (Table 3.10), supporting our bioinformatic analyses that predicted that prednisolone acts on pathways associated with inflammatory and metabolic pathways (Tables 3.5-8) as well as neuromuscular and metabolic disorders (Table 3.9). Notably, 71 of these compounds are already clinically approved such as Mecasermin, metformin and various forms of insulin (Table 3.10).

However, a caveat with only using the first approach is that the drugs were assigned based on their protein targets, not the modulation of gene expression patterns [654]. In addition, the pathways did not represent the entire 3056 DEGs identified in prednisolone-treated *Smn*$^{-/-}$*;SMN2* SMA mice. To ensure a complete and exhaustive list of potential drug candidates, we used the iPathwayGuide predicted upstream regulators derived from the list of DEGs following prednisolone treatment. We selected 308 upstream regulators that had >2 downstream targets and analysed them through DGIdb v3.0 [659], which predicts drug-gene interactions based on algorithms encompassing information from journals, databases, and online resources [659]. We therefore generated a list of drugs predicted to target and mimic the expression of the DEGs affected by prednisolone [659] (i.e. agonists for upregulated genes and antagonists for downregulated genes). We initially identified 125 agonist and 320 antagonist

drugs and again catalogued the compounds using the various databases and criteria described above. This generated a final list of 82 agonists (59 of these approved, 4 of these elicit) and 51 antagonists (28 of these approved) drugs, all of which targeted the DEGs (Tables 3.11-12). The majority of the agonists targeted androgynous genes such as *androgen receptor* (*Ar*) and *oestrogen receptor 1* (*Esr1*) (Table 3.11). Despite their gender-specific functions, both genes also play roles in skeletal muscle regulation (*Ers1* in metabolism [183–185] and *Ar* in anabolic growth and metabolism [803–805]). Indeed, anabolic steroids [806] and selective androgen receptor modulators (SARMs) [807] have been associated with approved drugs and clinical trials for NMD, myopathies and muscle-wasting-associated conditions (Table 3.11). On the other hand, the majority of the antagonistic drugs targeted *Endothelin receptor type B* (*Ednrb)*, *Catechol-O-methyltransferase* (*Comt)* and *Interleukin-6 receptor, alpha* (*Il6ra)* (Table 3.12). Although *Ednrb* drugs are used to treat vascular diseases, *Comt* and *Il6ra* have been associated with skeletal muscle mass regulation (Table 3.12). Indeed, *COMT* LOF polymorphisms are associated with greater skeletal muscle mass in elderly females [808] and *Il6ra* inhibition ameliorates muscle atrophy in murine models [745]. Similar to the iPathwayGuide approach, we found that the drugs identified with DGIdb v3.0 are primarily used to treat myopathies and muscle wasting (10), inflammatory disorders (24), metabolic diseases (8) and neuromuscular and neurodegenerative diseases (6) (Tables 3.11-12).

Finally, both approaches revealed drug candidates that have been previously investigated in SMA such as colforsin [809] and celecoxib [615] (ClinicalTrials ID: NCT02876094), further supporting the strength of our computational predictions (Tables 3.10-12). Although it should be noted that both colforsin and celecoxib's

potential usage in SMA therapeutics was as SMN-dependent drug candidates [615,809] rather than a muscle-specific SMN-independent treatment.

Overall, we have shown that drugs primarily used to treat metabolic, inflammatory, and muscle-wasting disorders are predicted to have similar pharmacological activities as prednisolone and have the potential to improve muscle pathologies in SMA.

Table 3.10. KEGG database drugs predicted to target components within the predicted iPathwayGuide KEGG pathways in skeletal muscle of prednisolone-treated $Smn^{-/-}$;SMN2 SMA mice.

Pathways	Drug	KEGG ID	Activity	Bioavailability	Disease(s)	Target(s)	Status
12	Leniolisib (USAN/INN)	D11158	Immunomodulator, PI3K Inhibitor	Oral	APDS, Lymphadenopathy, Immunodeficiency	*Pik3r1-3, Pik3cb*	Phase 3
	Leniolisib phosphate (USAN)	D11159	Immunomodulator, PI3K Inhibitor	Oral	APDS, Lymphadenopathy, Immunodeficiency	*Pik3r1-3, Pik3cb*	Phase 3
	Nemiralisib (USAN/INN)	D11267	Anti-asthmatic, Anti-inflammatory, Phosphatidylinositol 3-kinase inhibitor	Oral	COPD, Asthma	*Pik3r1-3, Pik3cb*	Phase 2
	Nemiralisib succinate (USAN)	D11354	Anti-asthmatic, Anti-inflammatory, Phosphatidylinositol 3-kinase inhibitor	Oral	COPD, Asthma	*Pik3r1-3, Pik3cb*	Phase 2
10	Ibutamoren mesylate (USAN)	D04491	Growth hormone releasing hormone receptor agonist	Oral	Fibromyalgia, Growth hormone deficiencies	*Igf1r, Egfr, Insr*	Phase 2
	Mecasermin (genetical recombination) (JAN)	D03297	Recombinant IGF-1	Subcutaneous	ALS, Type 1 and 2 diabetes mellitus	*Igf1r*	Approved
	Mecasermin rinfabate (USAN/INN)	D04870	Recombinant IGF-1	Intravenous	Chronic lung disease, Retinopathy	*Igf1r*	Phase 2
9	Lubeluzole (USAN/INN); Prosynap (TN)	D04789	Calmodulin inhibitor	Intravenous	Stroke	*Calm1-4*	Preclinical
	Teprotumumab (USAN/INN)	D09680	IGF-1R monoclonal antibody inhibitor	Intravenous	Graves diseases, Inflammatory disorders	*Igf1r*	Phase 3

8	Buformin (USAN/INN)	D00595	Biguanide hypoglycaemic agent, AMPK Agonist	Oral	Type 2 diabetes mellitus	*Prkag3*	Withdrawn
	Buformin hydrochloride (JP16)	D02206	Biguanide hypoglycaemic agent, AMPK Agonist	Oral	Type 2 diabetes mellitus	*Prkag3*	Withdrawn
	Metformin (USAN/INN)	D04966	Biguanide hypoglycaemic agent, AMPK Agonist	Oral	Type 2 diabetes mellitus	*Prkag3*	Approved
	Metformin hydrochloride (JP16/USP)	D00944	Biguanide hypoglycaemic agent, AMPK Agonist	Oral	Type 2 diabetes mellitus	*Prkag3*	Approved
	Phenformin hydrochloride	D08352	Biguanide hypoglycaemic agent, AMPK Agonist	Oral	Type 2 diabetes mellitus	*Prkag3*	Withdrawn
7	Colforsin (USAN/INN)	D03584	Adenylyl cyclase activator	Oral	Asthma	*Adcy1, Adcy6-7*	Phase 2
	Colforsin daropate hydrochloride (JAN)	D01697	Adenylyl cyclase activator	Oral	Acute heart failure	*Adcy1, Adcy6-7*	Approved
6	Iguratimod (JAN/INN)	D01146	Cyclooxygenase inhibitor	Oral	Rheumatoid arthritis	*Nfkb1*	Phase 4
	Pimagedine hydrochloride (USAN)*	D05479	Diamine oxidase, nitric oxide synthase inhibitor	Intravitreal, oral	Diabetic retinopathy and nephropathy	*Nos1-3*	Phase 1
	Tanzisertib (USAN)*	D10168	JNK Inhibitor	Oral	Idiopathic pulmonary fibrosis	*Mapk8-10*	Phase 2
	Tilarginine acetate (USAN)*	D09018	Nitric oxide synthase inhibitor	Intravenous	Obesity, Type 2 diabetes mellitus, Septic shock	*Nos1-3*	Phase 4

5	Acamprosate (INN) *	D07058	NMDA Receptor antagonist	Oral	Alcoholism, Addictive disorders	*Grin1, Grin2a-d*	Approved
	Acamprosate calcium (JAN/USAN) *	D02780	NMDA Receptor antagonist	Oral	Alcoholism, Addictive disorders	*Grin1, Grin2a-d*	Approved
	Acitretin (USP/INN); Soriatane (TN)	D02754	Retinoic acid receptor agonist	Oral	Psoriasis	*Rarb, Rxrb, Rxrg*	Approved
	Adapalene (JAN/USAN/INN); Differin (TN)	D01112	Retinoic acid receptor agonist	Topical	Acne	*Rarb, Rxrb, Rxrg*	Approved
	Amantadine (INN) *	D07441	Glutamate antagonist	Oral	Influenza A, Parkinson's	*Grin1, Grin2a-d*	Approved
	Amantadine hydrochloride (JP16/USP) *	D00777	Glutamate antagonist	Oral	Influenza A, Parkinson's	*Grin1, Grin2a-d*	Approved
	Apimostinel (USAN) *	D11299	NMDA receptor agonist	Oral	Depression	*Grin1, Grin2a-d*	Phase 3
	Aptiganel hydrochloride (USAN) *	D02973	NMDA receptor antagonist	Intravenous	Stroke	*Grin1, Grin2a-d*	Withdrawn
	Besonprodil (USAN) *	D03100	NMDA receptor antagonist	Oral	Parkinson's	*Grin2b*	Preclinical
	Bevantolol hydrochloride (JAN/USAN) *	D01369	Beta-1 adrenoreceptor antagonists	Oral	Hypertension, Angina pectoris	*Cacna1c-d, Cacna1f, Cacna1s, Arda1a-b, Arda1d, Ardb1*	Withdrawn
	Budipine (INN) *	D07306	NMDA receptor antagonist	Oral	Parkinson's	*Grin1, Grin2a-d*	Approved
	Budipine hydrochloride; Parkinsan (TN) *	D07589	NMDA receptor antagonist	Oral	Parkinson's	*Grin1, Grin2a-d*	Approved
	Delucemine hydrochloride (USAN) *	D03679	NMDA receptor antagonist	Intravenous	Stroke, Depression	*Grin1, Grin2a-d*	Phase 1

5	Dextromethorphan (USP) *	D03742	NMDA receptor antagonist	Oral	Cough, Cold virus	*Grin1, Grin2a-d*	Approved
	Dextromethorphan hydrobromide hydrate (JP16) *	D00848	NMDA receptor antagonist	Oral	Cough, Cold virus	*Grin1, Grin2a-d*	Approved
	Dextromethorphan polistirex (USAN) *	D03744	NMDA receptor antagonist	Oral	Cough, Cold virus	*Grin1, Grin2a-d*	Approved
	Dextrorphan hydrochloride (USAN) *	D03746	NMDA receptor antagonist	Oral	Cough, Cold virus	*Grin1, Grin2a-d*	Approved
	Dizocilpine maleate (USAN) *	D03878	NMDA receptor antagonist	Oral	Neurodegenerative disorders	*Grin1, Grin2a-d*	Preclinical
	Dronedarone (INN) *	D02537	Adrenergic receptor antagonist	Oral	Arrhythmia	*Cacna1c-d, Cacna1f, Cacna1s, Arda1a-b, Arda1d, Ardb1*	Approved
	Dronedarone hydrochloride (USAN) *	D03914	Adrenergic receptor antagonist	Oral	Arrhythmia	*Cacna1c-d, Cacna1f, Cacna1s, Arda1a-b, Arda1d, Ardb1*	Approved
	Ertiprotafib (USAN/INN) *	D04050	PTP1B inhibitor, PPAR agonist	Oral	Type 2 diabetes mellitus	*Ikbkb*	Preclinical
	Esketamine (INN) *	D07283	NMDA receptor antagonist	Nasal	Depression, Anaesthetic	*Grin1, Grin2a-d*	Approved
	Esketamine hydrochloride (USAN) *	D10627	NMDA receptor antagonist	Nasal	Depression, Anaesthetic	*Grin1, Grin2a-d*	Approved
	Etretinate (JAN/USAN/INN); Tegison (TN)	D00316	Retinoic acid receptor agonist	Oral	Psoriasis	*Rarb, Rxrb, Rxrg*	Withdrawn
	Felbamate (USAN/INN); Felbatol (TN) *	D00536	GABA receptor inhibitor	Oral	Epilepsy	*Grin1, Grin2a-d, Grin3a-b*	Approved

5	Gavestinel (USAN/INN) *	D04308	NMDA receptor antagonist	Oral	Stroke	*Grin1, Grin2a-d*	Phase 3
	Insulin (JAN/USP)	D00085	Recombinant insulin protein	Intravenous, subcutaneous, intramuscular	Type 1 and 2 Diabetes mellitus	*Insr*	Approved
	Insulin aspart (genetical recombination) (JAN)	D04475	Recombinant insulin protein	Intravenous, subcutaneous	Type 1 and 2 Diabetes mellitus	*Insr*	Approved
	Insulin degludec (genetical recombination) (JAN)	D09727	Recombinant insulin protein	Subcutaneous	Type 1 and 2 Diabetes mellitus	*Insr*	Approved
	Insulin detemir (genetical recombination) (JAN)	D04539	Recombinant insulin protein	Subcutaneous	Type 1 and 2 Diabetes mellitus	*Insr*	Approved
	Insulin glargine (genetical recombination) (JAN)	D03250	Recombinant insulin protein	Subcutaneous	Type 1 and 2 Diabetes mellitus	*Insr*	Approved
	Insulin glulisine (genetical recombination) (JAN)	D04540	Recombinant insulin protein	Intravenous, subcutaneous	Type 1 and 2 Diabetes mellitus	*Insr*	Approved
	Insulin human (genetical recombination) (JP16)	D03230	Recombinant insulin protein	Intravenous, subcutaneous, intramuscular, inhalation	Type 1 and 2 Diabetes mellitus	*Insr*	Approved
	Insulin human zinc (USP)	D04542	Recombinant insulin protein	Intravenous, subcutaneous, intramuscular, inhalation	Type 1 and 2 Diabetes mellitus	*Insr*	Approved
	Insulin human zinc, extended (USP)	D04543	Recombinant insulin protein	Intravenous, subcutaneous, intramuscular, inhalation	Type 1 and 2 Diabetes mellitus	*Insr*	Approved

5	Insulin human, isophane (USP)	D04541	Recombinant insulin protein	Subcutaneous	Type 1 and 2 Diabetes mellitus	*Insr*	Approved
	Insulin I 125 (USAN)	D04544	Recombinant insulin protein	Intravenous, Subcutaneous	Type 1 and 2 Diabetes mellitus	*Insr*	Labelling, not treatment
	Insulin I 131 (USAN)	D04545	Recombinant insulin protein	Intravenous, Subcutaneous	Type 1 and 2 Diabetes mellitus	*Insr*	Labelling, not treatment
	Insulin injection, biphasic isophane (BAN)	D08080	Recombinant insulin protein	Subcutaneous	Type 1 and 2 Diabetes mellitus	*Insr*	Approved
	Insulin lispro (genetical recombination) (JAN)	D04477	Recombinant insulin protein	Intravenous, subcutaneous, intramuscular	Type 1 and 2 Diabetes mellitus	*Insr*	Approved
	Insulin peglispro (USAN/INN)	D10473	Recombinant insulin protein	Intravenous, subcutaneous, intramuscular	Type 1 and 2 Diabetes mellitus	*Insr*	Approved
	Insulin zinc (USP)	D04551	Recombinant insulin protein	Intravenous, subcutaneous, intramuscular	Type 1 and 2 Diabetes mellitus	*Insr*	Approved
	Insulin zinc, extended (USP)	D04549	Recombinant insulin protein	Intravenous, subcutaneous, intramuscular	Type 1 and 2 Diabetes mellitus	*Insr*	Approved
	Insulin zinc, prompt (USP)	D04550	Recombinant insulin protein	Intravenous, subcutaneous, intramuscular	Type 1 and 2 Diabetes mellitus	*Insr*	Approved
	Insulin, dalanated (USAN)	D04546	Recombinant insulin protein	N/A	Type 1 and 2 Diabetes mellitus	*Insr*	Preclinical
	Insulin, neutral (USAN)	D04548	Recombinant insulin protein	Intravenous, subcutaneous, intramuscular	Type 1 and 2 Diabetes mellitus	*Insr*	Approved
	Isophane insulin injection (aqueous suspension) (JAN)	D04547	Recombinant insulin protein	Subcutaneous	Type 1 and 2 Diabetes mellitus	*Insr*	Approved
	Ketamine (INN) *	D08098	NMDA receptor antagonist	Intravenous, Intramuscular	Anaesthesia	*Grin1, Grin2a-d*	Approved

5	Ketamine hydrochloride (JP16/USP) *	D00711	NMDA receptor antagonist	Intravenous, Intramuscular	Anaesthesia	*Grin1, Grin2a-d*	Approved
	Latrepirdine (USAN/INN) *	D09917	Non-selective antihistamine	Oral	Alzheimer's, Huntington's	*Grin1, Grin2a-d*	Phase 3
	Latrepirdine dihydrochloride (USAN) *	D09918	Non-selective antihistamine	Oral	Alzheimer's, Huntington's	*Grin1, Grin2a-d*	Phase 3
	Levomethadone (INN) *	D08121	Opioid receptor agonist	Oral	Opioid dependency, Pain management	*Grin1, Grin2a-d, Oprm1*	Approved
	Levomethadone hydrochloride *	D08122	Opioid receptor agonist	Oral	Opioid dependency, Pain management	*Grin1, Grin2a-d, Oprm1*	Approved
	Licostinel (USAN/INN) *	D04728	NMDA receptor antagonist	Intravenous	Stroke	*Grin1, Grin2a-d*	Phase 1
	Memantine (INN) *	D08174	NMDA receptor antagonist	Oral	Alzheimer's	*Grin1, Grin2a-d*	Approved
	Memantine hydrochloride (JAN/USAN) *	D04905	NMDA receptor antagonist	Oral	Alzheimer's	*Grin1, Grin2a-d*	Approved
	Methadone (BAN) *	D08195	Opioid receptor agonist	Oral	Opioid dependency, Pain management	*Grin1, Grin2a-d, Oprm1*	Approved
	Methadone hydrochloride (JAN/USP) *	D02102	Opioid receptor agonist	Oral	Opioid dependency, Pain management	*Grin1, Grin2a-d, Oprm1*	Approved
	Monatepil maleate (JAN/USAN) *	D01171	Calcium antagonist	Oral	Angina, Hypertension	*Cacna1c-d, Cacna1f, Cacna1s*	Preclinical
	Neramexane mesylate (USAN) *	D05145	NMDA receptor antagonist	Oral	Alzheimer's	*Grin1, Grin2a-d*	Phase 3
	Orphenadrine (INN) *	D08305	Anticholinergic, Histamine H1 receptor, NMDA receptor inhibitor	Oral, intramuscular, intravenous	Parkinson's, Skeletal muscle relaxant	*Chrm1-5, Grin1, Grin2a-d, Grin3a-b, Hrh1*	Approved

5	Orphenadrine citrate (USP) *	D00774	Anticholinergic, Histamine H1 receptor, NMDA receptor inhibitor	Oral, intramuscular, intravenous	Parkinson's, Skeletal muscle relaxant	*Chrm1-5, Grin1, Grin2a-d, Grin3a-b, Hrh1*	Approved
	Orphenadrine hydrochloride *	D02599	Anticholinergic, Histamine H1 receptor, NMDA receptor inhibitor	Oral, intramuscular, intravenous	Parkinson's, Skeletal muscle relaxant	*Chrm1-5, Grin1, Grin2a-d, Grin3a-b, Hrh1*	Approved
	Perhexiline (INN) *	D08340	Vasodilator, Calcium channel blocker	Oral	Angina, Hypertrophic cardiomyopathy	*Cacna1c-d, Cacna1f, Cacna1s*	Phase 3
	Perhexiline maleate (USAN) *	D05442	Vasodilator, Calcium channel blocker	Oral	Angina, Hypertrophic cardiomyopathy	*Cacna1c-d, Cacna1f, Cacna1s*	Phase 3
	Perzinfotel (USAN/INN) *	D05447	NMDA receptor antagonist	Oral	Diabetic mellitus and neuropathy	*Grin1 Grin2a-d*	Phase 2
	Phencyclidine hydrochloride (USAN) *	D05453	NMDA receptor antagonist	Oral	Anaesthesia	*Grin1 Grin2a-d*	Withdrawn
	Proinsulin human (USAN)	D05622	Recombinant proinsulin protein	Intravenous, subcutaneous	Type 1 diabetes mellitus	*Insr*	Phase 2
	Remacemide hydrochloride (USAN) *	D05714	NMDA receptor antagonist	Oral , intravenous	Stroke, Neurodegenerative diseases	*Grin1 Grin2a-d*	Phase 3
	Rislenemdaz (USAN) *	D11340	NMDA receptor antagonist	Oral	Parkinson's, Depression	*Grin2b*	Phase 2
	Selfotel (USAN/INN) *	D02410	NMDA receptor antagonist	Intravenous	Stroke	*Grin1 Grin2a-d*	Withdrawn
	Tazarotene (JAN/USAN/INN); Avage (TN); Fabior (TN); Tazorac (TN)	D01132	Retinoic acid receptor agonist	Topical	Acne	*Rarb, Rxrb, Rxrg*	Approved
	Tiletamine (INN) *	D08596	NMDA receptor antagonist	Intramuscular	Anaesthesia	*Grin1 Grin2a-d*	Approved

5	Tiletamine hydrochloride (USP) *	D06146	NMDA receptor antagonist	Intramuscular	Anaesthesia	*Grin1 Grin2a-d*	Approved
	Traxoprodil mesylate (USAN) *	D06204	NMDA receptor antagonist	Intravenous	Parkinson's	*Grin2b*	Phase 2
	Troriluzole (USAN) *	D11414	Glutamate modulator	Oral, intravenous	Spinocerebellar ataxia, Alzheimer's	*Gria1-4, Grik1-5, Grin1, Grin2a-d*	Phase 3
4	Aleglitazar (USAN)	D08845	PPAR agonist	Oral	Type 2 diabetes mellitus	*Ppara, Pparg*	Phase 3
	Arhalofenate (USAN/INN) *	D09579	PPAR agonist	Oral	Type 2 diabetes mellitus	*Pparg*	Phase 3
	Ciglitazone (USAN/INN) *	D03493	PPAR agonist	Oral	Type 2 diabetes mellitus	*Pparg*	Phase 2
	Cipemastat (USAN/INN); Trocade (TN)	D03517	Matrix metalloproteinase inhibitor	Oral	Rheumatoid arthritis	*Mmp2, Mmp9*	Withdrawn
	Darvadstrocel (INN); Alofisel (TN) *	D11397	Stem cell therapy	Fistula injections	Crohn's disease	*Ifng*	Approved
	Edaglitazone sodium (USAN) *	D03941	PPAR gamma agonist	Oral	Type 2 diabetes mellitus	*Pparg*	Phase 2
	Efungumab (USAN/INN)	D09711	Antifungal monoclonal antibody	Intravenous	*C. albicans* infection	*Hsp90ab1, Hsp90aa1*	Phase 2
	Englitazone sodium (USAN) *	D03996	PPAR gamma agonist	Oral	Type 2 diabetes mellitus	*Pparg*	Preclinical
	Farglitazar (USAN/INN) *	D04132	PPAR gamma agonist	Oral	Type 2 diabetes mellitus	*Pparg*	Withdrawn
	Fontolizumab (USAN/INN) *	D04242	Anti-IFN-gamma monoclonal antibody	Intravenous	Crohn's disease, Rheumatoid arthritis	*Ifng*	Phase 2
	Halofenate (USAN/INN) *	D04411	PPAR gamma modulator	Oral	Type 2 diabetes mellitus, Dyslipidaemia	*Pparg*	Preclinical

4	Indeglitazar (USAN)	D09350	PPAR agonist	Oral	Type 2 diabetes mellitus	*Ppara , Ppard, Pprarg*	Phase 2
	Isometheptene mucate (USP) *	D07097	Alpha-1a adrenergic receptor agonist	Oral	Migraines	*Ardra1a, Slc18a1-2*	Approved
	Isotretinoin (USP); Absorica (TN); Accutane (TN); Sotret (TN)	D00348	Retinoic acid receptor agonist	Oral, topical	Acne	*Rarb, Rxrb, Rxrg*	Approved
	Isotretinoin anisatil (USAN)	D04636	Retinoic acid receptor agonist	Oral, topical	Acne	*Rarb, Rxrb, Rxrg*	Approved
	Mifobate (USAN/INN) *	D05030	PPAR antagonist	Oral	Type 2 diabetes mellitus	*Pparg*	Phase 2
	Muraglitazar (USAN/INN)	D05091	PPAR agonist	Oral	Type 2 diabetes mellitus	*Ppara, Pparg*	Phase 3
	Netoglitazone (USAN/INN) *	D05150	PPAR agonist	Oral	Type 2 diabetes mellitus	*Pparg*	Phase 2
	Peliglitazar (USAN)	D05397	PPAR agonist	Oral	Type 2 diabetes mellitus	*Ppara, Pparg*	Phase 2
	Pioglitazone (INN) *	D08378	PPAR agonist	Oral	Type 2 diabetes mellitus	*Pparg*	Approved
	Pioglitazone hydrochloride (JP16/USP) *	D00945	PPAR agonist	Oral	Type 2 diabetes mellitus	*Pparg*	Approved
	Propiverine (INN) *	D08441	Muscarinic acetylcholine receptor inhibitor	Oral	Overactive urinary bladder	*Chrm1-5*	Approved
	Propiverine hydrochloride (JP16) *	D01007	Muscarinic acetylcholine receptor inhibitor	Oral	Overactive urinary bladder	*Chrm1-5*	Approved
	Reglitazar (JAN/INN) *	D01971	PPAR agonist	Oral	Type 2 diabetes mellitus	*Pparg*	Phase 2
	Retinol acetate (JP16)	D01621	Retinoic acid receptor agonist	Oral, topical	Acne, Vitamin A deficiency	*Rarb, Rxrb, Rxrg*	Approved

4	Retinol palmitate (JP16); Aquasol A (TN)	D00164	Retinoic acid receptor agonist	Oral, topical	Acne, Vitamin A deficiency	*Rarb, Rxrb, Rxrg*	Approved
	Retinol propionate; Microvit a dlc [veterinary] (TN)	D08477	Retinoic acid receptor agonist	Oral, topical	Acne, Vitamin A deficiency	*Rarb, Rxrb, Rxrg*	Approved
	Rivoglitazone (USAN/INN) *	D05739	PPAR gamma agonist	Oral	Type 2 diabetes mellitus	*Pparg*	Phase 3
	Rosiglitazone (INN) *	D08491	PPAR gamma agonist	Oral	Type 2 diabetes mellitus	*Pparg*	Approved
	Rosiglitazone maleate (JAN/USAN) *	D00596	PPAR gamma agonist	Oral	Type 2 diabetes mellitus	*Pparg*	Approved
	Seladelpar (USAN/INN) *	D11256	PPAR delta agonist	Oral	Dyslipidaemia, Metabolic syndrome, Type 2 diabetes mellitus	*Pparg*	Phase 3
	Seladelpar lysine (USAN); Seladelpar lysine dihydrate *	D11257	PPAR delta agonist	Oral	Dyslipidaemia, Metabolic syndrome, Type 2 diabetes mellitus	*Pparg*	Phase 3
	Siltuximab (USAN/INN) *	D09669	Anti-IL6 monoclonal antibody	Intravenous	Castleman's disease	*Il-6*	Phase 3
	Sirukumab (USAN) *	D10080	Anti-IL6 monoclonal antibody	Intravenous	Rheumatoid arthritis	*Il-6*	Phase 3
	Sodelglitazar (USAN)	D06647	PPAR agonist	Oral	Type 2 diabetes mellitus	*Ppara , Ppard, Pprarg*	Phase 2
	Tesaglitazar (JAN/USAN/INN)	D01274	PPAR agonist	Oral	Type 2 diabetes mellitus	*Ppara, Pparg*	Phase 3
	Topiramate (JAN/USAN/INN) *	D00537	AMPA receptor antagonist	Oral	Epilepsy	*Cacna1c-d, Gria1-4*	Approved
	Troglitazone (JAN/USAN/INN) *	D00395	PPAR gamma agonist	Oral	Type 2 diabetes mellitus	*Pparg*	Withdrawn
	Vitamin A (USP); Retinol; Vitamin	D06543	Retinoic acid receptor agonist	Oral	Vitamin A deficiency	*Rarb, Rxrb, Rxrg*	Approved

	A1; Aquasol A (TN)

* Represents drugs that target components within the iPathwayGuide predicted KEGG pathways that are not encoded by the DEGs listed in the prednisolone treated *Smn$^{-/-}$;SMN2* mice vs untreated *Smn$^{-/-}$;SMN2* mice.
Activated PI3K delta syndrome (APDS); Chronic obstructive pulmonary disease (COPD); Amyotrophic lateral sclerosis (ALS)
International Non-proprietary Names (INN); Japanese Approved Name (JAN); United States Adopted Name (USAN); United States Pharmacopeia (USP); Japanese Pharmacopeia, 16th edition (JP16); British Approved Name (BAN).

Table 3.11. DGIdb list of drugs predicted to mimic the upregulation of upregulated upstream regulators in skeletal muscle of prednisolone-treated Smn$^{-/-}$;SMN2 SMA mice.

Gene	Drug	Interaction	Activity	Bioavailability	Disease	Regulatory status
Adk	Ribavirin	Activator	Antiviral nucleoside analogue	Oral, inhalation	Hepatitis C infection	Approved
Adk	Adenosine phosphate *	Product of	Nucleotide	Oral, nasal, intraarterial	Supplementation, asthma	Approved
Amhr2	Tranexamic acid	Agonist	Antifibrinolytic	Oral, topical, intravenous	Haemophilia, Excessive haemorrhaging	Approved
Ar	Levonorgestrel	Agonist	Progesterone receptor agonist	Oral	Contraceptive	Approved
Ar	Oxandrolone	Agonist	Androgen receptor agonist, anabolic steroid	Oral	Turner syndrome, muscle wasting, osteoporosis	Approved
Ar	Nandrolone phenpropionate	Agonist	Androgen receptor agonist, anabolic steroid	Oral	Anaemia, cachexia, osteoporosis, muscle wasting	Approved (Illicit)
Ar	Fluoxymesterone	Agonist	Androgen receptor agonist, anabolic steroid	Oral	Hypogonadism, male puberty delay	Approved (Illicit)
Ar	Danazol	Agonist	Androgen receptor agonist, progesterone receptor agonist	Oral	Endometriosis, fibrocystic breast disease	Approved
Ar	Testosterone propionate	Agonist	Androgen receptor agonist, anabolic steroid	Intramuscular	Hypogonadism, male puberty delay	Approved
Ar	Boldenone undecylenate	Agonist	Androgen receptor agonist, anabolic steroid	Intramuscular	N/A	Illicit
Ar	Prasterone	Agonist	Androgen receptor agonist, anabolic steroid	Vaginal	Dyspareunia	Approved

Ar	Methyltestosterone	Agonist	Androgen receptor agonist, anabolic steroid	Oral	Hypogonadism, male puberty delay	Approved
Ar	Nandrolone decanoate	Agonist	Androgen receptor agonist, anabolic steroid	Intramuscular	Anaemia, cachexia, osteoporosis, muscle wasting	Approved (Illicit)
Ar	Norgestrel	Agonist	Progesterone receptor agonist	Oral	Contraceptive	Approved
Ar	Esculin	Agonist	Coumarin glucoside	Transdermal	Venous insufficiency, Inflammatory disorders	Approved
Ar	Nandrolone	Agonist	Androgen receptor agonist, anabolic steroid	Intramuscular	Anaemia, cachexia, osteoporosis, muscle wasting	Approved
Ar	Testosterone	Agonist	Androgen receptor agonist, anabolic steroid	Buccal, nasal, oral, topical, transdermal, subcutaneous	Hypogonadism, male puberty delay	Approved
Ar	Ethylestrenol	Agonist	Androgen receptor agonist, anabolic steroid	Oral	Sexual development disorders	Withdrawn
Ar	Mibolerone	Agonist	Androgen and progesterone receptor agonists, anabolic steroid	Oral	N/A	Only veterinary approved
Ar	Testosterone cypionate	Agonist	Androgen receptor agonist, anabolic steroid	Topical	Hypogonadism	Approved
Ar	Testosterone undecanoate	Agonist	Androgen receptor agonist, anabolic steroid	Oral, intramuscular	Hypogonadism	Approved
Ar	Stanozolol	Agonist	Androgen receptor agonist, anabolic steroid	Oral	Hereditary angioedema	Approved

Ar	Testosterone enanthate	Agonist	Androgen receptor agonist, anabolic steroid	Intramuscular, subcutaneous	Hypogonadism	Approved
Ar	Oxymetholone	Agonist, activator	Androgen receptor agonist, anabolic steroid	Oral	Anaemia, myelofibrosis	Approved (Illicit)
Ar	Ketoconazole	Binder	CP450 inhibitor, androgen receptor binding agent	Oral, topical	Fungal infections	Approved
Ar	Enobosarm	Modulator	Selective androgen receptor modulator	Oral	Muscular atrophy, cachexia	Phase 3
Ar	GSK2849466	Modulator	Selective androgen receptor modulator	Oral	Cachexia	Phase 1
Ar	VK5211	Modulator	Selective androgen receptor modulator	Oral	Hip fracture	Phase 2
Ar	GLPG0492	Modulator	Selective androgen receptor modulator	Oral	Sarcopenia, Duchenne muscular dystrophy	Phase 1
Ar	LGD-2941	Modulator	Selective androgen receptor modulator	Oral	Hypogonadism	Phase 1
Ar	GSK2881078	Modulator	Selective androgen receptor modulator	Oral	Chronic disease associated muscle wasting	Phase 1
Ar	MK-0773	Modulator	Selective androgen receptor modulator	Oral	Sarcopenia	Phase 2
Cnr1	Dronabinol	Agonist	Synthetic THC	Oral	Anorexia, nausea, vomiting	Approved
Cnr1	Protriptyline	Agonist	Tricyclic norepinephrine transporter inhibitor	Oral	Depression	Approved
Cnr1	CP-55940	Agonist	Cannabinoid receptor agonist	Oral	N/A	Preclinical (illicit)
Cnr1	WIN-552122	Agonist	Cannabinoid receptor agonist	Oral	N/A	Preclinical (illicit)

Cnr1	Anandamide	Agonist	Endocannabinoid neurotransmitter	Oral	N/A	Preclinical
Cnr1	Cannabinol	Agonist	Cannabinoid receptor agonist	Oral	N/A	Preclinical
Cnr1	Nonabine	Agonist	Cannabinoid receptor agonist	Oral	N/A	Preclinical
Cnr1	SAD448	Agonist	Cannabinoid receptor agonist	Topical	Ocular hypertension	Phase 1
Cnr1	Nabilone	Agonist, partial agonist	Cannabinoid receptor agonist	Oral	Nausea, pain, multiple sclerosis	Approved
Cnr1	Cannabidiol	Allosteric modulator	Cannabinoid receptor agonist	Oral	Nausea, pain, multiple sclerosis	Approved
Cnr1	Droperidol	Allosteric modulator	Dopamine antagonist	Intravenous, intramuscular	Chemotherapy induced nausea	Approved
Creb1	Adenosine phosphate *	Activator	Nucleotide	Oral, nasal, intraarterial	Supplementation, asthma	Approved
Crhr2	Sauvagine	Agonist	Neuropeptide	N/A	N/A	Preclinical
Cxcl12	Tinzaparin sodium	Binder	Antithrombin 3 activator	Subcutaneous	Clotting, deep vein thrombosis	Approved
Dnmt1	Flucytosine	Other	Antifungal nucleic acid biosynthesis inhibitor	Oral	Fungal infections	Approved
Egf	Sucralfate	Inducer	Protectant/anti-ulcer	Oral	Stomach ulcers	Approved
Esr1	Oestrogens, conjugated	Agonist	Oestrogen receptor agonist, oestrogen	Oral, vaginal, topical, intramuscular, intravenous	Menopause	Approved
Esr1	Etonogestrel	Agonist	Progesterone receptor agonist	Transdermal	Contraceptive	Approved
Esr1	Desogestrel	Agonist	Progesterone receptor agonist	Oral	Contraceptive	Approved
Esr1	Progesterone	Agonist	Progesterone receptor agonist	Oral, vaginal, intramuscular	Amenorrhea, uterine haemorrhage, female infertility	Approved

Esr1	Estrone	Agonist	Oestrogen receptor agonist, oestrogen	Vaginal	Menopause	Approved
Esr1	Dienestrol	Agonist	Oestrogen receptor agonist, oestrogen	Vaginal	Atrophic vaginitis, kraurosis vulvae	Approved
Esr1	Norgestimate	Agonist	Progesterone receptor agonist	Oral	Menopause	Approved
Esr1	Estriol	Agonist	Oestrogen receptor agonist	Vaginal	Menopause	Approved
Esr1	Prinaberel	Agonist	Oestrogen receptor beta agonist	Oral	Rheumatoid arthritis	Phase 2
Esr1	Propylpyrazoletriol	Agonist	Oestrogen receptor alpha agonist	N/A	N/A	Preclinical
Esr1	Mestranol	Agonist	Oestrogen receptor agonist, oestrogen	Oral	Contraceptive	Approved
Esr1	Allylestrenol	Agonist	Progesterone receptor agonist	Oral	Miscarriages	Approved
Esr1	Estropipate	Agonist	Oestrogen receptor agonist, oestrogen	Oral, vaginal	Menopause	Approved
Esr1	Tibolone	Agonist	Oestrogen receptor agonist, oestrogen	Oral	Menopause	Approved
Esr1	Estradiol	Agonist	Oestrogen receptor agonist, oestrogen	Oral, topical, vaginal, transdermal, subcutaneous	Atrophic vaginitis, primary ovarian insufficiency	Approved
Esr1	Estradiol cypionate	Agonist	Oestrogen receptor agonist, oestrogen	Intramuscular	Atrophic vaginitis, primary ovarian insufficiency	Approved
Esr1	Oestrogens, esterified	Agonist	Oestrogen receptor agonist, oestrogen	Oral	Atrophic vaginitis, primary ovarian insufficiency	Approved
Esr1	Estradiol acetate (CHEMBL1200430)	Agonist	Oestrogen receptor agonist, oestrogen	Oral, vaginal	Atrophic vaginitis, primary ovarian insufficiency	Approved
Esr1	MK-6913	Agonist	Oestrogen receptor agonist	Oral	Menopause	Phase 2

Esr1	Raloxifene	Agonist, modulator	Selective oestrogen receptor modulator	Oral	Osteoporosis	Approved
Esr1	Ospemifene	Agonist, modulator	Selective oestrogen receptor modulator	Oral	Dyspareunia	Approved
Esr1	Chlorotrianisene	Agonist, binder	Oestrogen receptor agonist, oestrogen	Oral	Menopause, infertility	Withdrawn
Esr1	Lasofoxifene	Agonist, modulator	Selective oestrogen receptor modulator	Oral	Osteoporosis, vaginal atrophy	Approved
Esr1	Quinestrol	Agonist, modulator	Oestrogen receptor agonist, oestrogen	Oral	Menopause	Approved
Esr1	Bazedoxifene	Agonist, antagonist	Selective oestrogen receptor modulator	Oral	Osteoporosis, menopause	Approved
Esr1	Prasterone	Binder	Oestrogen receptor agonist	Vaginal	Dyspareunia	Approved
Esr1	Oestrogens, conjugated synthetic A	Ligand, agonist	Oestrogen receptor agonist, oestrogen	Oral	Menopause	Approved
Esr1	Synthetic conjugated Oestrogens, B	Ligand, agonist	Oestrogen receptor agonist, oestrogen	Oral	Menopause, dyspareunia	Approved
Esr1	Clomiphene citrate	Modulator	Oestrogen receptor agonist/antagonist (tissue dependent)	Oral	Infertility	Approved
Esr1	Bazedoxifene acetate	Modulator	Oestrogen receptor modulator	Oral	Osteoporosis, menopause	Approved
Esr1	CHF4227	Modulator	Oestrogen receptor modulator	Oral	Osteoporosis, menopause	Phase 1
Esr1	Levonorgestrel	Other	Progesterone receptor agonist	Oral, intrauterine, subcutaneous	Contraceptive	Approved
Kdr	Telbermin	Agonist	Recombinant vascular endothelial growth factor	Topical	Diabetic foot ulcers	Phase 2

Scly	Pyridoxal phosphate	Cofactor	Vitamin B6	Oral	Supplementation	Approved

* Drug has >1 DEG target

Table 3.12. DGIdb list of drugs predicted to mimic the downregulation of downregulated upstream regulators in skeletal muscle of prednisolone-treated Smn$^{-/-}$;SMN2 SMA mice.

Gene	Drug	Interaction	Activity	Bioavailability	Disease	Regulatory status
Bcl2l1	Isosorbide	Inhibitor	Hyperosmotic agent	Oral	Ocular hypertension, glaucoma	Approved
Brd2	Apabetalone *	Antagonist	BRD4 inhibitor	Oral	Type 2 diabetes mellitus, atherosclerosis, coronary heart disease	Phase 3
Brd4	Apabetalone *	Antagonist	BRD4 inhibitor	Oral	Type 2 diabetes mellitus, atherosclerosis, coronary heart disease	Phase 3
Brd4	Chlormezanone	Inhibitor	Benzodiazepine receptor binding agent	Oral	Muscle spasms	Withdrawn
Brd4	Stavudine	Inhibitor	Nucleoside reverse transcriptase inhibitor	Oral	HIV-1 Infections	Approved
C1qb	Ropinirole	Inhibitor	Dopamine receptor agonist	Oral	Parkinson's, Restless leg syndrome	Approved
C1qb	Fenclonine	Inhibitor	Tryptophan 5-hydroxylase inhibitor	Oral	Carcinoid syndrome	Withdrawn
C1qb	Fenfluramine	Inhibitor	Serotonin secretion activator	Oral	Obesity	Withdrawn
Carm1	Pregnenolone	Inhibitor	Neurosteroid	Oral	Depression, OCD, bipolar	Phase 4
Comt	S-Adenosyl-l-Methionine	Cofactor	S-Adenosyl-l-Methionine synthase binding agent	Oral, intravenous, intramuscular	Osteoarthritis, fibromyalgia	Approved
Comt	Tolcapone	Inhibitor	Catechol O-methyltransferase inhibitor	Oral	Parkinson's	Approved

Comt	Entacapone	Inhibitor	Catechol O-methyltransferase inhibitor	Oral	Parkinson's	Approved
Comt	D-proline	Inhibitor	Amino acid isomer	N/A	N/A	Preclinical
Ccn2	FG-3019 (Pamrevlumab)	Inhibitor	CTGF monoclonal antibody inhibitor	Intravenous	Type 2 diabetes mellitus, kidney disease, fibrotic disorders, DMD	Phase 2
Ednrb	Ambrisentan	Antagonist	Endothelin receptor antagonist	Oral	Pulmonary arterial hypertension	Approved
Ednrb	Bosentan	Antagonist	Endothelin receptor antagonist	Oral	Pulmonary arterial hypertension	Approved
Ednrb	A-192621	Antagonist	Endothelin B receptor antagonist	Oral	N/A	Preclinical
Ednrb	Galantamine	Antagonist	Acetylcholinesterase inhibitor	Oral	Alzheimer's	Approved
Ednrb	Macitentan	Antagonist	Endothelin receptor antagonist	Oral	Pulmonary arterial hypertension	Approved
Ednrb	Sitaxentan	Antagonist	Endothelin A receptor antagonist	Oral	Pulmonary arterial hypertension	Withdrawn
Ednrb	Enrasentan	Antagonist	Endothelin receptor antagonist	Oral	Heart failure	Phase 2
Ednrb	Tezosentan	Antagonist	Endothelin receptor antagonist	Intravenous	Heart failure	Phase 3
Ednrb	Darusentan	Antagonist	Endothelin receptor antagonist	Oral	Hypertension	Phase 3
Fos	Nadroparin calcium	Inhibitor	Platelet aggregation inhibitor (low molecular weight heparin)	Subcutaneous	Thrombosis	Approved
Igf1r	Mecasermin	Agonist, inhibitor	Recombinant IGF-1	Subcutaneous	ALS, Type 1 and 2 diabetes mellitus	Approved
Igf1r	Teprotumumab	Antagonist, inhibitor	IGF-1 receptor monoclonal antibody inhibitor	Intravenous	Thyroid eye disease	Approved

Igf1r	Dimethisterone	Inhibitor	IGF-1 receptor inhibitor	Oral	Pregnancy	Withdrawn
Il-6ra	SA237 (Satralizumab)	Antagonist	Anti-IL-6 receptor antibody inhibitor	Subcutaneous	Neuromyelitis Optica	Phase 3
Il-6ra	Sarilumab	Antagonist	Anti-IL-6 receptor antibody inhibitor	Subcutaneous	Rheumatoid arthritis	Approved
Il-6ra	Vobarilizumab	Antibody inhibitor	Anti-IL-6 receptor antibody inhibitor	Subcutaneous	Rheumatoid arthritis, lupus	Phase 2
Il-6ra	Tocilizumab	Antibody inhibitor	Anti-IL-6 receptor antibody inhibitor	Intravenous, subcutaneous	Rheumatoid arthritis	Approved
Insr	Insulin, neutral	Binder	Recombinant insulin protein	Intravenous, intramuscular, subcutaneous	Type 1 and 2 diabetes mellitus	Approved
Kdm1a	Diphenhydramine hydrochloride	Inhibitor	Histamine receptor antagonist	Oral	Allergic reactions	Approved
Kdm1a	Tranylcypromine	Inhibitor	Monoamine oxidase inhibitor	Oral	Depression	Approved
Mt2	Luzindole	Antagonist	Selective melatonin receptor antagonist	Oral	N/A	Preclinical
Pdgfra	Phenobarbital	Inhibitor	GABA-A receptor positive allosteric modulator	Oral, intravenous, intramuscular	Insomnia, epilepsy, anxiety, seizures	Approved
Pdpk1	Celecoxib	Inhibitor	Selective COX2 inhibitor	Oral	Rheumatoid arthritis	Approved
Pdpk1	BX-795	Inhibitor	PDK1 inhibitor	N/A	N/A	Preclinical
Pgf	Conbercept	Inhibitor	Vascular endothelial growth factor inhibitor	Intravitreal	Age related macular degeneration	Phase 3
Pkn1	Tofacitinib	Inhibitor	JAK inhibitor	Oral	Rheumatoid arthritis	Approved
Pkn1	Quercetin	Inhibitor	Bioflavonoid	Oral	Thromboembolism	Phase 3
Ptpn1	Tiludronic acid	Inhibitor	ATP inhibitor bisphosphate	Oral	Paget's disease of bone	Approved
Sik1	Pseudoephedrine hydrochloride	Inhibitor	Alpha- and beta-adrenergic receptor agonist	Oral	Coughing	Approved

Sirt1	Sodium lauryl sulfate	Inhibitor	Surfactant	Oral, topical, dental	N/A	Approved
Sirt1	Splitomicin	Inhibitor	NAD-dependent histone deacetylase SIR2 inhibitor	N/A	N/A	Preclinical
Stat3	Acitretin	Inhibitor	Retinoid X and retinoic acid receptor agonist	Oral	Psoriasis	Approved
Stat3	Bardoxolone methyl	Inhibitor	NF-kappa-B inhibitor	Oral	Alport syndrome, pulmonary hypertension, diabetic nephropathy	Phase 3
Tgfbr1	Trihexyphenidyl	Inhibitor	Muscarinic acetylcholine receptor antagonist	Oral	Parkinson’s	Approved
Tgfbr1	Neostigmine bromide	Inhibitor	Acetylcholinesterase inhibitor	Oral, intravenous, subcutaneous, intramuscular	Myasthenia gravis	Approved
Thra	Liothyronine	Antagonist, agonist	Thyroid hormone receptor alpha and beta agonist	Oral, intravenous	Hyper- and hypo-thyroidism	Approved

* Drug has >1 DEG target

3.3. Discussion

Although short term prednisolone treatment ameliorated skeletal muscle pathologies and improved survival in SMA mice [53], the consequence of muscle-wasting associated with chronic GC use [628] emphasises the need to develop alternative approaches to minimise these risks. Here, we used transcriptomics, ingenuity, and ORA analyses alongside drug-gene interaction databases to identify existing pharmacological compounds that have similar activities to prednisolone without GC-associated adverse risks in SMA skeletal muscle and could thus be repositioned as novel SMN-independent therapies.

In the first instance, we identified prednisolone-targeted genes and pathways and observed that many were involved in skeletal muscle size, metabolism, and regulatory function. Notably, a number of the pathways listed in the KEGG database have previously been reported as dysregulated in SMA patients and models. These include FoxO signalling [56], longevity regulating pathway [53,56,389,767,779–783], p53 signalling [779,780], AMPK signalling [389,781,782], mitophagy [388,784], circadian rhythm [356], PPAR signalling [389], and autophagy – animal [56,389], providing further support for prednisolone's efficacy as a beneficial treatment in SMA skeletal muscle.

However, it is unclear whether the restoration of these pathways was due to them being directly targeted by prednisolone or merely a consequence of improved muscle health in SMA mice. A prime example of the latter was the downregulation of *PTEN-induced kinase 1* (*Pink1*), which encodes a mitochondrial serine/threonine-protein kinase, that along with Parkin, acts as a damaged mitochondria sensor and primes them for autophagosomal-induced

degradation for mitophagy [810,811]. With mitochondrial dysfunction and damage being a hallmark feature in SMA skeletal muscle [388,784], the reduced expression of *Pink1* following prednisolone treatment suggests a lower proportion of damaged mitochondria, which could be attributed to overall improved muscle health.

Conversely, an important pathway that may be directly targeted by prednisolone is FoxO signalling. The *FoxO* genes (*FoxO1*, *FoxO3*, *FoxO4*, and *FoxO6*) encode four conserved transcription factors that modulate gene expression through a conserved Forkhead box structure DNA binding domain [364,365,812,813]. *FoxO* genes regulate auto-phagosomal and proteasomal pathways through *atrogin-1* and *MuRF-1* [363], atrogenes that contribute to muscle atrophy in a variety of different muscle-wasting conditions (e.g. disuse [814], cachexia [815], organ injury [816], denervation [637], metabolic dysregulation [817], starvation [366]) including SMA [56]. Our analysis predicted that short-term prednisolone treatment downregulated *FoxO1*, *FoxO3*, and *FoxO4* expression, whilst the computational perturbation calculations further predicted these would downregulate *atrogin-1* (*Fbxo32* and *Fbxo35*). FoxO isoforms in skeletal muscle are also involved in muscle differentiation [818–822] and glucose and FA metabolism [823–826], processes that have been reported as dysregulated in SMA [157–159,195,301,310,342,827,828] and also listed as restored in our GO pathways. Thus, our transcriptomic and pathway analyses were able to identify potential mechanisms by which prednisolone ameliorated skeletal muscle pathologies in the *Smn$^{-/-}$;SMN2* SMA mouse model.

Although we identified a number of potential pathways worth further mechanistic investigations, we instead used the targeted pathways and predicted upstream regulators as templates for finding predicted drugs that emulate similar effects as prednisolone. To do so, we used drug-gene interaction tools within

iPathwayGuide [651–654] and DGIdb [659] to provide suitable drug candidates, once those listed as withdrawn or linked to muscle-wasting had been removed.

Furthermore, we chose to focus on drugs that have not been investigated in SMA, that can be administered orally and that are clinically approved as they provide opportunities for cheaper and non-invasive novel SMN-independent therapies. In addition, they potentially can complement both invasive (Spinraza® and Zolgensma®) and non-invasive (Evrysdi®) SMN-dependent therapies. Based on these parameters, we chose to not further investigate promising candidates such as celecoxib [615] (investigated in SMA), tocilizumab [745,747] (non-oral) and GLPG0492 [829] (not clinically approved). Although celecoxib's progress onto the clinical trial stage in SMA patients (Clinical Trial ID: NCT02876094) supports the validity of our approach and the potential therapeutic usefulness of the drugs on our list.

Following this elimination process, a few leading candidates remain for further investigation, with two that are particularly and equally interesting. The first one is metformin, a biguanide AMPK agonist used as an anti-hyperglycaemic agent in type 2 DM (T2DM) [830]. Interestingly, metformin was predicted to downregulate the *FoxO* genes through its upregulation of *Prkag3*, which encodes for the AMPK-γ3 isoform in the α2/β2/γ3 AMPK complex that is highly expressed in normal skeletal muscle [831,832]. The second drug candidate is oxandrolone, a synthetic anabolic steroid used for growth disorders [833], myopathies [834], NMD [835] and muscle-wasting [836] that has a higher ratio of anabolic: androgynous effects [837,838]. Unsurprisingly, oxandrolone was predicted to upregulate the *Ar*, which in turn was further predicted to upregulate genes important for skeletal muscle cell differentiation (*Myogenin* (*MyoG*) [175], *Insulin-like growth factor binding protein 5*

(*Igfbp5*) [839] and *A-kinase anchor protein 6* (*Akap6*) [840]) and glucose metabolism (*Docking protein 5*(*Dok5*) [841]). However, all of these findings are based on computational predictions and thus, their suitability for SMA treatment would require experimental validation in appropriate cellular and animal models.

Although using *in silico* methods for drug repositioning provides many advantages, there are limitations to using transcriptomics data to generate pharmacological candidates. For our own data, one limitation was the low replicate numbers of N=3 for untreated *Smn*$^{+/-}$*;SMN2* healthy and untreated and prednisolone-treated *Smn*$^{-/-}$*;SMN2* SMA mice and N=2 for prednisolone-treated *Smn*$^{+/-}$*;SMN2* SMA mice. Ideally, replicate sizes of N=6 or more are suggested for enhanced detection of significant DEGs and improved reliability [743,842]. However, in our case a high N number and replicability was not feasible, because of cost, personnel, time and accessibility issues. Another limitation of transcriptomics is that it only defines gene expression based on mRNA levels and a high transcription rate does not always correspond to high protein levels or activity (and vice versa) due to factors such as mRNA degradation, mRNA instability and inefficient translation [843–847]. Furthermore, protein activity is not only measured by abundance, but also by post-translational modifications (PTMs) such as phosphorylation, methylation, acetylation and glycosylation as well as protein complex formation [848–850]. These are parameters that cannot be detected by transcriptomics, which can sometimes be problematic for pathway analysis as they are mostly built from protein-protein interaction data [655]. Thus, the transcriptomic profiles may not be a true reflection of the activity of prednisolone in skeletal muscle of SMA mice for certain molecular effectors. An example being mTOR, whose activity in the mTORC1 complex has been extensively associated

with muscle hypertrophy [362,851,852], yet in our study the prednisolone-treated SMA mice showed reduced mTOR transcript levels despite the attenuation of muscle atrophy [53]. Furthermore, the expression levels of negative regulators of mTORC1 (e.g. *Klf15* [368], *Ddit4* [368], *Eif4a* [853]) were also decreased in prednisolone-treated SMA mice, which suggests enhanced mTORC1 activity. One explanation is that mTOR in the mTORC1 complex is usually activated by phosphorylation in Serine 2448 position (p-mTOR S2448) that leads to its binding of RAPTOR and RICTOR [854], which certain studies have measured as a marker of mTORC1 activity [855], a read-out that our transcriptomics analysis could not detect. A way to overcome this limitation that would more accurately define the perturbed pathways and component interactions in prednisolone-treated SMA skeletal muscle would be to combine proteomics with our transcriptomics data. The advantages of a proteomic approach is that it can strengthen the identification of *bona fide* molecular targets for which the expression patterns at both the transcript and protein level are similar and it can also detect PTMs, thus better defining a protein's activity status [856,857]. We have indeed previously demonstrated the success of this approach in SMA, where a multi-omics strategy predicted harmine as a potential SMN-independent therapy, which was supported by validation experiments in cellular and animal models [716].

Combined, our previous and current results demonstrate the effectiveness of *in silico* drug repositioning methods for the identification of novel SMN-independent therapies. These have allowed us herein to uncover the pathways targeted by prednisolone in skeletal muscle of SMA mice and to generate a list of non-invasive oral drug candidates suitable for testing in SMA cellular and animal models.

Chapter 4.

Therapeutic potential of metformin to treat muscle pathologies in SMA.

4.1. Introduction

In chapter 2, we used bioinformatics to identify orally bioavailable pharmacological compounds that could emulate the ergogenic benefits of prednisolone in SMA skeletal muscle without the adverse myopathy effects of chronic use [53,628]. A leading candidate was metformin, a synthetic asymmetric dimethyl-biguanide compound that is based on natural phytochemicals from the *Galega officinalis* plant [858,859] (Figure 4.1). First synthesised in 1922, metformin is a cost-effective generic compound that has been used as an oral hypo-glycaemic agent in T2DM for over 60 years with a well-known safety profile [830,859–861].

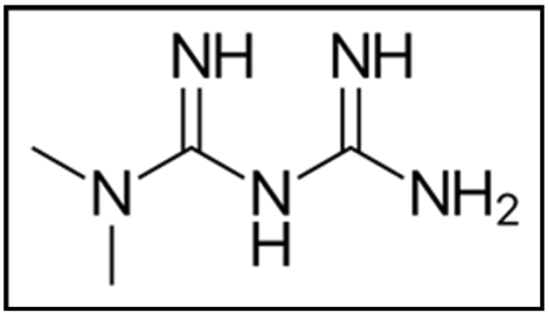

Figure 4.1. Metformin chemical structure (skeletal formula).

Metformin is classed as an AMPK agonist, which most research suggests arises indirectly via a specific and mild inhibition of the mitochondrial electron transport complex 1 (NADH: ubiquinone reductase) that subsequently activates AMPK by an increase in AMP: ATP and ADP: ATP ratios [862–867]. However, it has also been recently demonstrated that metformin can directly activate AMPK by strongly binding to cystathionine β-synthetase 1 (CBS1) and CBS4 sites in the regulatory AMPK-γ subunit [868–870].

AMPK is a conserved heterotrimeric serine/threonine protein kinase [871–874] that serves as a master regulator of cellular ATP metabolism by inhibiting anabolic processes (e.g. protein synthesis [875], lipogenesis [876], gluconeogenesis [877] and glycogenesis [878]) and promoting catabolic pathways (e.g. fatty acid oxidation [879], glycolysis [880], glucose uptake [881], and autophagy [882]). Composed of three subunits [873] (catalytic α [883–885], scaffolding β [878,886–888] and regulatory γ [889–891]), AMPK is expressed as cell type-dependent isoforms. In human skeletal muscle, 3 different AMPK isoform complexes have been identified (α1β2γ1, α2β2γ1, and α2β2γ3) [832,892–897].

With skeletal muscle being a highly metabolic organ that accounts for 40% of human body mass in a healthy individuals [280], metformin could potentially ameliorate muscle and metabolic dysfunctions that have been reported in SMA pathology (Figure 4.2). Indeed, metformin is well-known to promote glucose uptake and insulin sensitivity in skeletal muscle of T2DM patients [300,898,899] and, as mentioned previously (see section 1.3.3.1), there are several reports of insulin and glucose metabolism defects in both SMA patients and pre-clinical models [301–309] (Figure 4.2).

Another key target for metformin in SMA skeletal muscle is FA oxidation (Figure 4.2). Indeed, *in vivo* experiments have shown that metformin reduced intramyocellular accumulation in obese adult mice [900], high fat diet (HFD)-insulin resistant Wistar rats [901]. Although, *in vivo* experiments highlight the systemic effects of metformin treatment, *in vitro* studies on C2C12 myotubes have shown that direct metformin treatment in muscle upregulated FA oxidation genes for direct promotion of FA oxidation and decreased intramyocellular lipid content in muscle [900] (Figure 4.2). Importantly, these studies highlight metformin's potential

of promoting FA oxidation in SMA muscle, since type 1-3 SMA skeletal muscle biopsies displayed diminished β-oxidation enzyme activity [339,342].

Metformin could also ameliorate the mitochondrial dysfunctions observed in SMA muscle [129,388–393,395]. Indeed, AMPK plays an important regulatory role in mitochondrial biogenesis and function by activating PGC-1α [902,903] (Figure 4.2). In addition, PGC-1α governs skeletal muscle regulatory processes like glucose and lipid metabolism [904,905], NMJ regulation [906,907], inflammatory response [908] and hypertrophy-atrophy balance [909,910], which all have reported defects in SMA.

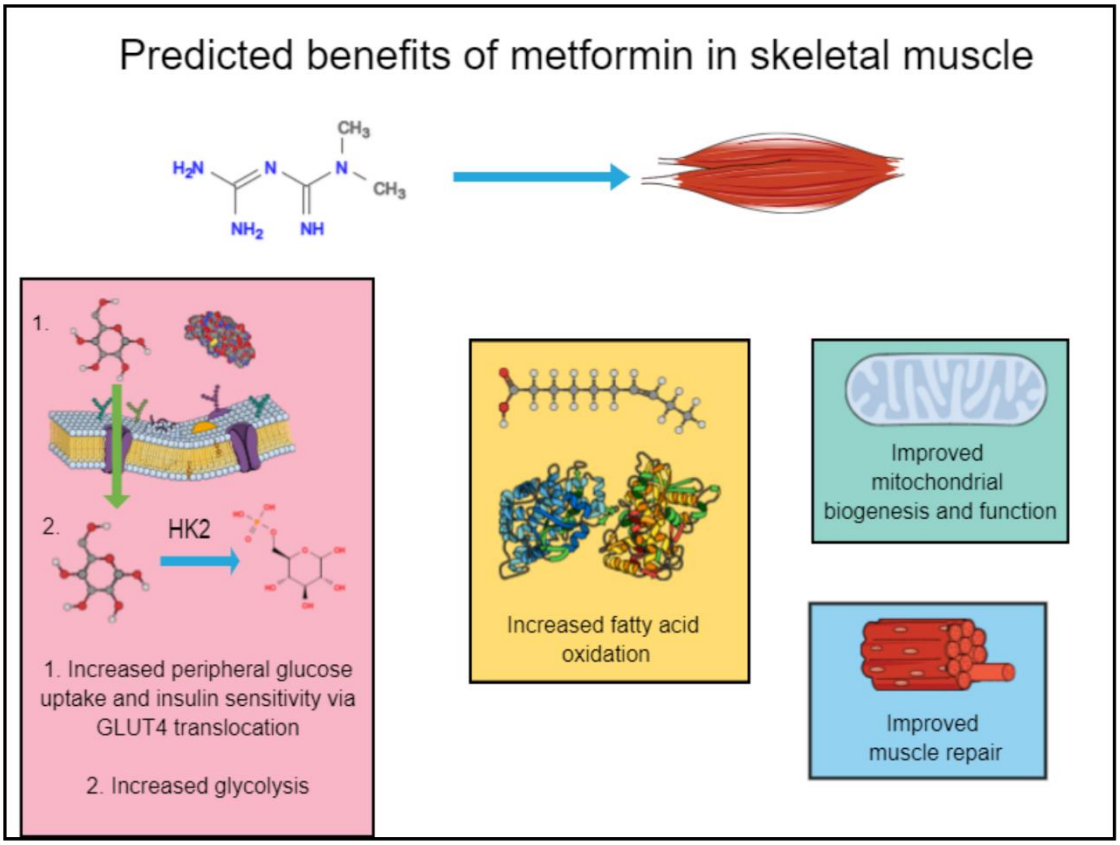

Figure 4.2. Benefits of metformin for skeletal muscle health.
Metformin modulates many skeletal muscle functions and processes that have been reported as dysfunctional in SMA. These include glucose metabolism, fatty acid metabolism, mitochondrial biogenesis and function and muscle repair. Figure was created on Mind the Graph.

An additional benefit of metformin in SMA could be the possible ergogenic effects it could bestow on the muscle wasting pathology. Indeed, metformin alleviated muscle wasting in pre-clinical models of cachexia, cardiotoxin and burn-injury via improved muscle regeneration, elevated $Pax7^{+}$ muscle progenitor cells, and increased net muscle protein synthesis (MPS) [911–913]. Furthermore, metformin treatment has improved neuromuscular and myopathic defects in disorders such as DMD [914] and congenital muscular dystrophy type 1 A (CMDT1A) [915]. Overall, the metabolic and muscle-specific improvements conferred by metformin in other conditions warrant its investigation in SMA.

Thus, the aim of this chapter is to evaluate the suitability of metformin as a skeletal muscle treatment for SMA. We will address this aim by the following objectives.

1. Validate the expression of predicted metformin targets genes in human and murine SMA cellular and animal models.
2. Investigate the effects of metformin, *Smn* depletion and canonical atrophy on the predicted metformin target genes in C2C12 myoblast-like cells.
3. Evaluate the therapeutic potential of metformin in $Smn^{2B/-}$ SMA mice.

4.2. Methods

4.2.1. *In vitro* metformin treatment.

Proliferating C2C12 myoblasts were seeded in 6-well plates (x4 wells per group). At 50-60% confluency for C2C12 myoblasts and D7 stage for differentiated C2C12 myotubes, they were treated with metformin (Sigma-Aldrich) dissolved in sterile PBS at concentrations of 0.3, 0.6, 1 and 2 mM for 24 hours against a PBS control (0.1% v/v).

4.2.2. *In vivo* metformin treatment.

Litters containing *Smn*$^{2B/-}$ SMA and *Smn*$^{2B/+}$ healthy mice were phenotypically analysed daily from P0. At P5, mice were either untreated, vehicle-treated (0.9% physiological saline) or received 200 or 400 mg/kg/day metformin hydrochloride (Sigma-Aldrich), dissolved in 0.9% physiological saline by gavage using a 25 µl syringe (Hamilton) and 1.25 mm gavage needle (Cadence Science), daily and up to humane endpoint (N>10). Skeletal muscle (*Triceps brachii* and TA), liver and spinal cord (N >4) were harvested from P14 untreated, and metformin hydrochloride-treated *Smn*$^{2B/-}$ SMA and *Smn*$^{2B/+}$ healthy mice 2 hours after final treatment. Furthermore, blood glucose levels (mmol/L) were measured immediately after euthanasia in non-fasted pups via True Metrix Go blood glucose monitoring system (Trividia Health).

4.3. Results

4.3.1. Metformin is predicted to emulate prednisolone's targeting of *Prkag3* and *FoxO* isoforms in SMA skeletal muscle.

In chapter 2, our bioinformatics and pathway analyses predicted metformin as a suitable candidate for emulating prednisolone's activity in skeletal muscle of *Smn*$^{-/-}$*;SMN2* SMA mice. Indeed, both prednisolone and metformin were predicted to upregulate *Prkag3*, which encodes the AMPK-γ3 subunit of the predominant skeletal muscle AMPK α2β2γ3 complex isoform [832] (Figure 4.3.a-b). Furthermore, the upregulated *Prkag3* was predicted to coherently downregulate the expression of *FoxO1*, *FoxO3* and *FoxO4* isoforms, whilst upregulating *FoxO6,* based on impact analysis calculations (Figure 4.3.a-b). Interestingly, previous studies have associated the activation of *FoxO1*, *FoxO3* and *FoxO4* isoforms to atrophy pathways in SMA skeletal muscle [56], whilst decreased expression of *FoxO6* has been linked with canonical muscle atrophy [916]. Importantly, the expression levels of *Prkag3* and the *FoxO* isoforms were normalised in skeletal muscle of prednisolone-treated *Smn*$^{-/-}$*;SMN2* SMA mice (Figure 4.3.c), validating the usefulness of restoring the expression pattern of these predicted metformin target genes in SMA skeletal muscle. Thus, we decided to investigate if metformin's targeting of *Prkag3* and *FoxO* isoforms could similarly ameliorate skeletal muscle pathologies in SMA cellular and animal models.

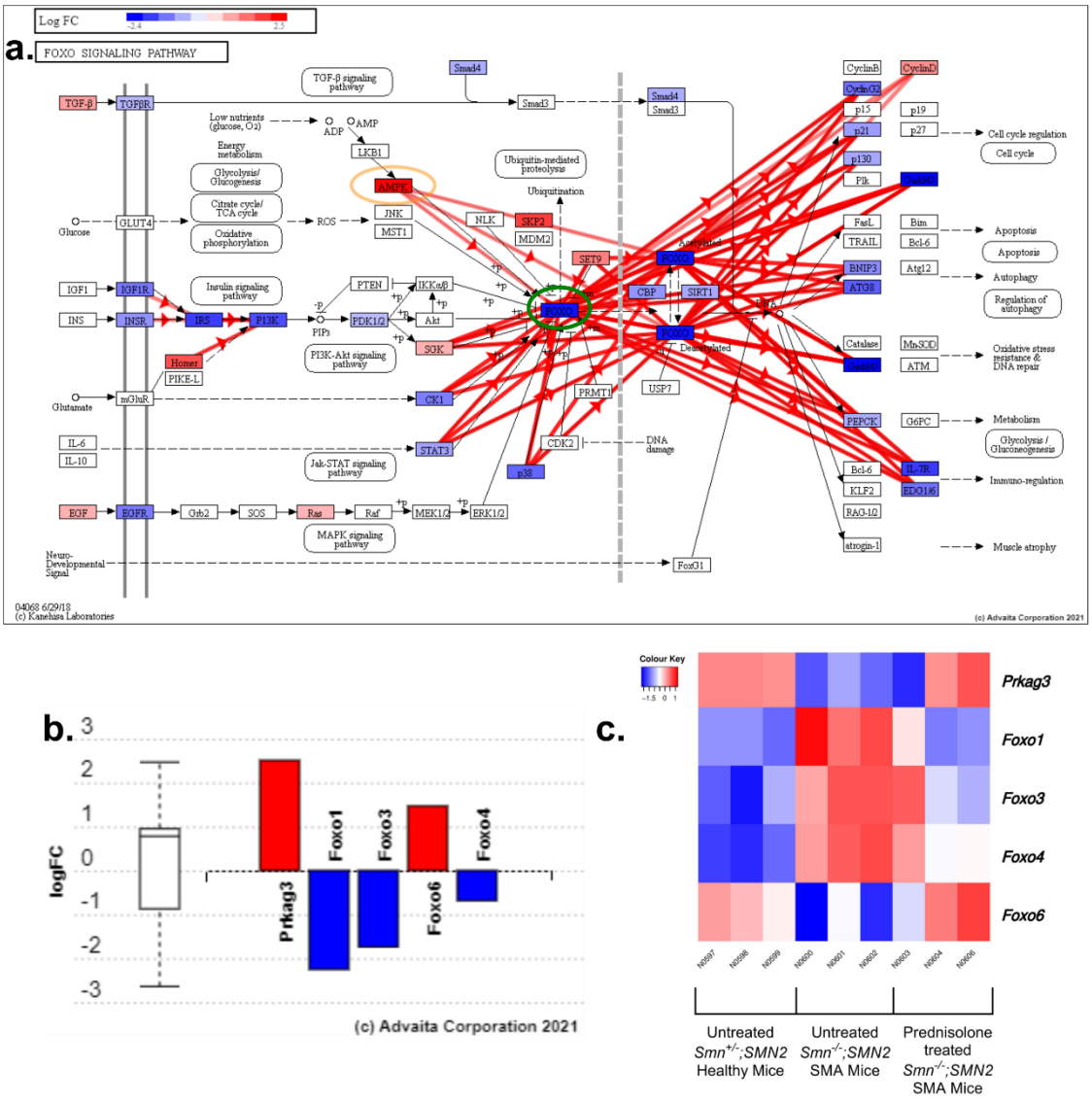

Figure 4.3. Bioinformatic identification of shared target genes between metformin and prednisolone in SMA skeletal muscle.

a. The pathway diagram contains proteins within the FOXO signalling pathway (KEGG: 04068) encoded by the predicted differentially expressed genes from prednisolone vs untreated *Smn*$^{-/-}$;*SMN2* SMA skeletal muscle. The AMPK protein (yellow circle) represents the AMPK-γ3 isoform gene *Prkag3*. Its activity on the iPathwayGuide interactive server highlights that it can be targeted by metformin via a built-in KEGG Drugs database. The red lines represent coherent cascades, which supports the consistency of the transcriptomic data and published pathway activity. In the FOXO signalling pathway activation of AMPK represented by *Prkag3* coherently downregulates the FOXO protein (green circle), which represents *FoxO1*, *FoxO3*, *FoxO4* and *FoxO6* isoforms. The highest logFC patterns are shown in dark red and lowest in dark blue as indicated in the legend value box. Graph generated in iPathwayGuide (Advaita). **b.** Differential gene expression pattern by LogFC (Y-axis) of predicted metformin targets *Prkag3*, *FoxO1*, *FoxO3*, *FoxO4*, and *FoxO6* based on transcriptomic data from prednisolone vs untreated *Smn*$^{-/-}$;*SMN2* SMA skeletal muscle. Upregulated genes above X-axis are highlighted in red and downregulated genes below X-axis highlighted in blue. The box and whisker plot on Y axis represents 1st quartile, median and 3rd quartile. Graph generated in iPathwayGuide (Advaita). **c.** Heatmap visualisation for predicted metformin targets *Prkag3*, *FoxO1*, *FoxO3*, *FoxO4*, and *FoxO6* (Log2FC >0.6; FDR <0.05) between untreated *Smn*$^{+/-}$;*SMN2* healthy mice (left), untreated *Smn*$^{-/-}$;*SMN2* SMA mice (centre), and prednisolone-treated *Smn*$^{-/-}$;*SMN2* SMA mice (right). Colour key represents the Log2FC for upregulated (red) and downregulated (blue) genes. Heatmap was generated by Heatmap2 v2.2.1+galaxy1.

4.3.2. *Prkag3* is downregulated in skeletal muscle of both severe *Smn$^{-/-}$;SMN2* and intermediate *Smn$^{2B/-}$* SMA mice.

We firstly wanted to validate our bioinformatic predictions on whether the metformin target genes were indeed dysregulated in SMA mice. For that purpose, we decided to measure the gene expression levels of the metformin target genes in the triceps of P7 symptomatic, untreated severe *Smn$^{-/-}$;SMN2* SMA and *Smn$^{+/-}$;SMN2* healthy mice by qPCR (Figure 4.4). For the main metformin target *Prkag3*, we found a significant downregulation of *Prkag3* in symptomatic severe *Smn$^{-/-}$;SMN2* SMA mice (-0.7 FC, p =0.0359) (Figure 4.4.a), supporting the predicted bioinformatics data and suggesting it may play a role in muscle pathologies. However, for the *FoxO* isoforms (*FoxO1* (1.1 FC, p =0.8161), *FoxO3* (1.4 FC, p =0.5441), *FoxO4* (-0.3 FC, p =0.3684), and *FoxO6* (-0.3 FC, p =0.3447) we found no significant difference in their expression levels between severe *Smn$^{-/-}$;SMN2* SMA and *Smn$^{+/-}$;SMN2* healthy mice (Figures 4.4.b-e). Although a previous study similarly found no significant difference in the qPCR expression of *FoxO* isoforms in symptomatic severe *Smn$^{-/-}$;SMN2* SMA mice [56], the distinction to our previous RNA-Seq data (Figure 4.3) suggests the possibility that our sequencing depth coverage was not conservative enough, which allowed for detection of low expressed genes [917], highlighting the importance of wet lab validation.

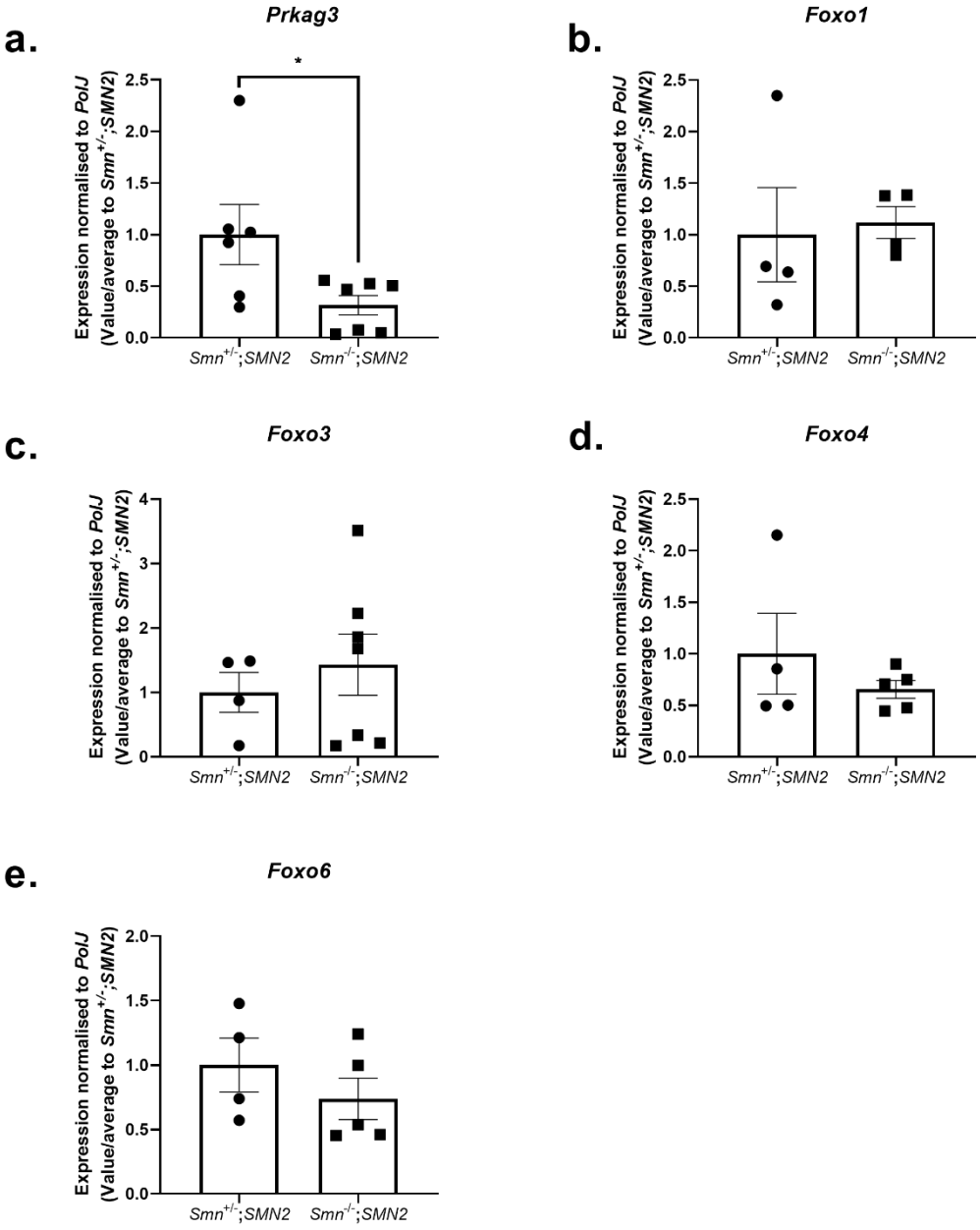

Figure 4.4. The metformin target gene *Prkag3* is downregulated in the skeletal muscle of symptomatic *Smn$^{-/-}$;SMN2* SMA mice.
The mRNA expression by qPCR of predicted metformin targets **a.** *Prkag3*, **b.** *Foxo1*, **c.** *Foxo3*, **d.** *Foxo4* and **e.** *Foxo6* in symptomatic P7 skeletal muscle (triceps) of *Smn$^{+/-}$;SMN2* healthy (N= 4 - 6) and *Smn$^{-/-}$;SMN2* SMA (N= 5 - 7) mice. Error bars represents +/- SEM with individual value points as black dot; unpaired t-test, *p <0.05.

Although our bioinformatic analyses were performed on muscles from severe *Smn$^{-/-}$;SMN2* SMA mice, we also decided to validate the metformin target genes in the milder *Smn$^{2B/-}$* SMA mice, as we have previously shown that both models share pathological pathways targeted by prednisolone [53]. Thus, we measured the gene expression levels of the metformin target genes in the triceps of untreated WT (C57BL/6J background) and intermediate *Smn$^{2B/-}$* SMA mice at pre-symptomatic (P10) and symptomatic (P19) stages [38,57] (Figure 4.5).

Interestingly, we found that *Prkag3* was significantly downregulated in both pre-symptomatic (-0.5 FC, p =0.0262) and symptomatic *Smn$^{2B/-}$* SMA mice (-0.8FC, p =0.0200) (Figures 4.5.a-b). For the downstream *FoxO* isoforms (*FoxO1* (1.5 FC, p =0.5520), *FoxO3* (1.4 FC, p =0.6803), *FoxO4* (5.0 FC, p= 0.0966), and *FoxO6* (1.1 FC, p =0.8460)), we found no significant difference in the triceps between WT and *Smn$^{2B/-}$* SMA mice in pre-symptomatic stages (Figures 4.5.c, e, g, i), coinciding with an absence of overt atrophy at that time-point [56]. However, we also did not observe any significant differences in symptomatic stages either (*FoxO1* (36.6 FC, p =0.3929), *FoxO3* (1.6 FC, p =0.2721), *FoxO4* (1.5 FC, p= 0.4819), and *FoxO6* (-0.3 FC, p =0.3335)) (Figures 4.5.d, f, h, j), which could be attributed to the wide variation in individual *Smn$^{2B/-}$* SMA samples.

Although the *FoxO* isoforms did not significantly reflect their transcriptomic predictions, we did find that *Prkag3* is downregulated in both severe *Smn$^{-/-}$;SMN2* and intermediate *Smn$^{2B/-}$* SMA mice, suggesting that this gene may be involved in both severe and milder SMA muscle pathologies. Furthermore, the significant downregulation of *Prkag3* in pre-symptomatic *Smn$^{2B/-}$* SMA mice suggests that this gene may impact muscle health in early disease stages, prior to symptomatic onset.

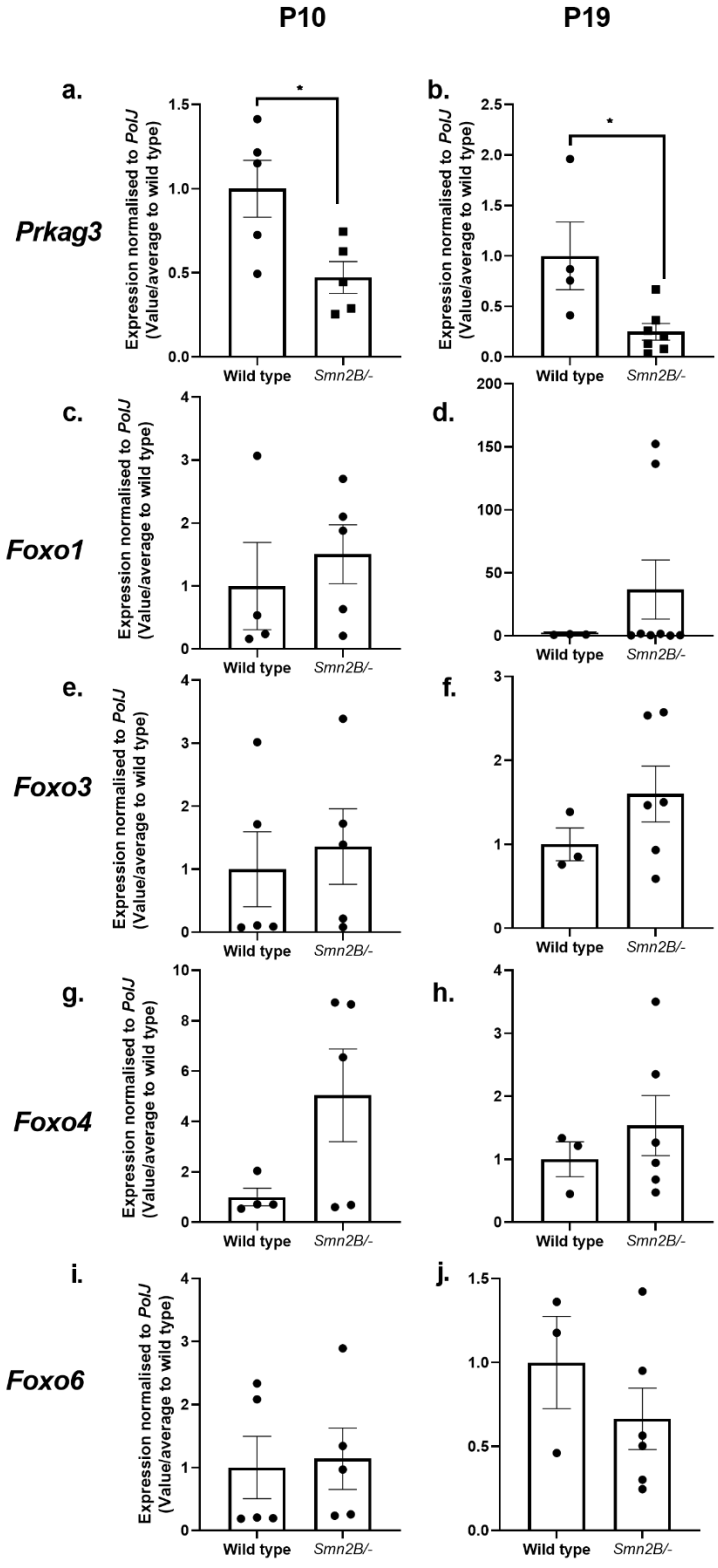

Figure 4.5. The metformin target gene *Prkag3* is downregulated in the skeletal muscle of both pre-symptomatic and symptomatic *Smn*$^{2B/-}$ SMA mice.
The mRNA expression by qPCR of predicted metformin targets *Prkag3* , *Foxo1*, *Foxo3*, *Foxo4* and *Foxo6* in pre-symptomatic stages (left) at post-natal day (P)10 (**a, c, e, g** and **i**) and at symptomatic stages (right) at P19 (**b, d, f, h,** and **j**) in skeletal muscle (triceps) of wild type (N= 4-6) and *Smn*$^{2B/-}$ SMA (N=6-8) mice. Error bars represents +/- SEM with individual value points as black dot; unpaired t-test, *p <0.05.

4.3.3. Main metformin target *PRKAG3* is upregulated in type 3 SMA deltoid myoblasts.

We next wanted to determine if the predicted metformin target genes were also dysregulated in SMA patients. For that purpose, we used primary myoblasts from deltoid biopsies of healthy control and type 3 SMA patients [13] (in collaboration with Dr Stephanie Duguez; Chapter 2, Table 2.2). Interestingly, we found that the expression of *PRKAG3* was significantly upregulated (4.5 FC , p =0.0037) in type 3 SMA myoblasts compared to healthy controls (Figure 4.6.a), contradicting the inverse patterns observed in *Smn*$^{-/-}$*;SMN2* and *Smn*$^{2B/-}$ SMA mice (Figures 4.4-5). Although we cannot rule out species (human vs mouse) and muscle type (deltoid vs triceps) differences, we also must take into consideration that these human myoblasts are no longer *in vivo* samples [918], and thus there could be an experimental (*in vitro* vs *in vivo*) difference. However, another explanation could be that *Smn*$^{-/-}$*;SMN2* and *Smn*$^{2B/-}$ SMA mice present severe phenotypes compared to type 3 SMA patients [13,38,57]. Thus, one explanation for the observed inverse expression is the greater ambulatory ability of type 3 SMA patients, which could lead to greater requirements of the AMPK α2β2γ3 isoform that is predominantly associated with intense exercises [13,832].

On the other hand, the expression levels of *FOXO1* (1.5 FC, p =0.4881) and *FOXO3* (1.7 FC, p =0.1731) isoforms were not significantly different between controls and type 3 SMA myoblasts (Figures 4.6.b-c), aligning with previous reports of normal FOXO signalling in similar cells [359]. In summary, we find that *PRKAG3* expression is potentially influenced by several factors including experimental status, species, severity, and/or muscle type. Nevertheless, *PRKAG3* expression is dysregulated in muscle from both SMA mice and patients.

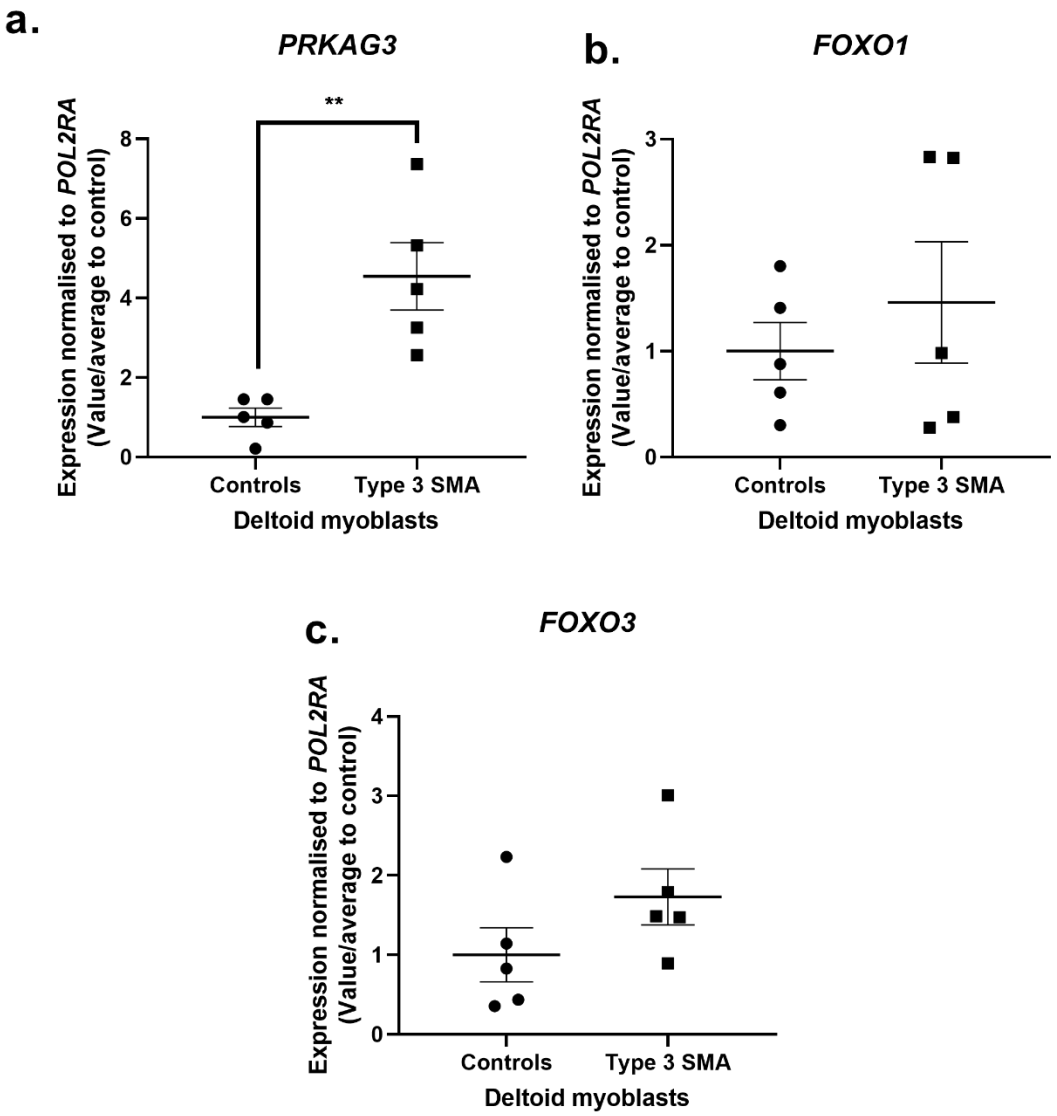

Figure 4.6. The metformin target gene *PRKAG3* is significantly upregulated in type 3 SMA deltoid myoblasts.
The mRNA expression by qPCR of metformin target genes **a.** *PRKAG3*, **b.** *FOXO1* and **c.** *FOXO3* in primary myoblasts from deltoid muscle biopsies from healthy controls and type 3 SMA patients (N=5). Individual samples are plotted as black dots, centre line represents mean and error bars represent +/- SEM; unpaired t-test, $^{**}p < 0.01$.

4.3.4. Dysregulation of predicted metformin target genes in C2C12 myoblasts and myotubes is mostly SMN-independent.

In the symptomatic muscle samples from SMA pre-clinical models and patients, the presence of both denervation and intrinsic SMN depletion can make it difficult to distinguish which factor had the greater influence on the metformin target genes. Thus, we wanted to investigate if intrinsic SMN depletion in skeletal muscle had a direct effect on the expression of metformin's target genes. In order to address this, we used an siRNA-mediated *Smn* depletion approach in immortalised murine C2C12 myoblast-like cells, making it a useful *in vitro* model of intrinsic SMA muscle defects independent of motor neuron denervation [159].

In our study, we transfected C2C12 myoblasts for 48 hours and differentiation day (D)8 myotubes for 192 hours with *Smn* siRNA to investigate its effects on the metformin target genes in different stages of muscle development. In addition, we also used a scrambled siRNA control to rule out any gene perturbations influenced by the lipofectamine transfection or presence of random genetic material. We initially determined by qPCR that siRNA-mediated *Smn* KD in both C2C12 myoblasts (-0.9 FC, p <0.0001) and myotubes (-0.9 FC, p <0.0001) decreased *Smn* mRNA levels by 90% (Figures 4.7.a-b), which is similar to the FL-SMN levels observed in type 1 SMA with one or two *SMN2* gene copies [38,41,161].

Next, we investigated the effect of *Smn* depletion on the predicted metformin target genes. In C21C2 myoblasts, we only found a significant upregulation of the *FoxO3* gene (1.7 FC, p =0.0020) when *Smn* was depleted, whilst the other metformin targets remained unchanged (*Prkag3* (1.1 FC, p =0.2760), *FoxO1* (1.4

FC, *p* =0.0882), *FoxO4* (not significant (ns), *p* =0.7900), and *FoxO6* (ns, *p* =0.8265) (Figure 4.7.c). Interestingly, previous microarray analyses in isolated iPSC-derived type 1 SMA myoblasts also revealed a selective upregulation of certain *FOXO* isoforms [359].

We also show that the expression of the predicted metformin target genes was not significantly different between siRNA-mediated *Smn* KD and control D8 C2C12 myotubes (*Prkag3* (ns, *p* =0.9561), *FoxO1* (-0.2 FC, *p* =0.1383), *FoxO3* (1.1 FC, *p* =0.7966), *FoxO4* (ns, *p* =0.8550), and *FoxO6* (-0.3 FC, *p* =0.0742) (Figure 4.7.d), suggesting that intrinsic *Smn* depletion has no effect on the expression of these genes in in mature muscle fibres.

In summary, our results indicate that although *FoxO3* is perturbed by intrinsic siRNA-mediated *Smn* KD in C2C12 myoblasts, overall, *in vitro Smn* depletion does not have a significant impact on the expression of metformin target genes in proliferating and differentiated C2C12 cells.

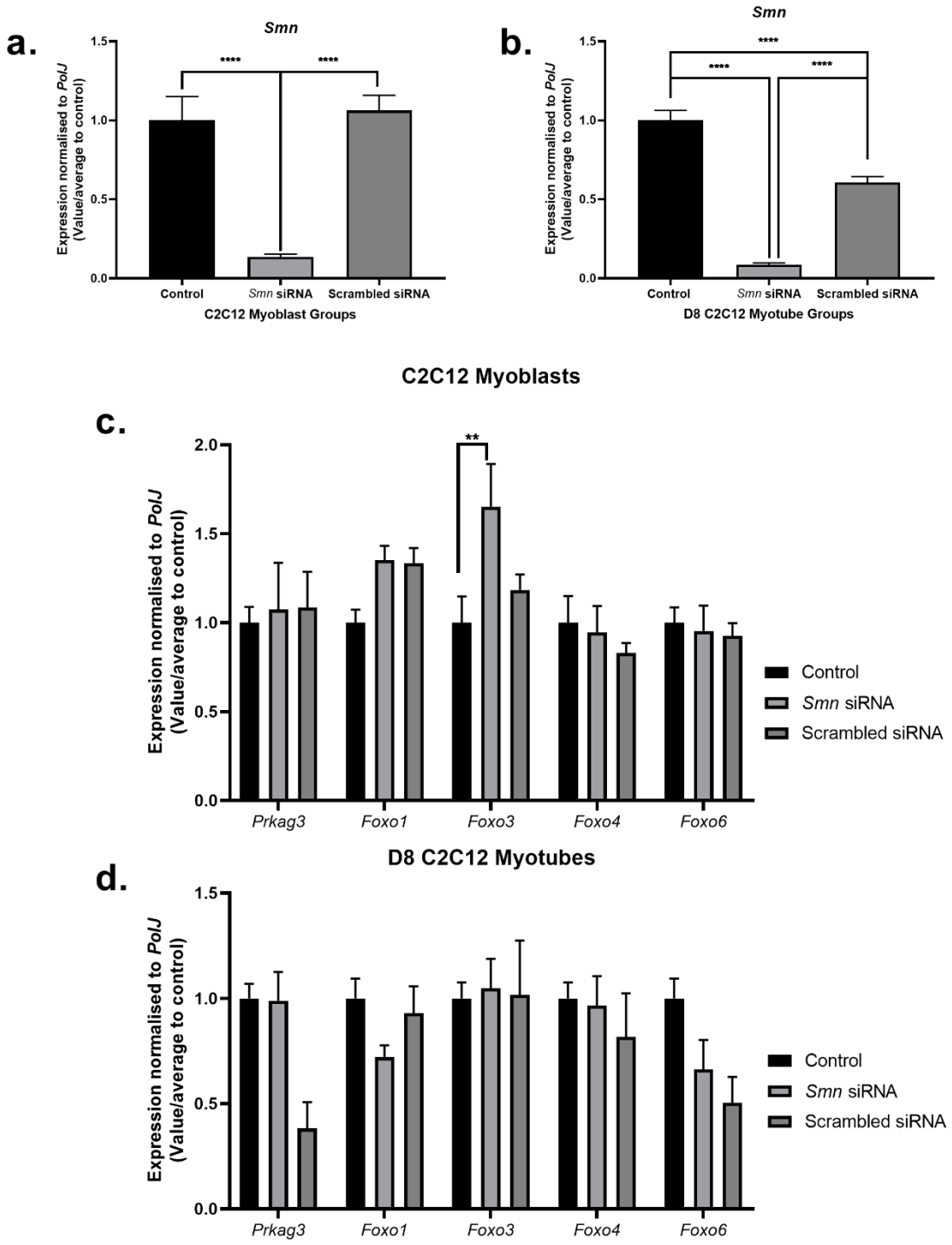

Figure 4.7. Majority of the metformin target genes are not affected by *Smn* depletion in C2C12 myoblasts and myotubes.
The mRNA expression by qPCR of *Smn* and predicted metformin target genes *Prkag3*, *Foxo1*, *Foxo3*, *Foxo4* and *Foxo6* in control, *Smn* siRNA and scrambled siRNA groups in C2C12 myoblasts (**a** and **c**) and D8 myotubes (**b** and **d**). Data represents N= 3-4 samples per group across two independent experiments; error bars represent +/- SEM; Two-way ANOVA with post-hoc uncorrected Fishers LSD test, **p* <0.05, ***p* <0.01.

4.3.5. Administration of both physiological and supraphysiological metformin concentrations did not emulate the predicted expression patterns of target genes in C2C12 myoblasts and myotubes.

Next, we wanted to evaluate metformin's predicted ability to influence the expression of *Prkag3* and *FoxO* genes as observed in our transcriptomic data (Figure 4.3). In our investigation, we used the C2C12 myoblast-like cell line as they are a frequently used *in vitro* model for skeletal muscle studies [665,666] and would allow us to evaluate the direct effect of metformin on the target genes in muscle. Based on previous research in C2C12 cells, we used "physiological" metformin concentrations were in a range of 30 – 60 µM as these are representative of skeletal muscle concentrations in diabetic patients who receive 1g of metformin twice a day [919,920]. We also investigated "supraphysiological" concentrations of around 1 – 2 mM as these have been key for *in vitro* metformin pharmacodynamics studies [865,920,921].

Importantly, prior investigations of both physiological and supraphysiological metformin concentrations in C2C12 cells ruled out any signs of toxicity [912]. Furthermore, we selected a treatment duration of 24 hours based on findings that 3 days of > 2 mM metformin treatment negatively impacted C2C12 myoblast proliferation via cell cycle arrest and impaired myotube fusion during myogenic differentiation [922].

When we compared 24 hours of physiological and supraphysiological metformin treatment in proliferating C2C12 myoblasts, we identified neither concentration had a significant effect on the expression of the main metformin target, *Prkag3* (Figure 4.8.a). However, for *FoxO* targets, only *FoxO3* was significantly

upregulated by the physiological 60 µM concentration (1.6 FC, *p* =0.0263), whilst both *FoxO3* (2.2 FC, *p* <0.0001) and *FoxO4* (1.8 FC, *p* =0.0009) were significantly upregulated by the supraphysiological 2 mM concentration (Figure 4.8.a). Thus, our C2C12 myoblasts revealed that metformin did not significantly upregulate *Prkag3* and *FoxO6* or downregulate *FoxO1*, *FoxO3* and *FoxO4* in accordance with our bioinformatic predictions (Figure 4.3).

Next, we evaluated metformin's effects on the predicted target genes in differentiated D8 C2C12 myotubes. Interestingly, both physiological (60 µM) (-0.5 FC, *p* =0.0218) and supraphysiological (1 (-0.6 FC, *p* =0.0049) and 2 mM (-0.6 FC, *p* =0.0068)) metformin concentrations significantly reduced *Prkag3* expression in D8 C2C12 myotubes (Figure 4.8.b). In addition, the physiological 60 µM concentration significantly upregulated *FoxO3* (1.5 FC, *p* =0.0276), whilst the supraphysiological 1 mM concentration significantly reduced *FoxO6* expression (-0.4 FC, *p* =0.0490) in D8 C2C12 myotubes (Figure 4.8.b), revealing in the myotube stage, metformin acts opposingly to the predicted bioinformatic expression patterns (Figure 4.3).

It was unclear why the main metformin target *Prkag3* was not significantly upregulated in C2C12 myoblasts and myotubes, as previous research showed that AMPKα2β2γ3 can be upregulated by metformin treatment [300]. However, in patients and mice, metformin is primarily metabolised in the liver to inhibit gluconeogenesis [923]. Thus, one possibility could be that direct metformin treatment inhibits gluconeogenesis in the C2C12 myotubes resulting in a breakdown of glycogen stores for glucose production. If this occurred, then *Prkag3* activity in theory would reduce as it plays important roles for glycogen storage [831,924].

Nevertheless, our *in vitro* metformin results revealed that neither physiological nor supraphysiological metformin concentrations emulated the predicted perturbation pattern of our target genes in C2C12 myoblasts and myotubes.

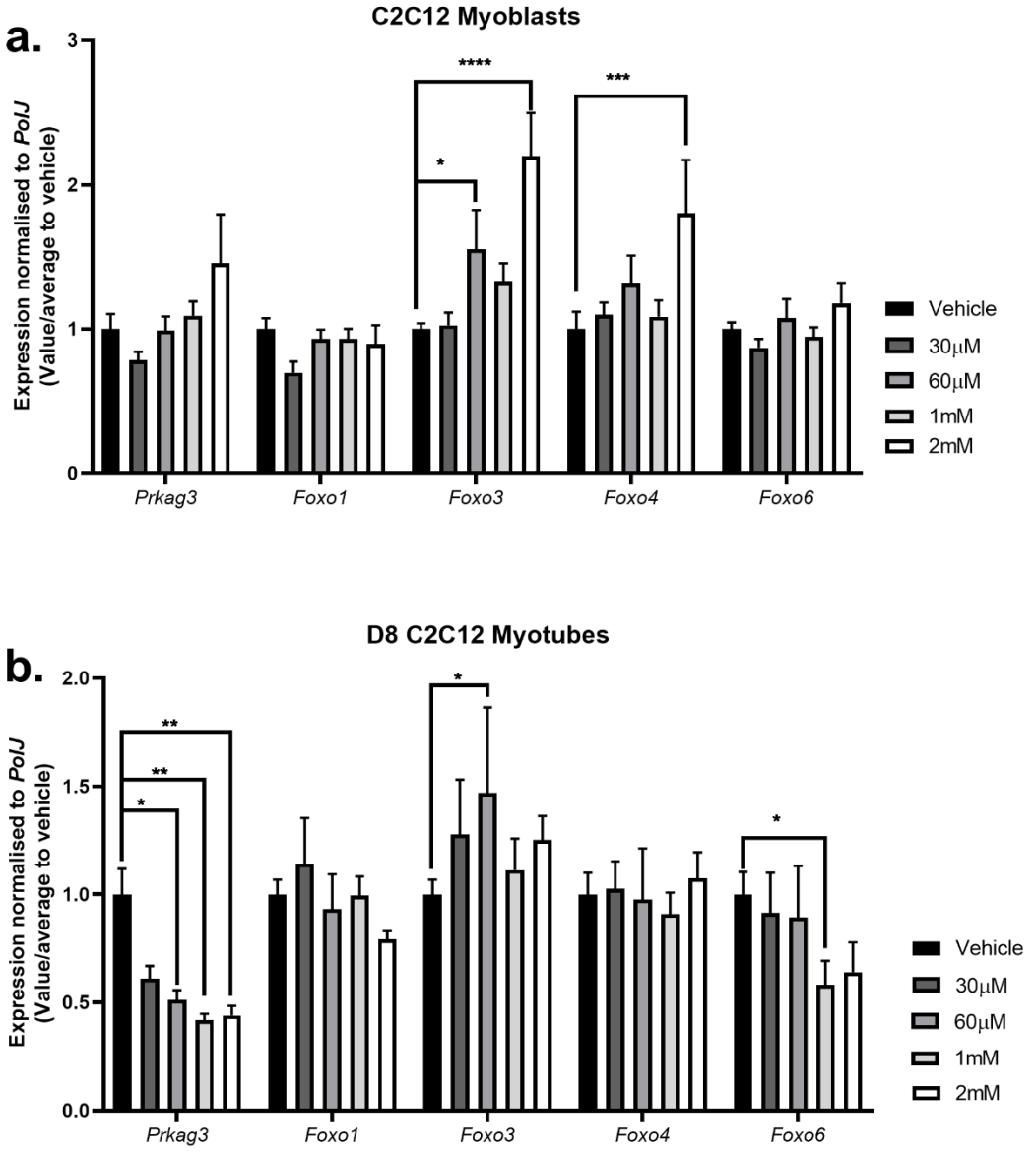

Figure 4.8. *In vitro* physiological and supraphysiological metformin treatments do not emulate the transcriptomic predicted expression of metformin target genes in C2C12 myoblasts and myotubes.
The mRNA expression by qPCR of predicted metformin targets *Prkag3*, *Foxo1*, *Foxo3*, *Foxo4* and *Foxo6* across C2C12 **a.** myoblasts and **b.** myotubes treated for 24 hours with PBS vehicle (black), 30 μM (dark grey), 60 μM (grey), 1 mM (light grey) and 2 mM (white) metformin concentrations. Data represents N=4 samples per group across two independent experiments; error bars represent +/- SEM; Two-way ANOVA with post-hoc uncorrected Fishers LSD test, **p* <0.05, ***p* <0.01, ****p* <0.001, *****p* <0.0001.

4.3.6. Metformin treatment does not attenuate canonical atrophy in C2C12 myotubes.

In our final *in vitro* investigation, we wanted to determine if metformin could attenuate muscle atrophy. Here, we used a validated method of serum-starvation-induced atrophy in differentiated C2C12 cells [667,668]. After 24 hours of starvation in serum-free high glucose DMEM, we observed a significant upregulation of *atrogin-1* mRNA (2.3 FC, p =0.0006) alongside myotube loss, confirming our *in vitro* atrophy model (Figures 4.9.a-c). Evaluation of the metformin target genes in the serum-deprived C2C12 myotubes revealed a significant upregulation of the *FoxO3* (1.9 FC, p =0.0096) and *FoxO4* (2.2 FC, p =0.0004) isoforms (Figure 4.9.d), which reflects the role these *FoxO* isoforms play in atrophy-dependent ubiquitin-proteasome pathways [363], further validating our model.

Next, we investigated whether metformin could modulate the serum-starvation-induced atrophy and dysregulated expression of *FoxO3* and *FoxO4* (Figure 4.9.d). Based on metformin's activity in control D8 C2C12 myotubes (Figure 4.8.b), we treated the serum-starved C2C12 myotubes with 2 mM metformin for 24 hours. Interestingly, we found that 2 mM metformin enhanced the significant upregulation of *atrogin-1* mRNA levels (2.7 FC, p =0.0137) (Figure 4.9.e), suggesting that supraphysiological concentrations of metformin may exacerbate muscle atrophy in our *in vitro* model (Figure 4.9.f). However, analysis of the *FoxO* genes revealed only a significant upregulation of *FoxO6* (2.1 FC, p =0.0233) (Figure 4.9.g), an isoform that is normally downregulated in atrophy [916], suggesting that the exacerbation of atrophy in our model by metformin could be through effectors outside of our predicted target genes.

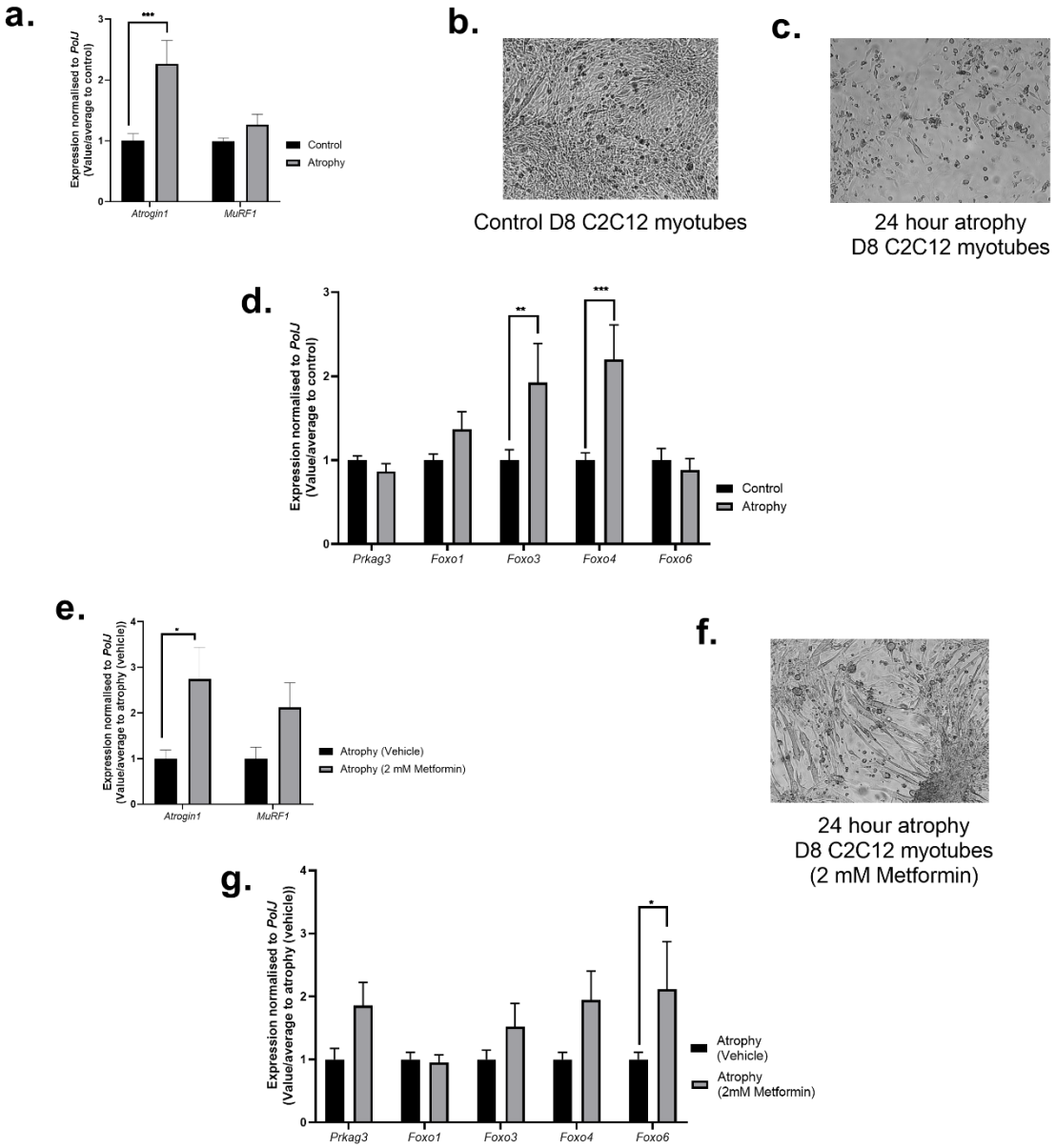

Figure 4.9. Supraphysiological metformin treatment exacerbates canonical atrophy in serum-starved D8 C2C12 myotubes.
a. Atrogene (a*trogin-1* and *MuRF1*) mRNA expression by qPCR between healthy control and 24-hour serum-deprived D8 C2C12 myotubes. 10x magnification of **b.** healthy control and **c.** 24-hour serum-deprived atrophy in D8 C2C12 myotubes. **d.** mRNA expression by qPCR of predicted target genes between healthy control and 24-hour serum-deprived D8 C2C12 myotubes. **e.** Atrogene (*atrogin-1* and *MuRF1*) mRNA expression by qPCR between vehicle control and 2 mM metformin treated 24-hour serum-deprived D8 C2C12 myotubes. **f.** 10 x magnification of 2 mM metformin treated 24-hour serum-deprived D8 C2C12 myotubes. **g.** mRNA expression by qPCR of predicted target genes between vehicle control and 2 mM metformin treated 24-hour serum-deprived D8 C2C12 myotubes. Data represents N=4 samples per group across two independent experiments; error bars represent +/- SEM; Two-way ANOVA with post-hoc uncorrected Fishers LSD test, *p <0.05, **p <0.01, ***p <0.001.

Seeing as supraphysiological levels of metformin appeared to exacerbate atrophy in our differentiated C2C12 myotubes, we next investigated if a lower physiological metformin concentration could have an inverse effect on canonical atrophy. However, we found that treating cells with 30 µM metformin for 24 hours did not significantly downregulate *atrogin-1* expression (ns, p =0.4230), suggesting that it does not attenuate atrophy (Figure 4.10). Interestingly, the 30 µM concentration did not exacerbate atrophy either, highlighting a relationship between metformin concentration and perturbation of atrophy signalling.

In summary, our findings revealed that metformin treatment did not attenuate canonical atrophy in C2C12 myotubes and higher concentrations could promote further muscle wasting. However, it is important to consider that although distinct atrophic stimuli may share similar signalling pathways [925], there are still differences between denervation- and starvation-induced muscle wasting and metformin may possibly have a different effect in denervated skeletal muscle.

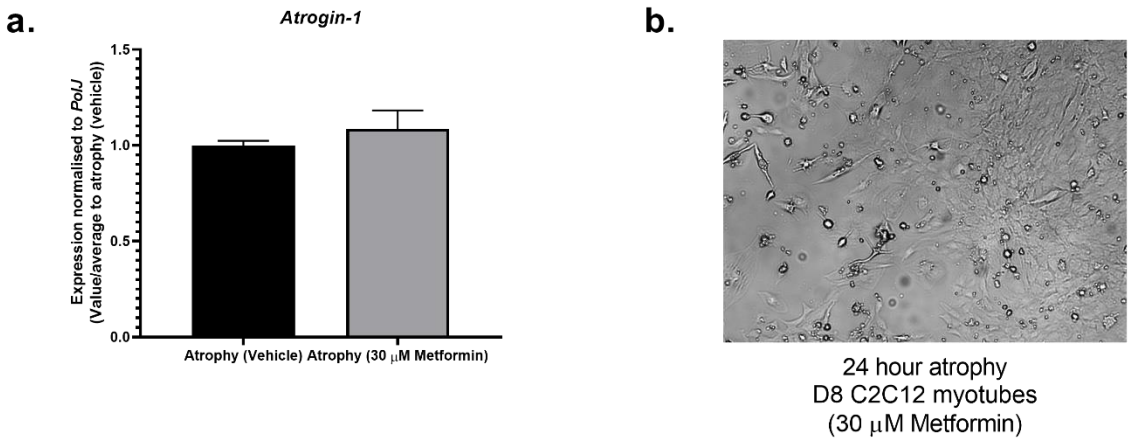

Figure 4.10. Physiological metformin treatment does not attenuate canonical atrophy in serum-starved D8 C2C12 myotubes.
a. Atrogene (*atrogin-1*) mRNA expression by qPCR between vehicle control and 30 µM metformin treated 24-hour serum-deprived D8 C2C12 myotubes. **b.** 10 x magnification of 30 µM metformin treated 24-hour serum-deprived D8 C2C12 myotubes. Data represents N=4 samples per group; error bars represent +/- SEM; unpaired t-test.

4.3.7. Metformin treatment does not improve survival, weight, or motor function in *Smn$^{2B/-}$* SMA mice.

The purpose of our study was to evaluate the effects of metformin on muscle pathologies in SMA. Although our *in vitro* work delivered interesting results, the C2C12 cell lines alone are not a true representation of SMA skeletal muscle. A primary limitation is that they are isolated cells that do not experience the reciprocal cross-talk regulation with interacting tissues compared to primary muscle biopsies [926–928]. Being that SMA is a NMD [1], we also need to take into consideration the systemic effects of metformin treatment on skeletal muscle.

Although our prediction for metformin was based on prednisolone treatment in *Smn$^{-/-}$;SMN2* SMA mice, we performed our *in vivo* experiments in the intermediate *Smn$^{2B/-}$* SMA mice. Not only do *Smn$^{2B/-}$* SMA mice share overlap for prednisolone-targeted pathways [53], but muscle from both *Smn$^{-/-}$;SMN2* and *Smn$^{2B/-}$* SMA mice reported a significant downregulation of *Prkag3* (Figures 4.4-5). Furthermore, the extended lifespan and later symptomatic onset in *Smn$^{2B/-}$* SMA mice allows for clearer distinctions of pre-symptomatic and symptomatic stages and also enables longer durations of metformin treatment [57,138,605]. Thus, from P0 we monitored the survival, weight and motor function (righting reflex) of untreated, vehicle-treated and metformin-treated *Smn$^{2B/-}$* SMA and *Smn$^{2B/+}$* healthy mice to evaluate the potential effect of metformin on life expectancy and disease progression.

Based on a previous study in CMDT1A [915], we began metformin treatment doses at 200 mg/kg/day in pups from P5 up until their humane endpoint. We observed that both untreated and metformin-treated *Smn$^{2B/-}$* SMA mice had a median

survival of 21 days, showing that metformin did not significantly improve life expectancy in SMA mice (Figure 4.11.a).

Next, we assessed body weight, since factors of muscle-wasting, delayed development and metabolic defects can possibly influence weight loss in *Smn*$^{2B/-}$ SMA mice [57]. As previously reported, we observed progressive weight loss starting at around P15 in untreated *Smn*$^{2B/-}$ SMA mice [57] (Figure 4.11.b). Although metformin treatment did not delay progressive weight loss in these mice, on average they remained at a significantly lower body weight from P7 (-0.3 kg average), just two days after initial treatment (Figure 4.11.b). However, the significantly smaller weights of metformin-treated *Smn*$^{2B/-}$ SMA mice at P4 (one day before starting treatment) (-0.4 kg average) suggests that the animals in those litters may have been naturally smaller (Figure 4.11.b).

Another important assessment for therapeutic intervention in SMA is motor function [929]. We observed no significant difference in the righting reflex time in 200 mg/kg/day metformin-treated *Smn*$^{2B/-}$ SMA mice, suggesting that metformin treatment did not improve motor function (Figure 4.11.c).

Importantly, our assessment of 200 mg/kg/day treatment in *Smn*$^{2B/+}$ healthy mice revealed no adverse effects in survival, weight, or motor function, compared to their untreated peers (Figure 4.12). Furthermore, this lack of adverse effects in *Smn*$^{2B/+}$ healthy mice suggests that the bodyweight-lowering effects specifically impacted *Smn*$^{2B/-}$ SMA mice across pre-symptomatic and symptomatic stages.

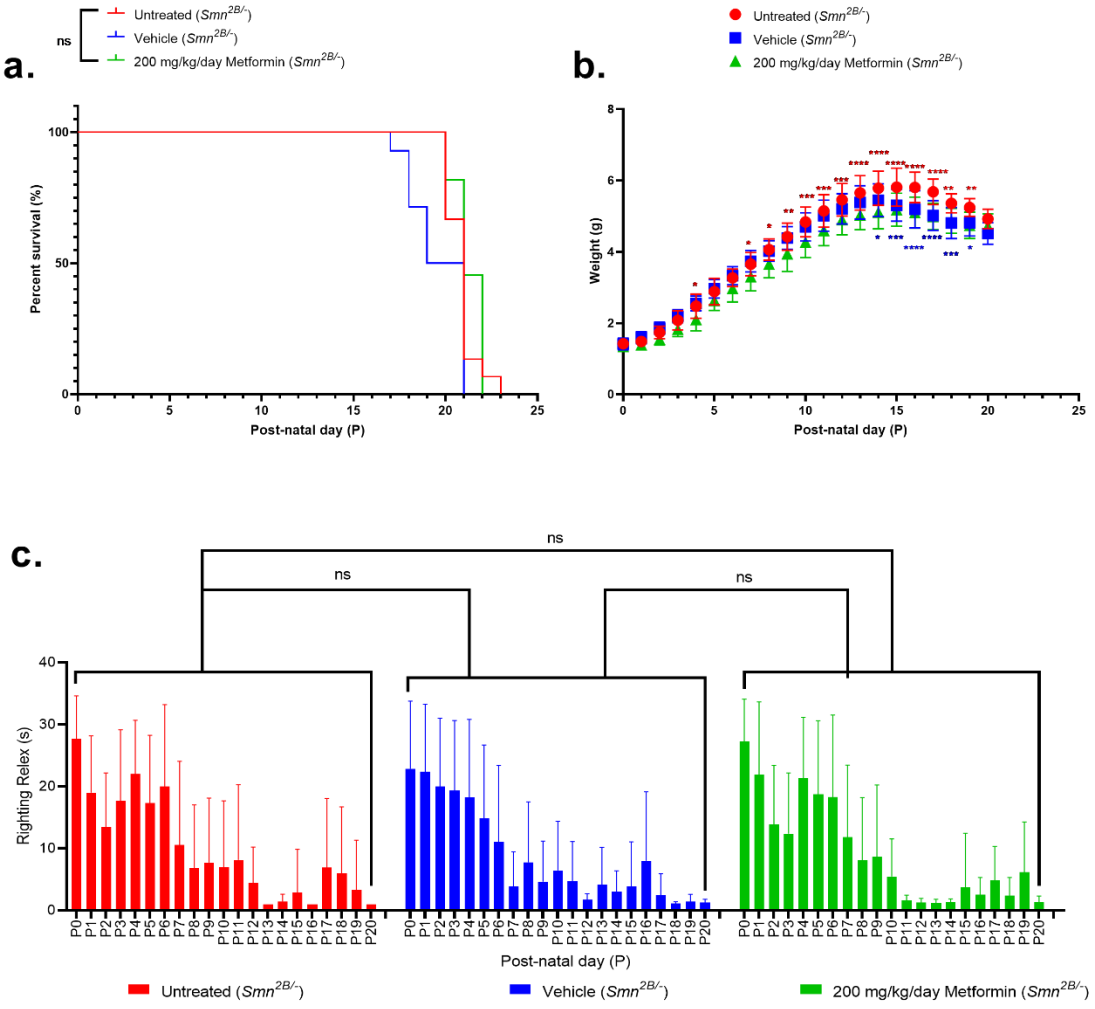

Figure 4.11. 200 mg/kg/day oral metformin treatment did not improve survival, weight or motor function in *Smn$^{2B/-}$* SMA mice.
All treated animals received a daily dose of metformin (200 mg/kg/day, diluted in 0.9% saline) or vehicle by gavage starting at P5.
a. Kaplan-Meier survival curves for n= 13 untreated (red, median survival: 21 days), n= 14 vehicle-treated (blue, median survival: 20 days) and n= 11 200 mg/kg/day metformin-treated (green, median survival: 21 days) *Smn$^{2B/-}$* SMA mice. Long-rank (Mantel-Cox) test ns= not significant.
b. Daily weights of untreated (red, n= 13), vehicle-treated (blue, n= 14) and 200 mg/kg/day metformin-treated (green n= 11) *Smn$^{2B/-}$* SMA mice. Data represents mean and +- SD error bars, Two-way ANOVA with post-hoc Sidak's multiple comparisons test between untreated and 200 mg/kg/day metformin (red star) and untreated vs vehicle-treated (blue star), **p* <0.05, ***p* <0.01, ****p* <0.001, *****p* <0.0001.
c. Daily righting reflex test up to a 30 second max time point of untreated (red, n= 13), vehicle-treated (blue, n= 14) and 200 mg/kg/day metformin-treated (green n= 11) *Smn$^{2B/-}$* SMA mice. Data represents mean and +- SD error bars, One-way ANOVA with post-hoc Tukey's multiple comparisons test, ns = not significant.

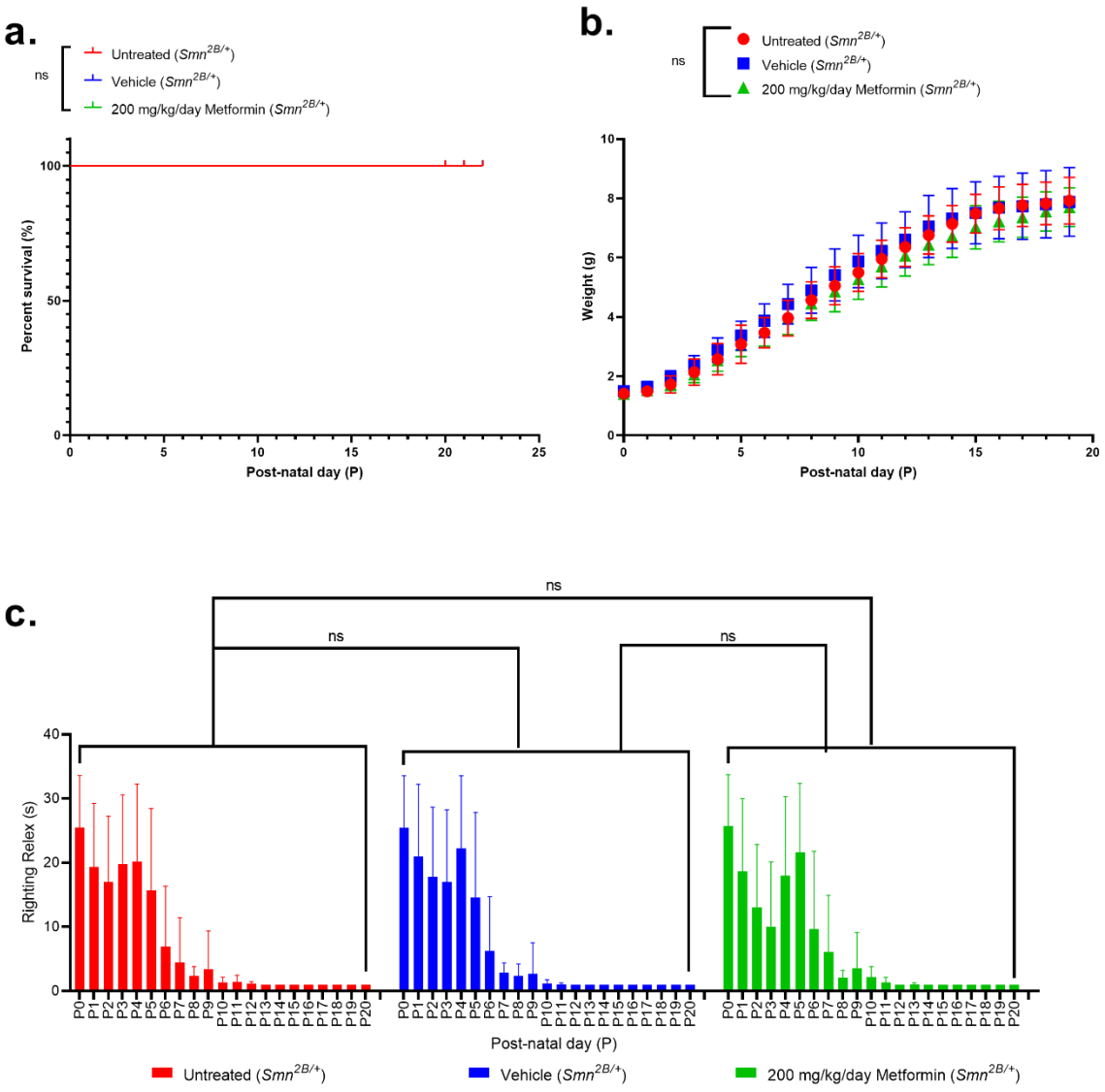

Figure 4.12. 200 mg/kg/day oral metformin treatment had no adverse effects in *Smn$^{2B/+}$* healthy mice.
All treated animals received a daily dose of metformin (200 mg/kg/day, diluted in 0.9% saline) or vehicle by gavage starting at P5.
a. Kaplan-Meier survival curves for n= 16 untreated (red, median survival: 21 days), n= 22 vehicle-treated (blue, median survival: 20 days) and n= 20 200 mg/kg/day metformin-treated (green, median survival: 21 days) *Smn$^{2B/+}$* healthy mice. Long-rank (Mantel-Cox) test ns= not significant.
b. Daily weights of untreated (red, n= 16), vehicle-treated (blue, n= 22) and 200 mg/kg/day metformin-treated (green n= 20) *Smn$^{2B/+}$* healthy mice. Data represents mean and +- SD error bars, Two-way ANOVA with post-hoc Sidak's multiple comparisons test between untreated and 200 mg/kg/day metformin and untreated vs vehicle-treated, ns= not significant.
c. Daily righting reflex test up to a 30 second max time point of untreated (red, n= 16), vehicle-treated (blue, n= 22) and 200 mg/kg/day metformin-treated (green n= 20) *Smn$^{2B/-}$* SMA mice. Data represents mean and +- SD error bars, One-way ANOVA with post-hoc Tukey's multiple comparisons test, ns = not significant.

Since 200 mg/kg/day metformin treatment did not improve disease onset or progression in *Smn*$^{2B/-}$ SMA mice (Figure 4.11), we instead ran pilot studies at later time points (P8) and lower doses (100 mg/kg/day) that resulted in similar effects as those reported for 200 mg/kg/day at P5 (*data not shown*). We therefore tried a higher dose of 400 mg/kg/day metformin, starting at P5. Astonishingly, we observed that 400 mg/kg/day metformin significantly lowered the median survival of *Smn*$^{2B/-}$ SMA pups by 5 days to P16 (Figure 4.13.a). Furthermore, the 400 mg/kg/day metformin-treated *Smn*$^{2B/-}$ SMA pups began to significantly lose weight at P13 (-0.5 kg average) compared to their untreated counterpart, suggesting the higher dose promoted weight loss (Figure 4.13.b). However, motor function was not significantly affected (Figure 4.13.c). On the other hand, 400 mg/kg/day metformin treatment had no adverse effects in healthy *Smn*$^{2B/+}$ mice (Figure 4.14), suggesting that higher metformin doses specifically reduced life expectancy in *Smn*$^{2B/-}$ SMA mice

Overall, our results demonstrated that 200 mg/kg/day metformin treatment did not improve survival or delay disease progression in intermediate *Smn*$^{2B/-}$ SMA mice. On the other hand, the higher 400 mg/kg/day dose reduced life expectancy specifically in SMA mice, suggesting dose- and disease-dependent adverse effects.

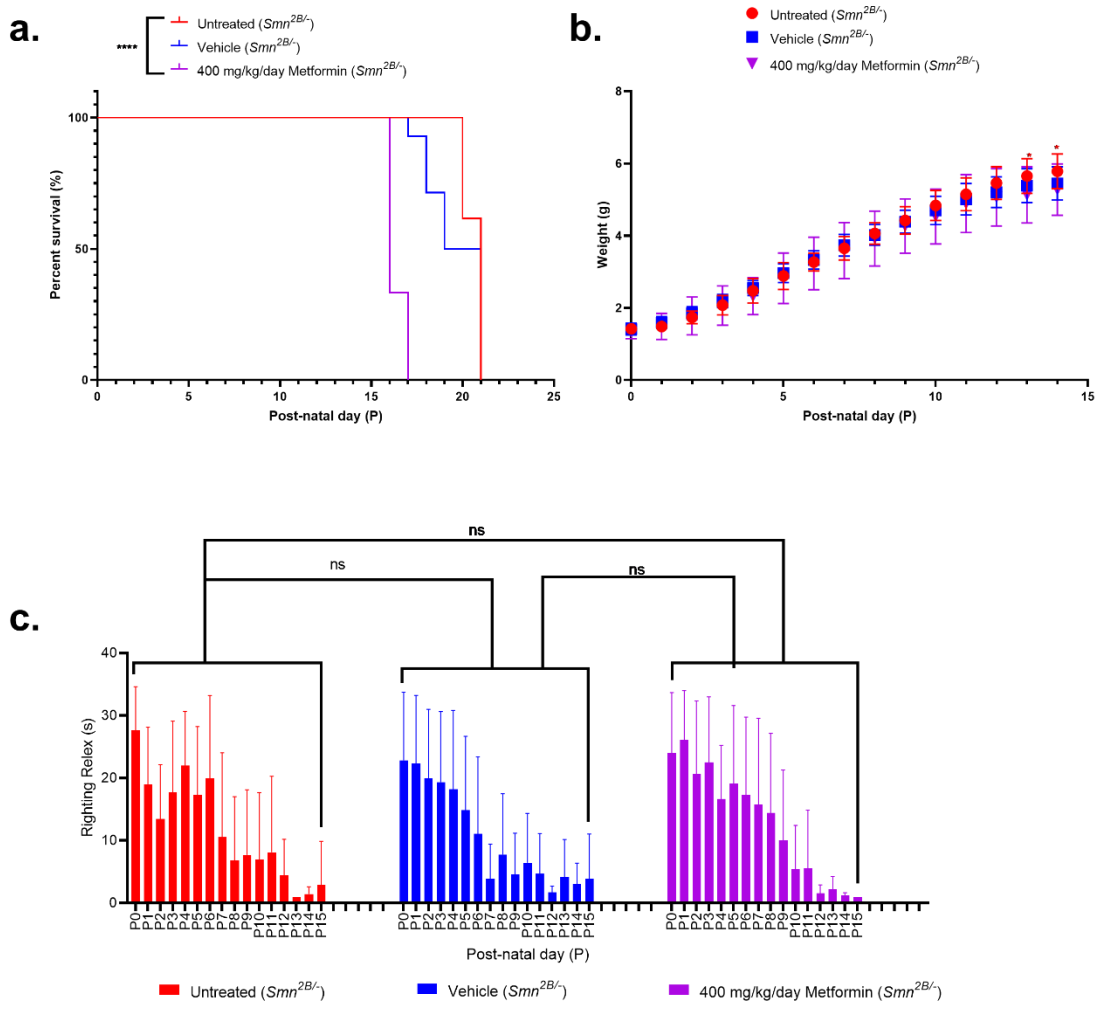

Figure 4.13. 400 mg/kg/day oral metformin treatment reduced life expectancy in *Smn$^{2B/-}$* SMA mice.
All treated animals received a daily dose of metformin (400 mg/kg/day, diluted in 0.9% saline) or vehicle by gavage starting at P5.
a. Kaplan-Meier survival curves for n= 13 untreated (red, median survival: 21 days), n= 14 vehicle-treated (blue, median survival: 20 days) and n= 4 400 mg/kg/day metformin-treated (purple, median survival: 21 days) *Smn$^{2B/-}$* SMA mice. Long-rank (Mantel-Cox) test, ****p <0.0001.
b. Daily weights of untreated (red, n= 13), vehicle-treated (blue, n= 14) and 400 mg/kg/day metformin-treated (purple, n= 9) *Smn$^{2B/-}$* SMA mice. Data represents mean and +- SD error bars, Two-way ANOVA with post-hoc Sidak's multiple comparisons test between untreated and 200 mg/kg/day metformin (red star) and untreated vs vehicle-treated (blue star), *p <0.05.
c. Daily righting reflex test up to a 30 second max time point of untreated (red, n= 13), vehicle-treated (blue, n= 14) and 400 mg/kg/day metformin-treated (purple, n= 9) *Smn$^{2B/-}$* SMA mice. Data represents mean and +- SD error bars, One-way ANOVA with post-hoc Tukey's multiple comparisons test, ns = not significant.

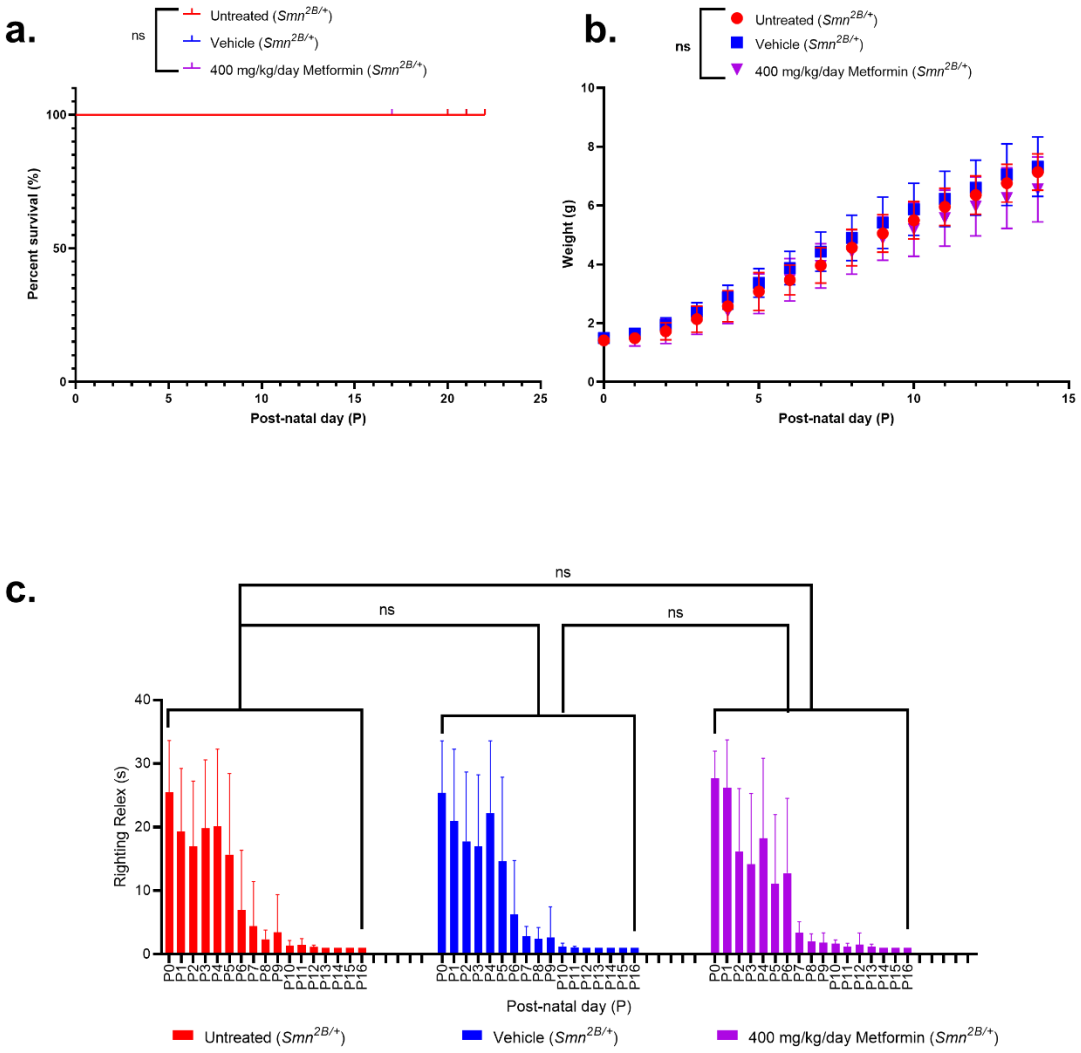

Figure 4.14. 400 mg/kg/day oral metformin treatment had no adverse effects in *Smn$^{2B/+}$* healthy mice
All treated animals received a daily dose of metformin (400 mg/kg/day, diluted in 0.9% saline) or vehicle by gavage starting at P5.
a. Kaplan-Meier survival curves for n= 16 untreated (red, median survival: 21 days), n= 22 vehicle-treated (blue, median survival: 20 days) and n= 3 400 mg/kg/day metformin-treated (purple, median survival: 21 days) *Smn$^{2B/+}$* healthy mice. Long-rank (Mantel-Cox) test, ns = not significant.
b. Daily weights of untreated (red, n= 16), vehicle-treated (blue, n= 22) and 400 mg/kg/day metformin-treated (purple, n= 15) *Smn$^{2B/+}$* healthy mice. Data represents mean and +- SD error bars, Two-way ANOVA with post-hoc Sidak's multiple comparisons test between untreated and 200 mg/kg/day metformin (red star) and untreated vs vehicle-treated (blue star), ns= not significant.
c. Daily righting reflex test up to a 30 second max time point of untreated (red, n= 16), vehicle-treated (blue, n= 22) and 400 mg/kg/day metformin-treated (purple, n= 15) *Smn$^{2B/+}$* healthy mice. Data represents mean and +- SD error bars, One-way ANOVA with post-hoc Tukey's multiple comparisons test, ns = not significant.

4.3.8. Daily 200 and 400 mg/kg/day metformin treatment in non-fasted *Smn$^{2B/-}$* SMA mice induces hypoglycaemia.

The reduced life expectancy observed only in 400 mg/kg/day metformin-treated *Smn$^{2B/-}$* SMA mice (Figure 4.13-14) led us to investigate why this dose had adverse effects. We firstly assessed blood glucose levels, since metformin is a blood glucose lowering agent [863] and could therefore exacerbate the hypoglycaemia reported in both pre-clinical SMA models and patients [301–303].

To address this, we first selected P14 as the experimental time-point, to compensate for the lower median survival of P16 in 400 mg/kg/day metformin-treated *Smn$^{2B/-}$* SMA mice. We then measured the blood glucose levels in non-fasted untreated, 200 and 400 mg/kg/day metformin-treated *Smn$^{2B/+}$* healthy and *Smn$^{2B/-}$* SMA mice 2 hours after metformin treatment [863]. Initially, we observed no significant difference in glucose levels between untreated *Smn$^{2B/-}$* SMA and *Smn$^{2B/+}$* healthy mice (Figure 4.15). Furthermore, we observed no significant difference between untreated and metformin-treated *Smn$^{2B/+}$* healthy mice (Figure 4.15.a). However, we interestingly found that both metformin concentrations significantly reduced the blood glucose levels in *Smn$^{2B/-}$* SMA mice (Figure 4.15.b). While hypoglycaemia could be a possible factor in metformin's inability to ameliorate disease progression in SMA mice, the similar effects of the 200 and 400 mg/kg/day doses in *Smn$^{2B/-}$* SMA mice (Figure 4.15.b) suggests that it was probably not the main cause behind the earlier death in the 400 mg/kg/day higher dose cohort.

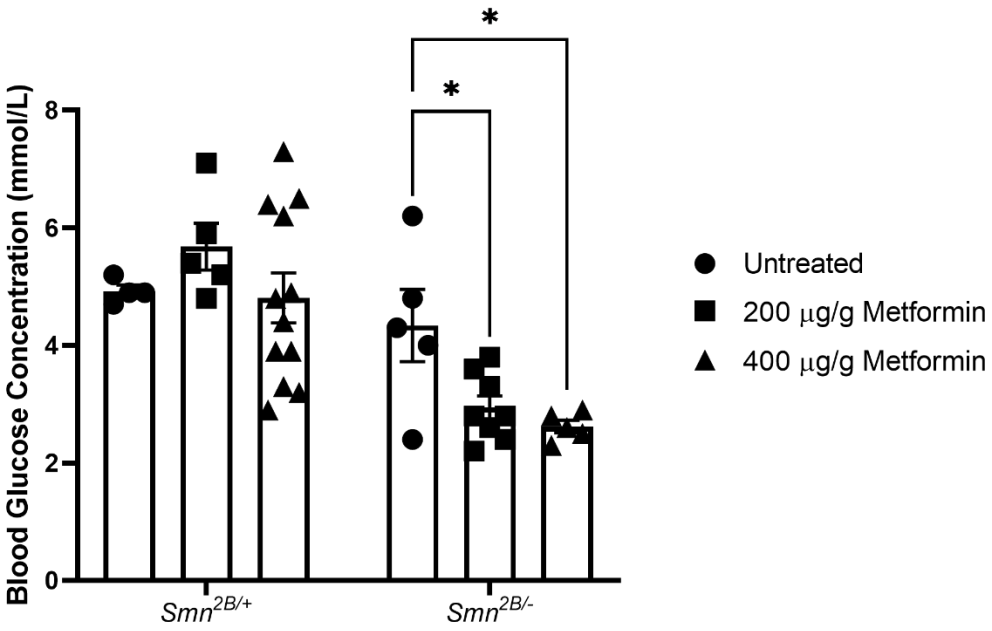

Figure 4.15. Administration of both 200 and 400 mg/kg/day metformin to *Smn$^{2B/-}$* SMA mice significantly reduces blood glucose levels.
All treated animals received a daily dose of either 200 or 400 mg/kg/day metformin (diluted in 0.9% saline) by gavage starting at P5. At P14, blood glucose concentrations (mmol/L) were measured in untreated and metformin-treated, non-fasted *Smn$^{2B/+}$* healthy and *Smn$^{2B/-}$* SMA mice, 2 hours after final metformin treatment. Data represents mean and +- SEM error bars of N = 5-12 animals per group, Two-way ANOVA with post-hoc uncorrected Fishers LSD test, *p <0.05.

4.3.9. 400 mg/kg/day metformin did not impact skeletal muscle targets associated with glucose metabolism, atrophy and mitochondrial function

Given that the rationale for selecting metformin was to evaluate its effectiveness in treating muscle pathologies in SMA, we next investigated if metformin had any adverse effects in muscle that could contribute to its inability to improve disease progression. As above, we used P14 untreated, 200 and 400 mg/kg/day metformin-treated *Smn*$^{2B/+}$ healthy and *Smn*$^{2B/-}$ SMA mice, 2 hours post final administration.

Initially, we wanted to investigate if metformin impacted the expression of the target genes previously predicted by our bioinformatics analyses (Figure 4.3). As aforementioned, our qPCR validation revealed that only *Prkag3* was significantly downregulated in untreated *Smn*$^{2B/-}$ SMA mice at both pre-symptomatic and symptomatic stages (Figure 4.5). Similarly, we only observed a significant downregulation of *Prkag3* (-0.4 FC, p =0.0086) and no change in the *FoxO* isoforms in the muscle between untreated *Smn*$^{2B/-}$ SMA and *Smn*$^{2B/+}$ healthy mice (Figure 4.16). Contrary to our iPathwayGuide predictions (Figure 4.3), both 200- (-0.3 FC, p =0.0188) and 400 mg/kg/day (-0.3 FC, p =0.0141) metformin doses actually exacerbated *Prkag3* downregulation in muscle of *Smn*$^{2B/-}$ SMA mice (Figure 4.16.a). Furthermore, the similar effect of both doses on *Prkag3* expression in *Smn*$^{2B/-}$ SMA mice alongside the significant reduction of *Prkag3* levels in muscle of *Smn*$^{2B/+}$ healthy mice after 200 mg/kg/day metformin (Figure 4.16.a), suggests this gene was probably not involved with the adverse effects of 400 mg/kg/day metformin treatment in *Smn*$^{2B/-}$ SMA mice (Figure 4.13).

However, these finding combined with our previous observations of hypoglycaemia in metformin-treated *Smn*$^{2B/-}$ SMA mice (Figure 4.15) and *Prkag3* downregulation in metformin-treated C2C12 myotubes (Figure 4.8), support our proposal that muscle-specific metformin-induced *Prkag3* downregulation may be due to compensatory glycogen depletion in response to hepatic gluconeogenesis inhibition [923] (see section 4.3.5). On the other hand, across all *FoxO* isoforms in both metformin-treated *Smn*$^{2B/+}$ healthy and *Smn*$^{2B/-}$ SMA mice, we only observed a significant downregulation of *FoxO6* at 200 mg/kg/day metformin in the latter group (-0.5 FC, p =0.0150) (Figures 4.16.b-e), suggesting that metformin does not impact the overall expression of *FoxO* isoforms in SMA skeletal muscle.

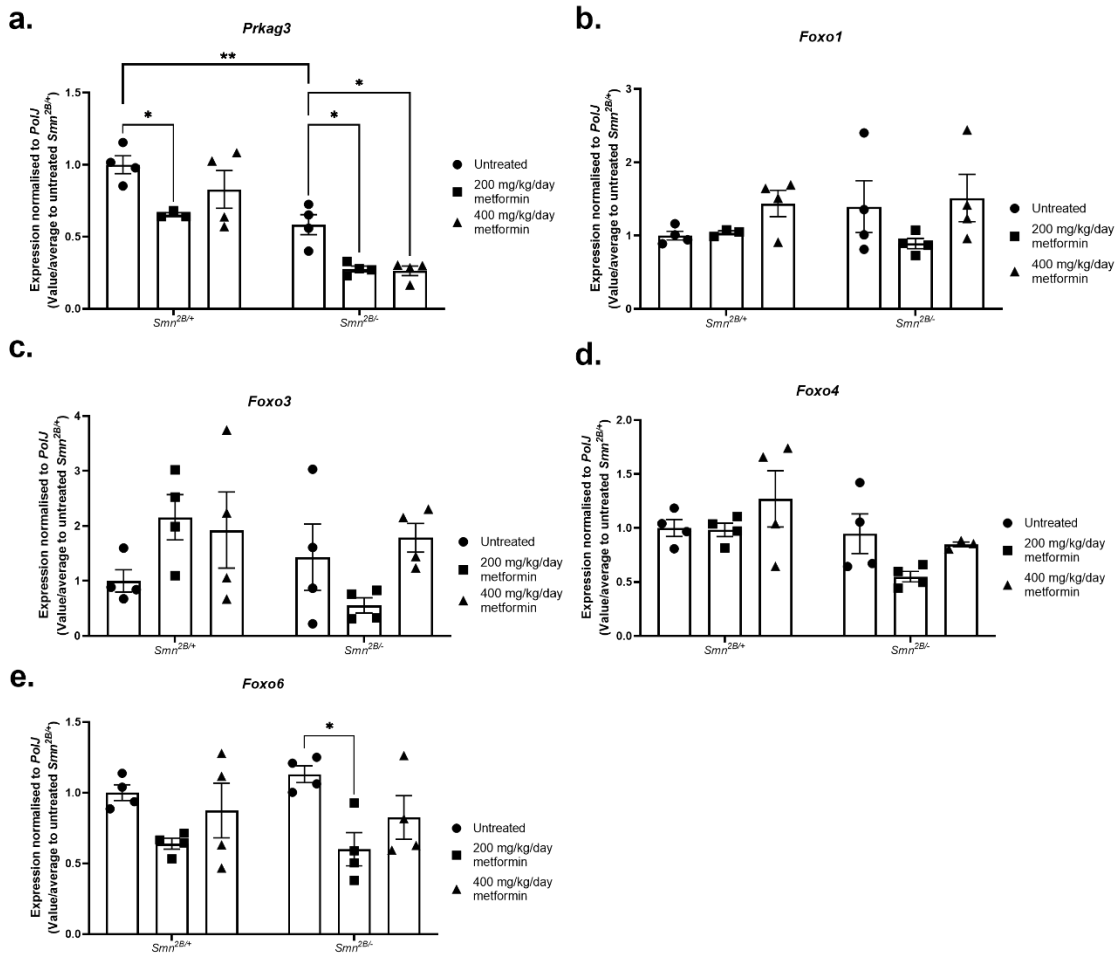

Figure 4.16. Administration of both 200 and 400 mg/kg/day metformin to *Smn$^{2B/-}$* SMA mice significantly reduced *Prkag3* in muscle.
All treated animals received a daily dose of either 200 or 400 mg/kg/day metformin (diluted in 0.9% saline) by gavage starting at P5. At P14, TA muscle was harvested from untreated and metformin-treated, non-fasted *Smn$^{2B/+}$* healthy and *Smn$^{2B/-}$* SMA mice, 2 hours after final metformin treatment. The mRNA expression of metformin target genes **a.** *Prkag3*, **b.** *Foxo1* **c.** *Foxo3*, **d.** *Foxo4*, and **e.** *Foxo6* was measured by qPCR . Data represents mean and +- SEM error bars of N = 4 animals per group, Two-way ANOVA with post-hoc Sidak's multiple comparison test, **p* <0.05, ***p* <0.01.

As progressive muscle atrophy is a hallmark feature in SMA [1–3], we wanted to evaluate if metformin affected this pathology, as previous studies have reported mixed results regarding metformin-associated attenuation of muscle-wasting [911–913,930]. We therefore investigated the atrogenes *atrogin-1* and *MurF1*, since they have previously been associated with muscle atrophy in symptomatic *Smn$^{2B/-}$* SMA mice [56]. Initially, our comparisons between untreated *Smn$^{2B/-}$* SMA mice and *Smn$^{2B/+}$* healthy mice revealed no significant difference between *atrogin-1* (-0.2

FC, *p* =0.9998) and *MuRF1* (-0.2 FC, *p* =0.9703) (Figure 4.17), which could be attributed to the P14 timepoint before weight loss in these SMA mice. Interestingly, we found no significant difference in *atrogin-1* or *MuRF1* expression between untreated and metformin-treated $Smn^{2B/+}$ healthy and $Smn^{2B/-}$ SMA mice either (Figure 4.17), suggesting that neither metformin dose exacerbated muscle atrophy in the $Smn^{2B/-}$ SMA mice.

Next, we assessed metformin's effects on glucose metabolism as metformin's primary action in skeletal muscle is the improvement of insulin sensitivity and glucose uptake [300,931]. Furthermore, both 200 and 400 mg/kg/day metformin-treated $Smn^{2B/-}$ SMA mice developed hypoglycaemia (Figure 4.15), suggesting that metformin impacts glucose metabolism in these mice. Two features associated with metformin and glucose metabolism in skeletal muscle are increased glucose uptake and glycolysis [300,898,899]. Hence, we investigated *Glut4* [295,296] and *Hk2* [311] expression, as these are important markers for the aforementioned functions and dysregulated in type 1 SMA iliopsoas and $Smn^{2B/-}$ TA muscle [312]. Although we found no significant difference for *Glut4* in the $Smn^{2B/+}$ healthy and $Smn^{2B/-}$ SMA groups (Figure 4.18.a), we surprisingly found that *Hk2* expression was only significantly reduced in 200 mg/kg/day metformin-treated $Smn^{2B/+}$ healthy mice (-0.4 FC, *p* =0.0029), with no significant difference between the $Smn^{2B/-}$ SMA groups (Figure 4.18.b) Given that metformin primarily lowers blood glucose levels via inhibition of hepatic gluconeogenesis [923], one possibility is that metformin's effects on systemic glucose metabolism are associated with non-muscular tissue in SMA.

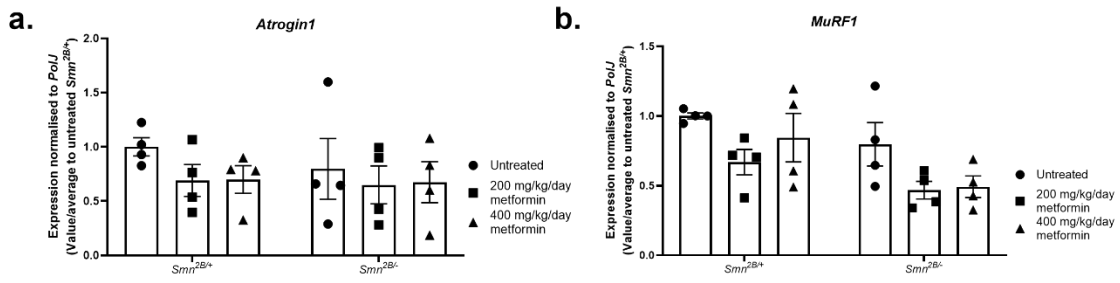

Figure 4.17. Administration of both 200 and 400 mg/kg/day metformin had no impact on atrogenes in the muscle of *Smn$^{2B/-}$* SMA mice.
All treated animals received a daily dose of either 200 or 400 mg/kg/day metformin (diluted in 0.9% saline) by gavage starting at P5. At P14, TA muscle was harvested from untreated and metformin-treated, non-fasted *Smn$^{2B/+}$* healthy and *Smn$^{2B/-}$* SMA mice, 2 hours after final metformin treatment. The mRNA expression of atrogenes **a.** *atrogin-1*, and **b.** *MuRF1* was measured by qPCR. Data represents mean and +- SEM error bars of N = 4 animals per group, Two-way ANOVA with post-hoc Sidak's multiple comparison test.

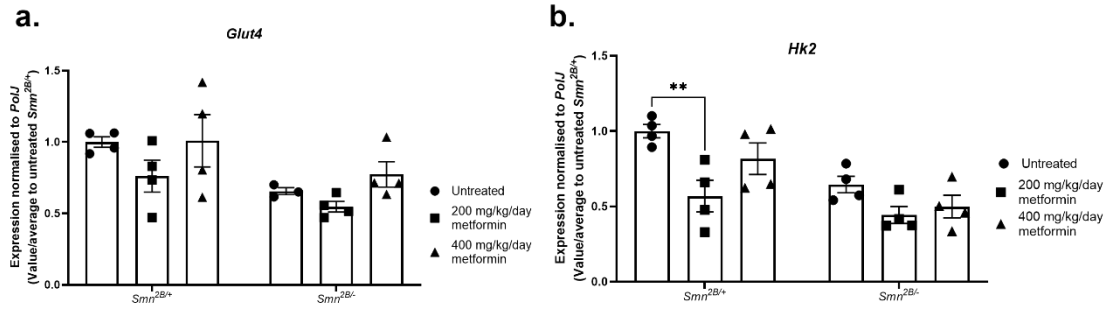

Figure 4.18. Administration of both 200 and 400 mg/kg/day metformin had no impact on glucose uptake and metabolism genes in the muscle of *Smn$^{2B/-}$* SMA mice.
All treated animals received a daily dose of either 200 or 400 mg/kg/day metformin (diluted in 0.9% saline) by gavage starting at P5. At P14, TA muscle was harvested from untreated and metformin-treated, non-fasted *Smn$^{2B/+}$* healthy and *Smn$^{2B/-}$* SMA mice, 2 hours after final metformin treatment. The mRNA expression of glucose uptake and metabolism genes **a.** *Glut4*, and **b.** *Hk2* was measured by qPCR . Data represents mean and +- SEM error bars of N = 4 animals per group, Two-way ANOVA with post-hoc Sidak's multiple comparison test, $^{**}p$ <0.01.

Having ruled out most of our predicted target genes as well as atrophy and glucose metabolism effectors as factors behind the adverse effects of the 400 mg/kg/day metformin treatment in *Smn$^{2B/-}$* SMA mice (Figure 4.13), we next evaluated metformin's effects on mitochondrial biogenesis and function, since it is a pathology in SMA muscle [129,388–393,395]. Furthermore, previous research has established that metformin can indirectly activate AMPK by mild inhibition of

mitochondrial electron transport complex 1 (or NADH:ubiquinone oxidoreductase) [862–867], so we wanted to observe if this had any impact in SMA skeletal muscle. We specifically focused on the expression of *Pgc1-α*, *Tfam* and *Nrf1* due to their importance in governing general mitochondrial biogenesis and function [396–401] and of *NADH-ubiquinone oxidoreductase 75 kDa subunit, mitochondrial* (*Ndufs1*), as this encodes the largest subunit of the mitochondrial electron transport complex 1 [932,933].

Our initial comparisons between untreated *Smn*$^{2B/-}$ SMA and *Smn*$^{2B/+}$ healthy mice revealed that *Pgc1-α* levels were significantly reduced (-0.4 FC, p =0.0072) in SMA muscle (Figure 4.19.a), supporting previous studies of *Pgc1-α* expression in the *Smn*$^{2B/-}$ SMA mouse model [389] and the role its reduction can have on mitochondrial dysfunction in SMA muscle [388]. Although 200 mg/kg/day metformin treatment significantly reduced *Pgc1-α* (-0.3 FC, p =0.0100), *Tfam* (-0.3 FC, p =0.0242), and *Ndufs1* (-0.4 FC, p =0.0053) levels in *Smn*$^{2B/+}$ healthy mice, none of the mitochondrial targets were significantly dysregulated by metformin in the muscle of *Smn*$^{2B/-}$ SMA mice (Figure 4.19). One possibility for the downregulation of mitochondrial targets in healthy muscle could be that since mitochondrial biogenesis and function are hallmarks in SMA skeletal muscle [129,388–393,395], they may be too dysregulated for metformin to have any significant mild inhibitory impact as observed with *Pgc1-α* (Figure 4.19.a)

Overall, the collective data in skeletal muscle suggests that metformin treatment did not have a direct impact on the predicted targets, glucose metabolism, atrophy, or mitochondrial function in *Smn*$^{2B/-}$ SMA skeletal muscle, suggesting that some of the adverse effects could occur in additional non-muscle tissues.

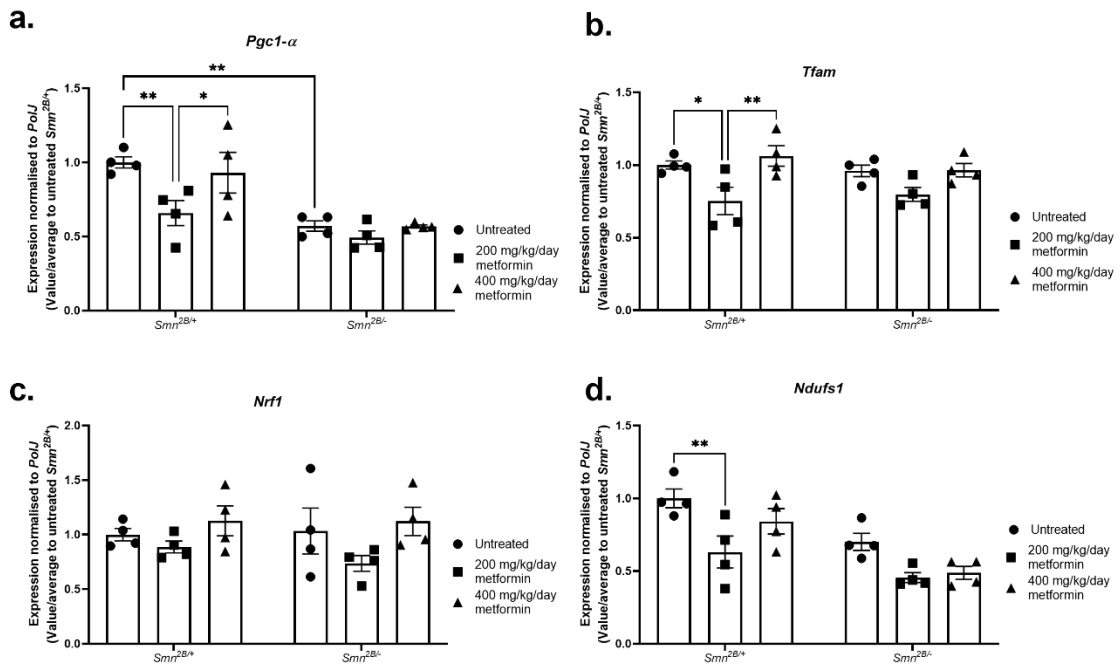

Figure 4.19. Administration of both 200 and 400 mg/kg/day metformin does not impact mitochondrial function and biogenesis genes in the muscle of *Smn*$^{2B/-}$ SMA mice.
All treated animals received a daily dose of either 200 or 400 mg/kg/day metformin (diluted in 0.9% saline) by gavage starting at P5. At P14, TA muscle was harvested from untreated and metformin-treated, non-fasted *Smn*$^{2B/+}$ healthy and *Smn*$^{2B/-}$ SMA mice, 2 hours after final metformin treatment. The mRNA expression of mitochondrial function and biogenesis genes **a.** *Pgc1-α*, **b.** *Tfam* **c.** *Nrf1*, and **d.** *Ndufs1* was measured by qPCR. Data represents mean and +- SEM error bars of N = 4 animals per group, Two-way ANOVA with post-hoc Sidak's multiple comparison test, *p <0.05, **p <0.01.

4.3.10. 400 mg/kg/day metformin treatment impacts genes important for mitochondrial function and biogenesis in the spinal cord of *Smn$^{2B/-}$* SMA mice.

Although we primarily focused on muscular pathologies, SMA is still a NMD [1], with systemic pathologies in multiple tissue types [77,150,151] (see section 1.3). Given that metformin is systemically distributed across different tissues [934], it led us to investigate whether metformin's inability to improve disease progression in *Smn$^{2B/-}$* SMA mice was a result of adverse effects in non-muscular tissues. One tissue relevant to SMA that is targeted by metformin is the spinal cord, since this drug has the ability to cross the BBB [935]. In particular, metformin has been discovered to impact the mitochondria in the spinal cord [936]. Thus, with neuronal mitochondrial dysfunctions naturally occurring in both *in vitro* and *in vivo* SMA models [129,145,146], we decided to investigate whether metformin had any impact on mitochondrial genes in the SMA spinal cord.

As above, we investigated the mitochondrial targets *Pgc1-α*, *Tfam*, *Nrf1,* and *Ndufs1* in the spinal cord of P14 untreated, 200 and 400 mg/kg/day metformin-treated *Smn$^{2B/+}$* healthy and *Smn$^{2B/-}$* SMA mice, 2 hours-post final administration. Our initial comparisons revealed that none of the mitochondrial targets were dysregulated between *Smn$^{2B/-}$* SMA and *Smn$^{2B/+}$* healthy mice (Figure 4.20). Interestingly, we found a significant downregulation of both *Pgc1-α* (-0.3 FC, p =0.0055) and *Ndufs1* (-0.2 FC, p =0.0298) in the 400 mg/kg/day metformin-treated *Smn$^{2B/-}$* SMA mice only (Figure 4.20.a and .d). Furthermore, we found that 200 mg/kg/day metformin treatment in *Smn$^{2B/+}$* healthy mice significantly downregulated *Pgc1-α* (-0.3 FC, p =0.0012) and *Nrf1* (-0.3 FC, p =0.0155) (Figure 4.20.a and c), whilst 400 mg/kg/day also downregulated both *Pgc1-α* (-

0.3 FC, *p* =0.0014) and *Nrf1* (-0.3 FC, *p* =0.0066) alongside *Ndufs1* (-0.2 FC, *p* =0.0298) (Figure 4.20.a and c-d).

Intriguingly, the comparative evidence between disease state and metformin treatment highlights that the *Pgc1-α* and *Ndufs1* mitochondrial target genes only became significantly downregulated in the spinal cord of $Smn^{2B/-}$ SMA mice after 400 mg/kg/day metformin treatment and not due to the disease itself (Figure 4.20.a and .d).

In the wider context, our evidence of selective exacerbation of mitochondrial target genes only in the spinal cord of $Smn^{2B/-}$ SMA mice (Figure 4.19-20) following metformin treatment is supported by evidence of tissue-dependent differences in conserved cellular processes between SMA motor neurons and skeletal muscle [937] alongside reports that the mitochondrial electron transport complex 1 is naturally dysfunctional in SMA motor neurons [146].

Thus, our results suggest that these particular mitochondrial genes are metformin targets in the spinal cord, highlighting the possibility that their downregulation in $Smn^{2B/-}$ SMA mice exacerbated neuronal mitochondrial dysfunction and contributed to the adverse effects of the high metformin dose.

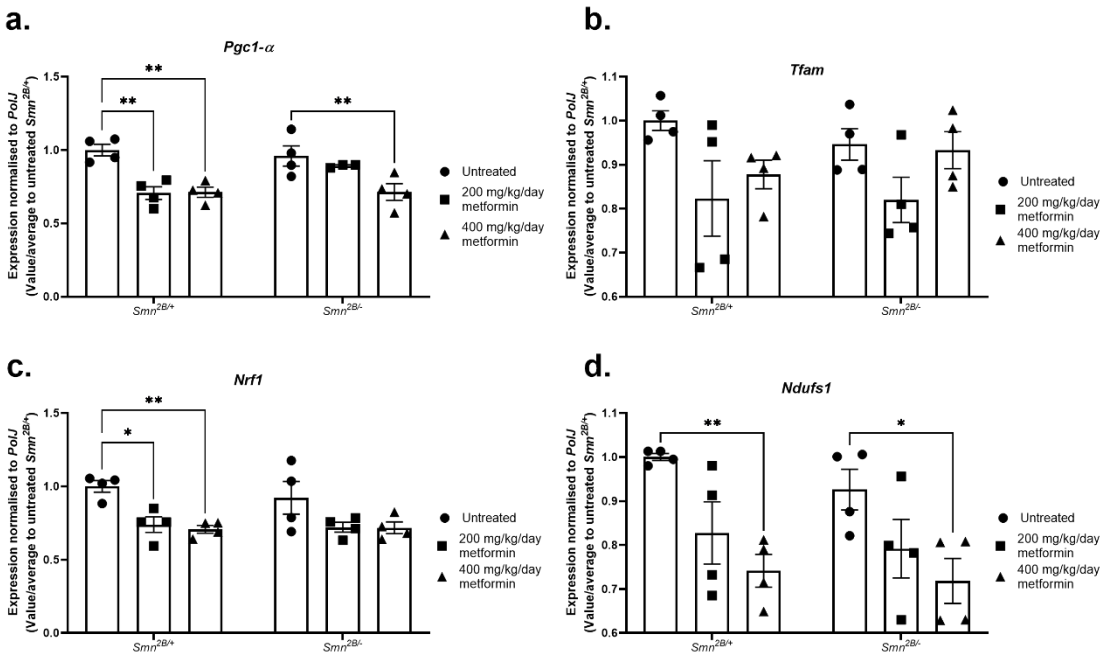

Figure 4.20. Administration of 400 mg/kg/day metformin significantly downregulates mitochondrial function and biogenesis genes *Pgc1-α* and *Ndufs1* in the spinal cord of *Smn$^{2B/-}$* SMA mice.
All treated animals received a daily dose of either 200 or 400 mg/kg/day metformin (diluted in 0.9% saline) by gavage starting at P5. At P14, spinal cord was harvested from untreated and metformin-treated, non-fasted *Smn$^{2B/+}$* healthy and *Smn$^{2B/-}$* SMA mice, 2 hours after final metformin treatment. The mRNA expression of mitochondrial function and biogenesis genes **a.** *Pgc1-α*, **b.** *Tfam* **c.** *Nrf1*, and **d.** *Ndufs1* was measured by qPCR. Data represents mean and +-SEM error bars of N = 4 animals per group, Two-way ANOVA with post-hoc Sidak's multiple comparison test, **p* <0.05, ***p* <0.01.

4.4. Discussion

In our study, metformin was evaluated for its suitability as a second-generation skeletal muscle therapy in SMA based on its predictive emulation of prednisolone activity on *Prkag3* and *FoxO* isoforms. However, our investigations of metformin treatment in C2C12 myoblast-like cells and *Smn*$^{2B/-}$ SMA mice revealed no improvements in disease phenotypes.

Interestingly, we validated that the metformin target *Prkag3*, which encodes for the AMPK-γ3 subunit was significantly downregulated in the muscle of severe *Smn*$^{-/-}$*;SMN2* and milder *Smn*$^{2B/-}$ SMA mice compared to their healthy *Smn*$^{+/-}$*;SMN2* and WT controls. Furthermore, *Prkag3* was also downregulated in the pre-symptomatic *Smn*$^{2B/-}$ SMA mice suggesting that its dysregulation is an early event in SMA muscle pathogenesis. Normally, the AMPK-γ3 isoform that is encoded by *Prkag3* is predominantly expressed in skeletal muscle after intense exercise and is more associated with glucose and FA metabolism rather than muscle size regulation [831,938,939]. Incidentally, these roles of *Prkag3* makes it an interesting target for metabolic dysfunctions in SMA. Indeed, *Prkag3*$^{-/-}$ null mice [831,938,939] share certain pathological similarities with SMA mice such as increased fat mass [344,827,828], lower glycogen content [940], as well as dysregulations in mitochondrial function [388,784] and glucose and FA metabolism [301–303,338–343]. Furthermore, the upregulation of *Prkag3* expression in SMA could be beneficial, since the over-expressing transgenic *Tg-Prkag3*^{225Q} mutant mice displayed the opposite phenotypes than the *Prkag3*$^{-/-}$ null counterparts [831,938,939].

Although there are no pre-clinical AMPK-γ3 -specific agonists currently available to test Prkag3 modulation [831,938,939], we could in a future study ectopically

overexpress *Prkag3* in SMA skeletal muscle via intravenous scAAV2/8 vector injections, as this method has previously been useful in SMA pre-clinical studies [941]. However, before we consider these future studies, we need to first address the inverse upregulation of *PRKAG3* in type 3 SMA deltoid myoblasts and evaluate the factor(s) such as experimental status, species, severity and/or muscle type.

Interestingly, we found that both 200 and 400 mg/kg/day metformin doses in *Smn*$^{2B/-}$ SMA mice resulted in a significant downregulation of *Prkag3* in muscle. Furthermore, we observed the same pattern in physiological and supraphysiological metformin-treated C2C12 myotubes, indicating that metformin does not have the *Prkag3* agonist ability that our bioinformatics software predicted. Even though it is unclear why metformin significantly downregulated *Prkag3* levels, one theory is that the treatment negatively affected glycogen synthesis (Figure 4.22.a). Indeed, metformin is known to inhibit gluconeogenesis [923] and we theorised that this inhibition occurred directly in C2C12 myotubes, while in *Smn*$^{2B/-}$ SMA mice, we think this occurred indirectly via the liver [923] (Figure 4.22.a). Given that metformin primarily lowers blood glucose levels via inhibition of hepatic gluconeogenesis [923], it could be possible that the hypoglycaemia in the *Smn*$^{2B/-}$ SMA mice triggered glycogen depletion in skeletal muscle [942] (Figure 4.22.a). In turn, the increased glycogen breakdown would account for the reduced *Prkag3* activity, since it is involved in glycogen storage [831,924] (Figure 4.22.a).

This indirect model could also provide an explanation for the atrogene-independent body weight reduction in 200 mg/kg/day metformin-treated *Smn*$^{2B/-}$ SMA mice as glycogen depletion would reduce water retention [942]. However,

corroboration of this model would require glycogen measurements in untreated and metformin-treated *Smn*$^{2B/-}$ SMA muscle. Regardless, our hypoglycaemia model was probably not the main contributor to the adverse effects observed in SMA mice, since both metformin doses impacted glucose levels.

Contrary to what was expected, metformin's negative effects on SMA pathogenesis is different to previous studies of AMPK activity in SMA, as these found that AMPK activation via exercise and AICAR treatment actually improved the muscle phenotype [389,782]. Despite both being AMPK agonists, there are differences between AICAR [943] and metformin [862,944] that could explain the negative effects of the latter in SMA. The key one being that only metformin can pass the BBB [935,945], suggesting that AICAR would have no direct impact on neuronal tissue as evident in the AICAR-treated *SMNΔ7* SMA mice [782]. This is important as direct AMPK activation in neuronal tissue actually has negative consequences in related-NMDs like ALS [946,947], whereby metformin was unable to delay disease progression in *SOD1*^{G93A} ALS mice [948]. Thus, metformin's adverse effects in *Smn*$^{2B/-}$ SMA mice could be due to exacerbation of neuronal dysfunction.

Indeed, we observed that the higher and toxic 400 mg/kg/day metformin dose specifically impacted the mitochondrial targets *Pgc1-α* and *Ndufs1* in the spinal cord of *Smn*$^{2B/-}$ SMA mice. Previous studies have in fact established endogenous mitochondrial dysfunction in SMA neurons, including the downregulation of the metformin target mitochondrial respiratory complex 1 [146,862 146]. Furthermore, the tissue-dependent differences in conserved cellular processes between SMA motor neurons and skeletal muscle [937] could explain the differential impact of metformin on spinal cord and muscle in SMA mice. We thus theorise that 400

mg/kg/day metformin reduced the life expectancy of our *Smn*$^{2B/-}$ SMA mice via exacerbation of neuronal mitochondrial dysfunction (Figure 4.21.b), as higher metformin doses have indeed previously been linked to reduced mitochondrial oxidative activity in pre-clinical *in vivo* models [949]. However, we would need to strengthen this model with experiments that measured mitochondrial respiratory complex 1 activity and oxygen consumption rates directly in SMA spinal cords before we can draw any firm conclusions.

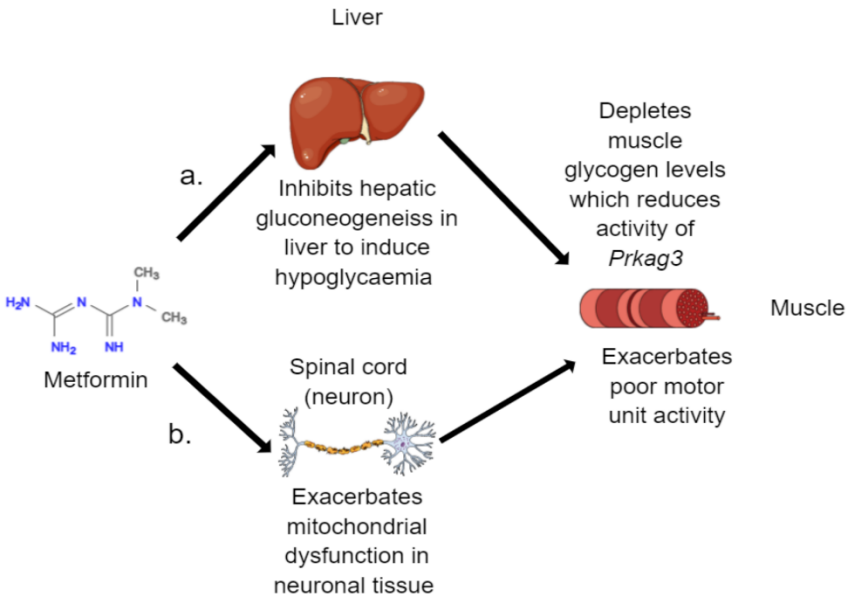

Figure 4.21. Predicted systemic actions of metformin in SMA.
Theorised model summarising metformin's systemic effects on *Smn*$^{2B/-}$ SMA mice regarding **a.** hypoglycaemia and *Prkag3* downregulation and **b.** dysregulation of mitochondrial genes in the spinal cord**.** Figure was created with Mind the Graph.

Despite the lack of phenotypic improvement in metformin-treated SMA mice, our data could provide significant information in a different clinical context of drug safety in SMA patients. Indeed, pre-clinical models and patient case studies have established aberrant glucose metabolism as a feature of SMA [301–303] and that diabetes is a co-morbidity in certain patients [306–310]. Traditionally, metformin is a generic pharmacological intervention for disease management of T2DM patients [830]. However, in the context of SMA, careful consideration should be taken by clinicians before using metformin, as the reduced quality of life observed in the 400 mg/kg/day metformin-treated *Smn*$^{2B/-}$ SMA mice suggests that SMA patients may benefit from either lower metformin doses or non-biguanide diabetes drugs [950] for successful diabetes management.

In conclusion, our pre-clinical data suggests that metformin is not a suitable repositioning candidate for SMA. However, further investigations could be useful to establish its suitability for treating diabetes-like co-morbidities in SMA patients safely.

Chapter 5.

Therapeutic potential of oxandrolone to treat skeletal muscle pathologies in SMA.

5.1. Introduction

In chapter 4, we evaluated the efficacy of metformin as a potential skeletal muscle treatment for SMA based on our *in silico* drug repositioning predictions in chapter 2. In this chapter, we investigate another oral-based pharmacological candidate, oxandrolone, a synthetic anabolic steroid [837,838]. First synthesised in 1962, oxandrolone shares a similar chemical structure to testosterone, albeit with the absence of a Δ^4-3-oxo-group that is replaced by an oxygen atom in the carbon 2 position and alkylation in the C17-α position that enables oral bioavailability [837,838] (Figure 5.1).

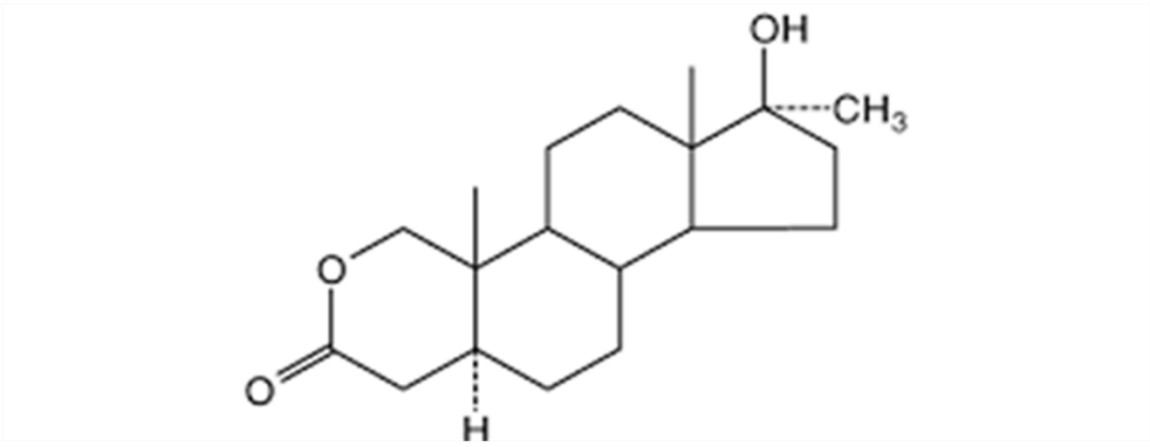

Figure 5.1. Oxandrolone chemical structure (skeletal formula).

As an oral anabolic steroid, oxandrolone directly targets the cytosolic AR across various tissues [837,838] (Figure 5.2.a), as opposed to endogenous testosterone, which is initially converted into dihydrotestosterone (DHT) by the 5α-reductase prior to AR activation (Figure 5.2.b) [951,952]. However, in both cases, the oxandrolone- or DHT-activated AR translocates to the nucleus and binds to the

palindromic, dihexameric androgen response element (ARE) motif in the promoter or enhancer regions of AR-responsive genes [952,953] (Figure 5.2). Interestingly, the 5α-reduced structure of oxandrolone is an important feature, as bypassing DHT formation promotes a higher ratio of anabolism to androgyny by 10:1 [837,952] (Figure 5.2.a). In the context of SMA, this makes oxandrolone a treatment suitable for all patients. Indeed, a meta-analysis of 27 studies of oxandrolone treatment in mixed gender patients reported minimal androgynous side effects [837,954,955].

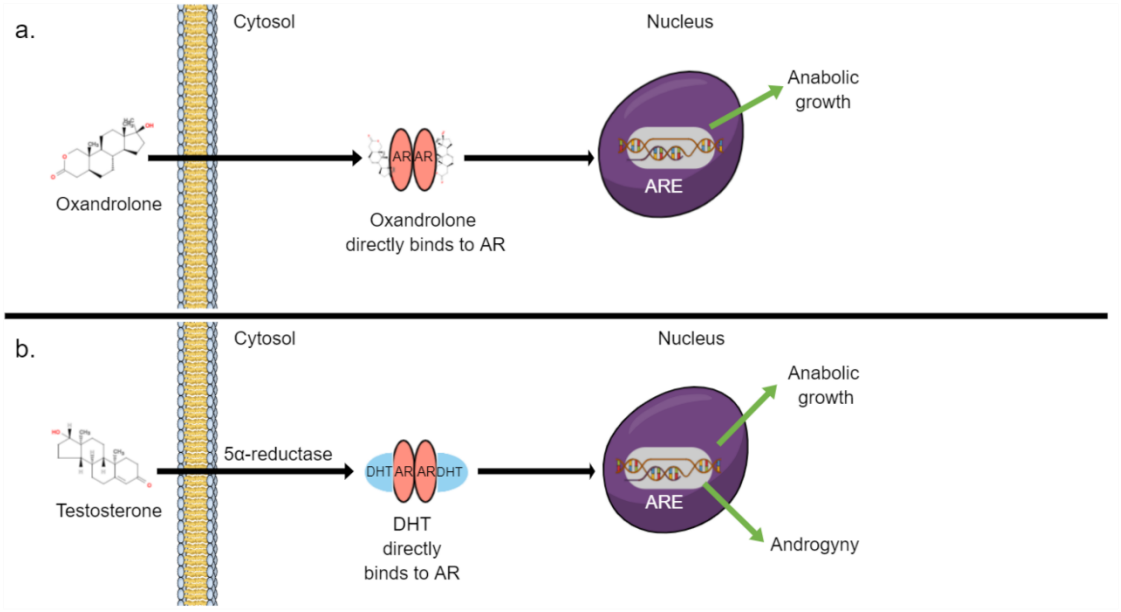

Figure 5.2. Pharmacodynamics of oxandrolone activity.
a. Oxandrolone directly activates androgen receptor (AR) in the cytosol due to its 5α-reduced structure not requiring the catalytic step of 5α-reductase interaction. The active AR homodimer translocates the nucleus where it recognises the androgen response element (ARE) in promoter/enhancer regions of androgen-targeted genes. For these genes, oxandrolone has a higher ratio of activating anabolic growth genes compared to androgynous.
b. Testosterone is reduced to dihydrotestosterone (DHT) by 5α-reductase in the cytosol, which makes it active to directly binding to AR homodimer. The active AR homodimer translocates the nucleus where it recognises the ARE in promoter/enhancer regions of androgen-targeted genes. Testosterone being an androgen is able to activate anabolic growth and androgyny genes.
Figure was created on Mind the Graph.

As a skeletal muscle therapy, oxandrolone and anabolic steroids are useful as the androgen-AR signalling pathways govern skeletal muscle development, growth, repair and metabolism [804,805,956–959] (Figure 5.3). Although the AR plays a greater role in male skeletal muscle, oxandrolone is popular with both male and female bodybuilders and athletes due to its ability to increase muscle growth and limit fatigue [954,956,960–962]. Furthermore, the anabolic benefits of oxandrolone are prolonged, compared to other anabolic steroids, since the absence of a Δ^4-3-oxo-group prevents its breakdown by 3β-hydroxysteroid dehydrogenase (3β-HSD) [954,963].

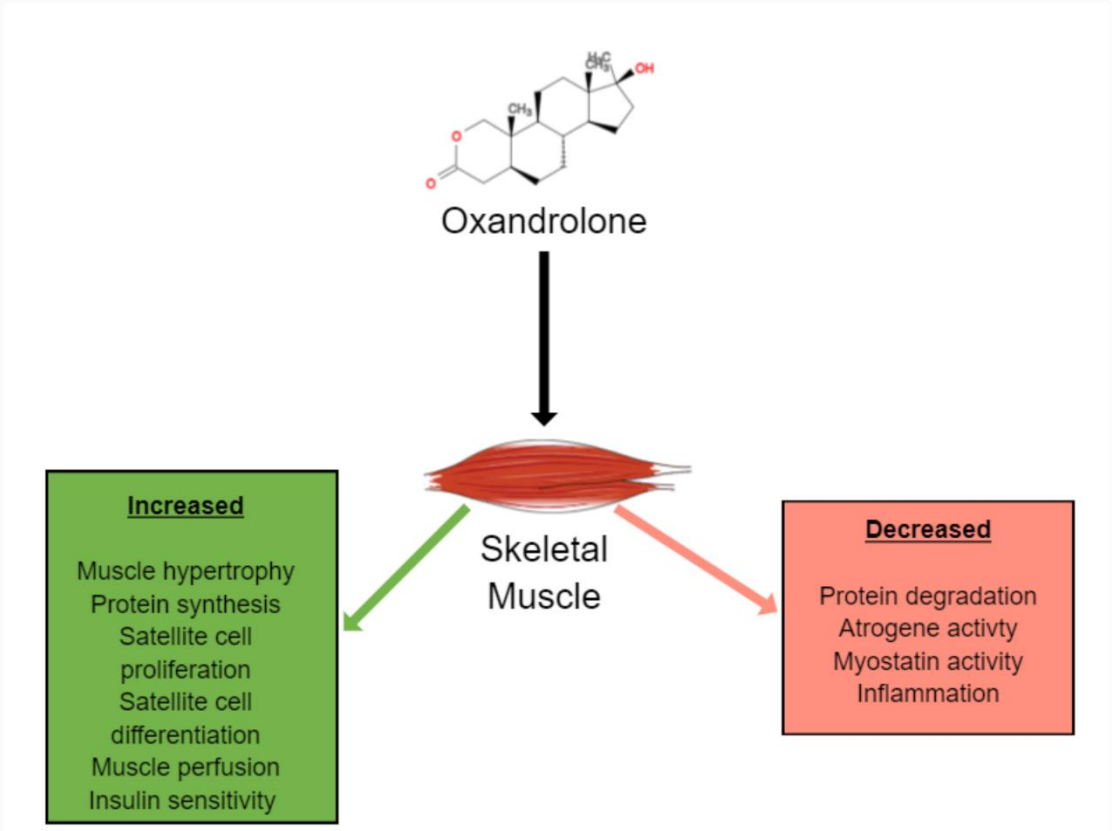

Figure 5.3. Benefits of oxandrolone and anabolic steroids in skeletal muscle.
Schematic representation of oxandrolone targeting skeletal muscle to increase (green box) pathways associated with skeletal muscle growth and decrease (red box) pathways associated with skeletal muscle atrophy.
Figure was created on Mind the Graph.

In addition to athletic performance, the ergogenic benefits of oxandrolone have also been reported in various diseases, which include NMD and myopathies such as DMD [964], SCI [965], ALS [966], Charcot-Marie Tooth disease type 1 A (CMT1A) [835], Inclusion body myositis (IBM) [967], Human immunodeficiency virus (HIV) [968], cachexia [969] and burn injuries [836], to name a few [837]. Importantly for SMA, clinical trials in juvenile DMD [964] and mixed gender burn injury patients [836] have reported increased lean body mass growth, elevated MPS and minimal androgynous side effects suggesting that oxandrolone confers anabolic growth with minimal androgynous risks in pre-pubescent patients [837].

Thus, the aim of this chapter is to evaluate the suitability of oxandrolone as a skeletal muscle treatment for SMA. We will address this aim with the following objectives.

1. Validate the expression of predicted oxandrolone target genes in human and murine SMA cellular and animal models.
2. Investigate the effects of oxandrolone, *Smn* depletion and canonical atrophy on the predicted oxandrolone target genes in C2C12 myoblast-like cells.
3. Evaluate the therapeutic potential of oxandrolone in *Smn*$^{2B/-}$ SMA mice.

5.2. Methods

5.2.1. *In vitro* drug treatment.

Proliferating C2C12 myoblasts were seeded in 6-well plates (x4 wells per group). At 60% confluency for C2C12 myoblasts and D2, D4 and D7 stages for differentiated C2C12 myotubes, they were treated with oxandrolone (Sigma-Aldrich) dissolved in absolute ethanol (Fisher Scientific) at 1, 10 and 100 µM concentrations for 24 hours against an absolute ethanol vehicle control (0.1% v/v).

5.2.2. Lactate dehydrogenase (LDH) assay for cytotoxicity.

Drug cytotoxicity was measured by the lactate dehydrogenase (LDH)-Glo™ Cytotoxicity assay kit (Promega). In principle the LDH-Glo™ assay involves a two-stage process, the first stage utilises the release of LDH enzyme into the cell culture media from damaged and/or dead cells, which oxidises lactate via reduction of NAD+ into NADH [970,971]. The second stage involves the NADH catalysing the reduction of a reductase substrate into luciferin, which then generates a bioluminescent signal proportional to the LDH levels released into the cell culture medium via an Ultra-Glo™ rluciferase [970,971].

Culture supernatant from cells exposed to either absolute ethanol vehicle or oxandrolone for 24 and 72 hours alongside a blank media control and a maximum LDH release control (1% Triton-X incubation for 15 minutes) (N=6) were diluted in storage buffer (200 mM Tris-HCL (pH 7.3), 10% glycerol, 1% BSA, and PBS) in ratios of 1:300 for myoblasts and 1:100 for myotubes. In 96-well plates, 50 µl aliquots of these solutions alongside 50 µl of LDH detection solution (1:200 concentration of LDH detection enzyme mix and reductase)

(Promega) were incubated for 30-60 minutes in the dark. For the final 10 minutes, these plates underwent luminescence detections at 400 nm within the GloMax Explorer (Promega).

5.2.3. Bromodeoxyuridine (BrDU) cell proliferation assay

Cell proliferation was measured by the bromodeoxyuridine (BrDU) cell proliferation assay kit (Merck). C2C12 myoblasts that were untreated, absolute ethanol vehicle- and oxandrolone-treated (N=6) for 24- or 72-hours alongside a blank control (no cells) were labelled with a 1:2000 non-isotopic BrDU solution for 2 hours. We also used an unlabelled and untreated C2C12 myoblast group as a control. After 2 hours, the labelled media was removed, and each well was incubated for 30 minutes with a fixative/denaturing solution. These samples were then incubated with a 100X anti-BrDU antibody (1:100 dilution buffer) for 1 hour at room temperature. Afterwards, the samples were washed with a 1X wash buffer and then incubated with a secondary goat anti-mouse IgG horseradish peroxidase (HRP) conjugate for 30 minutes at room temperature. Following consecutive washes with 1X wash buffer and distilled (d)H_2O, the samples were then treated with a substrate solution and incubated in the dark at room temperature for 15 minutes. Finally, these samples were treated with a stop solution for 30 minutes before their absorbance readings were taken with a GloMax Explorer (Promega) at 450-540 nm.

5.2.4. Animal Treatment.

Litters containing *Smn*$^{2B/-}$ SMA and *Smn*$^{2B/+}$ healthy mice were phenotypically analysed by weight and righting reflex daily from P0. At P5, mice were either untreated or vehicle-treated (0.5% carboxymethylcellulose (CMC) (Sigma-Aldrich)). For drug treatment groups, these mice received 4 mg/kg/day oxandrolone (Sigma-Aldrich) ultrasonicated in 0.5% CMC from P8. Both vehicle- and oxandrolone-treatments were delivered by gavage using a 25 µl syringe (Hamilton) and 1.25 mm animal feeding needle (Cadence Science), daily from their respective start points and up to humane endpoint (N>10).

5.3. Results

5.3.1. Oxandrolone is predicted to emulate prednisolone's activity on *Ar* and its downstream effectors.

The potential of oxandrolone to emulate the beneficial effects of prednisolone treatment in SMA skeletal muscle was based on the upregulation of the *Ar* gene in prednisolone-treated *Smn*$^{-/-}$*;SMN2* SMA mice compared to untreated *Smn*$^{-/-}$*;SMN2* SMA mice and the DGIdb database selection of oxandrolone as an Ar agonist (See Chapter 3, Table 3.11). Furthermore, we identified downstream effectors in iPathwayGuide that prednisolone-targeted *Ar* was predicted to coherently modulate (Figures 5.4.a-b). In this case, the two upregulated downstream effectors directly targeted by *Ar* were *Igfbp5* and *Myogenin* (Figures 5.4.a-b), which both regulate muscle differentiation, regeneration and myofiber growth [839,972,973].

Subsequently, bioinformatic analyses revealed that *Igfbp5* and *Myogenin* also had predicted downstream targeted genes (Figures 5.4.a-b). Indeed, *Igfbp5* was predicted to upregulate *Dok5* a signalling protein linked to insulin and IGF-1 activity [841] (Figure 5.4.a-b). On the other hand, *Myogenin* upregulation was predicted to upregulate *Akap6*, which is involved in modulation of muscle differentiation and regeneration [840] (Figures 5.4.a-b). In addition to these downstream effectors, we also selected *DNA damage inducible transcript 4* (*Ddit4*) as a predicted oxandrolone target gene based on its direct relationship with Ar [749] and it being one of the top 20 downregulated targets of prednisolone in the skeletal muscle of *Smn*$^{-/-}$*;SMN2* SMA mice (See Chapter 3, Table 3.4) (Figures 5.4.a-b).

Importantly, the expression of all the predicted downstream *Ar* target genes in the skeletal muscle of prednisolone-treated *Smn*$^{-/-}$*;SMN2* SMA mice was normalised to the log2FC patterns observed in untreated *Smn*$^{+/-}$*;SMN2* healthy mice instead of untreated *Smn*$^{-/-}$*;SMN2* SMA mice (Figure 5.4.c). However, there was no significant difference in the expression of the *Ar* gene itself between untreated *Smn*$^{-/-}$*;SMN2* SMA and *Smn*$^{+/-}$*;SMN2* healthy mice (Figure 5.4.c). Although it is unclear why only prednisolone and not disease phenotype affected *Ar* expression, one possibility is that ectopic expression of *Ar* could be beneficial to skeletal muscle health in SMA. Regardless, we decided to investigate if oxandrolone could indeed ameliorate skeletal muscle pathologies in SMA cellular and animal models.

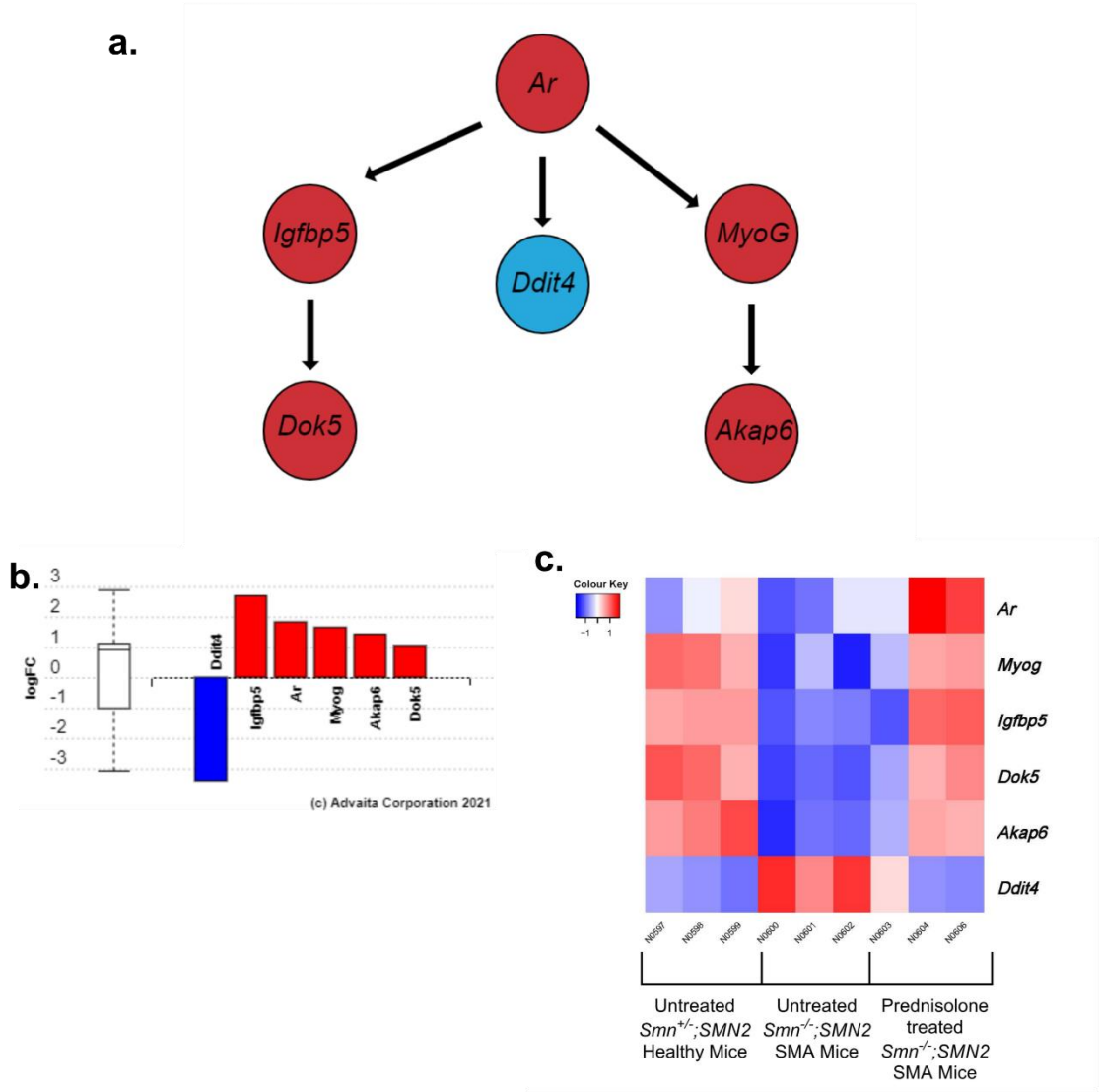

Figure 5.4. Oxandrolone is predicted to emulate the target patterns of prednisolone treatment in the skeletal muscle (Triceps) of *Smn$^{-/-}$;SMN2* SMA mice.

a. The pathway diagram is based on upstream regulator pattern predicted by iPathwayGuide in prednisolone vs untreated *Smn$^{-/-}$;SMN2* SMA skeletal muscle. *Ar* upregulates downstream targets *Igfbp5* and *MyoG*, whilst it downregulates *Ddit4*. *Igfbp5* upregulates *Dok5* and *MyoG* upregulates *Akap6*. Upregulated genes shaded in red, downregulated genes shaded in blue. **b.** Differential gene expression pattern by LogFC (Y-axis) of predicted oxandrolone targets *Ddit4*, *Igfbp5*, *Ar*, *MyoG*, *Akap6* and *Dok5* based on transcriptomic data from prednisolone vs untreated *Smn$^{-/-}$;SMN2* SMA skeletal muscle. Upregulated genes above X-axis are highlighted in red and downregulated genes below X-axis highlighted in blue. The box and whisker plot on Y axis represents 1st quartile, median and 3rd quartile. Graph generated in iPathwayGuide (Advaita). **c.** Heatmap visualisation for predicted oxandrolone targets *Ar*, *MyoG*, *Igfbp5*, *Dok5*, *Akap6*, and *Ddit4* (Log2FC >0.6; FDR <0.05) between untreated *Smn$^{+/-}$;SMN2* healthy mice (left), untreated *Smn$^{-/-}$;SMN2* SMA mice (centre), and prednisolone-treated *Smn$^{-/-}$;SMN2* SMA mice (right). Colour key represents the Log2FC for upregulated (red) and downregulated (blue) genes. Heatmap was generated by Heatmap2 v2.2.1+galaxy1.

5.3.2. Predicted oxandrolone target gene *Ddit4* is upregulated in skeletal muscle of severe *Smn$^{-/-}$;SMN2* SMA mice.

Similar to chapter 4, we wanted to validate whether our predicted oxandrolone target genes were indeed dysregulated in the skeletal muscle of SMA mice. Thus, we measured the gene expression levels of the oxandrolone target genes in the triceps of P7 symptomatic, untreated severe *Smn$^{-/-}$;SMN2* SMA and *Smn$^{+/-}$;SMN2* healthy mice (Figure 5.5). Interestingly, only *Ddit4* (6.7 FC, p =0.0196) was significantly upregulated in symptomatic severe *Smn$^{-/-}$;SMN2* SMA mice (Figure 5.5.f), supporting both our bioinformatics data and the known pro-atrophic role of Ddit4 [748,749,758], thus indicating that it may play a role in SMA muscle pathologies.

In addition, we compared the expression of our predicted oxandrolone target genes in both pre-symptomatic (P10) and symptomatic (P19) stages of intermediate *Smn$^{2B/-}$* SMA mice to evaluate if their dysregulation is associated with or precedes muscle atrophy (Figure 5.6). Overall, we found no significant difference before and after symptomatic onset for any of the predicted oxandrolone targets (Figure 5.6). However, it should be noted that we observed variation of target gene expression in *Smn$^{2B/-}$* SMA mice (Figure 5.6), suggesting possibility of technical variations. One reason could be that retention of ECM proteins after fibrous RNA extraction [974] or a difference in muscle fibre composition between biological samples [975] fluctuated the total purified RNA content.

In summary, the majority of the predicted oxandrolone target genes did not significantly reflect their transcriptomic predictions.

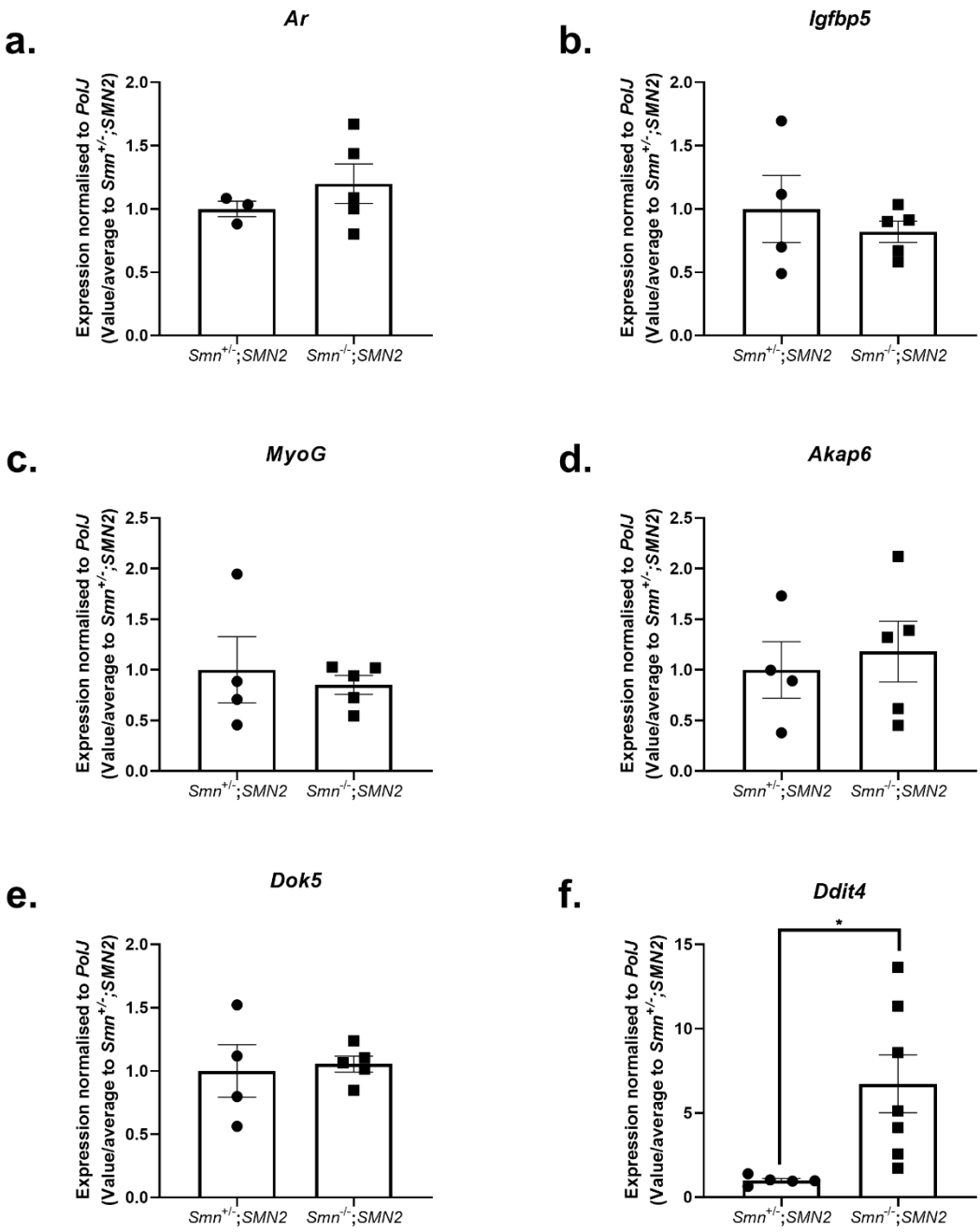

Figure 5.5. The oxandrolone target gene *Ddit4* is upregulated in the skeletal muscle of symptomatic *Smn$^{-/-}$;SMN2* SMA mice.
The mRNA expression by qPCR of predicted metformin targets **a.** *Ar*, **b.** *Igfbp5*, **c.** *MyoG*, **d.** *Akap6*, **e.** *Dok5* and **f.** *Ddit4* in symptomatic post-natal day (P)7 skeletal muscle (triceps) of *Smn$^{+/-}$;SMN2* healthy (N= 4 - 6) and *Smn$^{-/-}$;SMN2* SMA (N= 5 - 7) mice. Error bars represents +/- SEM with individual value points as black dot; unpaired t-test, *p <0.05.

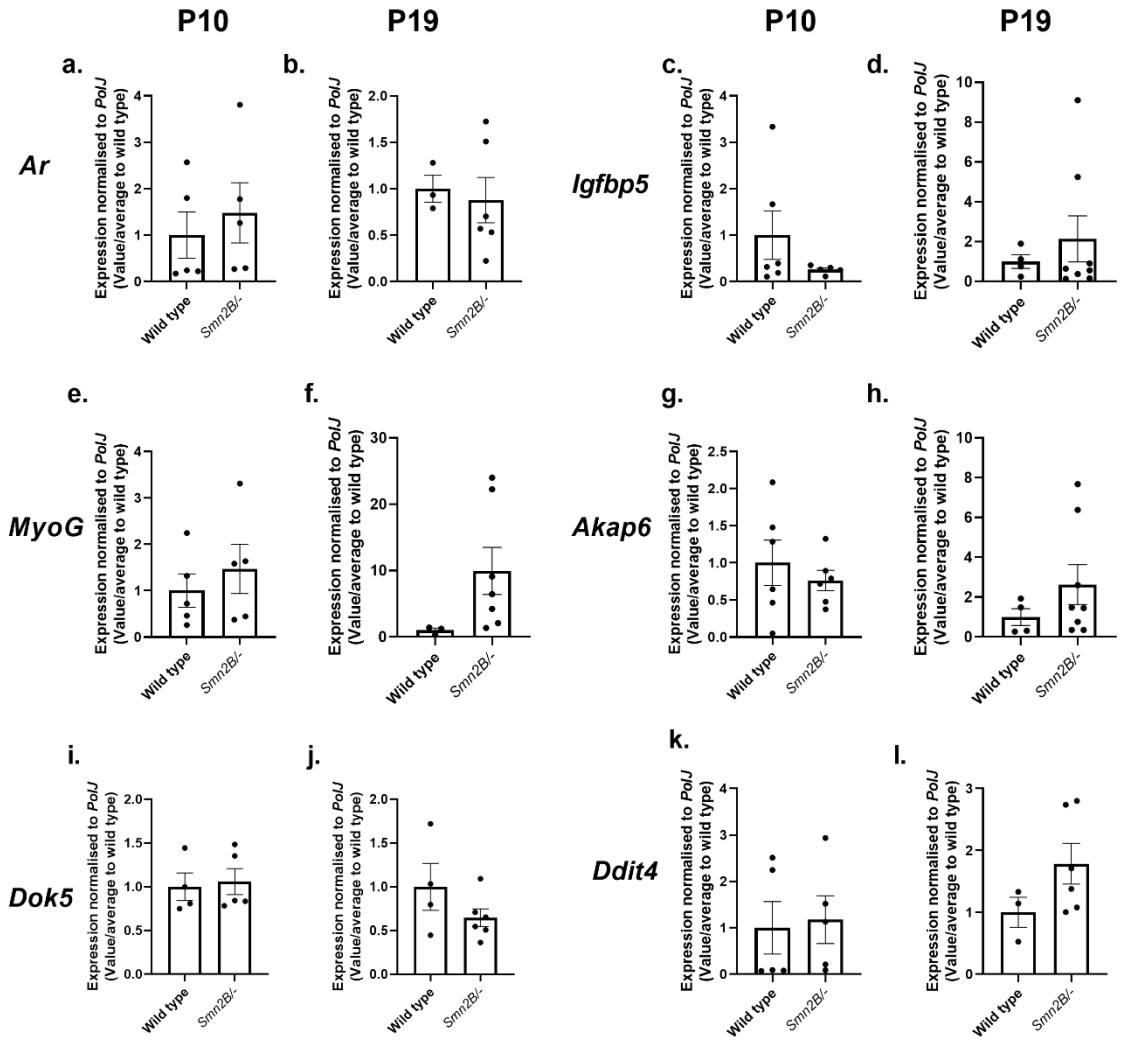

Figure 5.6. None of the oxandrolone target genes are significantly dysregulated in the skeletal muscle of both pre-symptomatic and symptomatic *Smn*$^{2B/-}$ SMA mice.
The mRNA expression by qPCR of predicted metformin targets *Ar*, *Igfbp5*, *MyoG*, *Akap6*, *Dok5* and *Ddit4* in pre-symptomatic stages (left) at post-natal day (P)10 (**a, c, e, g, i** and **k**) and at symptomatic stages (right) at P19 (**b, d, f, h, j,** and **l**) in skeletal muscle (triceps) of wild type (N= 4-6) and *Smn*$^{2B/-}$ SMA (N=6-8) mice. Error bars represents +/- SEM with individual value points as black dot; unpaired t-test, **p* <0.05.

5.3.3. Oxandrolone target genes *DOK5* and *DDIT4* are significantly upregulated in type 3 SMA deltoid myoblasts.

Similar to chapter 4, we next investigated the predicted oxandrolone target genes in primary control and type 3 SMA deltoid myoblasts [13] (in collaboration with Dr Stephanie Duguez; Chapter 2, Table 2.2) to determine if they are dysregulated in human muscle cell lines. Although we observed no significant difference in *AR* (1.5 FC, p =0.3007) and *MYOG* (2.0 FC, p =0.3925) expression between control and type 3 SMA myoblasts (Figures 5.7.a-b), both *DOK5* (20.97 FC, p =0.0221) and *DDIT4* (2.4 FC, p =0.0424) were significantly upregulated in the latter (Figures 5.7.c-d). Although little is known about the function of *DOK5* in muscle, one possibility for its upregulation relates to its proposed competitive and inhibitory activity on IRS-1 and IRS-2 [976], and could contribute to the previously described glucose homeostatic defects in SMA [301–303,305,306]. Interestingly, the significant upregulation of *DDIT4* in *Smn$^{-/-}$;SMN2* mice and type 3 SMA myoblasts not only supports its established pro-atrophy role in muscle-wasting conditions [748,749], but also suggests that it could play an important role in severe and mild muscle pathologies in SMA.

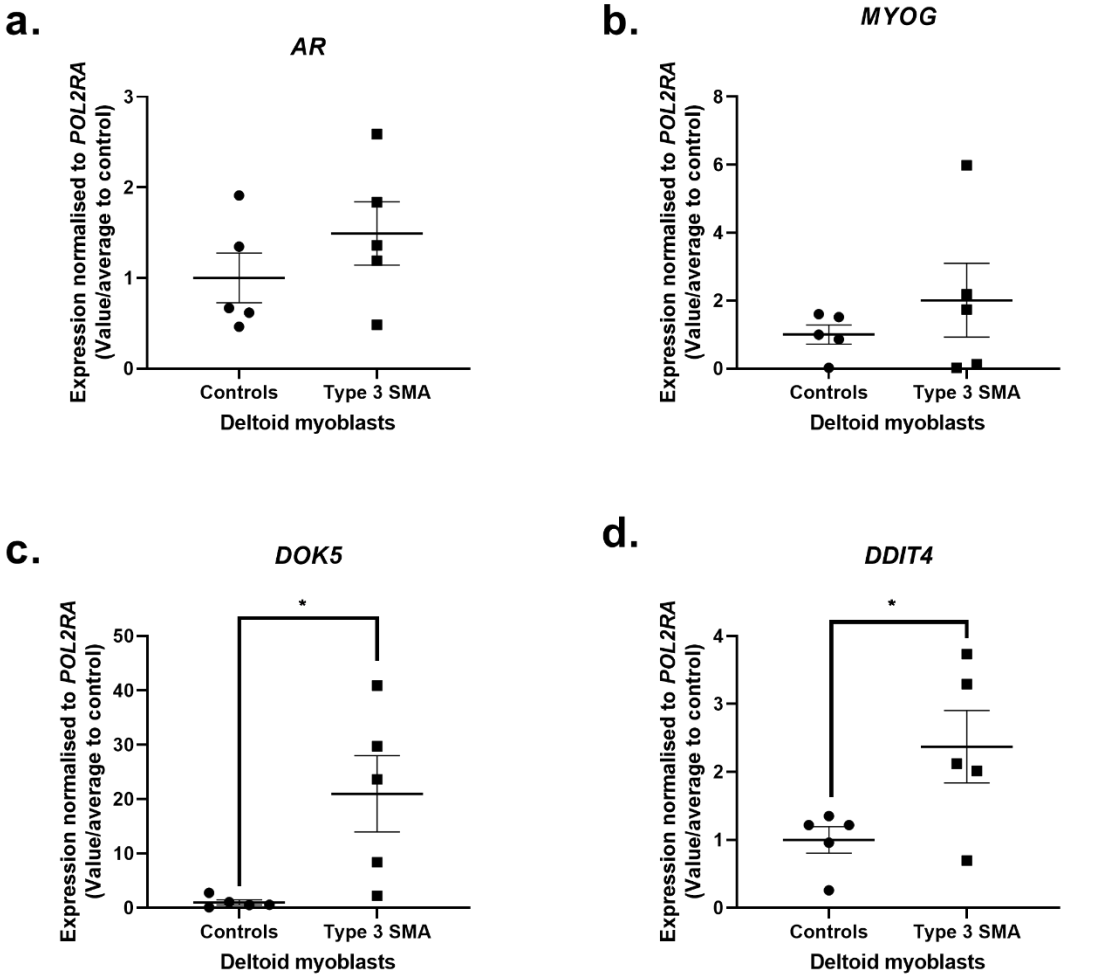

Figure 5.7. *DOK5* and *DDIT4* are significantly upregulated in type 3 SMA deltoid myoblasts. The mRNA expression by qPCR of predicted oxandrolone target genes **a.** *AR*, **b.** *MYOG* ,**c.** *DOK5* and **d.** *DDIT4* in primary myoblasts from deltoid muscle biopsies from healthy controls and type 3 SMA patients (N=5). Individual samples are plotted as black dots, centre line represents mean and error bars represent +/-SEM; unpaired t-test, **p* <0.05.

5.3.4. The expression of the majority of oxandrolone targets is SMN-independent in C2C12 myoblasts and myotubes.

We next determined whether any of the predicted oxandrolone targets are associated with SMN expression. Similar to our metformin investigation (see chapter 4, section 4.3.4), we used *Smn*-depleted C2C12 myoblasts and myotubes generated by siRNA transfection. In the C2C12 myoblasts, none of the oxandrolone targets were significantly affected by *Smn* depletion alone (Figure 5.8.a), suggesting that *Smn* does not influence the expression of these genes in proliferating cells. However, in *Smn*-depleted C2C12 myotubes, *Dok5* is significantly upregulated (3.5 FC, p <0.0001) in the *Smn*-siRNA group alone (Figure 5.8.b), suggesting that this oxandrolone target could be SMN-dependent. Despite *Dok5* being upregulated in *Smn*-depleted C2C12 myotubes, the main oxandrolone target *Ar* (-0.1 FC, p =0.6686) and the other downstream genes are not impacted by *Smn* depletion (Figure 5.8.b), indicating that their expression is most likely SMN-independent in this myoblast-like cell line.

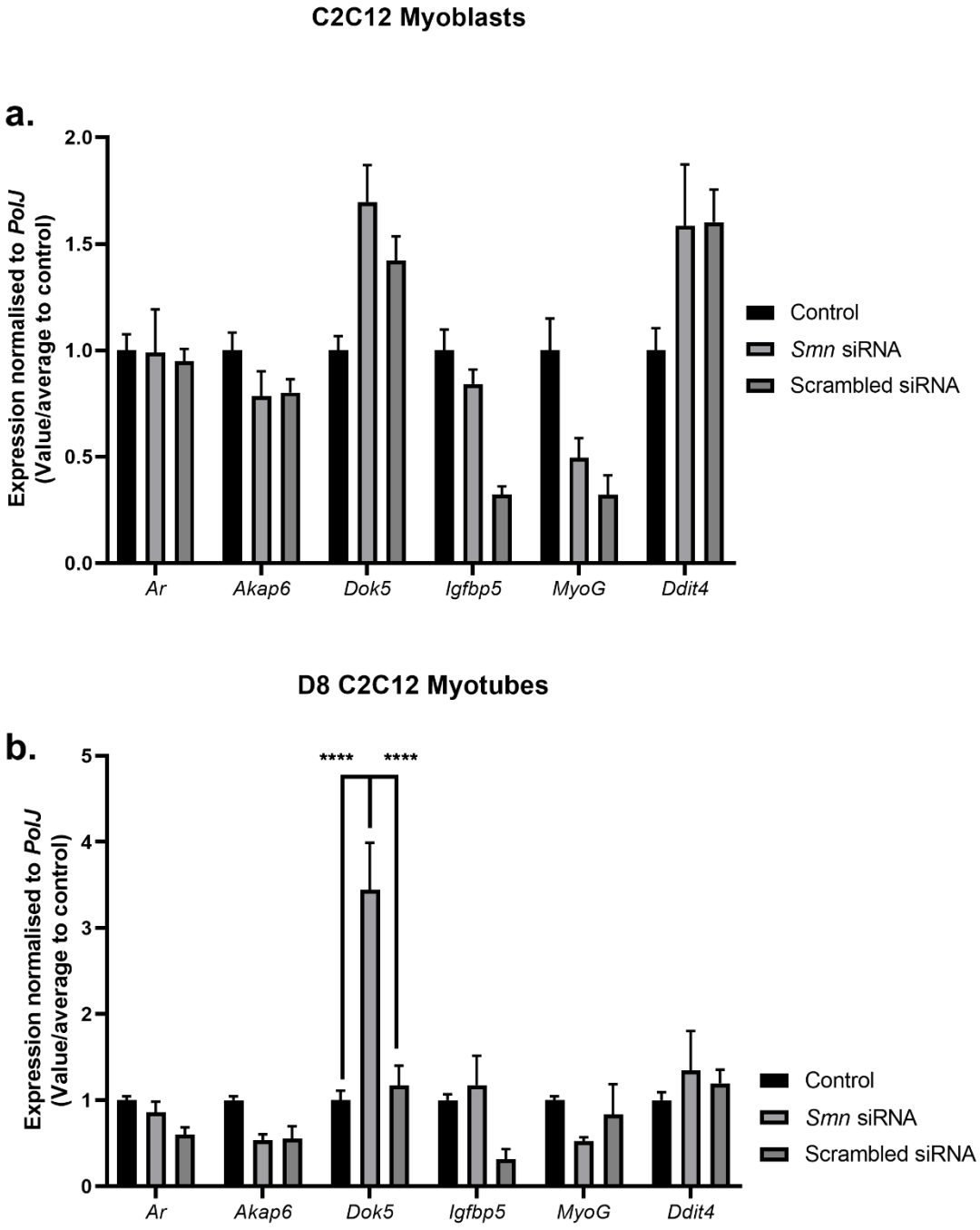

Figure 5.8. *Dok5* is significantly upregulated by *Smn* depletion in C2C12 myotubes.
The mRNA expression by qPCR of oxandrolone target genes *Ar*, *Akap6*, *Dok5*, *Igfbp5*, *MyoG* and *Ddit4* across control, *Smn* siRNA and scrambled siRNA groups in **a.** C2C12 myoblasts and **b.** D8 myotubes. Data represents N=3-4 samples per group across two independent experiments; error bars represent +/- SEM; Two-way ANOVA with post-hoc uncorrected Fishers LSD test, ****p <0.0001.

5.3.5. Low oxandrolone concentration modulates a subset of the predicted target genes in C2C12 myoblasts only.

We next evaluated whether oxandrolone treatment can affect the expression of our predicted target genes. To the best of our knowledge, oxandrolone has not previously been investigated in C2C12 cells. However, 10 µM of the structurally related DHT stimulated both proliferation and differentiation in the C2C12 myoblast-like cell line [837,977]. Thus, we evaluated 10 µM of oxandrolone alongside lower (1 µM) and higher (100 µM) doses in both C2C12 myoblasts and myotubes for a period of 24 hours.

Interestingly, both the low (2.1 FC, p =0.0019) and medium (1.8 FC, p =0.337) oxandrolone doses significantly increased the expression levels of the main target *Ar* in C2C12 myoblasts, validating its reported Ar agonist activity [837,838] (Figure 5.9.a). In addition, the lower oxandrolone dose also upregulated *Igfbp5* (2.5 FC, p <0.0001), *Akap6* (1.9 FC, p =0.0141), *Myogenin* (2.2 FC, p =0.0009) and *Ddit4* (2.2 FC, p =0.0014), whilst the medium dose only upregulated *Igfbp5* (1.77 FC, p =0.0255) and *Ddit4* (2.2 FC, p =0.0013) (Figure 5.9.a).

Conversely, none of the oxandrolone doses significantly upregulated *Ar* expression in the D8 C2C12 myotubes (Figure 5.9.b), which may be due to the fact that C2C12 cells express only 0.1% of endogenous Ar mRNA and protein compared to adult mouse gastrocnemius muscle [978]. Furthermore, analysis of downstream targets affected by oxandrolone in C2C12 myoblasts such as *Igfbp5* and *Myogenin* revealed no significant difference either (Figure 5.9.c), suggesting an absence of oxandrolone-Ar signalling in differentiated C2C12 myotubes.

Based on the known low oxandrolone dose-Ar activity in C2C12 myoblasts (Figure 5.9.a), we therefore decided to compare low oxandrolone treatment across earlier differentiation stages of D3 and D5. Although we observed a significant downregulation of the main *Ar* target in D3 C2C12 myotubes (-0.3 FC, *p* =0.0203) (Figure 5.9.d), there was a slight significant *Ar* upregulation in D5 C2C12 myotubes (1.4 FC, *p* =0.0480) (Figure 5.9.e). However, our investigations of the downstream target genes in D5 C2C12 myotubes revealed no significant modulation by oxandrolone (Figure 5.g.f), again validating the absence of oxandrolone-Ar signalling in differentiated C2C12 myotubes. Although it is unclear why oxandrolone-Ar signalling only occurred in C2C12 myoblasts, one possibility could be that it facilitates the transition of proliferation to differentiation, as evidenced by previous AR activity research [979,980] and the upregulation of muscle differentiation genes *Igfbp5* [839], *Akap6* [840] and *Myogenin* [173,840,980] in our C2C12 myoblasts (Figure 5.9.a).

Another finding we need to take into consideration is the upregulation of *Ddit4* in only C2C12 myoblasts by lower and medium oxandrolone doses (Figure 5.9.a & .f). Although there would be concern of exacerbating significantly upregulated *Ddit4* in severe *Smn*$^{-/-}$*;SMN2* mice (Figure 5.5.f), previous studies of androgen treatment downregulating *Ddit4* activity to ameliorate atrophy in dexamethasone-treated L6.AR myotubes and rat gastrocnemius muscle [749], suggest this upregulation may be linked to the myoblast stage.

Overall, our investigations revealed that oxandrolone has a stronger influence on the expression of our predicted target genes in proliferating C2C12 myoblasts compared to differentiated C2C12 myotubes.

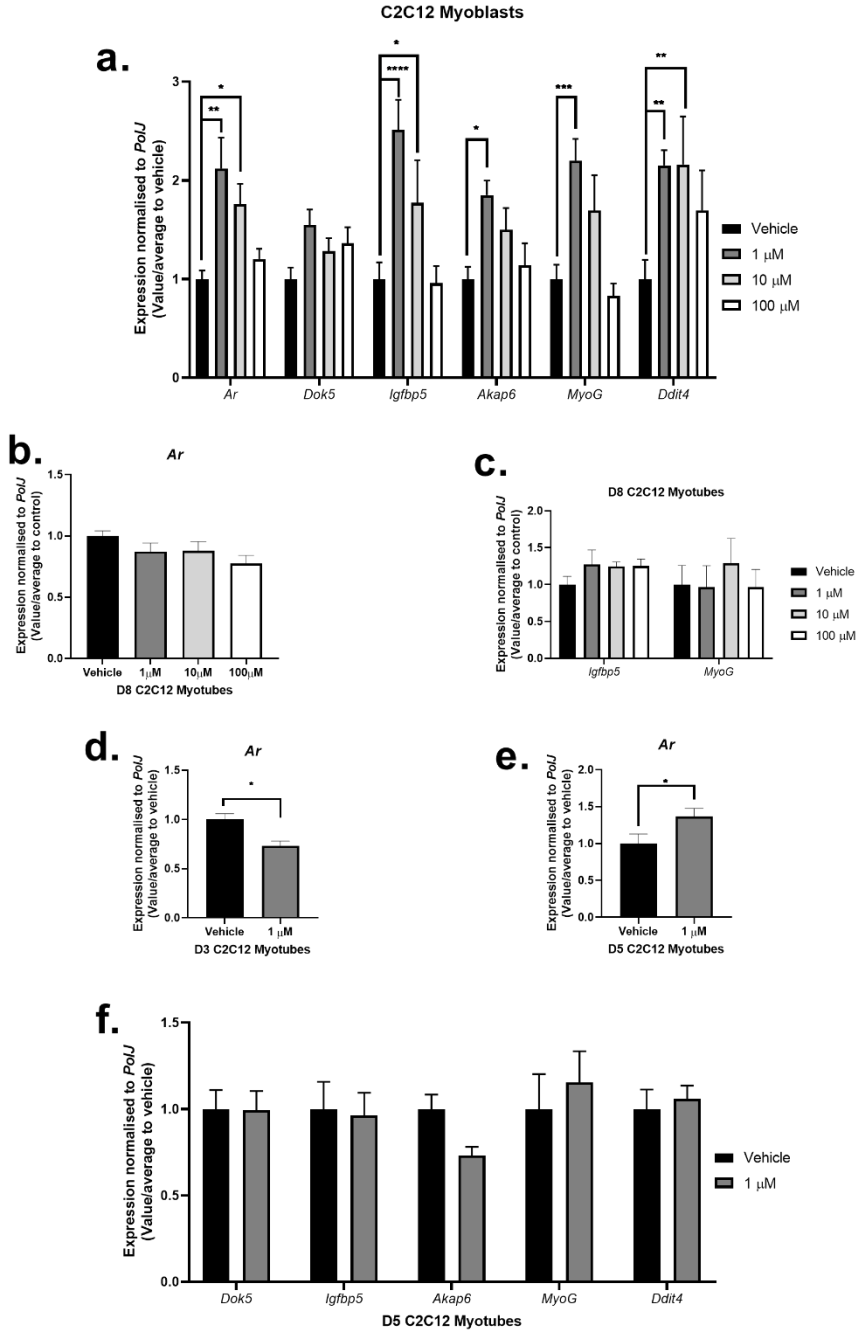

Figure 5.9. Oxandrolone only perturbs specific target genes in C2C12 myoblasts.
The mRNA expression by qPCR to investigate vehicle (absolute ethanol), low 1 μM, medium 10 μM and high 100 μM oxandrolone treatment. **a.** Effects of increasing oxandrolone doses on targets *Ar*, *Dok5*, *Igfbp5*, *Akap6*, *MyoG* and *Ddit4* in C2C12 myoblasts by Two-way ANOVA with post-hoc uncorrected Fishers LSD test. **b.** *Ar* expression in C2C12 D8 myotubes by One-way ANOVA with post-hoc Sidak's test. **c.** *Igfbp5* and *MyoG* expression in C2C12 D8 myotubes by Two-way ANOVA with post-hoc uncorrected Fishers LSD test. Unpaired T-test of *Ar* expression across **d.** D3 and **e.** D5 C2C12 myotubes treated with low 1 μM oxandrolone for 24 hours. **f.** Effects of low 1 μM oxandrolone on downstream targets *Dok5*, *Igfbp5*, *Akap6*, *MyoG* and *Ddit4* in D5 C2C12 myotubes. Data represents N=4 samples per group across two independent experiments; error bars represent +/- SEM;, **p* <0.05, ***p* <0.01, ****p* <0.001, *****p* <0.0001.

5.3.6. Low oxandrolone concentrations are non-toxic in C2C12 myoblasts and myotubes.

Although previous research investigating testosterone, DHT and other anabolic steroids in C2C12 cells have reported little toxicity [978,979,981], the distinct chemical modification of oxandrolone and its first use in C2C12 cells led us to investigate its potential adverse effects [837,838]. In our investigation, we used LDH assay to evaluate for potential toxicity of 1 µM oxandrolone treatment in C2C12 myoblasts and myotubes [982]. Compared to the traditional 3-(4,5-dimethylthiazol-2-yl)-2,5-diphenyl-2H-tetrazolium bromide (MTT) assay method [983], the LDH assay is advantageous in detecting the extent of cell damage and death by proportionally measuring released LDH levels [982].

For C2C12 myoblasts, the LDH assay revealed that both 24- and 72-hours 1 µM oxandrolone treatment had significantly lower absorption rates compared to the cytotoxic control (Figure 5.10.a). Although, 24 hours of ethanol vehicle and 1 µM oxandrolone treatment had no significant difference to the untreated control, both of the 72 hour duration groups had significantly higher absorbances (Figure 5.10.a), indicating that 72 hours of ethanol vehicle treatment has toxicity in proliferating cells. On the other hand, the absorbances for 24- and -72 hours 1 µM oxandrolone treatment in D5 C2C12 myotubes were not significantly different from the cytotoxic control (Figure 5.10.b). Although both of the drug durations were not significantly different from the untreated control, the absorption rate for the 72 hour ethanol vehicle was significantly higher (Figure 5.10.b), again suggesting the possibility that the toxicity in the differentiated myotubes could be due to this vehicle. Overall, our LDH assay revealed that lower doses of oxandrolone did not induce any major toxicity in our C2C12 cells.

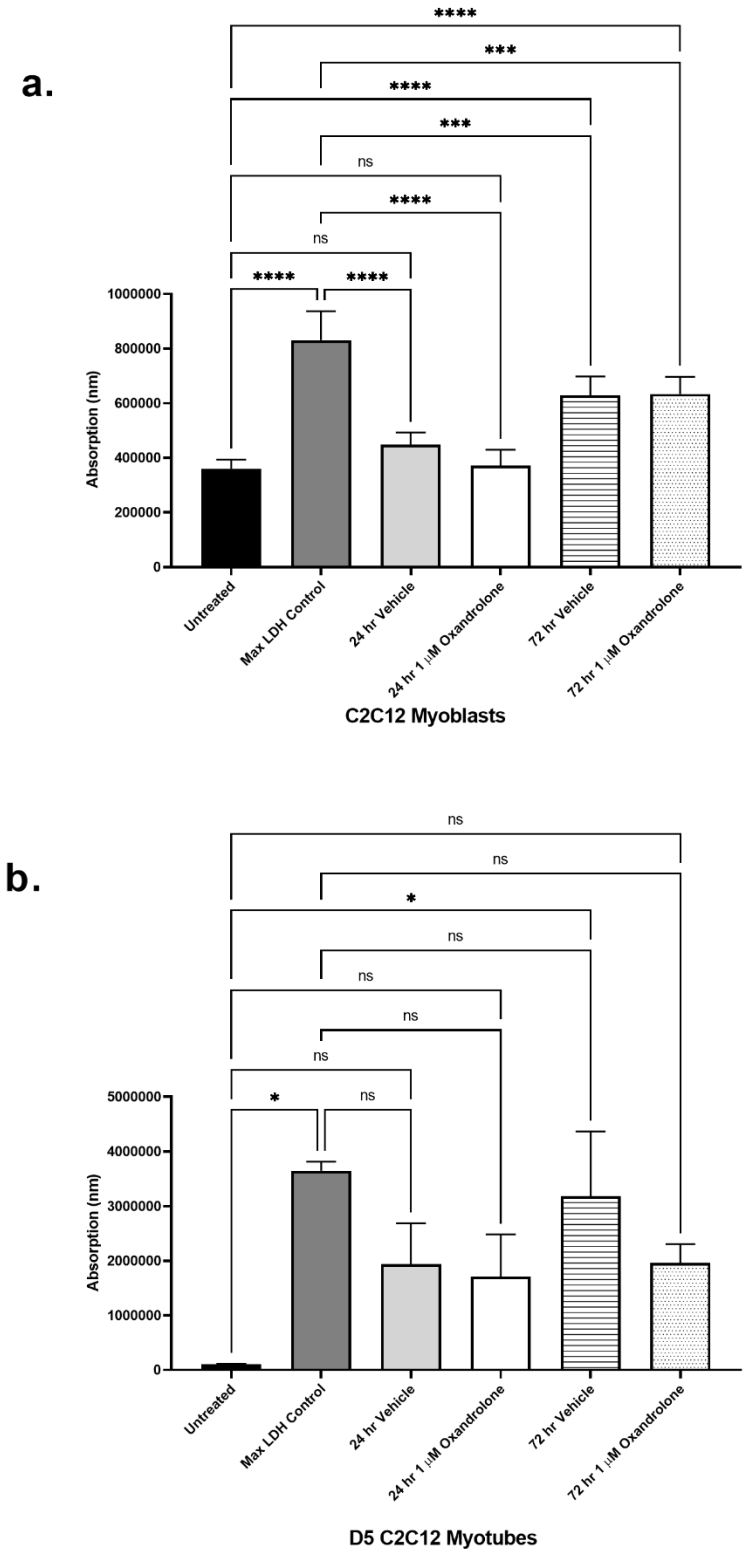

Figure 5.10. Low 1 μM oxandrolone treatment is non-toxic in C2C12 myoblasts and myotubes.
Absorption readings (nm) from released lactate dehydrogenase (LDH) in cell culture supernatant from untreated , max LDH control (1% Triton-X), 24-hour ethanol vehicle, 24 hour 1 μM oxandrolone, 72 hour vehicle, and 72 hour 1 μM oxandrolone treatment in **a.** C2C12 myoblasts and **b.** D5 C2C12 myoblasts. Data represents N=6 samples; error bars represent +/- SEM; One-way ANOVA with post-hoc Dunnett's multiple comparisons test, ns = not significant, *p <0.01, ***p <0.001, ****p <0.0001.

5.3.7. Low oxandrolone concentrations do not affect proliferation of C2C12 myoblasts.

Previously, in section 5.3.5, we observed that oxandrolone-Ar activity only affected the target genes in proliferating C2C12 myoblasts (Figure 5.9.a). Furthermore, the target genes such as *Igfbp5* [839], *Akap6* [840] and *Myogenin* [173,840,980] have previously been associated with promoting muscle differentiation. Thus, we wanted to investigate if oxandrolone affected proliferation of C2C12 myoblasts. For this, we labelled the C2C12 myoblasts with BrDU, a synthetic analog that incorporates into replicating DNA allowing us to proportionally measure proliferation via primary anti-BrDU and secondary colourimetric antibody staining [984,985]. As above, we evaluated the effects of 24- and 72-hours of ethanol vehicle and 1 µM oxandrolone treatment. Interestingly, there was no significant difference between untreated and oxandrolone-treated C2C12 myoblasts across 24- and 72-hour time periods (Figure 5.11), suggesting that oxandrolone does not impact proliferation of C2C12 myoblasts.

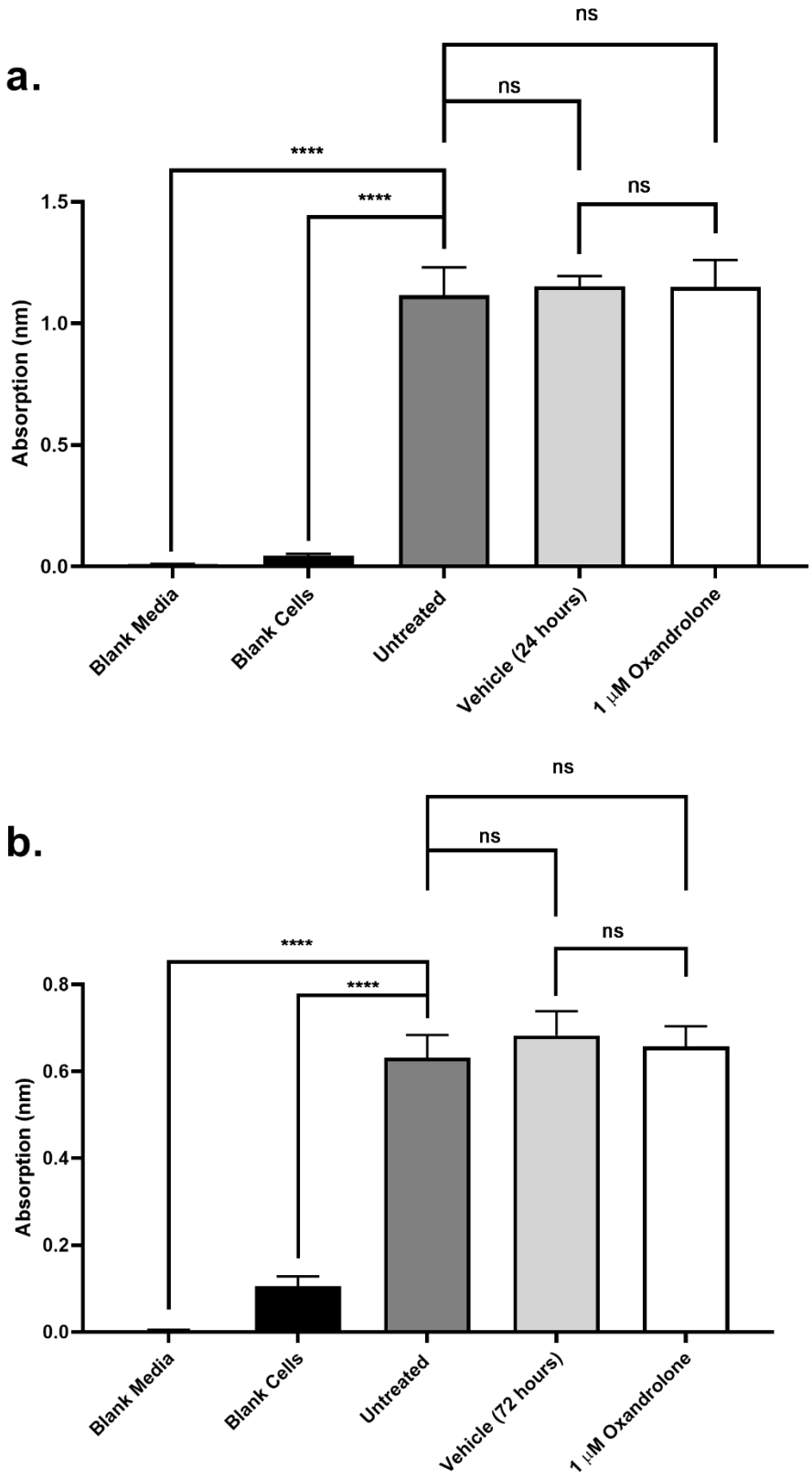

Figure 5.11.Low 1 μM oxandrolone treatment does not affect C2C12 myoblast proliferation. Absorption readings (nm)of blank media, blank C2C12 myoblasts and anti-BrDU antibody immunostained untreated, vehicle- (absolute ethanol) and 1 μM oxandrolone-treated C2C12 myoblasts for **a.** 24 hours and **b.** 72 hours. Data represents N=6 samples; error bars represent +/- SEM; One-way ANOVA with post-hoc Dunnett's multiple comparisons test, ns = not significant, ****p <0.0001.

5.3.8. Low oxandrolone doses attenuate canonical atrophy in serum-deprived C2C12 myotubes independent of predicted target genes.

We next wanted to evaluate the ability of oxandrolone to attenuate canonical muscle atrophy by using the same serum-deprivation method that we previously described and performed in metformin-treated C2C12 myotubes (see chapter 4, section 4.3.6). However, in our metformin investigation, we used D8 C2C12 myotubes, whilst our prior results for oxandrolone showed that D5 C2C12 myotubes are required to elicit an androgen response (Figure 5.9.e). Thus, we initially wanted to determine if *in vitro* serum-deprivation muscle atrophy can be similarly replicated in D5 C2C12 myotubes. We confirmed that both atrogenes *atrogin-1* (2.0 FC, p =0.0197) and *MuRF1* (2.6 FC, p =0.0005) were significantly upregulated after 24 hours of serum deprivation, validating a muscle atrophy phenotype in D5 C2C12 myotubes (Figures 5.12.a-c). Furthermore, specific oxandrolone target genes were significantly downregulated in atrophied D5 C2C12 myotubes such as *MyoG* (-0.6 FC, p =0.0003), *Akap6* (-0.5 FC, p =0.0014), *Igfbp5* (-0.7 FC, p <0.0001) and *Ddit4* (-0.6 FC, p =0.0004) (Figure 5.12.d).

Next, we wanted to evaluate whether oxandrolone treatment can attenuate the serum-starvation induced muscle atrophy and furthermore, if it can restore the expression of the dysregulated target genes (Figure 5.12.d). Interestingly, a 24-hour treatment of 1 µM oxandrolone delayed progressive atrophy in serum-deprived C2C12 myotubes, as evidenced by the significant downregulation of *atrogin-1* (-0.3 FC, p =0.0354) (Figures 5.12.e-f). However, the levels of *Myogenin* (-0.3 FC, p =0.0112) and *Igfbp5* (-0. 3FC, p =0.0151) were in fact further downregulated by oxandrolone treatment (Figure 5.12.g), suggesting that

the ameliorative effects were governed via Ar-independent effectors. Overall, a low dose of oxandrolone attenuated canonical atrophy in C2C12 myotubes, supporting its therapeutic potential in SMA mice.

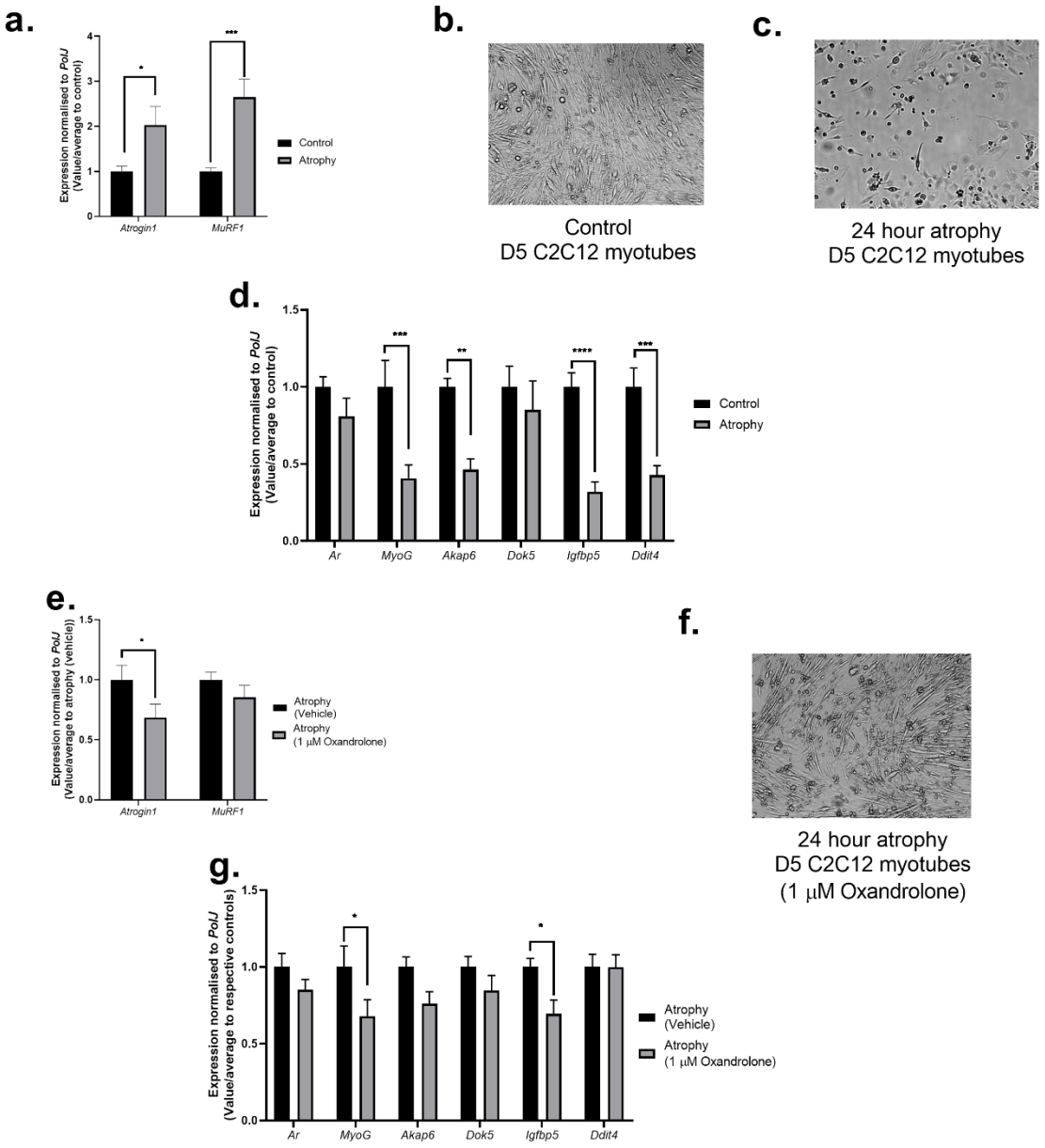

Figure 5.12. Low 1 μM oxandrolone treatment attenuates canonical atrophy in serum-starved D5 C2C12 myotubes. **a**. Atrogene (*Atrogin-1* and *MuRF1*) mRNA expression between control and 24-hour serum-deprived D5 C2C12 myotubes by qPCR. 10x magnification of **b.** control and **c.** 24-hour serum-deprived atrophy in D5 C2C12 myotubes. **d.** mRNA expression of predicted target genes between control and 24-hour serum-deprived D5 C2C12 myotubes by qPCR. **e.** Atrogene (*Atrogin-1* and *MuRF1*) mRNA expression between vehicle control and 1 μM oxandrolone treated 24-hour serum-deprived D5 C2C12 myotubes by qPCR. **f.** 10 x magnification of1 μM oxandrolone treated 24-hour serum-deprived D5 C2C12 myotubes. **g.** mRNA expression of predicted target genes between vehicle control and 1 μM oxandrolone treated 24-hour serum-deprived D5 C2C12 myotubes by qPCR. Data represents N=4 samples per group across two independent experiments; error bars represent +/- SEM; Two-way ANOVA with post-hoc uncorrected Fishers LSD test, *p <0.05, **p <0.01, ***p <0.001.

5.3.9. Oxandrolone treatment improves survival in *Smn$^{2B/-}$* SMA mice.

Similar to Chapter 4, our purpose of investigating oxandrolone was to evaluate its effects on muscle pathologies in SMA. Thus, we conducted preliminary treatment regimens of 1 – 8 mg/kg/day starting at P5 and P8, based on oxandrolone's prior use in mouse models of SCI [965] and burn injury [986]. In these pilot studies, we also stopped oxandrolone treatment at P21, as previous research showed that shorter oxandrolone treatments are more effective than long-term [965]. In the end, our daily assessment of survival, weight and motor function from P0 up to humane endpoint (*Data now shown*) suggested that daily gavage of oxandrolone at 4 mg/kg/day and starting at P8 was the optimum regimen.

Indeed, we observed that this dose significantly improved the median survival of *Smn$^{2B/-}$* SMA mice by 3 days (Figure 5.13.a). Next, we assessed body weight and noticed the weight of the 4 mg/kg/day oxandrolone oxandrolone-treated *Smn$^{2B/-}$* SMA mice were significantly lower compared to their untreated counterparts (Figure 5.13.b). However, the significantly lower body weight in 4 mg/kg/day oxandrolone-treated *Smn$^{2B/-}$* SMA mice began 4 days prior to the initial treatment start date of P8 (-0.4 kg average) (Figure 5.13.b), suggesting that these animals were naturally smaller.

In terms of motor function, we observed no significant difference in the righting reflex time between untreated, vehicle- and 4 mg/kg/day oxandrolone-treated *Smn$^{2B/-}$* SMA mice (Figure 5.13.c), suggesting that oxandrolone does not improve motor function.

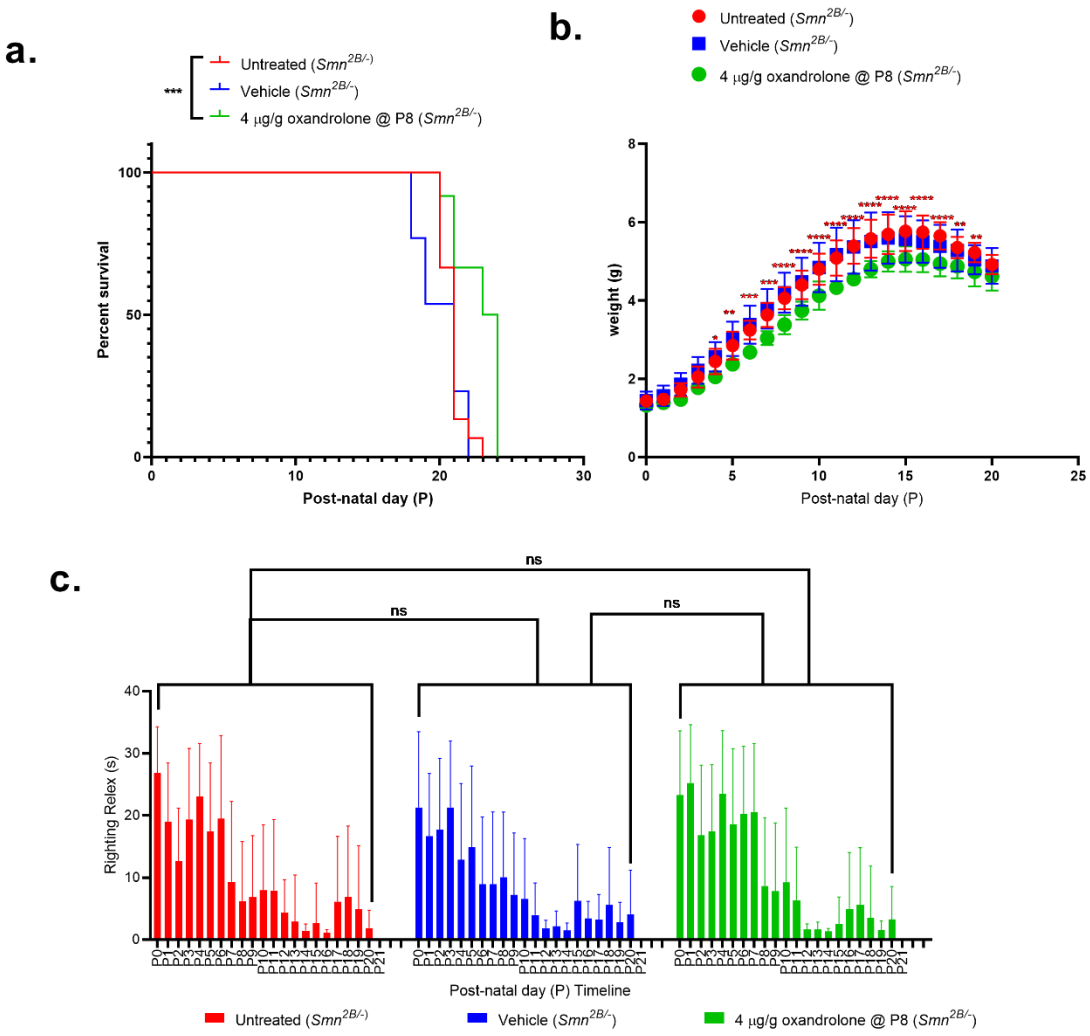

Figure 5.13. 4 mg/kg/day oral oxandrolone treatment improved survival in *Smn*$^{2B/-}$ SMA mice.
All treated animals received a daily dose of oxandrolone (200 mg/kg/day, suspended in 0.5% carboxymethylcellulose) by gavage starting at P8 or vehicle by gavage starting at P5.
a. Kaplan-Meier survival curves for n= 15 untreated (red, median survival: 21 days), n= 13 vehicle-treated (blue, median survival: 20 days) and n= 12 4 mg/kg/day oxandrolone-treated (green, median survival: 21 days) *Smn*$^{2B/-}$ SMA mice. Long-rank (Mantel-Cox) test ***p <0.001.
b. Daily weights of untreated (red, n= 15), vehicle-treated (blue, n= 13) and 4 mg/kg/day oxandrolone-treated (green n= 12) *Smn*$^{2B/-}$ SMA mice. Data represents mean and +- SD error bars, Two-way ANOVA with post-hoc Sidak's multiple comparisons test between untreated and 4 mg/kg/day oxandrolone (red star) and untreated vs vehicle-treated (blue star), *p <0.05, **p <0.01, ***p <0.001, ****p <0.0001.
c. Daily righting reflex test up to a 30 second max time point of untreated (red, n= 15), vehicle-treated (blue, n= 13) and 4 mg/kg/day oxandrolone-treated (green n= 12) *Smn*$^{2B/-}$ SMA mice. Data represents mean and +- SD error bars, One-way ANOVA with post-hoc Tukey's multiple comparisons test, ns = not significant.

On the other hand, although 4 mg/kg/day oxandrolone had no effect on survival or motor function, we did observe a significant downregulation of body weight in *Smn*$^{2B/+}$ healthy mice starting from P9 (-0.7 kg average) (Figure 5.14). Thus, both the *Smn*$^{2B/-}$ SMA and *Smn*$^{2B/+}$ healthy data suggests that oxandrolone may have an impact on body weight.

Nevertheless, our results demonstrated that 4 mg/kg/day oxandrolone treatment mildly improved survival in intermediate *Smn*$^{2B/-}$ SMA mice. However, it remains unclear on whether muscle pathologies were affected.

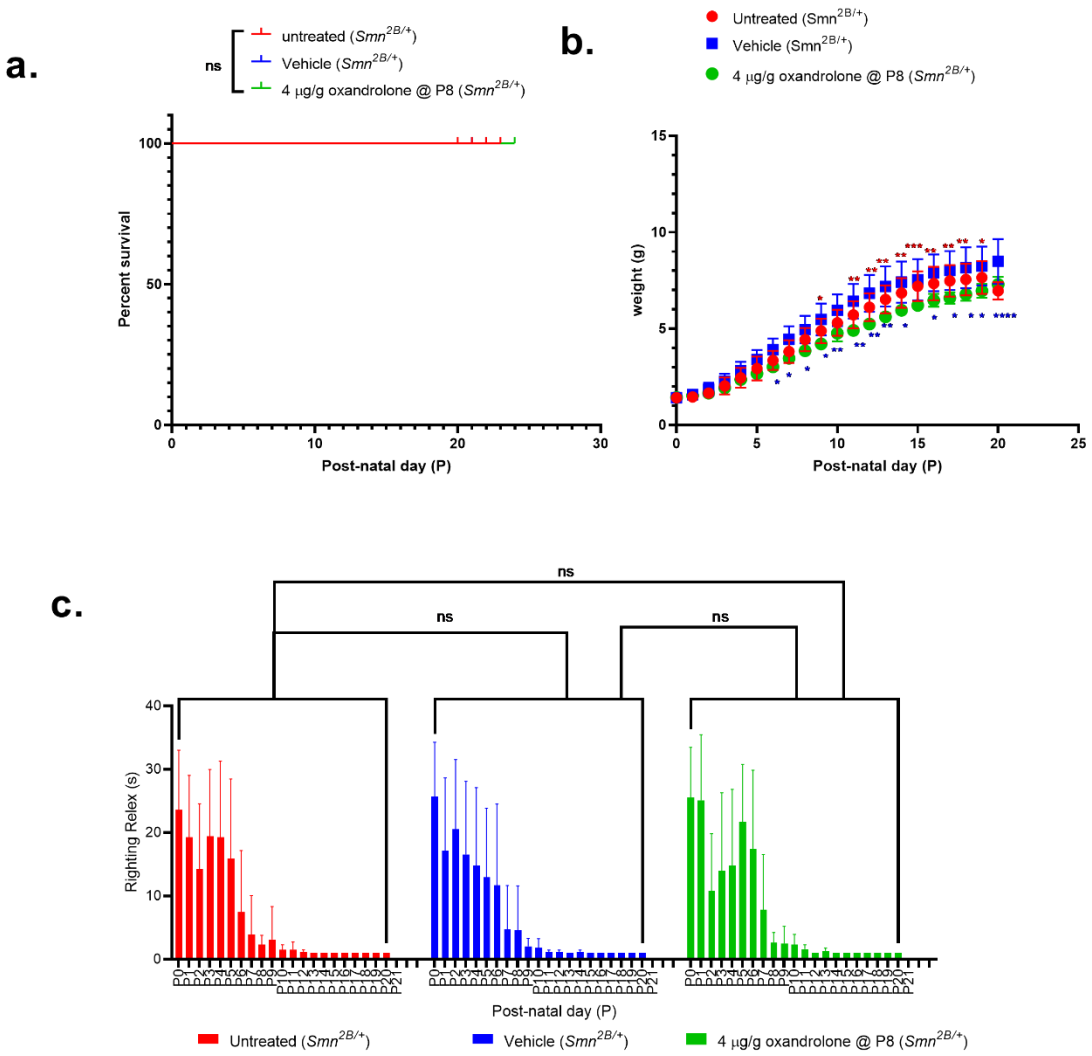

Figure 5.14. 4 mg/kg/day oral oxandrolone treatment significantly lowered weight in *Smn*$^{2B/+}$ healthy mice.
All treated animals received a daily dose of oxandrolone (200 mg/kg/day, suspended in 0.5% carboxymethylcellulose) by gavage starting at P8 or vehicle by gavage starting at P5.
a. Kaplan-Meier survival curves for n= 21 untreated (red, median survival: 21 days), n= 16 vehicle-treated (blue, median survival: 20 days) and n= 10 4 mg/kg/day oxandrolone-treated (green, median survival: 21 days) *Smn*$^{2B/+}$ healthy mice Long-rank (Mantel-Cox) test ns = not significant.
b. Daily weights of untreated (red, n= 21), vehicle-treated (blue, n= 16) and 4 mg/kg/day oxandrolone-treated (green n= 10) *Smn*$^{2B/+}$ healthy mice. Data represents mean and +- SD error bars, Two-way ANOVA with post-hoc Sidak's multiple comparisons test between untreated and 4 mg/kg/day oxandrolone (red star) and untreated vs vehicle-treated (blue star), **p* <0.05, ***p* <0.01, ****p* <0.001, *****p* <0.0001.
c. Daily righting reflex test up to a 30 second max time point of untreated (red, n= 21), vehicle-treated (blue, n= 16) and 4 mg/kg/day oxandrolone-treated (green n= 10)*Smn*$^{2B/+}$ healthy mice. Data represents mean and +- SD error bars, One-way ANOVA with post-hoc Tukey's multiple comparisons test, ns = not significant.

5.4. Discussion

Although we have not finalised our investigations, the pre-clinical evidence so far suggests potential for oxandrolone as a skeletal muscle therapy in SMA. However, compared to prednisolone we observed minimal ameliorations [53]. Indeed, despite the median survival increase of 3 days in 4 mg/kg/day oxandrolone-treated *Smn*$^{2B/-}$ SMA mice, this did not triple their life expectancy as previously observed in prednisolone-treated *Smn*$^{2B/-}$ SMA mice [53], suggesting that oxandrolone is not as effective as prednisolone in improving survival in SMA. One reason could be that prednisolone targets a greater number of pathways that may be important for SMA pathology. However, comparisons between prednisolone and oxandrolone-targeted pathways in SMA skeletal muscle by RNA-Seq would be needed to investigate this further.

In terms of neuromuscular phenotype, we observed no difference in motor function and a significantly lower bodyweight in both *Smn*$^{2B/-}$ SMA and *Smn*$^{2B+}$ healthy mice. However, a previous study has shown that deletion of pro-atrophy factors like *atrogin-1* in *SMNΔ7* SMA mice can still increase myofiber size without improvements to survival and total body weight [155]. Thus, future experiments would therefore need to evaluate by histological and molecular analyses if oxandrolone improved neuromuscular pathologies like myofiber size and impacted the expression of the predicted target (e.g., *Ddit4* and *Dok5*) and muscle health (atrogenes, MRFs) genes in *Smn*$^{2B/-}$ SMA mice.

Indeed, we found a significant upregulation of *Ddit4* in the skeletal muscle of both severe *Smn*$^{-/-}$*;SMN2* SMA mice (triceps) and type 3 SMA human myoblasts (deltoid), suggesting that Ddit4 could be influential in severe and mild SMA

muscle pathologies, regardless of species or muscle differences. Interestingly, the upregulation of *Ddit4* in both symptomatic severe and mild SMA skeletal muscle could be linked to the fact that alongside Klf15, it is also a downstream GC receptor (GR) target that negatively modulates myofiber size [368,987]. Furthermore, with prednisolone's GC-dependent amelioration of disease phenotypes in both severe *Smn*$^{-/-}$*;SMN2* and milder *Smn*$^{2B/-}$ SMA mice, one possibility could be that the GC-Ddit4 pathway acts as a Klf15-independent mechanism for muscle improvement [53]. In the context of oxandrolone, Ddit4 could also be an interesting target as previous studies have shown that AR directly prevents its upregulation, thus ameliorating muscle-wasting [749].

Another interesting target that we validated was *Dok5*, which was significantly upregulated in type 3 SMA deltoid myoblasts and *Smn*-depleted C2C12 myotubes, suggesting it is an SMN-dependent target. Although the physiological role of Dok5 and how SMN influences its expression remain poorly understood [976], previous studies have so far identified it as a downstream kinase for IRS-6 [841]. Furthermore, IRS-6 constitutively binds to IRS-1 as evidenced by bioluminescence resonance energy transfer (BRET) activity [976], suggesting it acts as a competitive inhibitor in insulin and IGF-1 signalling. In the context of SMA, studies from mice have shown that increase of IGF-1 levels is linked to improved phenotype [988,989]. Thus, one possibility could be that *Dok5* upregulation via depleted SMN levels promotes reduced IGF-1 activity in SMA through competitively inhibiting IRS1/2 signalling [350,841,976]. However, future studies on the relationship between SMN activity and Dok5 would be needed to corroborate this theory.

Even though we have not evaluated oxandrolone's effects on SMA skeletal muscle, our *in vitro* investigations revealed that doses of 1 µM oxandrolone ameliorated canonical atrophy in C2C12 myotubes. Although we used serum-starvation to induce atrophy in this model [748,758], meta-analysis of transcriptomic studies have revealed that starvation and denervation both promote autophagy pathways [925]. Furthermore, autophagy contributes to muscle atrophy in symptomatic *Smn*$^{2B/-}$ SMA mice [56], supporting the potential for oxandrolone to reduce muscle wasting in SMA. Nevertheless, despite ameliorating atrophy in C2C12 cells, our analyses revealed that this effect was independent of the expression of our predicted target genes. In fact, *Ddit4* was inversely downregulated in atrophied C2C12 myotubes. However, one possible explanation could be the glucose and FA metabolic defects associated with starvation [990], as these could have negatively modulated Ddit4 activity [991], as observed in the muscle of *Ddit4*-KO mice [759,992].

In terms of how oxandrolone ameliorated atrophy independently of our predicted targets in C2C12 myotubes, there are two possibilities that could be further investigated. One is that oxandrolone promoted differentiation, as AR and oxandrolone have previously been linked to muscle differentiation, which in turn has benefited muscle growth [834,979 993]. However, our only evidence so far in support of differentiation is the upregulation of our pro-differentiation target genes *Igfbp5* [839], *Akap6* [840] and *Myogenin* [173,840,980] in C2C12 myoblasts and oxandrolone having no significant impact on proliferation. We would therefore need to perform MHC immunostaining to further evaluate if differentiation was being promoted by oxandrolone [994]. In addition to the impact on differentiation, another explanation could be the promotion of myocellular protein levels, as

previous oxandrolone and AR studies in muscle have also associated muscle growth with elevated myocellular protein levels [962,978]. Importantly, these future *in vitro* studies would be useful for determining the possible mechanisms behind the ways in which oxandrolone could benefit SMA skeletal muscle.

One limitation that we need to take into consideration regarding our *in vitro* experiments is that C2C12 cells were not an effective muscle model for Ar activity. Indeed, previous research has established that Ar expression levels in C2C12 myoblasts reflected only 0.1% of the mRNA and protein content of adult mouse skeletal muscle [978]. Similarly, patterns of low endogenous Ar activity have also been reported in L6 rat myoblasts [995,996], suggesting that immortalised murine skeletal muscle cell lines are not effective tools for measuring androgen treatment. Although primary mouse myoblasts could be a useful alternative based on the higher Ar content in muscle biopsies [978,997], these would have a limited growth potential and require optimum culture conditions compared to immortalised cell myoblasts [998,999]. Thus, one consideration for improving our *in vitro* oxandrolone experiments could be the use of human AR plasmid transfection in our C2C12 myoblasts, since previous studies overcame poor Ar signalling by designing androgen responsive C2C12 (or C2C12.AR) and L6 (or L6.AR) myoblasts [978,996]. However, a less labourious alternative for human AR plasmid transfection could be testing oxandrolone in a human immortalised muscle cell line like LHCN-M2 myoblasts [1000]

In the context of SMA therapies, there are still some factors that need to be taken into consideration when discussing the suitability of oxandrolone as a long-term skeletal muscle treatment. In our study we mainly focused on mixed gender cohorts. However, *Ar* KO models have shown that its absence does not impact

female muscle size to the same extent as in males [956]. Furthermore, female mice have higher expression of *oestrogen related receptor alpha* (EsrrA) compared to *Ar* and different transcriptomic responses to DHT treatment [1001]. With intramuscular Ar content a stronger influence on hypertrophy than systemic hormone levels [1002] and suggestions that SMA males are linked to more severe skeletal muscle pathologies [1003], it remains unclear whether oxandrolone would have equal benefits in males and females. One way that we could address this is with sex-specific phenotypic, molecular and histological analyses of oxandrolone treatment in our *Smn*$^{2B/-}$ SMA mice. Another possibility would be the evaluation of pro-oestrogen drugs in female *Smn*$^{2B/-}$ SMA mice as prior studies have shown that oestrogen receptor-α (*Erα*) depletion negatively affects muscle contraction and health in female mice [1004,1005]. In addition, our bioinformatics and DGIdb v3.0 data showed that *Esr1* was significantly upregulated by prednisolone, which led to the identification of 31 potential oestrogen-agonist orally bioavailable drugs (see Chapter 3, Table 3.11).

Another unknown regarding oxandrolone treatment in SMA relates to the long-term adverse effects. Although studies in paediatric patients have not reported any myopathic adverse risks from chronic treatment after 6 months [1006], an independent study did see a rise in liver enzyme activity that was restored after discontinuation of oxandrolone use [1007,1008]. With liver pathologies being a feature in SMA [343,348,349], it is possible that oxandrolone may be limited to short treatment durations like prednisolone [53,628]. To overcome this issue, future studies could investigate non-steroidal (ns)-SARMs [1009]. The advantage that ns-SARMs would have over oxandrolone is that certain compounds would be specifically designed to target skeletal muscle-expressed Ar and in theory, limit adverse systemic

effects [1009]. Despite the fact that none of the ns-SARMs are approved, pre-clinical studies of these compounds in muscle-wasting and disease models such as DMD [829,1010], chronic GC usage [1011] and hypogonadism [1011] have reported anabolic muscle growth with minimal Ar activity in other organs. Furthermore, ns-SARMs were also identified in our DGIdb v3.0 drugs list (see Chapter 3, Table 3.11), making them interesting candidates for future SMA drug repositioning studies.

In summary, the pre-clinical data for oxandrolone has so far shown it could slightly improve survival and possibly muscle pathologies in SMA. However, further investigations are still needed to address whether it can significantly improve health in SMA mice and if it is a suitable long-term substitute for prednisolone treatment.

Chapter 6.

Discussion

6.1. Project outcomes

The necessity for combinatorial and synergistic treatments to improve the quality of life of all SMA patients has been delayed due to the absence of clinically approved SMN-independent therapies (as of 2021) that target hallmark pathologies in the CNS and skeletal muscle. In particular, skeletal muscle is an important treatment target as SMA pre-clinical models and patients display pathophysiological progressive muscle weakness and atrophy [56,359,360], delayed myogenesis [54,55,157,158] and dysfunctional metabolism [161,301,303,342]. Although two novel therapies designed for SMA skeletal muscle are being clinically investigated at this time [544,545,572], another avenue for consideration is drug repositioning since this approach undergoes a shorter discovery pipeline that produces cost-effective treatments if successful [586,587,590].

One recent example of drug repositioning in SMA is with the synthetic GC prednisolone, which improved muscle health and survival in both severe *Smn*$^{-/-}$*;SMN2* and milder *Smn*$^{2B/-}$ SMA mice [53]. However, to overcome the adverse myopathic effects of chronic GC use [628], this thesis has focused on identifying existing clinically approved drugs that could emulate the beneficial effects of prednisolone in SMA skeletal muscle.

In chapter 3, we analysed RNA-Seq data obtained from triceps of prednisolone-treated and untreated symptomatic *Smn*$^{-/-}$*;SMN2* SMA and *Smn*$^{+/-}$*;SMN2* healthy mice. Interestingly, the transcriptomics revealed that prednisolone treatment normalised a specific subset of genes in symptomatic SMA skeletal muscle to those similarly observed in untreated healthy cohorts. Notably, these genes were linked to myofiber size regulation as well as metabolic and functional muscle

pathways such as FoxO signalling [56], AMPK signalling [389,781,782], mitophagy [388,784], autophagy [56,389] and circadian rhythm [356], which have previously been associated with SMA. Importantly, our findings confirmed the ameliorative benefits of prednisolone and uncovered different pathways to those previously published of its activity in SMA skeletal muscle [53]. In addition, these predicted pathways were vital for our thesis as iPathwayGuide [651–655] and the DGIdb v3.0 database [659] used them to identify 223 clinically approved compounds that were not primarily developed for cancer and have been used in disorders that share pathological overlaps with SMA. Furthermore, the identification of colforsin [809] and celecoxib [615] (ClinicalTrials ID: NCT02876094), which have previously been investigated in SMA, provided support for the validity of our *in silico* strategy. For this thesis, drug candidates to be further experimentally evaluated were selected based on the criteria of novelty in SMA and oral bioavailability, due to the lack of non-invasive treatments approved at the time.

In chapters 4 and 5 we assessed the efficacy of our selected candidates using C2C12 myoblasts and *Smn*$^{2B/-}$ SMA mice. The two drugs selected were metformin, an AMPK agonist biguanide used primarily as a hypoglycaemic agent in T2DM [300,858,923,931] and oxandrolone, an anabolic steroid therapeutically used for muscle wasting and growth conditions [837]. Counterintuitively, metformin treatment did not improve disease phenotypes or survival and it had an inverse impact on its predicted gene target *Prkag3*. Furthermore, higher metformin doses actually reduced survival, which molecular analyses potentially attributed to the dysregulation of genes linked to mitochondrial activity in the spinal cord [145,146,862] and gluconeogenesis in the liver [348,349,923]. Consequently, these results led us to consider the possibility of adverse systemic side effects that could negatively

impact disease progression in *Smn*$^{2B/-}$ SMA mice and affect the suitability of metformin as a skeletal muscle therapy [926,927].

On the other hand, the data collected so far for oxandrolone presented a more promising outcome as *in vitro* treatment (1 µM for 24 hours) attenuated canonical atrophy in serum-starved C2C12 myotubes. Furthermore, phenotypic analyses revealed a significantly increased survival of 3 days in 4 mg/kg/day oxandrolone-treated *Smn*$^{2B/-}$ SMA mice. However, it still remains unclear if oxandrolone's ameliorative effects were attributed to its activity on the predicted gene targets.

Retrospectively, although our bioinformatics data have provided new evidence for how prednisolone impacts skeletal muscle in SMA, our computational predictions for metformin and oxandrolone to emulate these effects have not come to fruition in our experimental investigations. Upon reflection, the data in our thesis has showcased the importance of experimental validation for bioinformatic predictions and exposed the limitations of transcriptomics-based *in silico* drug repositioning that need to be taken into consideration for future SMA drug discovery studies.

6.2. Candidates for future SMA drug repositioning studies.

In the latter part of this thesis, we focused on the experimental validation of metformin and oxandrolone in SMA cellular and animal models. Although these drugs did not emulate prednisolone's ameliorative abilities in SMA muscle, they were not the only drug candidates identified by our bioinformatics and drug database analyses. Indeed, a total of 223 commercially approved compounds were identified. Even though most of these drugs did not pass the strict selection criteria, the pharmacological activity in specific compounds still make them interesting candidates for future SMA drug repositioning research.

6.2.1. Insulin

Intriguingly, the metabolic pathways in SMA skeletal muscle targeted by prednisolone led to the prediction of various DM-related drugs. One reoccurring candidate was insulin. Although pre-clinical studies have not associated insulin resistance with aberrant glucose metabolism in *Smn*$^{2B/-}$ SMA mice [301,310], an observational endocrine study across 63 mixed gender type 1-3 SMA patients linked insulin resistance with muscle atrophy severity [305,1012]. The association between muscle atrophy and insulin resistance is also reported in DM research with protein anabolism resistance being an early marker in the higher risk offspring of T2DM patients [1013]. Furthermore, a meta-analysis of insulin treatment across 69 independent investigations revealed a significantly increased net balance of skeletal muscle protein levels in insulin-treated patients [1014]. Although ongoing, in-depth studies have reported that insulin increases net skeletal muscle protein levels via minor involvement in MPS and major involvement in muscle

protein breakdown (MPB) [314,1014–1018]. Indeed, insulin has been found to reduce amino acid efflux and reverse atrogin-1 activity, suggesting that it acts on proteasomal degradation [314,1015–1017]. Intriguingly, this mechanism could make insulin therapy advantageous for SMA skeletal muscle since proteasomal degradation is a key pathway involved in its progressive atrophy [56]. However, similar to what we observed with metformin, hypoglycaemia could also be a risk factor with insulin treatment [1019]. Nevertheless, the dual role insulin could serve in management of glucose metabolism and protein anabolism could be beneficial for skeletal muscle health in SMA.

6.2.2. Thiazolidinediones

Another class of clinically approved DM drugs predicted in our list were the thiazolidinedione compounds pioglitazone and rosiglitazone, which are PPAR-γ) agonists [1020]. The PPAR isoforms (PPARα, PPARβ/δ and PPARγ) play crucial regulatory roles in skeletal muscle such as metabolism, development, regeneration and inflammation [1021]. Importantly for SMA, they also play a role in the inhibition of muscle-wasting and myosteatosis (fat infiltration) [1021]. Indeed, inhibition and activation studies of the thiazolidinediones' main target PPARγ highlight its anti-atrophy benefits [1022]. Furthermore, the activity of its co-activator PGC1-α is downregulated in SMA skeletal muscle, suggesting a potential use for these drugs as second-generation therapies in SMA [388,389]. In addition, pioglitazone and rosiglitazone treatment in related diseases characterised by muscle wasting such as cachexia [1023,1024], ALS [1025] and spinal and bulbar muscular atrophy (SBMA) [1026], have reported ameliorative benefits.

Nevertheless, pioglitazone and rosiglitazone come with possible adverse risks of potential liver failure [1027], as exampled by a summary of 21 reported cases from patients receiving these drugs in the US across 1997 – 2006 [1028]. In the context of SMA, such risks could be detrimental via exacerbation of the existing liver pathologies [343,348,464], thus any future pre-clinical repositioning studies of these drugs in SMA need to evaluate their effects on the liver alongside neuromuscular tissue.

6.2.3. Interleukin-6 receptor inhibitors

The primary use of prednisolone in certain diseases is for its function as an anti-inflammatory agent [625,626]. As such, within our predicted analyses we observed pathways associated with inflammation being targeted by prednisolone in SMA skeletal muscle. Consequently, these led to the *in silico* prediction of various anti-inflammatory drugs being potential candidates to emulate prednisolone's activity in SMA. Although celecoxib has already been investigated in SMA [614,615], another category of anti-inflammatory drugs identified were IL6R monoclonal antibody inhibitors. Clinically approved examples of these include tocilizumab and sarilumab, which are used primarily for the treatment of rheumatoid arthritis [769,1029–1031]. IL6 itself is a cytokine and myokine involved in inflammation, metabolism, myogenesis and growth in skeletal muscle [769,1032]. Paradoxically, studies have also linked IL6 to both hypertrophic and atrophic effects in skeletal muscle [1032–1034]. Nevertheless, pre-clinical disuse-induced muscle atrophy and dystrophin KO DMD rodent models have demonstrated that Il6r inhibition via monoclonal antibody treatment improved muscle health and growth [745,747].

Despite these aforementioned studies not being focused on denervation-induced muscle atrophy, independent investigations using muscle biopsies from symptomatic *SMNΔ7* SMA mice revealed an association between increased Il6 levels and denervation [1035]. Furthermore, our transcriptomics screen identified a significant downregulation of *Il6ra* expression in the prednisolone-treated *Smn*$^{-/-}$*;SMN2* SMA mice compared to their untreated counterparts, suggesting that Il6 activity could play a pro-atrophic role in this disease. However, compared to our previously investigated candidates, IL6R monoclonal antibody inhibitors are more invasively administered, with requirements for subcutaneous and intravenous injections [1030]. Regardless, clinically approved examples like tocilizumab could be interesting candidates for skeletal muscle therapy in SMA.

6.3. Future considerations

6.3.1. A multi-omics strategy is a suitable option for *in silico* drug repositioning in SMA

In our study, *in silico* drug repositioning was an appropriate choice for identifying clinically approved drugs predicted to emulate prednisolone's effects in SMA skeletal muscle. We analysed the transcriptomic patterns across skeletal muscle from prednisolone-treated and untreated *Smn*$^{-/-}$*;SMN2* SMA and *Smn*$^{+/-}$*;SMN2* healthy mice as it allowed for an unbiased identification of dysregulated genes and pathways [680,681]. However, as previously explained in chapter 3, reliance on this method alone comes with limitations. The main limitation being that transcript expression levels do not proportionally represent protein activity in terms of abundance and PTM [843–850]. Thus, this can be a caveat for drug repositioning studies in particular as most of the candidates' pharmacodynamics involve drug-protein target interactions.

In our study, this is exemplified by metformin. We originally selected metformin based on the iPathwayGuide prediction that this drug can also activate the AMPK protein in certain prednisolone-targeted pathways. However, the predicted AMPK protein activation in these pathways was actually derived from the significant upregulation of the *Prkag3* gene in our transcriptomic data. Although prior studies have shown that the AMPK- γ-3 isoform encoded by *Prkag3* is important for AMPK activation [832,889,890,924], the protein's activity is usually measured by phosphorylation of the Thr-172 residue in the catalytic AMPK-α isoform [300,832,1036]. Upon reflection, it seems that integration of proteomics would have been advantageous to validate if AMPK activity was normalised to healthy levels after

prednisolone treatment in SMA skeletal muscle. This could have then allowed for a better evaluation of the suitability of metformin for further investigations in SMA cellular and animal models.

Indeed, we recently published a study that supports the benefits of multi-omics (transcriptomics and proteomics) for *in silico* drug repositioning in SMA [716]. In that study, harmine was selected for experimental validation as it appeared across both transcriptomic and proteomic drug perturbation signature lists [716]. Importantly, harmine treatment in C2C12 myoblasts and both severe *Smn*$^{-/-}$*;SMN2* and milder *Smn*$^{2B/-}$ SMA mice matched its predicted molecular activities and significantly improved muscle phenotypes [716].

Although the addition of proteomics to our bioinformatics platform would have allowed for a more detailed pathway analysis and more accurate representation of the pharmacodynamics patterns of the predicted drugs [1037], it would still not be enough to bridge the gap between drug interaction and phenotype [1038]. Indeed, a proteomics analysis of the cerebral spinal fluid of Spinraza®-treated type 2 and 3 SMA patients reported that no correlation was found between protein profiles and functional score improvements [1039]. However, one more recent omics platform that could help overcome this limitation is metabolomics, which is a high-throughput study of total metabolites within a biological sample [1040,1041]. Unlike other omics technologies, metabolomics is advantageous in that metabolites can closely link a pathway's activity to a specific phenotype [1038,1040–1043]. In our case, this would be drug treatment and disease status, which could be particularly useful in SMA as the canonical phenotype of muscle atrophy can be characterised by the rise in protein breakdown [56,1044,1045]. Furthermore, studies in SMA muscle have used ROS and metabolite intermediates to support the

evidence of dysfunction in the mitochondria [388,395], as well as glucose [161] and FA [339,342] metabolic reactions.

Although proteomics and metabolomics both have their advantages in biological research as standalone approaches, they do not present a fully detailed signalling pathway [651,1046–1048]. Optimally, we would want to integrate both proteomics and metabolomics to our established transcriptomics data. In theory, it would fit the hierarchal expression and activity of transcript > protein > metabolite and could better ensure the reliable and accurate prediction of prednisolone-targeted pathways that improved the SMA skeletal muscle phenotype [1046–1048]. Although metabolomic data cannot be uploaded into iPathwayGuide in the same instance that transcriptomics and proteomics data can [654], there are still many multi-platform tools that can analyse it. These include Metaboanalyst [1049], Cytoscape [1050] and MetExplore [1051]. Although they are limited by their reliance on set enrichment patterns for specific pathways [1049–1052]. However, a recently developed tool called Metaboverse is useful in annotating interlinked transcriptomics, proteomics and metabolomics data onto pathway networks [1052]. Thus, Metaboverse could help complement our iPathwayGuide data by allowing us to visualise the downstream and neighbouring effects of our predicted drug targets across canonical pathways important in SMA pathology to develop a greater detailed picture of pathological effectors and potential therapeutic targets [654,1052].

Despite these potential advantages, a multi-omics approach that combined transcriptomics, proteomics and metabolomics has, to the best of our knowledge, so far not been used for *in silico* drug repositioning in SMA research. However, this method has been used in SMA biomarker research including the BforSMA

study that identified 200 biomarkers as interesting candidates for measuring disease progression [1053]. Furthermore, multi-omics studies that comprised all of these three platforms have been useful for the prediction of repositioned drug candidates in other diseases such as AD [1054], diabetes [1055], cancer [1056] and most recently COVID-19 [1057]. Indeed, some of these candidates have even moved onto the clinical trial phase, as most recently exampled with a phase 2 clinical trial currently in recruitment of using dasatinib, a tyrosine kinase inhibitor originally designed for managing leukaemia to treat moderate and severe COVID-19 [1057,1058] (ClinicalTrials.gov ID: NCT04830735).

Thus, the strategy of isolated omics experiments to address biological problems is an inefficient strategy to reliably identify drugs that could emulate the beneficial effects of prednisolone in SMA skeletal muscle. Instead, it would have been useful to use a combined integration of transcriptomics, proteomics and metabolomics data from the samples as a prerequisite for drug candidate selection before later investigations in cellular and animal models.

6.3.2. Adverse systemic effects need to be considered when investigating skeletal muscle therapies in SMA

Although we solely focused on the skeletal muscle as a therapeutic target for SMA in this project, there are two important points that should be considered for future muscle-specific therapy research. The first is that as previously explained in Chapter 1, SMA is a systemic disease that consists of pathologies in both neuromuscular and peripheral organs [77,150,151]. Although the latter is not the predominant pathology in most untreated patients, the enhanced life expectancy

and quality of life provided by the SMN-dependent treatment [451,452,470,472,490,493] (especially in the severe types), could see novel pathologies emerge in these organs. Furthermore, if pathologies were exacerbated or ameliorated tissue(s) rendered dysfunctional by second-generation therapies, this would negatively impact the maximal benefits imparted by the primary SMN-dependent treatment.

The second point is that skeletal muscle is a highly plastic tissue whose size, contractile strength and metabolism [277–282] is also governed by cross-talk with interacting cells and organs such as neurons [926], liver [927] and pancreas [928] to name a few. Thus, any adverse effects on these neighbouring tissues could have an indirect negative impact on skeletal muscle itself. One particular example are drugs that have the ability to cross the BBB. Recently, it was shown that conserved pathways such as autophagy are regulated in a tissue-dependent manner in SMA neuronal and muscle tissue [937]. For example, if an mTOR agonist with the ability to cross the BBB was chosen as a treatment option in SMA, it could promote hypertrophy of SMA skeletal muscle [851,852]. However, the exacerbation of the already active p-Ser2448 mTOR in SMA motor neurons could lead to adverse side effects such as hypersensitivity in patients [937,1059].

Such adverse systemic risks were indeed observed in our study. In chapter 4, we found that 400 mg/kg/day metformin treatment in *Smn*$^{2B/-}$ SMA mice significantly reduced their life expectancy, exacerbated hypoglycaemia and dysregulated mitochondrial targets in the spinal cord. Oxandrolone, our second drug candidate, could also lead to long-term adverse effects such as prostate cancer development via its *Ar* agonist ability [837,1060]. Other independent investigations of second-generation therapies for SMA have also noted adverse risks. These include the emergence of tremors in harmine-treated *Smn*$^{2B/-}$ SMA mice [716] and

increased risks of cancer in *SMNΔ7* SMA mice when the PTEN tumour suppressor gene was depleted via a scAAV6-shRNA [1061].

One approach that could be used to overcome this issue is the use of meta-analysis across the transcriptomics data obtained from skeletal muscle and key interacting tissue types. Retrospectively, in our study, we could have also performed transcriptomics in the liver and spinal cord of prednisolone-treated and untreated *Smn*$^{-/-}$*;SMN2* SMA and *Smn*$^{+/-}$*;SMN2* healthy pups. Importantly, iPathwayGuide possessed a meta-analysis feature that would have allowed us to cross-examine these separate tissues for prednisolone-impacted pathways [654,1062]. In theory, the meta-analysis would have allowed us to select drugs that appeared beneficial across all tissue types and targeted similar genes and pathways as prednisolone [654,1062]. Thus, we would have had a predicted drug and pathway dataset across skeletal muscle and the tissues with which it interacts. Literature searches and preliminary experimentation would have then allowed us to predict drugs with minimal adverse side effects in non-muscle tissue in SMA mice. Interestingly, this approach has recently been useful to predict methylprednisolone as a treatment option for COVID-19 infected patients, which showcases its potential for *in silico* drug repositioning research [1062].

In summary, *in silico* drug repositioning for skeletal muscle therapies in SMA should also implement the omics data from interacting tissues that are crucial for its regulation via reciprocal crosstalk. Not only would this predict drugs with minimised adverse effects, but it could also potentially maximise the benefits of treatment in SMA skeletal muscle both directly and indirectly if successful.

6.4. Conclusion

The optimum treatment strategy for SMA most likely requires a combination of first-generation SMN-dependent and second-generation SMN-independent therapies. Skeletal muscle is an important target for second-generation therapies since SMN restoration is currently not a cure and pre-clinical studies have shown that systemic administration of SMN restoration treatment is more effective compared to CNS delivery alone [350]. Although two novel muscle-specific therapies are currently in clinical trial, the limitations of prolonged developmental timeline, expensive costs, safety risks and unknown longitudinal effects, makes drug repositioning a useful complementary approach or alternative [584–586]. We have previously shown that SMA mice treated with the GC prednisolone demonstrated improved muscle health and survival [53]. However, the adverse effects of chronic GC treatment limit prednisolone's long-term use in SMA [628].

In this thesis, we thus used transcriptomics-based *in silico* drug repositioning followed by experimental validation to evaluate if any clinically approved, non-invasive drugs could emulate prednisolone's benefits in SMA skeletal muscle. Interestingly, our bioinformatics data presented a wide array of prednisolone-targeted pathways linked to skeletal muscle functions and hundreds of interesting drugs for future repositioning studies. However, experimentally, metformin and oxandrolone's activity in SMA cellular and animal models were not able to emulate prednisolone's to the same effect. Nevertheless, our work highlighted the importance of experimental validation for bioinformatics and called attention to the importance of multi-omics and systemic effects for possible future *in silico* studies. Overall, our thesis shows that with refinement an *in silico* drug

repositioning strategy is a useful alternative to discover novel less expensive second-generation therapies for SMA skeletal muscle.

References

1. Kolb, S. J. & Kissel, J. T. Spinal Muscular Atrophy. *Neurologic Clinics* **33**, 831–846 (2015).
2. Ling, K. K. Y., Gibbs, R. M., Feng, Z. & Ko, C.-P. Severe neuromuscular denervation of clinically relevant muscles in a mouse model of spinal muscular atrophy. *Hum. Mol. Genet.* **21**, 185–195 (2012).
3. De Sanctis, R. *et al.* Clinical phenotypes and trajectories of disease progression in type 1 spinal muscular atrophy. *Neuromuscular Disorders* **28**, 24–28 (2018).
4. Munsat, T. L. & Davies, K. E. International SMA consortium meeting. (26-28 June 1992, Bonn, Germany). *Neuromuscul Disord* **2**, 423–428 (1992).
5. Dubowitz, V. Very severe spinal muscular atrophy (SMA type 0): an expanding clinical phenotype. *Eur. J. Paediatr. Neurol.* **3**, 49–51 (1999).
6. Al Dakhoul, S. Very severe spinal muscular atrophy (Type 0). *Avicenna J Med* **7**, 32–33 (2017).
7. Audic, F. & Barnerias, C. Spinal muscular atrophy (SMA) type I (Werdnig-Hoffmann disease). *Arch Pediatr* **27**, 7S15-17S17 (2020).
8. Finkel, R. S. *et al.* Observational study of spinal muscular atrophy type I and implications for clinical trials. *Neurology* **83**, 810–817 (2014).
9. Finkel, R. S., Weiner, D. J., Mayer, O. H., McDonough, J. M. & Panitch, H. B. Respiratory muscle function in infants with spinal muscular atrophy type I. *Pediatr. Pulmonol.* **49**, 1234–1242 (2014).
10. Cancès, C., Richelme, C., Barnerias, C. & Espil, C. Clinical features of spinal muscular atrophy (SMA) type 2. *Arch Pediatr* **27**, 7S18-17S22 (2020).
11. Wijngaarde, C. A. *et al.* Population-based analysis of survival in spinal muscular atrophy. *Neurology* **94**, e1634–e1644 (2020).
12. Wijngaarde, C. A. *et al.* Natural history of lung function in spinal muscular atrophy. *Orphanet Journal of Rare Diseases* **15**, 88 (2020).

13. Salort-Campana, E. & Quijano-Roy, S. Clinical features of spinal muscular atrophy (SMA) type 3 (Kugelberg-Welander disease). *Archives de Pédiatrie* **27**, 7S23-7S28 (2020).
14. Zerres, K. *et al.* A collaborative study on the natural history of childhood and juvenile onset proximal spinal muscular atrophy (type II and III SMA): 569 patients. *J. Neurol. Sci.* **146**, 67–72 (1997).
15. Piepers, S. *et al.* A natural history study of late onset spinal muscular atrophy types 3b and 4. *J. Neurol.* **255**, 1400–1404 (2008).
16. Sugarman, E. A. *et al.* Pan-ethnic carrier screening and prenatal diagnosis for spinal muscular atrophy: clinical laboratory analysis of >72 400 specimens. *Eur J Hum Genet* **20**, 27–32 (2012).
17. Hendrickson, B. C. *et al.* Differences in SMN1 allele frequencies among ethnic groups within North America. *Journal of Medical Genetics* **46**, 641–644 (2009).
18. Prior, T. W. *et al.* Newborn and carrier screening for spinal muscular atrophy. *American Journal of Medical Genetics Part A* **152A**, 1608–1616 (2010).
19. Kay, D. M. *et al.* Implementation of population-based newborn screening reveals low incidence of spinal muscular atrophy. *Genet Med* **22**, 1296–1302 (2020).
20. Brzustowicz, L. M. *et al.* Genetic mapping of chronic childhood-onset spinal muscular atrophy to chromosome 5q11.2-13.3. *Nature* **344**, 540–541 (1990).
21. Lefebvre, S. *et al.* Identification and characterization of a spinal muscular atrophy-determining gene. *Cell* **80**, 155–165 (1995).
22. Rodrigues, N. R. *et al.* Deletions in the survival motor neuron gene on 5q13 in autosomal recessive spinal muscular atrophy. *Human Molecular Genetics* **4**, 631–634 (1995).
23. Bowen, B. M. *et al.* SMA Identified: Clinical and Molecular Findings From a Sponsored Testing Program for Spinal Muscular Atrophy in More Than 2,000 Individuals. *Front Neurol* **12**, 663911 (2021).

24. Sun, Y. *et al.* Molecular and functional analysis of intragenic SMN1 mutations in patients with spinal muscular atrophy. *Human Mutation* **25**, 64–71 (2005).
25. Melki, J. *et al.* De novo and inherited deletions of the 5q13 region in spinal muscular atrophies. *Science* **264**, 1474–1477 (1994).
26. Prior, T. W., Swoboda, K. J., Scott, H. D. & Hejmanowski, A. Q. Homozygous SMN1 Deletions in Unaffected Family Members and Modification of the Phenotype by SMN2. *Am J Med Genet A* **0**, 307–310 (2004).
27. Wirth, B. *et al.* De novo rearrangements found in 2% of index patients with spinal muscular atrophy: mutational mechanisms, parental origin, mutation rate, and implications for genetic counseling. *Am J Hum Genet* **61**, 1102–1111 (1997).
28. Edens, B. M., Ajroud-Driss, S., Ma, L. & Ma, Y.-C. Molecular mechanisms and animal models of spinal muscular atrophy. *Biochimica et Biophysica Acta (BBA) - Molecular Basis of Disease* **1852**, 685–692 (2015).
29. Rochette, C. F., Gilbert, N. & Simard, L. R. SMN gene duplication and the emergence of the SMN2 gene occurred in distinct hominids: SMN2 is unique to Homo sapiens. *Hum Genet* **108**, 255–266 (2001).
30. Bürglen, L. *et al.* Structure and Organization of the Human Survival Motor Neurone (SMN) Gene. *Genomics* **32**, 479–482 (1996).
31. Lorson, C. L., Hahnen, E., Androphy, E. J. & Wirth, B. A single nucleotide in the SMN gene regulates splicing and is responsible for spinal muscular atrophy. *Proc Natl Acad Sci U S A* **96**, 6307–6311 (1999).
32. Monani, U. R. A single nucleotide difference that alters splicing patterns distinguishes the SMA gene SMN1 from the copy gene SMN2. *Human Molecular Genetics* **8**, 1177–1183 (1999).

33. Cartegni, L., Hastings, M. L., Calarco, J. A., de Stanchina, E. & Krainer, A. R. Determinants of Exon 7 Splicing in the Spinal Muscular Atrophy Genes, SMN1 and SMN2. *The American Journal of Human Genetics* **78**, 63–77 (2006).
34. Cartegni, L. & Krainer, A. R. Disruption of an SF2/ASF-dependent exonic splicing enhancer in SMN2 causes spinal muscular atrophy in the absence of SMN1. *Nature Genetics* **30**, 377–384 (2002).
35. Kashima, T. & Manley, J. L. A negative element in SMN2 exon 7 inhibits splicing in spinal muscular atrophy. *Nature Genetics* **34**, 460–463 (2003).
36. DiDonato, C. J. *et al.* Cloning, characterization, and copy number of the murine survival motor neuron gene: homolog of the spinal muscular atrophy-determining gene. *Genome Res* **7**, 339–352 (1997).
37. Schrank, B. *et al.* Inactivation of the survival motor neuron gene, a candidate gene for human spinal muscular atrophy, leads to massive cell death in early mouse embryos. *Proc Natl Acad Sci U S A* **94**, 9920–9925 (1997).
38. Hsieh-Li, H. M. *et al.* A mouse model for spinal muscular atrophy. *Nature Genetics* **24**, 66–70 (2000).
39. Michaud, M. *et al.* Neuromuscular defects and breathing disorders in a new mouse model of spinal muscular atrophy. *Neurobiol Dis* **38**, 125–135 (2010).
40. Monani, U. R. *et al.* The human centromeric survival motor neuron gene (SMN2) rescues embryonic lethality in Smn–/– mice and results in a mouse with spinal muscular atrophy. *Human Molecular Genetics* **9**, 333–339 (2000).
41. Harada, Y. *et al.* Correlation between SMN2 copy number and clinical phenotype of spinal muscular atrophy: three SMN2 copies fail to rescue some patients from the disease severity. *J Neurol* **249**, 1211–1219 (2002).
42. Feldkötter, M., Schwarzer, V., Wirth, R., Wienker, T. F. & Wirth, B. Quantitative Analyses of SMN1 and SMN2 Based on Real-Time LightCycler PCR: Fast and Highly Reliable Carrier

Testing and Prediction of Severity of Spinal Muscular Atrophy. *The American Journal of Human Genetics* **70**, 358–368 (2002).

43. Wirth, B. *et al.* Mildly affected patients with spinal muscular atrophy are partially protected by an increased SMN2 copy number. *Hum Genet* **119**, 422–428 (2006).
44. Butchbach, M. E. R. Copy Number Variations in the Survival Motor Neuron Genes: Implications for Spinal Muscular Atrophy and Other Neurodegenerative Diseases. *Front Mol Biosci* **3**, (2016).
45. Burghes, A. H. When is a deletion not a deletion? When it is converted. *Am J Hum Genet* **61**, 9–15 (1997).
46. Hao, L. T., Burghes, A. H. & Beattie, C. E. Generation and Characterization of a genetic zebrafish model of SMA carrying the human SMN2 gene. *Molecular Neurodegeneration* **6**, 24 (2011).
47. Chan, Y. B. *et al.* Neuromuscular defects in a Drosophila survival motor neuron gene mutant. *Hum Mol Genet* **12**, 1367–1376 (2003).
48. Ymlahi-Ouazzani, Q. *et al.* Reduced levels of survival motor neuron protein leads to aberrant motoneuron growth in a Xenopus model of muscular atrophy. *Neurogenetics* **11**, 27–40 (2010).
49. Miguel-Aliaga, I. *et al.* The Caenorhabditis Elegans Orthologue of the Human Gene Responsible for Spinal Muscular Atrophy Is a Maternal Product Critical for Germline Maturation and Embryonic Viability. *Human Molecular Genetics* **8**, 2133–2143 (1999).
50. Le, T. T. *et al.* SMNDelta7, the major product of the centromeric survival motor neuron (SMN2) gene, extends survival in mice with spinal muscular atrophy and associates with full-length SMN. *Hum Mol Genet* **14**, 845–857 (2005).
51. Riessland, M. *et al.* SAHA ameliorates the SMA phenotype in two mouse models for spinal muscular atrophy. *Hum Mol Genet* **19**, 1492–1506 (2010).

52. Lin, T.-L. *et al.* Selective Neuromuscular Denervation in Taiwanese Severe SMA Mouse Can Be Reversed by Morpholino Antisense Oligonucleotides. *PLoS ONE* **11**, e0154723 (2016).
53. Walter, L. M. *et al.* Interventions Targeting Glucocorticoid-Krüppel-like Factor 15-Branched-Chain Amino Acid Signaling Improve Disease Phenotypes in Spinal Muscular Atrophy Mice. *EBioMedicine* **31**, 226–242 (2018).
54. Boyer, J. G. *et al.* Myogenic program dysregulation is contributory to disease pathogenesis in spinal muscular atrophy. *Hum. Mol. Genet.* **23**, 4249–4259 (2014).
55. Boyer, J. G. *et al.* Early onset muscle weakness and disruption of muscle proteins in mouse models of spinal muscular atrophy. *Skeletal Muscle* **3**, 24 (2013).
56. Deguise, M.-O. *et al.* Differential induction of muscle atrophy pathways in two mouse models of spinal muscular atrophy. *Sci Rep* **6**, 28846 (2016).
57. Bowerman, M., Murray, L. M., Beauvais, A., Pinheiro, B. & Kothary, R. A critical smn threshold in mice dictates onset of an intermediate spinal muscular atrophy phenotype associated with a distinct neuromuscular junction pathology. *Neuromuscul. Disord.* **22**, 263–276 (2012).
58. Hammond, S. M. *et al.* Mouse Survival Motor Neuron Alleles That Mimic SMN2 Splicing and Are Inducible Rescue Embryonic Lethality Early in Development but Not Late. *PLoS ONE* **5**, (2010).
59. Eshraghi, M., McFall, E., Gibeault, S. & Kothary, R. Effect of genetic background on the phenotype of the Smn2B/- mouse model of spinal muscular atrophy. *Hum Mol Genet* **25**, 4494–4506 (2016).
60. Osborne, M. *et al.* Characterization of behavioral and neuromuscular junction phenotypes in a novel allelic series of SMA mouse models. *Human Molecular Genetics* **21**, 4431–4447 (2012).
61. Deguise, M.-O. *et al.* Motor transmission defects with sex differences in a new mouse model of mild spinal muscular atrophy. *EBioMedicine* **55**, (2020).

62. Coovert, D. D. *et al.* The Survival Motor Neuron Protein in Spinal Muscular Atrophy. *Human Molecular Genetics* **6**, 1205–1214 (1997).
63. Stump, A. D., Dillon-White, M. & Gu, S. Molecular evolution of the moonlighting protein SMN in metazoans. *Comp Biochem Physiol Part D Genomics Proteomics* **8**, 220–230 (2013).
64. Bertrandy, S. *et al.* The RNA-binding properties of SMN: deletion analysis of the zebrafish orthologue defines domains conserved in evolution. *Hum Mol Genet* **8**, 775–782 (1999).
65. Singh, R. N., Howell, M. D., Ottesen, E. W. & Singh, N. N. Diverse role of survival motor neuron protein. *Biochim Biophys Acta Gene Regul Mech* **1860**, 299–315 (2017).
66. Lorson, C. L. & Androphy, E. J. The domain encoded by exon 2 of the survival motor neuron protein mediates nucleic acid binding. *Hum Mol Genet* **7**, 1269–1275 (1998).
67. Côté, J. & Richard, S. Tudor Domains Bind Symmetrical Dimethylated Arginines *. *Journal of Biological Chemistry* **280**, 28476–28483 (2005).
68. Shafey, D., Boyer, J. G., Bhanot, K. & Kothary, R. Identification of Novel Interacting Protein Partners of SMN Using Tandem Affinity Purification. *J. Proteome Res.* **9**, 1659–1669 (2010).
69. Giesemann, T. *et al.* A Role for Polyproline Motifs in the Spinal Muscular Atrophy Protein SMN: PROFILINS BIND TO AND COLOCALIZE WITH SMN IN NUCLEAR GEMS *. *Journal of Biological Chemistry* **274**, 37908–37914 (1999).
70. Paushkin, S. *et al.* The survival motor neuron protein of Schizosacharomyces pombe. Conservation of survival motor neuron interaction domains in divergent organisms. *J Biol Chem* **275**, 23841–23846 (2000).
71. Seo, J., Singh, N. N., Ottesen, E. W., Lee, B. M. & Singh, R. N. A novel human-specific splice isoform alters the critical C-terminus of Survival Motor Neuron protein. *Sci Rep* **6**, 30778 (2016).
72. Martin, R., Gupta, K., Ninan, N. S., Perry, K. & Van Duyne, G. D. The Survival Motor Neuron protein forms soluble glycine zipper oligomers. *Structure* **20**, 1929–1939 (2012).

73. Gray, K. M. *et al.* Self-oligomerization regulates stability of survival motor neuron protein isoforms by sequestering an SCFSlmb degron. *Mol Biol Cell* **29**, 96–110 (2018).
74. Young, P. J. *et al.* The exon 2b region of the spinal muscular atrophy protein, SMN, is involved in self-association and SIP1 binding. *Human Molecular Genetics* **9**, 2869–2877 (2000).
75. Cho, S. & Dreyfuss, G. A degron created by SMN2 exon 7 skipping is a principal contributor to spinal muscular atrophy severity. *Genes Dev* **24**, 438–442 (2010).
76. Battaglia, G., Princivalle, A., Forti, F., Lizier, C. & Zeviani, M. Expression of the SMN gene, the spinal muscular atrophy determining gene, in the mammalian central nervous system. *Hum Mol Genet* **6**, 1961–1971 (1997).
77. Groen, E. J. N. *et al.* Temporal and tissue-specific variability of SMN protein levels in mouse models of spinal muscular atrophy. *Human Molecular Genetics* **27**, 2851–2862 (2018).
78. Navascues, J., Berciano, M. T., Lafarga, M., Tucker, K. E. & Matera, A. G. Targeting SMN to Cajal bodies and nuclear gems during neuritogenesis. *Chromosoma* **112**, 398–409 (2004).
79. Massenet, S., Pellizzoni, L., Paushkin, S., Mattaj, I. W. & Dreyfuss, G. The SMN complex is associated with snRNPs throughout their cytoplasmic assembly pathway. *Mol Cell Biol* **22**, 6533–6541 (2002).
80. Young, P. J., Le, T. T., thi Man, N., Burghes, A. H. & Morris, G. E. The relationship between SMN, the spinal muscular atrophy protein, and nuclear coiled bodies in differentiated tissues and cultured cells. *Exp Cell Res* **256**, 365–374 (2000).
81. Battle, D. J. *et al.* The SMN Complex: An Assembly Machine for RNPs. *Cold Spring Harbor Symposia on Quantitative Biology* **71**, 313–320 (2006).
82. Feng, W. *et al.* Gemins modulate the expression and activity of the SMN complex. *Human Molecular Genetics* **14**, 1605–1611 (2005).
83. Liu, Q. & Dreyfuss, G. A novel nuclear structure containing the survival of motor neurons protein. *EMBO J* **15**, 3555–3565 (1996).

84. Liu, J.-L. & Gall, J. G. U bodies are cytoplasmic structures that contain uridine-rich small nuclear ribonucleoproteins and associate with P bodies. *Proc Natl Acad Sci U S A* **104**, 11655–11659 (2007).

85. Bühler, D., Raker, V., Lührmann, R. & Fischer, U. Essential role for the tudor domain of SMN in spliceosomal U snRNP assembly: implications for spinal muscular atrophy. *Hum Mol Genet* **8**, 2351–2357 (1999).

86. Fischer, U., Liu, Q. & Dreyfuss, G. The SMN-SIP1 complex has an essential role in spliceosomal snRNP biogenesis. *Cell* **90**, 1023–1029 (1997).

87. Fischer, U., Sumpter, V., Sekine, M., Satoh, T. & Lührmann, R. Nucleo-cytoplasmic transport of U snRNPs: definition of a nuclear location signal in the Sm core domain that binds a transport receptor independently of the m3G cap. *EMBO J* **12**, 573–583 (1993).

88. Friesen, W. J. & Dreyfuss, G. Specific sequences of the Sm and Sm-like (Lsm) proteins mediate their interaction with the spinal muscular atrophy disease gene product (SMN). *J Biol Chem* **275**, 26370–26375 (2000).

89. Friesen, W. J., Massenet, S., Paushkin, S., Wyce, A. & Dreyfuss, G. SMN, the product of the spinal muscular atrophy gene, binds preferentially to dimethylarginine-containing protein targets. *Mol Cell* **7**, 1111–1117 (2001).

90. Huo, Q. *et al.* Splicing changes in SMA mouse motoneurons and SMN-depleted neuroblastoma cells: Evidence for involvement of splicing regulatory proteins. *RNA Biology* **11**, 1430–1446 (2014).

91. Li, D. K., Tisdale, S., Lotti, F. & Pellizzoni, L. SMN control of RNP assembly: From post-transcriptional gene regulation to motor neuron disease. *Seminars in Cell & Developmental Biology* **32**, 22–29 (2014).

92. Pellizzoni, L., Kataoka, N., Charroux, B. & Dreyfuss, G. A novel function for SMN, the spinal muscular atrophy disease gene product, in pre-mRNA splicing. *Cell* **95**, 615–624 (1998).

93. Custer, S. K. *et al.* Altered mRNA Splicing in SMN-Depleted Motor Neuron-Like Cells. *PLoS One* **11**, (2016).

94. Doktor, T. K. *et al.* RNA-sequencing of a mouse-model of spinal muscular atrophy reveals tissue-wide changes in splicing of U12-dependent introns. *Nucleic Acids Res.* **45**, 395–416 (2017).

95. Fuller, H. & Morris, G. SMN complexes of nucleus and cytoplasm: A proteomic study for SMA therapy. *Translational Neuroscience* **1**, 261–267 (2010).

96. Fuller, H. R. *et al.* The SMN Interactome Includes Myb-Binding Protein 1a. *J. Proteome Res.* **9**, 556–563 (2010).

97. Boyer, J. G., Bowerman, M. & Kothary, R. The many faces of SMN: deciphering the function critical to spinal muscular atrophy pathogenesis. *Future Neurology* **5**, 873–890 (2010).

98. Bowerman, M. *et al.* SMN, profilin IIa and plastin 3: a link between the deregulation of actin dynamics and SMA pathogenesis. *Mol Cell Neurosci* **42**, 66–74 (2009).

99. Zhao, D. Y. *et al.* SMN and symmetric arginine dimethylation of RNA polymerase II C-terminal domain control termination. *Nature* **529**, 48–53 (2016).

100. Jones, K. W. *et al.* Direct interaction of the spinal muscular atrophy disease protein SMN with the small nucleolar RNA-associated protein fibrillarin. *J Biol Chem* **276**, 38645–38651 (2001).

101. Bachand, F., Boisvert, F.-M., Côté, J., Richard, S. & Autexier, C. The product of the survival of motor neuron (SMN) gene is a human telomerase-associated protein. *Mol Biol Cell* **13**, 3192–3202 (2002).

102. Tisdale, S. *et al.* SMN is essential for the biogenesis of U7 small nuclear ribonucleoprotein and 3'-end formation of histone mRNAs. *Cell Rep* **5**, 1187–1195 (2013).

103. Fallini, C., Donlin-Asp, P. G., Rouanet, J. P., Bassell, G. J. & Rossoll, W. Deficiency of the Survival of Motor Neuron Protein Impairs mRNA Localization and Local Translation in the Growth Cone of Motor Neurons. *J Neurosci* **36**, 3811–3820 (2016).

104. Takizawa, Y. *et al.* GEMIN2 promotes accumulation of RAD51 at double-strand breaks in homologous recombination. *Nucleic Acids Res* **38**, 5059–5074 (2010).

105. Ottesen, E. W. *et al.* Severe impairment of male reproductive organ development in a low SMN expressing mouse model of spinal muscular atrophy. *Sci Rep* **6**, 20193 (2016).

106. Fayzullina, S. & Martin, L. J. DNA Damage Response and DNA Repair in Skeletal Myocytes From a Mouse Model of Spinal Muscular Atrophy. *J Neuropathol Exp Neurol* **75**, 889–902 (2016).

107. Fayzullina, S. & Martin, L. J. Skeletal Muscle DNA Damage Precedes Spinal Motor Neuron DNA Damage in a Mouse Model of Spinal Muscular Atrophy (SMA). *PLoS One* **9**, (2014).

108. Chaytow, H., Huang, Y.-T., Gillingwater, T. H. & Faller, K. M. E. The role of survival motor neuron protein (SMN) in protein homeostasis. *Cell Mol Life Sci* **75**, 3877–3894 (2018).

109. Sanchez, G. *et al.* A novel function for the survival motoneuron protein as a translational regulator. *Hum Mol Genet* **22**, 668–684 (2013).

110. Garcera, A., Bahi, N., Periyakaruppiah, A., Arumugam, S. & Soler, R. M. Survival motor neuron protein reduction deregulates autophagy in spinal cord motoneurons in vitro. *Cell Death Dis* **4**, e686 (2013).

111. Piras, A. *et al.* Inhibition of autophagy delays motoneuron degeneration and extends lifespan in a mouse model of spinal muscular atrophy. *Cell Death Dis* **8**, 3223 (2017).

112. Han, K.-J. *et al.* Ubiquitin-specific protease 9x deubiquitinates and stabilizes the spinal muscular atrophy protein-survival motor neuron. *J Biol Chem* **287**, 43741–43752 (2012).

113. Ramser, J. *et al.* Rare missense and synonymous variants in UBE1 are associated with X-linked infantile spinal muscular atrophy. *Am J Hum Genet* **82**, 188–193 (2008).

114. Wishart, T. M. *et al.* Dysregulation of ubiquitin homeostasis and β-catenin signaling promote spinal muscular atrophy. *J Clin Invest* **124**, 1821–1834 (2014).

115. Powis, R. A. *et al.* Systemic restoration of UBA1 ameliorates disease in spinal muscular atrophy. *JCI Insight* **1**, e87908 (2016).

116. Nölle, A. *et al.* The spinal muscular atrophy disease protein SMN is linked to the Rho-kinase pathway via profilin. *Hum. Mol. Genet.* **20**, 4865–4878 (2011).

117. Bowerman, M., Beauvais, A., Anderson, C. L. & Kothary, R. Rho-kinase inactivation prolongs survival of an intermediate SMA mouse model. *Hum Mol Genet* **19**, 1468–1478 (2010).

118. Rossoll, W. *et al.* Smn, the spinal muscular atrophy–determining gene product, modulates axon growth and localization of β-actin mRNA in growth cones of motoneurons. *The Journal of Cell Biology* **163**, 801–812 (2003).

119. Dimitriadi, M. *et al.* Decreased function of survival motor neuron protein impairs endocytic pathways. *Proc Natl Acad Sci U S A* **113**, E4377-4386 (2016).

120. Setola, V. *et al.* Axonal-SMN (a-SMN), a protein isoform of the survival motor neuron gene, is specifically involved in axonogenesis. *Proc Natl Acad Sci U S A* **104**, 1959–1964 (2007).

121. Soler-Botija, C. *et al.* Implication of Fetal SMN2 Expression in Type I SMA Pathogenesis: Protection or Pathological Gain of Function? *Journal of Neuropathology & Experimental Neurology* **64**, 215–223 (2005).

122. Zhang, H. *et al.* Multiprotein complexes of the survival of motor neuron protein SMN with Gemins traffic to neuronal processes and growth cones of motor neurons. *J. Neurosci.* **26**, 8622–8632 (2006).

123. Fan, L. & Simard, L. R. Survival motor neuron (SMN) protein: role in neurite outgrowth and neuromuscular maturation during neuronal differentiation and development. *Hum Mol Genet* **11**, 1605–1614 (2002).

124. Moradi, M. *et al.* Differential roles of α-, β-, and γ-actin in axon growth and collateral branch formation in motoneurons. *J Cell Biol* **216**, 793–814 (2017).

125. Nelson, J. C., Stavoe, A. K. H. & Colón-Ramos, D. A. The actin cytoskeleton in presynaptic assembly. *Cell Adh Migr* **7**, 379–387 (2013).

126. Chenouard, N., Xuan, F. & Tsien, R. W. Synaptic vesicle traffic is supported by transient actin filaments and regulated by PKA and NO. *Nature Communications* **11**, 5318 (2020).

127. van Bergeijk, J., Rydel-Könecke, K., Grothe, C. & Claus, P. The spinal muscular atrophy gene product regulates neurite outgrowth: importance of the C terminus. *FASEB J* **21**, 1492–1502 (2007).

128. Ebert, A. D. *et al.* Induced pluripotent stem cells from a spinal muscular atrophy patient. *Nature* **457**, 277–280 (2009).

129. Fulceri, F. *et al.* Ultrastructural characterization of peripheral denervation in a mouse model of Type III spinal muscular atrophy. *J Neural Transm (Vienna)* (2021) doi:10.1007/s00702-021-02353-9.

130. Mourelatos, Z., Abel, L., Yong, J., Kataoka, N. & Dreyfuss, G. SMN interacts with a novel family of hnRNP and spliceosomal proteins. *EMBO J* **20**, 5443–5452 (2001).

131. Glinka, M. *et al.* The heterogeneous nuclear ribonucleoprotein-R is necessary for axonal beta-actin mRNA translocation in spinal motor neurons. *Hum Mol Genet* **19**, 1951–1966 (2010).

132. Bunnell, T. M., Burbach, B. J., Shimizu, Y. & Ervasti, J. M. β-Actin specifically controls cell growth, migration, and the G-actin pool. *MBoC* **22**, 4047–4058 (2011).

133. Hensel, N. & Claus, P. The Actin Cytoskeleton in SMA and ALS: How Does It Contribute to Motoneuron Degeneration? *Neuroscientist* **24**, 54–72 (2018).

134. Walter, L. M. *et al.* Profilin2a-phosphorylation as a regulatory mechanism for actin dynamics. *The FASEB Journal* **34**, 2147–2160 (2020).

135. Amano, M., Nakayama, M. & Kaibuchi, K. Rho-Kinase/ROCK: A Key Regulator of the Cytoskeleton and Cell Polarity. *Cytoskeleton (Hoboken)* **67**, 545–554 (2010).

136. Bowerman, M., Shafey, D. & Kothary, R. Smn depletion alters profilin II expression and leads to upregulation of the RhoA/ROCK pathway and defects in neuronal integrity. *J Mol Neurosci* **32**, 120–131 (2007).

137. Walter, L. M., Rademacher, S., Pich, A. & Claus, P. Profilin2 regulates actin rod assembly in neuronal cells. *Scientific Reports* **11**, 10287 (2021).

138. Bowerman, M., Murray, L. M., Boyer, J. G., Anderson, C. L. & Kothary, R. Fasudil improves survival and promotes skeletal muscle development in a mouse model of spinal muscular atrophy. *BMC Med* **10**, 24 (2012).

139. Oprea, G. E. *et al.* Plastin 3 Is a Protective Modifier of Autosomal Recessive Spinal Muscular Atrophy. *Science* **320**, 524–527 (2008).

140. Shinomiya, H. Plastin Family of Actin-Bundling Proteins: Its Functions in Leukocytes, Neurons, Intestines, and Cancer. *International Journal of Cell Biology* **2012**, e213492 (2012).

141. Ackermann, B. *et al.* Plastin 3 ameliorates spinal muscular atrophy via delayed axon pruning and improves neuromuscular junction functionality. *Hum Mol Genet* **22**, 1328–1347 (2013).

142. Alrafiah, A. *et al.* Plastin 3 Promotes Motor Neuron Axonal Growth and Extends Survival in a Mouse Model of Spinal Muscular Atrophy. *Molecular Therapy - Methods & Clinical Development* **9**, 81–89 (2018).

143. Sareen, D. *et al.* Inhibition of Apoptosis Blocks Human Motor Neuron Cell Death in a Stem Cell Model of Spinal Muscular Atrophy. *PLoS One* **7**, (2012).

144. Parker, G. C. *et al.* Survival motor neuron protein regulates apoptosis in an in vitro model of spinal muscular atrophy. *Neurotox Res* **13**, 39–48 (2008).

145. Miller, N., Shi, H., Zelikovich, A. S. & Ma, Y.-C. Motor neuron mitochondrial dysfunction in spinal muscular atrophy. *Hum. Mol. Genet.* **25**, 3395–3406 (2016).

146. Thelen, M. P., Wirth, B. & Kye, M. J. Mitochondrial defects in the respiratory complex I contribute to impaired translational initiation via ROS and energy homeostasis in SMA motor neurons. *Acta Neuropathologica Communications* **8**, 223 (2020).

147. Siracusa, R., Fusco, R. & Cuzzocrea, S. Astrocytes: Role and Functions in Brain Pathologies. *Front. Pharmacol.* **0**, (2019).

148. Martin, J. E. *et al.* Decreased Motor Neuron Support by SMA Astrocytes due to Diminished MCP1 Secretion. *J Neurosci* **37**, 5309–5318 (2017).

149. Patitucci, T. N. & Ebert, A. D. SMN deficiency does not induce oxidative stress in SMA iPSC-derived astrocytes or motor neurons. *Hum Mol Genet* **25**, 514–523 (2016).

150. Nash, L. A., Burns, J. K., Chardon, J. W., Kothary, R. & Parks, R. J. Spinal Muscular Atrophy: More than a Disease of Motor Neurons? *Curr Mol Med* **16**, 779–792 (2016).

151. Shababi, M., Lorson, C. L. & Rudnik-Schöneborn, S. S. Spinal muscular atrophy: a motor neuron disorder or a multi-organ disease? *J Anat* **224**, 15–28 (2014).

152. Swoboda, K. J. *et al.* Natural history of denervation in SMA: relation to age, SMN2 copy number, and function. *Ann Neurol* **57**, 704–712 (2005).

153. Powis, R. A. & Gillingwater, T. H. Selective loss of alpha motor neurons with sparing of gamma motor neurons and spinal cord cholinergic neurons in a mouse model of spinal muscular atrophy. *J Anat* **228**, 443–451 (2016).

154. Farrar, M. A., Vucic, S., Johnston, H. M., du Sart, D. & Kiernan, M. C. Pathophysiological insights derived by natural history and motor function of spinal muscular atrophy. *J Pediatr* **162**, 155–159 (2013).

155. Iyer, C. C., McGovern, V. L., Wise, D. O., Glass, D. J. & Burghes, A. H. M. Deletion of atrophy enhancing genes fails to ameliorate the phenotype in a mouse model of spinal muscular atrophy. *Neuromuscul Disord* **24**, 436–444 (2014).

156. Iyer, C. C. *et al.* Low levels of Survival Motor Neuron protein are sufficient for normal muscle function in the SMNΔ7 mouse model of SMA. *Hum Mol Genet* **24**, 6160–6173 (2015).

157. Martínez-Hernández, R., Bernal, S., Alias, L. & Tizzano, E. F. Abnormalities in early markers of muscle involvement support a delay in myogenesis in spinal muscular atrophy. *J. Neuropathol. Exp. Neurol.* **73**, 559–567 (2014).

158. Martínez-Hernández, R. *et al.* The Developmental Pattern of Myotubes in Spinal Muscular Atrophy Indicates Prenatal Delay of Muscle Maturation. *Journal of Neuropathology & Experimental Neurology* **68**, 474–481 (2009).

159. Shafey, D., Côté, P. D. & Kothary, R. Hypomorphic Smn knockdown C2C12 myoblasts reveal intrinsic defects in myoblast fusion and myotube morphology. *Exp. Cell Res.* **311**, 49–61 (2005).

160. Hayhurst, M., Wagner, A. K., Cerletti, M., Wagers, A. J. & Rubin, L. L. A cell-autonomous defect in skeletal muscle satellite cells expressing low levels of survival of motor neuron protein. *Dev. Biol.* **368**, 323–334 (2012).

161. Hellbach, N. *et al.* Impaired myogenic development, differentiation and function in hESC-derived SMA myoblasts and myotubes. *PLoS ONE* **13**, e0205589 (2018).

162. Kim, J.-K. *et al.* Muscle-specific SMN reduction reveals motor neuron–independent disease in spinal muscular atrophy models. *The Journal of Clinical Investigation* **130**, 1271 (2020).

163. Chal, J. & Pourquié, O. Making muscle: skeletal myogenesis in vivo and in vitro. *Development* **144**, 2104–2122 (2017).

164. Zammit, P. S. Function of the myogenic regulatory factors Myf5, MyoD, Myogenin and MRF4 in skeletal muscle, satellite cells and regenerative myogenesis. *Semin. Cell Dev. Biol.* **72**, 19–32 (2017).

165. Buckingham, M. E., Lyons, G. E., Ott, M. O. & Sassoon, D. A. Myogenesis in the mouse. *Ciba Found Symp* **165**, 111–124; discussion 124-131 (1992).

166. Fürst, D. O., Osborn, M. & Weber, K. Myogenesis in the mouse embryo: differential onset of expression of myogenic proteins and the involvement of titin in myofibril assembly. *J Cell Biol* **109**, 517–527 (1989).

167. Bober, E., Franz, T., Arnold, H. H., Gruss, P. & Tremblay, P. Pax-3 is required for the development of limb muscles: a possible role for the migration of dermomyotomal muscle progenitor cells. *Development* **120**, 603–612 (1994).

168. Gros, J., Manceau, M., Thomé, V. & Marcelle, C. A common somitic origin for embryonic muscle progenitors and satellite cells. *Nature* **435**, 954–958 (2005).

169. Summerbell, D., Halai, C. & Rigby, P. W. J. Expression of the myogenic regulatory factor Mrf4 precedes or is contemporaneous with that of Myf5 in the somitic bud. *Mech. Dev.* **117**, 331–335 (2002).

170. Rudnicki, M. A. *et al.* MyoD or Myf-5 is required for the formation of skeletal muscle. *Cell* **75**, 1351–1359 (1993).

171. Mak, K. L., To, R. Q., Kong, Y. & Konieczny, S. F. The MRF4 activation domain is required to induce muscle-specific gene expression. *Mol Cell Biol* **12**, 4334–4346 (1992).

172. Hasty, P. *et al.* Muscle deficiency and neonatal death in mice with a targeted mutation in the myogenin gene. *Nature* **364**, 501–506 (1993).

173. Mastroyiannopoulos, N. P., Nicolaou, P., Anayasa, M., Uney, J. B. & Phylactou, L. A. Down-Regulation of Myogenin Can Reverse Terminal Muscle Cell Differentiation. *PLOS ONE* **7**, e29896 (2012).

174. Cusella-De Angelis, M. G. *et al.* MyoD, myogenin independent differentiation of primordial myoblasts in mouse somites. *J. Cell Biol.* **116**, 1243–1255 (1992).

175. Ganassi, M. *et al.* Myogenin promotes myocyte fusion to balance fibre number and size. *Nature Communications* **9**, 4232 (2018).

176. Montarras, D. *et al.* Developmental patterns in the expression of Myf5, MyoD, myogenin, and MRF4 during myogenesis. *New Biol.* **3**, 592–600 (1991).

177. Schiaffino, S., Rossi, A. C., Smerdu, V., Leinwand, L. A. & Reggiani, C. Developmental myosins: expression patterns and functional significance. *Skelet Muscle* **5**, (2015).

178. Relaix, F., Rocancourt, D., Mansouri, A. & Buckingham, M. A Pax3/Pax7-dependent population of skeletal muscle progenitor cells. *Nature* **435**, 948–953 (2005).

179. Matsakas, A., Otto, A., Elashry, M. I., Brown, S. C. & Patel, K. Altered primary and secondary myogenesis in the myostatin-null mouse. *Rejuvenation Res* **13**, 717–727 (2010).

180. Wilson, S. J., McEwan, J. C., Sheard, P. W. & Harris, A. J. Early stages of myogenesis in a large mammal: Formation of successive generations of myotubes in sheep tibialis cranialis muscle. *J Muscle Res Cell Motil* **13**, 534–550 (1992).

181. Van Horn, R. & Crow, M. T. Fast myosin heavy chain expression during the early and late embryonic stages of chicken skeletal muscle development. *Dev. Biol.* **134**, 279–288 (1989).

182. Olguin, H. C. & Olwin, B. B. Pax-7 up-regulation inhibits myogenesis and cell cycle progression in satellite cells: a potential mechanism for self-renewal. *Dev Biol* **275**, 375–388 (2004).

183. White, R. B., Biérinx, A.-S., Gnocchi, V. F. & Zammit, P. S. Dynamics of muscle fibre growth during postnatal mouse development. *BMC Developmental Biology* **10**, 21 (2010).

184. Zammit, P. S. *et al.* Pax7 and myogenic progression in skeletal muscle satellite cells. *J. Cell. Sci.* **119**, 1824–1832 (2006).

185. Moss, F. P. & Leblond, C. P. Satellite cells as the source of nuclei in muscles of growing rats. *The Anatomical Record* **170**, 421–435 (1971).

186. Collins, C. A. *et al.* Stem cell function, self-renewal, and behavioral heterogeneity of cells from the adult muscle satellite cell niche. *Cell* **122**, 289–301 (2005).

187. Relaix, F. *et al.* Pax3 and Pax7 have distinct and overlapping functions in adult muscle progenitor cells. *J Cell Biol* **172**, 91–102 (2006).

188. Beauchamp, J. R. *et al.* Expression of CD34 and Myf5 defines the majority of quiescent adult skeletal muscle satellite cells. *J. Cell Biol.* **151**, 1221–1234 (2000).

189. Koishi, K., Zhang, M., McLennan, I. S. & Harris, A. J. MyoD protein accumulates in satellite cells and is neurally regulated in regenerating myotubes and skeletal muscle fibers. *Dev. Dyn.* **202**, 244–254 (1995).

190. Meadows, E., Cho, J.-H., Flynn, J. M. & Klein, W. H. Myogenin regulates a distinct genetic program in adult muscle stem cells. *Dev. Biol.* **322**, 406–414 (2008).

191. Sambasivan, R. *et al.* Pax7-expressing satellite cells are indispensable for adult skeletal muscle regeneration. *Development* **138**, 3647–3656 (2011).

192. Wen, Y. *et al.* Constitutive Notch activation upregulates Pax7 and promotes the self-renewal of skeletal muscle satellite cells. *Mol. Cell. Biol.* **32**, 2300–2311 (2012).

193. Desmin/vimentin intermediate filaments are dispensable for many aspects of myogenesis. *J Cell Biol* **114**, 953–966 (1991).

194. Stevens, L. *et al.* Childhood spinal muscular atrophy induces alterations in contractile and regulatory protein isoform expressions. *Neuropathol. Appl. Neurobiol.* **34**, 659–670 (2008).

195. Bricceno, K. V. *et al.* Survival motor neuron protein deficiency impairs myotube formation by altering myogenic gene expression and focal adhesion dynamics. *Hum Mol Genet* **23**, 4745–4757 (2014).

196. Muses, S., Morgan, J. E. & Wells, D. J. A New Extensively Characterised Conditionally Immortal Muscle Cell-Line for Investigating Therapeutic Strategies in Muscular Dystrophies. *PLOS ONE* **6**, e24826 (2011).

197. Zamir, E. & Geiger, B. Molecular complexity and dynamics of cell-matrix adhesions. *Journal of Cell Science* **114**, 3583–3590 (2001).

198. Ziegler, W. H., Liddington, R. C. & Critchley, D. R. The structure and regulation of vinculin. *Trends Cell Biol.* **16**, 453–460 (2006).

199. Conti, F. J., Monkley, S. J., Wood, M. R., Critchley, D. R. & Müller, U. Talin 1 and 2 are required for myoblast fusion, sarcomere assembly and the maintenance of myotendinous junctions. *Development* **136**, 3597–3606 (2009).

200. Gautel, M. & Djinović-Carugo, K. The sarcomeric cytoskeleton: from molecules to motion. *The Journal of Experimental Biology* **219**, 135–145 (2016).

201. Yamaguchi, M., Izumimoto, M., Robson, R. M. & Stromer, M. H. Fine structure of wide and narrow vertebrate muscle Z-lines. A proposed model and computer simulation of Z-line architecture. *J. Mol. Biol.* **184**, 621–643 (1985).

202. Takahashi, K. & Hattori, A. Alpha-actinin is a component of the Z-filament, a structural backbone of skeletal muscle Z-disks. *J. Biochem.* **105**, 529–536 (1989).

203. Luther, P. K. The vertebrate muscle Z-disc: sarcomere anchor for structure and signalling. *J. Muscle Res. Cell. Motil.* **30**, 171–185 (2009).

204. Harris, B. Z., Lim, W. A., Harris, B. Z. & Lim, W. A. Mechanism and role of PDZ domains in signaling complex assembly. 13.

205. Hernández-Ochoa, E., Pratt, S., Lovering, R. & Schneider, M. Critical role of intracellular RyR1 calcium release channels in skeletal muscle function and disease. *Frontiers in Physiology* **6**, 420 (2016).

206. Gilchrist, J. S. C. *et al.* RyR1/SERCA1 cross-talk regulation of calcium transport in heavy sarcoplasmic reticulum vesicles. *Can J Physiol Pharmacol* **81**, 220–233 (2003).

207. Rajendra, T. K. *et al.* A Drosophila melanogaster model of spinal muscular atrophy reveals a function for SMN in striated muscle. *J Cell Biol* **176**, 831–841 (2007).

208. Walker, M. P. *et al.* SMN complex localizes to the sarcomeric Z-disc and is a proteolytic target of calpain. *Hum. Mol. Genet.* **17**, 3399–3410 (2008).

209. Berciano, M. T. *et al.* Mislocalization of SMN from the I-band and M-band in human skeletal myofibers in spinal muscular atrophy associates with primary structural alterations of the sarcomere. *Cell Tissue Res* **381**, 461–478 (2020).

210. Lange, S., Pinotsis, N., Agarkova, I. & Ehler, E. The M-band: The underestimated part of the sarcomere. *Biochimica et Biophysica Acta (BBA) - Molecular Cell Research* **1867**, 118440 (2020).

211. Huang, Y. & Wang, K. K. The calpain family and human disease. *Trends Mol Med* **7**, 355–362 (2001).

212. Smith, M. A. & Schnellmann, R. G. Calpains, mitochondria, and apoptosis. *Cardiovasc Res* **96**, 32–37 (2012).

213. Buffolo, M., Batista Possidonio, A. C., Mermelstein, C. & Araujo, H. A conserved role for calpains during myoblast fusion. *Genesis* **53**, 417–430 (2015).

214. Denny, J. B., Polan-Curtain, J., Ghuman, A., Wayner, M. J. & Armstrong, D. L. Calpain inhibitors block long-term potentiation. *Brain Res.* **534**, 317–320 (1990).

215. Wells, A., Huttenlocher, A. & Lauffenburger, D. A. Calpain proteases in cell adhesion and motility. *Int. Rev. Cytol.* **245**, 1–16 (2005).

216. Cheng, S., Wang, S., Lei, M., Wang, Z. & Xiong, K. Regulatory role of calpain in neuronal death. *Neural Regen Res* **13**, 556–562 (2018).

217. de la Fuente, S., Sansa, A., Periyakaruppiah, A., Garcera, A. & Soler, R. M. Calpain Inhibition Increases SMN Protein in Spinal Cord Motoneurons and Ameliorates the Spinal Muscular Atrophy Phenotype in Mice. *Mol. Neurobiol.* (2018) doi:10.1007/s12035-018-1379-z.

218. Wang, C.-H., Liang, W.-C., Minami, N., Nishino, I. & Jong, Y.-J. Limb-girdle Muscular Dystrophy Type 2A with Mutation in CAPN3: The First Report in Taiwan. *Pediatrics & Neonatology* **56**, 62–65 (2015).

219. El-Khoury, R. *et al.* Divergent Features of Mitochondrial Deficiencies in LGMD2A Associated With Novel Calpain-3 Mutations. *J. Neuropathol. Exp. Neurol.* **78**, 88–98 (2019).

220. Yalvac, M. E. *et al.* Impaired regeneration in calpain-3 null muscle is associated with perturbations in mTORC1 signaling and defective mitochondrial biogenesis. *Skelet Muscle* **7**, (2017).

221. Taveau, M. *et al.* Calpain 3 is activated through autolysis within the active site and lyses sarcomeric and sarcolemmal components. *Mol. Cell. Biol.* **23**, 9127–9135 (2003).

222. Beckmann, J. S. & Spencer, M. Calpain 3, the 'gatekeeper' of proper sarcomere assembly, turnover and maintenance. *Neuromuscul. Disord.* **18**, 913–921 (2008).

223. Charton, K. *et al.* CAPN3-mediated processing of C-terminal titin replaced by pathological cleavage in titinopathy. *Hum. Mol. Genet.* **24**, 3718–3731 (2015).

224. Hughes, B. W., Kusner, L. L. & Kaminski, H. J. Molecular architecture of the neuromuscular junction. *Muscle & Nerve* **33**, 445–461 (2006).

225. Creazzo, T. L. & Sohal, G. S. Neural control of embryonic acetylcholine receptor and skeletal muscle. *Cell Tissue Res.* **228**, 1–12 (1983).

226. Liu, Y. *et al.* Essential roles of the acetylcholine receptor -subunit in neuromuscular synaptic patterning. *Development* **135**, 1957–1967 (2008).

227. Vock, V. M., Ponomareva, O. N. & Rimer, M. Evidence for muscle-dependent neuromuscular synaptic site determination in mammals. *J. Neurosci.* **28**, 3123–3130 (2008).

228. Lin, W. *et al.* Distinct roles of nerve and muscle in postsynaptic differentiation of the neuromuscular synapse. *Nature* **410**, 1057–1064 (2001).

229. Tintignac, L. A., Brenner, H.-R. & Rüegg, M. A. Mechanisms Regulating Neuromuscular Junction Development and Function and Causes of Muscle Wasting. *Physiological Reviews* **95**, 809–852 (2015).

230. Sanes, J. R. & Lichtman, J. W. Development of the vertebrate neuromuscular junction. *Annu Rev Neurosci* **22**, 389–442 (1999).

231. Gan, W. B. & Lichtman, J. W. Synaptic segregation at the developing neuromuscular junction. *Science* **282**, 1508–1511 (1998).

232. Sanes, J. R. & Lichtman, J. W. Induction, assembly, maturation and maintenance of a postsynaptic apparatus. *Nature Reviews Neuroscience* **2**, 791–805 (2001).

233. Ac, M., Gc, C., Bj, K., Jr, S. & Jp, M. Maturation of the acetylcholine receptor in skeletal muscle: regulation of the AChR gamma-to-epsilon switch. *Dev Biol* **179**, 223–238 (1996).

234. Slater, C. R. Postnatal maturation of nerve-muscle junctions in hindlimb muscles of the mouse. *Developmental Biology* **94**, 11–22 (1982).

235. Marques, M. J., Conchello, J.-A. & Lichtman, J. W. From Plaque to Pretzel: Fold Formation and Acetylcholine Receptor Loss at the Developing Neuromuscular Junction. *J. Neurosci.* **20**, 3663–3675 (2000).

236. Yumoto, N., Wakatsuki, S. & Sehara-Fujisawa, A. The acetylcholine receptor γ-to-ε switch occurs in individual endplates. *Biochemical and Biophysical Research Communications* **331**, 1522–1527 (2005).

237. Low, L. K. & Cheng, H.-J. Axon pruning: an essential step underlying the developmental plasticity of neuronal connections. *Philosophical Transactions of the Royal Society B: Biological Sciences* **361**, 1531 (2006).

238. Clark, J. A., Southam, K. A., Blizzard, C. A., King, A. E. & Dickson, T. C. Axonal degeneration, distal collateral branching and neuromuscular junction architecture alterations occur prior to symptom onset in the SOD1(G93A) mouse model of amyotrophic lateral sclerosis. *J Chem Neuroanat* **76**, 35–47 (2016).

239. Bishop, D. L., Misgeld, T., Walsh, M. K., Gan, W.-B. & Lichtman, J. W. Axon branch removal at developing synapses by axosome shedding. *Neuron* **44**, 651–661 (2004).

240. Riley, D. A. Ultrastructural evidence for axon retraction during the spontaneous elimination of polyneuronal innervation of the rat soleus muscle. *J Neurocytol* **10**, 425–440 (1981).

241. Walsh, M. K. & Lichtman, J. W. In vivo time-lapse imaging of synaptic takeover associated with naturally occurring synapse elimination. *Neuron* **37**, 67–73 (2003).

242. Lichtman, J. W. & Colman, H. Synapse elimination and indelible memory. *Neuron* **25**, 269–278 (2000).

243. Wadman, R. I., Vrancken, A. F. J. E., van den Berg, L. H. & van der Pol, W. L. Dysfunction of the neuromuscular junction in spinal muscular atrophy types 2 and 3. *Neurology* **79**, 2050–2055 (2012).

244. Martínez-Hernández, R. *et al.* Synaptic defects in type I spinal muscular atrophy in human development. *The Journal of Pathology* **229**, 49–61 (2013).

245. Boido, M. & Vercelli, A. Neuromuscular Junctions as Key Contributors and Therapeutic Targets in Spinal Muscular Atrophy. *Front Neuroanat* **10**, (2016).

246. Hunter, G. *et al.* Restoration of SMN in Schwann cells reverses myelination defects and improves neuromuscular function in spinal muscular atrophy. *Hum Mol Genet* **25**, 2853–2861 (2016).

247. Hunter, G., Aghamaleky Sarvestany, A., Roche, S. L., Symes, R. C. & Gillingwater, T. H. SMN-dependent intrinsic defects in Schwann cells in mouse models of spinal muscular atrophy. *Human Molecular Genetics* **23**, 2235–2250 (2014).

248. Jablonka, S., Beck, M., Lechner, B. D., Mayer, C. & Sendtner, M. Defective Ca2+ channel clustering in axon terminals disturbs excitability in motoneurons in spinal muscular atrophy. *J Cell Biol* **179**, 139–149 (2007).

249. Lee, Y. il, Mikesh, M., Smith, I., Rimer, M. & Thompson, W. Muscles in a mouse model of spinal muscular atrophy show profound defects in neuromuscular development even in the absence of failure in neuromuscular transmission or loss of motor neurons. *Developmental biology* **356**, 432 (2011).

250. Cifuentes-Diaz, C. *et al.* Neurofilament accumulation at the motor endplate and lack of axonal sprouting in a spinal muscular atrophy mouse model. *Human Molecular Genetics* **11**, 1439–1447 (2002).

251. Herrmann, H., Bär, H., Kreplak, L., Strelkov, S. V. & Aebi, U. Intermediate filaments: from cell architecture to nanomechanics. *Nat Rev Mol Cell Biol* **8**, 562–573 (2007).

252. Bott, C. J. & Winckler, B. Intermediate filaments in developing neurons: Beyond structure. *Cytoskeleton* **77**, 110–128 (2020).

253. Dale, J. M. *et al.* The spinal muscular atrophy mouse model, SMAΔ7, displays altered axonal transport without global neurofilament alterations. *Acta Neuropathol* **122**, 331–341 (2011).

254. Torres-Benito, L., Ruiz, R. & Tabares, L. Synaptic defects in spinal muscular atrophy animal models. *Dev Neurobiol* **72**, 126–133 (2012).

255. Kariya, S. *et al.* Reduced SMN protein impairs maturation of the neuromuscular junctions in mouse models of spinal muscular atrophy. *Hum Mol Genet* **17**, 2552–2569 (2008).

256. Murray, L. M. *et al.* Selective vulnerability of motor neurons and dissociation of pre- and post-synaptic pathology at the neuromuscular junction in mouse models of spinal muscular atrophy. *Human Molecular Genetics* **17**, 949–962 (2008).

257. Kong, L. *et al.* Impaired Synaptic Vesicle Release and Immaturity of Neuromuscular Junctions in Spinal Muscular Atrophy Mice. *J. Neurosci.* **29**, 842–851 (2009).

258. Dachs, E. *et al.* Defective Neuromuscular Junction Organization and Postnatal Myogenesis in Mice With Severe Spinal Muscular Atrophy. *Journal of Neuropathology & Experimental Neurology* **70**, 444–461 (2011).

259. Biondi, O. *et al.* Exercise-Induced Activation of NMDA Receptor Promotes Motor Unit Development and Survival in a Type 2 Spinal Muscular Atrophy Model Mouse. *J. Neurosci.* **28**, 953–962 (2008).

260. Udina, E. *et al.* Compensatory axon sprouting for very slow axonal die-back in a transgenic model of spinal muscular atrophy type III. *J Physiol* **595**, 1815–1829 (2017).

261. Liu, D. W. & Westerfield, M. Clustering of muscle acetylcholine receptors requires motoneurons in live embryos, but not in cell culture. *J. Neurosci.* **12**, 1859–1866 (1992).

262. Yoshida, M. *et al.* Modeling the Early Phenotype at the Neuromuscular Junction of Spinal Muscular Atrophy Using Patient-Derived iPSCs. *Stem Cell Reports* **4**, 561–568 (2015).

263. Arnold, A.-S. *et al.* Reduced expression of nicotinic AChRs in myotubes from spinal muscular atrophy I patients. *Lab. Invest.* **84**, 1271–1278 (2004).

264. Lin, S., Landmann, L., Ruegg, M. A. & Brenner, H. R. The Role of Nerve- versus Muscle-Derived Factors in Mammalian Neuromuscular Junction Formation. *J. Neurosci.* **28**, 3333–3340 (2008).

265. Mazhar, S. & Herbst, R. The formation of complex acetylcholine receptor clusters requires MuSK kinase activity and structural information from the MuSK extracellular domain. *Molecular and Cellular Neuroscience* **49**, 475–486 (2012).

266. Zong, Y. & Jin, R. Structural mechanisms of the agrin-LRP4-MuSK signaling pathway in neuromuscular junction differentiation. *Cell Mol Life Sci* **70**, 3077–3088 (2013).

267. Zong, Y. *et al.* Structural basis of agrin-LRP4-MuSK signaling. *Genes Dev* **26**, 247–258 (2012).

268. Boido, M. *et al.* Increasing Agrin Function Antagonizes Muscle Atrophy and Motor Impairment in Spinal Muscular Atrophy. *Front Cell Neurosci* **12**, (2018).

269. Zhang, Z. *et al.* Dysregulation of synaptogenesis genes antecedes motor neuron pathology in spinal muscular atrophy. *Proc Natl Acad Sci U S A* **110**, 19348–19353 (2013).

270. Kim, J.-K., Caine, C., Awano, T., Herbst, R. & Monani, U. R. Motor neuronal repletion of the NMJ organizer, Agrin, modulates the severity of the spinal muscular atrophy disease phenotype in model mice. *Hum Mol Genet* **26**, 2377–2385 (2017).

271. Feng, Z. *et al.* Activation of Muscle-Specific Kinase (MuSK) Reduces Neuromuscular Defects in the Delta7 Mouse Model of Spinal Muscular Atrophy (SMA). *International Journal of Molecular Sciences* **22**, (2021).

272. Lavrnic, D. *et al.* The features of myasthenia gravis with autoantibodies to MuSK. *Journal of Neurology, Neurosurgery & Psychiatry* **76**, 1099–1102 (2005).

273. Huijbers, M. G. *et al.* MuSK myasthenia gravis monoclonal antibodies. *Neurol Neuroimmunol Neuroinflamm* **6**, (2019).

274. Perez-Garcia, M. J. & Burden, S. J. Increasing MuSK Activity Delays Denervation and Improves Motor Function in ALS Mice. *Cell Rep* **2**, 497–502 (2012).

275. Boehm, I. *et al.* Comparative anatomy of the mammalian neuromuscular junction. *Journal of Anatomy* **237**, 827–836 (2020).

276. Jones, R. A. *et al.* Cellular and Molecular Anatomy of the Human Neuromuscular Junction. *Cell Rep* **21**, 2348–2356 (2017).

277. Westerblad, H., Bruton, J. D. & Katz, A. Skeletal muscle: energy metabolism, fiber types, fatigue and adaptability. *Exp Cell Res* **316**, 3093–3099 (2010).

278. Larson, D. J. & Brown, S. H. M. The effects of trunk extensor and abdominal muscle fatigue on postural control and trunk proprioception in young, healthy individuals. *Human Movement Science* **57**, 13–20 (2018).

279. Manders, E. *et al.* Reduced force of diaphragm muscle fibers in patients with chronic thromboembolic pulmonary hypertension. *American Journal of Physiology-Lung Cellular and Molecular Physiology* **311**, L20–L28 (2016).

280. Baskin, K. K., Winders, B. R. & Olson, E. N. Muscle as a “Mediator“ of Systemic Metabolism. *Cell Metab* **21**, 237–248 (2015).

281. Hood, D. A., Irrcher, I., Ljubicic, V. & Joseph, A.-M. Coordination of metabolic plasticity in skeletal muscle. *Journal of Experimental Biology* **209**, 2265–2275 (2006).

282. Gallagher, D. *et al.* Organ-tissue mass measurement allows modeling of REE and metabolically active tissue mass. *Am J Physiol* **275**, E249-258 (1998).

283. Thiebaud, D. *et al.* The effect of graded doses of insulin on total glucose uptake, glucose oxidation, and glucose storage in man. *Diabetes* **31**, 957–963 (1982).

284. Wilden, P. A. *et al.* The role of insulin receptor kinase domain autophosphorylation in receptor-mediated activities. Analysis with insulin and anti-receptor antibodies. *J Biol Chem* **267**, 13719–13727 (1992).

285. Yu, K. T. & Czech, M. P. Tyrosine phosphorylation of the insulin receptor beta subunit activates the receptor-associated tyrosine kinase activity. *J Biol Chem* **259**, 5277–5286 (1984).

286. Lee, J., Pilch, P. F., Shoelson, S. E. & Scarlata, S. F. Conformational Changes of the Insulin Receptor upon Insulin Binding and Activation As Monitored by Fluorescence Spectroscopy. *Biochemistry* **36**, 2701–2708 (1997).

287. Myers, M. G. *et al.* IRS-1 activates phosphatidylinositol 3'-kinase by associating with src homology 2 domains of p85. *Proc Natl Acad Sci U S A* **89**, 10350–10354 (1992).

288. Alessi, D. R. *et al.* Mechanism of activation of protein kinase B by insulin and IGF-1. *EMBO J* **15**, 6541–6551 (1996).

289. Alessi, D. R. *et al.* Characterization of a 3-phosphoinositide-dependent protein kinase which phosphorylates and activates protein kinase Balpha. *Curr Biol* **7**, 261–269 (1997).

290. Wang, Q. *et al.* Protein Kinase B/Akt Participates in GLUT4 Translocation by Insulin in L6 Myoblasts. *Mol Cell Biol* **19**, 4008–4018 (1999).

291. Karlsson, H. K. R. *et al.* Insulin-stimulated phosphorylation of the Akt substrate AS160 is impaired in skeletal muscle of type 2 diabetic subjects. *Diabetes* **54**, 1692–1697 (2005).

292. Middelbeek, R. J. W. *et al.* Insulin stimulation regulates AS160 and TBC1D1 phosphorylation sites in human skeletal muscle. *Nutrition & Diabetes* **3**, e74–e74 (2013).

293. Chen, S., Wasserman, D. H., MacKintosh, C. & Sakamoto, K. Mice with AS160/TBC1D4-Thr649Ala Knockin Mutation Are Glucose Intolerant with Reduced Insulin Sensitivity and Altered GLUT4 Trafficking. *Cell Metabolism* **13**, 68–79 (2011).

294. Sun, Y., Bilan, P. J., Liu, Z. & Klip, A. Rab8A and Rab13 are activated by insulin and regulate GLUT4 translocation in muscle cells. *Proc Natl Acad Sci U S A* **107**, 19909–19914 (2010).

295. Birnbaum, M. J. Identification of a novel gene encoding an insulin-responsive glucose transporter protein. *Cell* **57**, 305–315 (1989).

296. Charron, M. J., Brosius, F. C., Alper, S. L. & Lodish, H. F. A glucose transport protein expressed predominately in insulin-responsive tissues. *Proc Natl Acad Sci U S A* **86**, 2535–2539 (1989).

297. Sun, Y., Jaldin-Fincati, J., Liu, Z., Bilan, P. J. & Klip, A. A complex of Rab13 with MICAL-L2 and α-actinin-4 is essential for insulin-dependent GLUT4 exocytosis. *Mol Biol Cell* **27**, 75–89 (2016).

298. Evans, P. L., McMillin, S. L., Weyrauch, L. A. & Witczak, C. A. Regulation of Skeletal Muscle Glucose Transport and Glucose Metabolism by Exercise Training. *Nutrients* **11**, (2019).

299. DeFronzo, R. A. & Tripathy, D. Skeletal Muscle Insulin Resistance Is the Primary Defect in Type 2 Diabetes. *Diabetes Care* **32**, S157–S163 (2009).

300. Musi, N. *et al.* Metformin Increases AMP-Activated Protein Kinase Activity in Skeletal Muscle of Subjects With Type 2 Diabetes. *Diabetes* **51**, 2074–2081 (2002).

301. Bowerman, M. *et al.* Glucose metabolism and pancreatic defects in spinal muscular atrophy. *Ann. Neurol.* **72**, 256–268 (2012).

302. Bruce, A. K., Jacobsen, E., Dossing, H. & Kondrup, J. Hypoglycaemia in spinal muscular atrophy. *Lancet* **346**, 609–610 (1995).

303. Djordjevic, S. A. *et al.* Glucose and lipid metabolism disorders in children and adolescents with spinal muscular atrophy types 2 and 3. *Neuromuscul Disord* (2021) doi:10.1016/j.nmd.2021.02.002.

304. Kölbel, H. *et al.* Hyperleptinemia in children with autosomal recessive spinal muscular atrophy type I-III. *PLoS One* **12**, (2017).

305. Brener, A. *et al.* Insulin-like growth factor-1 status is associated with insulin resistance in young patients with spinal muscular atrophy. *Neuromuscular Disorders* **30**, 888–896 (2020).

306. Borkowska, A. *et al.* Coexistence of type 1 diabetes mellitus and spinal muscular atrophy in an 8-year-old girl: a case report. *Acta Biochim Pol* **62**, 167–168 (2015).

307. Hossain, S. & Chao, J. MON-154 Abnormal Glucose Homeostasis in Spinal Muscular Atrophy (SMA) Leading to a Transient Episode of Diabetic Ketoacidosis (DKA). *J Endocr Soc* **3**, (2019).

308. Lamarca, N. H. *et al.* Diabetic Ketoacidosis in an Adult Patient With Spinal Muscular Atrophy Type II: Further Evidence of Extraneural Pathology Due to Survival Motor Neuron 1 Mutation? *J Child Neurol* **28**, 1517–1520 (2013).

309. Stoimenis, D. *et al.* Euglycemic Ketoacidosis in Spinal Muscular Atrophy. *Case Rep Pediatr* **2019**, (2019).

310. Bowerman, M. *et al.* Defects in pancreatic development and glucose metabolism in SMN-depleted mice independent of canonical spinal muscular atrophy neuromuscular pathology. *Hum Mol Genet* **23**, 3432–3444 (2014).

311. DeWaal, D. *et al.* Hexokinase-2 depletion inhibits glycolysis and induces oxidative phosphorylation in hepatocellular carcinoma and sensitizes to metformin. *Nature Communications* **9**, 446 (2018).

312. Meijboom, K. E. Spinal muscular atrophy: Disease mechanisms and therapeutic approaches. (University of Oxford, 2018).

313. Koopman, R., Ly, C. H. & Ryall, J. G. A metabolic link to skeletal muscle wasting and regeneration. *Front. Physiol.* **5**, (2014).

314. Wang, X., Hu, Z., Hu, J., Du, J. & Mitch, W. E. Insulin Resistance Accelerates Muscle Protein Degradation: Activation of the Ubiquitin-Proteasome Pathway by Defects in Muscle Cell Signaling. *Endocrinology* **147**, 4160–4168 (2006).

315. Perry, B. D. *et al.* Muscle atrophy in patients with Type 2 Diabetes Mellitus: roles of inflammatory pathways, physical activity and exercise. *Exerc Immunol Rev* **22**, 94–109 (2016).

316. Stein, T. P. & Wade, C. E. Metabolic consequences of muscle disuse atrophy. *J Nutr* **135**, 1824S-1828S (2005).

317. FREIDENBERG, G. R. & OLEFSKY, J. M. Dissociation of Insulin Resistance and Decreased Insulin Receptor Binding in Duchenne Muscular Dystrophy*. *The Journal of Clinical Endocrinology & Metabolism* **60**, 320–327 (1985).

318. Olichon-Berthe, C., Gautier, N., Van Obberghen, E. & Le Marchand-Brustel, Y. Expression of the glucose transporter GLUT4 in the muscular dystrophic mdx mouse. *Biochem J* **291 (Pt 1)**, 257–261 (1993).

319. Perseghin, G. *et al.* Contribution of Abnormal Insulin Secretion and Insulin Resistance to the Pathogenesis of Type 2 Diabetes in Myotonic Dystrophy. *Diabetes Care* **26**, 2112–2118 (2003).

320. Takeshima, K. *et al.* Myotonic dystrophy type 1 with diabetes mellitus, mixed hypogonadism and adrenal insufficiency. *Endocrinol Diabetes Metab Case Rep* **2018**, (2018).

321. Renna, L. V. *et al.* Receptor and post-receptor abnormalities contribute to insulin resistance in myotonic dystrophy type 1 and type 2 skeletal muscle. *PLOS ONE* **12**, e0184987 (2017).

322. Reyes, E. T., Perurena, O. H., Festoff, B. W., Jorgensen, R. & Moore, W. V. Insulin resistance in amyotrophic lateral sclerosis. *Journal of the Neurological Sciences* **63**, 317–324 (1984).

323. Pradat, P.-F. *et al.* Impaired glucose tolerance in patients with amyotrophic lateral sclerosis. *Amyotroph Lateral Scler* **11**, 166–171 (2010).

324. Röder, P. V., Wu, B., Liu, Y. & Han, W. Pancreatic regulation of glucose homeostasis. *Exp Mol Med* **48**, e219 (2016).

325. Rowe, P. A., Campbell-Thompson, M. L., Schatz, D. A. & Atkinson, M. A. The pancreas in human type 1 diabetes. *Semin Immunopathol* **33**, 29–43 (2011).

326. Melzer, K. Carbohydrate and fat utilization during rest and physical activity. *e-SPEN, the European e-Journal of Clinical Nutrition and Metabolism* **6**, e45–e52 (2011).

327. Luiken, J. J. F. P., Bonen, A. & Glatz, J. F. C. Cellular fatty acid uptake is acutely regulated by membrane-associated fatty acid-binding proteins. *Prostaglandins Leukot Essent Fatty Acids* **67**, 73–78 (2002).

328. Holloway, G. P. *et al.* Fatty acid binding protein facilitates sarcolemmal fatty acid transport but not mitochondrial oxidation in rat and human skeletal muscle. *J Physiol* **582**, 393–405 (2007).

329. Li, L. O. *et al.* Compartmentalized Acyl-CoA Metabolism in Skeletal Muscle Regulates Systemic Glucose Homeostasis. *Diabetes* **64**, 23–35 (2015).

330. Mashek, D. G., Li, L. O. & Coleman, R. A. Rat long-chain acyl-CoA synthetase mRNA, protein, and activity vary in tissue distribution and in response to diet. *J Lipid Res* **47**, 2004–2010 (2006).

331. Teodoro, B. G. *et al.* Long-chain acyl-CoA synthetase 6 regulates lipid synthesis and mitochondrial oxidative capacity in human and rat skeletal muscle. *J Physiol* **595**, 677–693 (2017).

332. Jogl, G. & Tong, L. Crystal Structure of Carnitine Acetyltransferase and Implications for the Catalytic Mechanism and Fatty Acid Transport. *Cell* **112**, 113–122 (2003).

333. Bruce, C. R. *et al.* Overexpression of carnitine palmitoyltransferase-1 in skeletal muscle is sufficient to enhance fatty acid oxidation and improve high-fat diet-induced insulin resistance. *Diabetes* **58**, 550–558 (2009).

334. Tucker, M. Z. & Turcotte, L. P. Impaired fatty acid oxidation in muscle of aging rats perfused under basal conditions. *Am J Physiol Endocrinol Metab* **282**, E1102-1109 (2002).

335. Heilbronn, L. K., Gregersen, S., Shirkhedkar, D., Hu, D. & Campbell, L. V. Impaired Fat Oxidation After a Single High-Fat Meal in Insulin-Sensitive Nondiabetic Individuals With a Family History of Type 2 Diabetes. *Diabetes* **56**, 2046–2053 (2007).

336. Lara-Castro, C. & Garvey, W. T. Intracellular Lipid Accumulation in Liver and Muscle and the Insulin Resistance Syndrome. *Endocrinol Metab Clin North Am* **37**, 841–856 (2008).

337. Kuhlmann, J. *et al.* Intramyocellular Lipid and Insulin Resistance: A Longitudinal In Vivo 1H-Spectroscopic Study in Zucker Diabetic Fatty Rats. *Diabetes* **52**, 138–144 (2003).

338. Kelley, R. I. & Sladky, J. T. Dicarboxylic aciduria in an infant with spinal muscular atrophy. *Ann Neurol* **20**, 734–736 (1986).

339. Harpey, J. P. *et al.* Secondary metabolic defects in spinal muscular atrophy type II. *Lancet* **336**, 629–630 (1990).

340. Crawford, T. O., Sladky, J. T., Hurko, O., Besner-Johnston, A. & Kelley, R. I. Abnormal fatty acid metabolism in childhood spinal muscular atrophy. *Ann Neurol* **45**, 337–343 (1999).

341. Sproule, D. M. *et al.* Increased fat mass and high incidence of overweight despite low body mass index in patients with Spinal Muscular Atrophy. *Neuromuscul Disord* **19**, 391–396 (2009).

342. Tein, I. *et al.* Fatty acid oxidation abnormalities in childhood-onset spinal muscular atrophy: primary or secondary defect(s)? *Pediatr. Neurol.* **12**, 21–30 (1995).

343. Deguise, M. *et al.* Abnormal fatty acid metabolism is a core component of spinal muscular atrophy. *Ann Clin Transl Neurol* **6**, 1519–1532 (2019).

344. Watson, K. S., Boukhloufi, I., Bowerman, M. & Parson, S. H. The Relationship between Body Composition, Fatty Acid Metabolism and Diet in Spinal Muscular Atrophy. *Brain Sci* **11**, (2021).

345. Costa, C. C. G., De Almeida, I. T., Jakobs, C., Poll-The, B.-T. & Duran, M. Dynamic Changes of Plasma Acylcarnitine Levels Induced by Fasting and Sunflower Oil Challenge Test in Children. *Pediatric Research* **46**, 440–440 (1999).

346. Alves-Bezerra, M. & Cohen, D. E. Triglyceride metabolism in the liver. *Comprehensive Physiology* **8**, 1 (2017).

347. Sattar, N., Forrest, E. & Preiss, D. Non-alcoholic fatty liver disease. *BMJ* **349**, g4596 (2014).

348. Deguise, M.-O. *et al.* A mouse model for spinal muscular atrophy provides insights into non-alcoholic fatty liver disease pathogenesis. *bioRxiv* 2020.04.29.051938 (2020) doi:10.1101/2020.04.29.051938.

349. Vitte, J. M. *et al.* Deletion of Murine Smn Exon 7 Directed to Liver Leads to Severe Defect of Liver Development Associated with Iron Overload. *Am J Pathol* **165**, 1731–1741 (2004).

350. Hua, Y. *et al.* Peripheral SMN restoration is essential for long-term rescue of a severe spinal muscular atrophy mouse model. *Nature* **478**, 123–126 (2011).

351. Högler, W. *et al.* IGFALS Gene Dosage Effects on Serum IGF-I and Glucose Metabolism, Body Composition, Bone Growth in Length and Width, and the Pharmacokinetics of Recombinant Human IGF-I Administration. *The Journal of Clinical Endocrinology & Metabolism* **99**, E703–E712 (2014).

352. Clemmons, D. R. Metabolic Actions of IGF-I in Normal Physiology and Diabetes. *Endocrinol Metab Clin North Am* **41**, 425–443 (2012).

353. Laron, Z. Insulin-like growth factor 1 (IGF-1): a growth hormone. *Mol Pathol* **54**, 311–316 (2001).

354. Kaymaz, A. Y. *et al.* Serum IGF1 and IGFBP3 levels in SMA patients. *Neuromuscular Disorders* **26**, S105 (2016).

355. Calderon-Dominguez, M. *et al.* Fatty acid metabolism and the basis of brown adipose tissue function. *Adipocyte* **5**, 98 (2016).

356. Walter, L. M. *et al.* Light modulation ameliorates expression of circadian genes and disease progression in spinal muscular atrophy mice. *Hum. Mol. Genet.* **27**, 3582–3597 (2018).

357. Goldberg, A. L. Protein synthesis during work-induced growth of skeletal muscle. *J Cell Biol* **36**, 653–658 (1968).

358. Figueiredo, V. C. Revisiting the roles of protein synthesis during skeletal muscle hypertrophy induced by exercise. *American Journal of Physiology-Regulatory, Integrative and Comparative Physiology* **317**, R709–R718 (2019).

359. Millino, C. *et al.* Different atrophy-hypertrophy transcription pathways in muscles affected by severe and mild spinal muscular atrophy. *BMC Medicine* **7**, 14 (2009).

360. Schiaffino, S. & Mammucari, C. Regulation of skeletal muscle growth by the IGF1-Akt/PKB pathway: insights from genetic models. *Skelet Muscle* **1**, 4 (2011).

361. Yoon, M.-S. mTOR as a Key Regulator in Maintaining Skeletal Muscle Mass. *Front Physiol* **8**, (2017).

362. Zhang, Q. *et al.* Lack of muscle mTOR kinase activity causes early onset myopathy and compromises whole-body homeostasis. *J Cachexia Sarcopenia Muscle* **10**, 35–53 (2019).

363. Sandri, M. *et al.* Foxo Transcription Factors Induce the Atrophy-Related Ubiquitin Ligase Atrogin-1 and Cause Skeletal Muscle Atrophy. *Cell* **117**, 399–412 (2004).

364. Biggs III, W. H. & CaveneeKaren C., W. K. Identification and characterization of members of the FKHR (FOX O) subclass of winged-helix transcription factors in the mouse. *Mammalian Genome* **12**, 416–425 (2001).

365. Wang, M., Zhang, X., Zhao, H., Wang, Q. & Pan, Y. FoxO gene family evolution in vertebrates. *BMC Evolutionary Biology* **9**, 222 (2009).

366. Mammucari, C. *et al.* FoxO3 Controls Autophagy in Skeletal Muscle In Vivo. *Cell Metabolism* **6**, 458–471 (2007).

367. Gray, S. *et al.* Regulation of gluconeogenesis by Krüppel-like factor 15. *Cell Metab* **5**, 305–312 (2007).

368. Shimizu, N. *et al.* Crosstalk between Glucocorticoid Receptor and Nutritional Sensor mTOR in Skeletal Muscle. *Cell Metabolism* **13**, 170–182 (2011).

369. Neishabouri, S. H., Hutson, S. M. & Davoodi, J. Chronic activation of mTOR complex 1 by branched chain amino acids and organ hypertrophy. *Amino Acids* **47**, 1167–1182 (2015).

370. Liu, Y. *et al.* Branched-Chain Amino Acid Negatively Regulates KLF15 Expression via PI3K-AKT Pathway. *Front Physiol* **8**, 853 (2017).

371. Cid-Díaz, T. *et al.* Obestatin signalling counteracts glucocorticoid-induced skeletal muscle atrophy via NEDD4/KLF15 axis. *Journal of Cachexia, Sarcopenia and Muscle* **12**, 493–505 (2021).

372. Xie, Y. *et al.* New Insights Into the Circadian Rhythm and Its Related Diseases. *Front. Physiol.* **10**, (2019).

373. Maury, E., Ramsey, K. M. & Bass, J. Circadian rhythms and metabolic syndrome: from experimental genetics to human disease. *Circulation research* **106**, 447 (2010).

374. Blume, C., Garbazza, C. & Spitschan, M. Effects of light on human circadian rhythms, sleep and mood. *Somnologie (Berl)* **23**, 147–156 (2019).

375. Gekakis, N. *et al.* Role of the CLOCK protein in the mammalian circadian mechanism. *Science* **280**, 1564–1569 (1998).

376. Chiou, Y.-Y. *et al.* Mammalian Period represses and de-represses transcription by displacing CLOCK–BMAL1 from promoters in a Cryptochrome-dependent manner. *PNAS* **113**, E6072–E6079 (2016).

377. Sancar, A. Regulation of the Mammalian Circadian Clock by Cryptochrome *. *Journal of Biological Chemistry* **279**, 34079–34082 (2004).

378. Harfmann, B. D., Schroder, E. A. & Esser, K. A. Circadian rhythms, the molecular clock, and skeletal muscle. *J. Biol. Rhythms* **30**, 84–94 (2015).

379. Froy, O. & Garaulet, M. The Circadian Clock in White and Brown Adipose Tissue: Mechanistic, Endocrine, and Clinical Aspects. *Endocr Rev* **39**, 261–273 (2018).

380. Sadacca, L. A., Lamia, K. A., deLemos, A. S., Blum, B. & Weitz, C. J. An intrinsic circadian clock of the pancreas is required for normal insulin release and glucose homeostasis in mice. *Diabetologia* **54**, 120 (2011).

381. Mukherji, A., Bailey, S. M., Staels, B. & Baumert, T. F. The circadian clock and liver function in health and disease. *Journal of Hepatology* **71**, 200–211 (2019).

382. Pera, M. C. *et al.* Sleep disorders in spinal muscular atrophy. *Sleep Med* **30**, 160–163 (2017).

383. Verrillo, E. *et al.* Sleep architecture in infants with spinal muscular atrophy type 1. *Sleep Med* **15**, 1246–1250 (2014).

384. Hatanaka, F. *et al.* Genome-wide profiling of the core clock protein BMAL1 targets reveals a strict relationship with metabolism. *Mol Cell Biol* **30**, 5636–5648 (2010).

385. Rudic, R. D. *et al.* BMAL1 and CLOCK, Two Essential Components of the Circadian Clock, Are Involved in Glucose Homeostasis. *PLoS Biol* **2**, (2004).

386. Bertram, R., Gram Pedersen, M., Luciani, D. S. & Sherman, A. A simplified model for mitochondrial ATP production. *J Theor Biol* **243**, 575–586 (2006).

387. Mishra, P., Varuzhanyan, G., Pham, A. H. & Chan, D. C. Mitochondrial dynamics is a distinguishing feature of skeletal muscle fiber types and regulates organellar compartmentalization. *Cell Metab* **22**, 1033–1044 (2015).

388. Ripolone, M. *et al.* Impaired Muscle Mitochondrial Biogenesis and Myogenesis in Spinal Muscular Atrophy. *JAMA Neurol* **72**, 666–675 (2015).

389. Ng, S. Y., Mikhail, A. & Ljubicic, V. Mechanisms of exercise-induced survival motor neuron expression in the skeletal muscle of spinal muscular atrophy-like mice. *J Physiol* **597**, 4757–4778 (2019).

390. Mancuso, M. *et al.* Mitochondrial DNA depletion: mutations in thymidine kinase gene with myopathy and SMA. *Neurology* **59**, 1197–1202 (2002).

391. Salviati, L. *et al.* Cytochrome c oxidase deficiency due to a novel SCO2 mutation mimics Werdnig-Hoffmann disease. *Arch Neurol* **59**, 862–865 (2002).

392. Tarnopolsky, M. A. *et al.* Novel SCO2 mutation (G1521A) presenting as a spinal muscular atrophy type I phenotype. *Am J Med Genet A* **125A**, 310–314 (2004).

393. Berger, A. *et al.* Severe depletion of mitochondrial DNA in spinal muscular atrophy. *Acta Neuropathol* **105**, 245–251 (2003).

394. James, R., Chaytow, H., Ledahawsky, L. M. & Gillingwater, T. H. Revisiting the role of mitochondria in spinal muscular atrophy. *Cell. Mol. Life Sci.* (2021) doi:10.1007/s00018-021-03819-5.

395. Montes, J. *et al.* Diminished muscle oxygen uptake and fatigue in spinal muscular atrophy. *Ann Clin Transl Neurol* **8**, 1086–1095 (2021).

396. Wu, Z. *et al.* Mechanisms controlling mitochondrial biogenesis and respiration through the thermogenic coactivator PGC-1. *Cell* **98**, 115–124 (1999).

397. Zhao, R.-Z., Jiang, S., Zhang, L. & Yu, Z.-B. Mitochondrial electron transport chain, ROS generation and uncoupling (Review). *International Journal of Molecular Medicine* **44**, 3–15 (2019).

398. Scarpulla, R. C. Nuclear Control of Respiratory Chain Expression by Nuclear Respiratory Factors and PGC-1-Related Coactivator. *Ann N Y Acad Sci* **1147**, 321–334 (2008).

399. Piantadosi, C. A. & Suliman, H. B. Mitochondrial transcription factor A induction by redox activation of nuclear respiratory factor 1. *J Biol Chem* **281**, 324–333 (2006).

400. Gleyzer, N., Vercauteren, K. & Scarpulla, R. C. Control of mitochondrial transcription specificity factors (TFB1M and TFB2M) by nuclear respiratory factors (NRF-1 and NRF-2) and PGC-1 family coactivators. *Mol Cell Biol* **25**, 1354–1366 (2005).

401. Bruni, F., Polosa, P. L., Gadaleta, M. N., Cantatore, P. & Roberti, M. Nuclear Respiratory Factor 2 Induces the Expression of Many but Not All Human Proteins Acting in Mitochondrial DNA Transcription and Replication 2. *Journal of Biological Chemistry* **285**, 3939–3948 (2010).

402. Schultz, J. *et al.* The secreted MSP domain of C. elegans VAPB homolog VPR-1 patterns the adult striated muscle mitochondrial reticulum via SMN-1. *Development* **144**, 2175–2186 (2017).

403. Hubers, L. *et al.* HuD interacts with survival motor neuron protein and can rescue spinal muscular atrophy-like neuronal defects. *Hum Mol Genet* **20**, 553–579 (2011).

404. Hong, Y. *et al.* RNA binding protein HuD contributes to β-cell dysfunction by impairing mitochondria dynamics. *Cell Death Differ* **27**, 1633–1643 (2020).

405. Bernkopf, D. B. *et al.* Pgam5 released from damaged mitochondria induces mitochondrial biogenesis via Wnt signaling. *J Cell Biol* **217**, 1383–1394 (2018).

406. Wu, H. *et al.* The BCL2L1 and PGAM5 axis defines hypoxia-induced receptor-mediated mitophagy. *Autophagy* **10**, 1712–1725 (2014).

407. Wijngaarde, C. A. *et al.* Cardiac pathology in spinal muscular atrophy: a systematic review. *Orphanet J Rare Dis* **12**, (2017).

408. Grotto, S. *et al.* Type 0 Spinal Muscular Atrophy: Further Delineation of Prenatal and Postnatal Features in 16 Patients. *J Neuromuscul Dis* **3**, 487–495 (2016).

409. Hamilton, G. & Gillingwater, T. H. Spinal muscular atrophy: going beyond the motor neuron. *Trends Mol Med* **19**, 40–50 (2013).

410. Heier, C. R., Satta, R., Lutz, C. & DiDonato, C. J. Arrhythmia and cardiac defects are a feature of spinal muscular atrophy model mice. *Hum Mol Genet* **19**, 3906–3918 (2010).

411. Shababi, M. *et al.* Cardiac defects contribute to the pathology of spinal muscular atrophy models. *Hum Mol Genet* **19**, 4059–4071 (2010).

412. Bevan, A. K. *et al.* Early heart failure in the SMNDelta7 model of spinal muscular atrophy and correction by postnatal scAAV9-SMN delivery. *Hum. Mol. Genet.* **19**, 3895–3905 (2010).

413. Shababi, M. *et al.* Partial restoration of cardio-vascular defects in a rescued severe model of spinal muscular atrophy. *J Mol Cell Cardiol* **52**, 1074–1082 (2012).

414. Lake, N. Loss of cardiac myofibrils: mechanism of contractile deficits induced by taurine deficiency. *Am J Physiol* **264**, H1323-1326 (1993).

415. Frank, D. & Frey, N. Cardiac Z-disc Signaling Network. *J Biol Chem* **286**, 9897–9904 (2011).

416. Šoltić, D. *et al.* Lamin A/C dysregulation contributes to cardiac pathology in a mouse model of severe spinal muscular atrophy. *Hum Mol Genet* **28**, 3515–3527 (2019).

417. Crasto, S., My, I. & Di Pasquale, E. The Broad Spectrum of LMNA Cardiac Diseases: From Molecular Mechanisms to Clinical Phenotype. *Front. Physiol.* **11**, (2020).

418. Gerbino, A., Procino, G., Svelto, M. & Carmosino, M. Role of Lamin A/C Gene Mutations in the Signaling Defects Leading to Cardiomyopathies. *Front. Physiol.* **9**, (2018).

419. Iwahara, N., Hisahara, S., Hayashi, T., Kawamata, J. & Shimohama, S. A novel lamin A/C gene mutation causing spinal muscular atrophy phenotype with cardiac involvement: report of one case. *BMC Neurol* **15**, (2015).

420. Somers, E. *et al.* Vascular Defects and Spinal Cord Hypoxia in Spinal Muscular Atrophy. *Ann Neurol* **79**, 217–230 (2016).

421. Nobutoki, T. & Ihara, T. Early disruption of neurovascular units and microcirculatory dysfunction in the spinal cord in spinal muscular atrophy type I. *Med Hypotheses* **85**, 842–845 (2015).

422. Araujo, A. prufer de Q. C., Araujo, M. & Swoboda, K. J. Vascular Perfusion Abnormalities in Infants with Spinal Muscular Atrophy. *J Pediatr* **155**, 292–294 (2009).

423. Somers, E., Stencel, Z., Wishart, T. M., Gillingwater, T. H. & Parson, S. H. Density, calibre and ramification of muscle capillaries are altered in a mouse model of severe spinal muscular atrophy. *Neuromuscul Disord* **22**, 435–442 (2012).

424. Schreml, J. *et al.* Severe SMA mice show organ impairment that cannot be rescued by therapy with the HDACi JNJ-26481585. *Eur J Hum Genet* **21**, 643–652 (2013).

425. Deguise, M. & Kothary, R. New insights into SMA pathogenesis: immune dysfunction and neuroinflammation. *Ann Clin Transl Neurol* **4**, 522–530 (2017).

426. Khairallah, M.-T. *et al.* SMN deficiency negatively impacts red pulp macrophages and spleen development in mouse models of spinal muscular atrophy. *Hum Mol Genet* **26**, 932–941 (2017).

427. Deguise, M.-O. *et al.* Immune dysregulation may contribute to disease pathogenesis in spinal muscular atrophy mice. *Hum. Mol. Genet.* **26**, 801–819 (2017).

428. Thomson, A. K. *et al.* Survival of motor neurone protein is required for normal postnatal development of the spleen. *J Anat* **230**, 337–346 (2017).

429. Cesta, M. F. Normal Structure, Function, and Histology of the Spleen. *Toxicol Pathol* **34**, 455–465 (2006).

430. THAPA, P. & FARBER, D. L. THE ROLE OF THE THYMUS IN THE IMMUNE RESPONSE. *Thorac Surg Clin* **29**, 123–131 (2019).

431. Ando, S. *et al.* Survival motor neuron protein regulates oxidative stress and inflammatory response in microglia of the spinal cord in spinal muscular atrophy. *Journal of Pharmacological Sciences* **144**, 204–211 (2020).

432. Wasserman, H. M. *et al.* Low bone mineral density and fractures are highly prevalent in pediatric patients with spinal muscular atrophy regardless of disease severity. *Neuromuscul Disord* **27**, 331–337 (2017).

433. Hensel, N. *et al.* Altered bone development with impaired cartilage formation precedes neuromuscular symptoms in spinal muscular atrophy. *Human Molecular Genetics* **29**, 2662–2673 (2020).

434. Nery, F. C. *et al.* Impaired kidney structure and function in spinal muscular atrophy. *Neurol Genet* **5**, (2019).

435. Allardyce, H. *et al.* Renal pathology in a mouse model of severe Spinal Muscular Atrophy is associated with downregulation of Glial Cell-Line Derived Neurotrophic Factor (GDNF). *Human Molecular Genetics* **29**, 2365–2378 (2020).

436. Hully, M. *et al.* Palliative Care in SMA Type 1: A Prospective Multicenter French Study Based on Parents' Reports. *Front Pediatr* **8**, (2020).

437. Wang, C. H. *et al.* Consensus statement for standard of care in spinal muscular atrophy. *J. Child Neurol.* **22**, 1027–1049 (2007).

438. Hardart, M. K. M., Burns, J. P. & Truog, R. D. Respiratory support in spinal muscular atrophy type I: a survey of physician practices and attitudes. *Pediatrics* **110**, e24 (2002).

439. Gillingwater, T. H. & Murray, L. M. How far away is spinal muscular atrophy gene therapy? *Expert Review of Neurotherapeutics* **15**, 965–968 (2015).

440. Faravelli, I., Nizzardo, M., Comi, G. P. & Corti, S. Spinal muscular atrophy—recent therapeutic advances for an old challenge. *Nature Reviews Neurology* **11**, 351–359 (2015).

441. Hua, Y., Vickers, T. A., Okunola, H. L., Bennett, C. F. & Krainer, A. R. Antisense masking of an hnRNP A1/A2 intronic splicing silencer corrects SMN2 splicing in transgenic mice. *Am. J. Hum. Genet.* **82**, 834–848 (2008).

442. Passini, M. A. *et al.* Antisense Oligonucleotides Delivered to the Mouse CNS Ameliorate Symptoms of Severe Spinal Muscular Atrophy. *Science Translational Medicine* **3**, 72ra18-72ra18 (2011).

443. Porensky, P. N. *et al.* A single administration of morpholino antisense oligomer rescues spinal muscular atrophy in mouse. *Hum Mol Genet* **21**, 1625–1638 (2012).

444. Hua, Y. *et al.* Antisense correction of SMN2 splicing in the CNS rescues necrosis in a type III SMA mouse model. *Genes Dev* **24**, 1634–1644 (2010).

445. Williams, J. H. *et al.* Oligonucleotide-mediated survival of motor neuron protein expression in CNS improves phenotype in a mouse model of spinal muscular atrophy. *J Neurosci* **29**, 7633–7638 (2009).

446. Rinaldi, C. & Wood, M. J. A. Antisense oligonucleotides: the next frontier for treatment of neurological disorders. *Nature Reviews Neurology* **14**, 9–21 (2018).

447. Gidaro, T. & Servais, L. Nusinersen treatment of spinal muscular atrophy: current knowledge and existing gaps. *Dev Med Child Neurol* **61**, 19–24 (2019).

448. Hoy, S. M. Nusinersen: First Global Approval. *Drugs* **77**, 473–479 (2017).

449. Min, H. S. *et al.* Systemic Brain Delivery of Antisense Oligonucleotides across the Blood–Brain Barrier with a Glucose-Coated Polymeric Nanocarrier. *Angewandte Chemie International Edition* **59**, 8173–8180 (2020).

450. Crawford, L., Rosch, J. & Putnam, D. Concepts, technologies, and practices for drug delivery past the blood–brain barrier to the central nervous system. *Journal of Controlled Release* **240**, 251–266 (2016).

451. Finkel, R. S. *et al.* Treatment of infantile-onset spinal muscular atrophy with nusinersen: a phase 2, open-label, dose-escalation study. *Lancet* **388**, 3017–3026 (2016).

452. Chiriboga, C. A. *et al.* Results from a phase 1 study of nusinersen (ISIS-SMNRx) in children with spinal muscular atrophy. *Neurology* **86**, 890–897 (2016).

453. SPINRAZA (nusinersen) injection, for intrathecal use. 13.

454. Finkel, R. S. *et al.* Nusinersen versus Sham Control in Infantile-Onset Spinal Muscular Atrophy. *New England Journal of Medicine* **377**, 1723–1732 (2017).

455. Mercuri, E. *et al.* Nusinersen versus Sham Control in Later-Onset Spinal Muscular Atrophy. *New England Journal of Medicine* **378**, 625–635 (2018).

456. De Vivo, D. C. *et al.* Nusinersen initiated in infants during the presymptomatic stage of spinal muscular atrophy: Interim efficacy and safety results from the Phase 2 NURTURE study. *Neuromuscul Disord* **29**, 842–856 (2019).

457. Osmanovic, A., Schreiber-Katz, O. & Petri, S. Nusinersen Wearing-Off in Adult 5q-Spinal Muscular Atrophy Patients. *Brain Sciences* **11**, 367 (2021).

458. Wurster, C. D. *et al.* Intrathecal administration of nusinersen in adolescent and adult SMA type 2 and 3 patients. *J. Neurol.* **266**, 183–194 (2019).

459. Jalali, A. *et al.* Cost-Effectiveness of Nusinersen and Universal Newborn Screening for Spinal Muscular Atrophy. *J Pediatr* **227**, 274-280.e2 (2020).

460. Fujak, A. *et al.* Natural course of scoliosis in proximal spinal muscular atrophy type II and IIIa: descriptive clinical study with retrospective data collection of 126 patients. *BMC Musculoskelet Disord* **14**, 283 (2013).

461. Rodillo, E., Marini, M. L., Heckmatt, J. Z. & Dubowitz, V. Scoliosis in Spinal Muscular Atrophy: Review of 63 Cases. *J Child Neurol* **4**, 118–123 (1989).

462. Nakao, S. *et al.* Intrathecal administration of nusinersen for spinal muscular atrophy: report of three cases with severe spinal deformity. *JA Clinical Reports* **6**, 28 (2020).

463. Lowes, L. *et al.* AVXS-101 phase 1 gene therapy clinical trial in SMA Type 1: patients treated early with the proposed therapeutic dose were able to sit unassisted at a younger age. *Neuromuscular Disorders* **27**, S208–S209 (2017).

464. Foust, K. D. *et al.* Rescue of the spinal muscular atrophy phenotype in a mouse model by early postnatal delivery of SMN. *Nat Biotechnol* **28**, 271–274 (2010).

465. McCarty, D. M., Monahan, P. E. & Samulski, R. J. Self-complementary recombinant adeno-associated virus (scAAV) vectors promote efficient transduction independently of DNA synthesis. *Gene Therapy* **8**, 1248–1254 (2001).

466. Commissioner, O. of the. FDA approves innovative gene therapy to treat pediatric patients with spinal muscular atrophy, a rare disease and leading genetic cause of infant

mortality. *FDA* https://www.fda.gov/news-events/press-announcements/fda-approves-innovative-gene-therapy-treat-pediatric-patients-spinal-muscular-atrophy-rare-disease (2020).

467. Merkel, S. F. *et al.* Trafficking of adeno-associated virus vectors across a model of the blood-brain barrier; a comparative study of transcytosis and transduction using primary human brain endothelial cells. *J Neurochem* **140**, 216–230 (2017).

468. Armbruster, N. *et al.* Efficacy and biodistribution analysis of intracerebroventricular administration of an optimized scAAV9-SMN1 vector in a mouse model of spinal muscular atrophy. *Mol Ther Methods Clin Dev* **3**, 16060 (2016).

469. Besse, A. *et al.* AAV9-Mediated Expression of SMN Restricted to Neurons Does Not Rescue the Spinal Muscular Atrophy Phenotype in Mice. *Molecular Therapy* **28**, 1887–1901 (2020).

470. Mendell, J. R. *et al.* Single-Dose Gene-Replacement Therapy for Spinal Muscular Atrophy. *New England Journal of Medicine* **377**, 1713–1722 (2017).

471. Lowes, L. P. *et al.* Impact of Age and Motor Function in a Phase 1/2A Study of Infants With SMA Type 1 Receiving Single-Dose Gene Replacement Therapy. *Pediatr Neurol* **98**, 39–45 (2019).

472. Mendell, J. R. *et al.* Five-Year Extension Results of the Phase 1 START Trial of Onasemnogene Abeparvovec in Spinal Muscular Atrophy. *JAMA Neurol* (2021) doi:10.1001/jamaneurol.2021.1272.

473. Shell, R. *et al.* S61 Onasemnogene abeparvovec gene-replacement therapy (GRT) for spinal muscular atrophy type 1 (SMA1): preliminary pulmonary and ventilatory findings from the phase 3 study (STR1VE). *Thorax* **74**, A42–A42 (2019).

474. Finkel, R. S. *et al.* S12 Onasemnogene abeparvovec gene therapy for spinal muscular atrophy type 1: phase 3 study (STR1VE-US). *Thorax* **76**, A10–A11 (2021).

475. Strauss, K. A. *et al.* Onasemnogene Abeparvovec-xioi Gene-Replacement Therapy in Presymptomatic Spinal Muscular Atrophy: SPR1NT Study Update (2384). *Neurology* **94**, (2020).

476. Novartis announces AVXS-101 intrathecal study update. *Novartis* https://www.novartis.com/news/media-releases/novartis-announces-avxs-101-intrathecal-study-update.

477. Kim, H. C. *et al.* Normal serum aminotransferase concentration and risk of mortality from liver diseases: prospective cohort study. *BMJ* **328**, 983 (2004).

478. Prabhu, N. *et al.* Thrombotic Microangiopathy (TMA): A potential adverse reaction post Zolgensma (onasemnogene abeparvovec-xioi) therapy for Spinal Muscular Atrophy (SMA) (5483). *Neurology* **94**, (2020).

479. Van Alstyne, M. *et al.* Gain of toxic function by long-term AAV9-mediated SMN overexpression in the sensorimotor circuit. *Nature Neuroscience* 1–11 (2021) doi:10.1038/s41593-021-00827-3.

480. Boutin, S. *et al.* Prevalence of serum IgG and neutralizing factors against adeno-associated virus (AAV) types 1, 2, 5, 6, 8, and 9 in the healthy population: implications for gene therapy using AAV vectors. *Hum Gene Ther* **21**, 704–712 (2010).

481. Dyer, O. Health ministers condemn Novartis lottery for Zolgensma, the world's most expensive drug. *BMJ* **368**, m580 (2020).

482. Dhillon, S. Risdiplam: First Approval. *Drugs* **80**, 1853–1858 (2020).

483. Singh, R. N., Ottesen, E. W. & Singh, N. N. The First Orally Deliverable Small Molecule for the Treatment of Spinal Muscular Atrophy. *J Exp Neurosci* **15**, 2633105520973985 (2020).

484. Poirier, A. *et al.* Risdiplam distributes and increases SMN protein in both the central nervous system and peripheral organs. *Pharmacol Res Perspect* **6**, (2018).

485. Naryshkin, N. A. *et al.* SMN2 splicing modifiers improve motor function and longevity in mice with spinal muscular atrophy. *Science* **345**, 688–693 (2014).

486. Ratni, H. *et al.* Specific Correction of Alternative Survival Motor Neuron 2 Splicing by Small Molecules: Discovery of a Potential Novel Medicine To Treat Spinal Muscular Atrophy. *J Med Chem* **59**, 6086–6100 (2016).

487. Kletzl, H. *et al.* The oral splicing modifier RG7800 increases full length survival of motor neuron 2 mRNA and survival of motor neuron protein: Results from trials in healthy adults and patients with spinal muscular atrophy. *Neuromuscular Disorders* **29**, 21–29 (2019).

488. Ratni, H. *et al.* Discovery of Risdiplam, a Selective Survival of Motor Neuron-2 (SMN2) Gene Splicing Modifier for the Treatment of Spinal Muscular Atrophy (SMA). *J. Med. Chem.* 17 (2018).

489. Sturm, S. *et al.* A phase 1 healthy male volunteer single escalating dose study of the pharmacokinetics and pharmacodynamics of risdiplam (RG7916, RO7034067), a SMN2 splicing modifier. *Br J Clin Pharmacol* **85**, 181–193 (2019).

490. Baranello, G. *et al.* P.353FIREFISH Part 1: 16-month safety and exploratory outcomes of risdiplam (RG7916) treatment in infants with type 1 spinal muscular atrophy. *Neuromuscular Disorders* **29**, S184 (2019).

491. Servais, L. *et al.* FIREFISH Part 2: Efficacy and Safety of Risdiplam (RG7916) in Infants with Type 1 Spinal Muscular Atrophy (SMA) (1302). *Neurology* **94**, (2020).

492. Mercuri, E. *et al.* Update from SUNFISH Part 1: Safety, Tolerability and PK/PD from the Dose-Finding Study, Including Exploratory Efficacy Data in Patients with Type 2 or 3 Spinal Muscular Atrophy (SMA) Treated with Risdiplam (RG7916) (S25.007). *Neurology* **92**, (2019).

493. Mercuri, E. *et al.* SUNFISH Part 2: Efficacy and Safety of Risdiplam (RG7916) in Patients with Type 2 or Non-Ambulant Type 3 Spinal Muscular Atrophy (SMA) (1260). *Neurology* **94**, (2020).

494. Wang, J., Schultz, P. G. & Johnson, K. A. Mechanistic studies of a small-molecule modulator of SMN2 splicing. *PNAS* **115**, E4604–E4612 (2018).

495. Ojala, K. S., Reedich, E. J., DiDonato, C. J. & Meriney, S. D. In Search of a Cure: The Development of Therapeutics to Alter the Progression of Spinal Muscular Atrophy. *Brain Sci* **11**, (2021).

496. Serra-Juhe, C. & Tizzano, E. F. Perspectives in genetic counseling for spinal muscular atrophy in the new therapeutic era: early pre-symptomatic intervention and test in minors. *Eur J Hum Genet* **27**, 1774–1782 (2019).

497. Dangouloff, T. & Servais, L. Clinical Evidence Supporting Early Treatment Of Patients With Spinal Muscular Atrophy: Current Perspectives. *Ther Clin Risk Manag* **15**, 1153–1161 (2019).

498. Matesanz, S. E., Battista, V., Flickinger, J., Jones, J. N. & Kichula, E. A. Clinical Experience With Gene Therapy in Older Patients With Spinal Muscular Atrophy. *Pediatric Neurology* **118**, 1–5 (2021).

499. Monnette, A. *et al.* Treatment preference among patients with spinal muscular atrophy (SMA): a discrete choice experiment. *Orphanet Journal of Rare Diseases* **16**, 36 (2021).

500. Veerapandiyan, A. *et al.* Nusinersen for older patients with spinal muscular atrophy: A real-world clinical setting experience. *Muscle Nerve* **61**, 222–226 (2020).

501. Poletti, A. & Fischbeck, K. H. Combinatorial treatment for spinal muscular atrophy. *Journal of Neurochemistry* **153**, 146–149 (2020).

502. Long, K. K. *et al.* Specific inhibition of myostatin activation is beneficial in mouse models of SMA therapy. *Hum Mol Genet* **28**, 1076–1089 (2019).

503. Dagbay, K. B. *et al.* Structural basis of specific inhibition of extracellular activation of pro- or latent myostatin by the monoclonal antibody SRK-015. *J Biol Chem* **295**, 5404–5418 (2020).

504. Pirruccello-Straub, M. *et al.* Blocking extracellular activation of myostatin as a strategy for treating muscle wasting. *Sci Rep* **8**, (2018).

505. Ac, M., Am, L. & Sj, L. Regulation of skeletal muscle mass in mice by a new TGF-beta superfamily member. *Nature* vol. 387 https://pubmed.ncbi.nlm.nih.gov/9139826/?dopt=Abstract (1997).

506. Reisz-Porszasz, S. *et al.* Lower skeletal muscle mass in male transgenic mice with muscle-specific overexpression of myostatin. *Am J Physiol Endocrinol Metab* **285**, E876-888 (2003).

507. Lee, S.-J. & McPherron, A. C. Regulation of myostatin activity and muscle growth. *PNAS* **98**, 9306–9311 (2001).

508. Anderson, S. B., Goldberg, A. L. & Whitman, M. Identification of a novel pool of extracellular pro-myostatin in skeletal muscle. *J Biol Chem* **283**, 7027–7035 (2008).

509. Thies, R. S. *et al.* GDF-8 propeptide binds to GDF-8 and antagonizes biological activity by inhibiting GDF-8 receptor binding. *Growth Factors* **18**, 251–259 (2001).

510. Wolfman, N. M. *et al.* Activation of latent myostatin by the BMP-1/tolloid family of metalloproteinases. *PNAS* **100**, 15842–15846 (2003).

511. Rebbapragada, A., Benchabane, H., Wrana, J. L., Celeste, A. J. & Attisano, L. Myostatin Signals through a Transforming Growth Factor β-Like Signaling Pathway To Block Adipogenesis. *Molecular and Cellular Biology* **23**, 7230–7242 (2003).

512. Pasteuning-Vuhman, S. *et al.* New function of the myostatin/activin type I receptor (ALK4) as a mediator of muscle atrophy and muscle regeneration. *FASEB J* **31**, 238–255 (2017).

513. Sartori, R. *et al.* Smad2 and 3 transcription factors control muscle mass in adulthood. *Am J Physiol Cell Physiol* **296**, C1248-1257 (2009).

514. McFarlane, C. *et al.* Myostatin induces cachexia by activating the ubiquitin proteolytic system through an NF-κB-independent, FoxO1-dependent mechanism. *Journal of Cellular Physiology* **209**, 501–514 (2006).

515. Allen, D. L. & Unterman, T. G. Regulation of myostatin expression and myoblast differentiation by FoxO and SMAD transcription factors. *American Journal of Physiology-Cell Physiology* **292**, C188–C199 (2007).

516. Lokireddy, S. *et al.* Myostatin promotes the wasting of human myoblast cultures through promoting ubiquitin-proteasome pathway-mediated loss of sarcomeric proteins. *American Journal of Physiology-Cell Physiology* **301**, C1316–C1324 (2011).

517. Trendelenburg, A. U. *et al.* Myostatin reduces Akt/TORC1/p70S6K signaling, inhibiting myoblast differentiation and myotube size. *American Journal of Physiology-Cell Physiology* **296**, C1258–C1270 (2009).

518. Costelli, P. *et al.* Muscle myostatin signalling is enhanced in experimental cancer cachexia. *Eur J Clin Invest* **38**, 531–538 (2008).

519. Kobayashi, M., Kasamatsu, S., Shinozaki, S., Yasuhara, S. & Kaneki, M. Myostatin deficiency not only prevents muscle wasting but also improves survival in septic mice. *American Journal of Physiology-Endocrinology and Metabolism* **320**, E150–E159 (2020).

520. Wagner, K. R., McPherron, A. C., Winik, N. & Lee, S.-J. Loss of myostatin attenuates severity of muscular dystrophy in mdx mice. *Ann Neurol* **52**, 832–836 (2002).

521. Bogdanovich, S., McNally, E. M. & Khurana, T. S. Myostatin blockade improves function but not histopathology in a murine model of limb-girdle muscular dystrophy 2C. *Muscle Nerve* **37**, 308–316 (2008).

522. Parsons, S. A., Millay, D. P., Sargent, M. A., McNally, E. M. & Molkentin, J. D. Age-Dependent Effect of Myostatin Blockade on Disease Severity in a Murine Model of Limb-Girdle Muscular Dystrophy. *Am J Pathol* **168**, 1975–1985 (2006).

523. Holzbaur, E. L. F. *et al.* Myostatin inhibition slows muscle atrophy in rodent models of amyotrophic lateral sclerosis. *Neurobiology of Disease* **23**, 697–707 (2006).

524. Walsh, F. S. & Rutkowski, J. L. Myostatin as a therapeutic target in Amyotrophic Lateral Sclerosis. *Neurochemistry International* **61**, 931–935 (2012).

525. Siriett, V. *et al.* Prolonged absence of myostatin reduces sarcopenia. *J Cell Physiol* **209**, 866–873 (2006).

526. Bergen, H. R. *et al.* Myostatin as a mediator of sarcopenia versus homeostatic regulator of muscle mass: insights using a new mass spectrometry-based assay. *Skeletal Muscle* **5**, 21 (2015).

527. Dial, A. G. *et al.* Muscle and serum myostatin expression in type 1 diabetes. *Physiol Rep* **8**, (2020).

528. McPherron, A. C. & Lee, S.-J. Double muscling in cattle due to mutations in the myostatin gene. *PNAS* **94**, 12457–12461 (1997).

529. Mosher, D. S. *et al.* A Mutation in the Myostatin Gene Increases Muscle Mass and Enhances Racing Performance in Heterozygote Dogs. *PLOS Genetics* **3**, e79 (2007).

530. Schuelke, M. *et al.* Myostatin Mutation Associated with Gross Muscle Hypertrophy in a Child. *New England Journal of Medicine* **350**, 2682–2688 (2004).

531. Rose, F. F., Mattis, V. B., Rindt, H. & Lorson, C. L. Delivery of recombinant follistatin lessens disease severity in a mouse model of spinal muscular atrophy. *Hum Mol Genet* **18**, 997–1005 (2009).

532. Sumner, C. J. *et al.* Inhibition of myostatin does not ameliorate disease features of severe spinal muscular atrophy mice. *Hum Mol Genet* **18**, 3145–3152 (2009).

533. Liu, M., Hammers, D. W., Barton, E. R. & Sweeney, H. L. Activin Receptor Type IIB Inhibition Improves Muscle Phenotype and Function in a Mouse Model of Spinal Muscular Atrophy. *PLoS One* **11**, (2016).

534. Kota, J. *et al.* Follistatin Gene Delivery Enhances Muscle Growth and Strength in Nonhuman Primates. *Sci Transl Med* **1**, 6ra15 (2009).

535. Morrison, B. M. *et al.* A soluble activin type IIB receptor improves function in a mouse model of amyotrophic lateral sclerosis. *Experimental Neurology* **217**, 258–268 (2009).

536. St Andre, M. *et al.* A mouse anti-myostatin antibody increases muscle mass and improves muscle strength and contractility in the mdx mouse model of Duchenne muscular dystrophy and its humanized equivalent, domagrozumab (PF-06252616), increases muscle volume in cynomolgus monkeys. *Skelet Muscle* **7**, 25 (2017).

537. Lee, S.-J. *et al.* Regulation of muscle growth by multiple ligands signaling through activin type II receptors. *Proc Natl Acad Sci U S A* **102**, 18117–18122 (2005).

538. Schneyer, A. L. *et al.* Differential antagonism of activin, myostatin and growth and differentiation factor 11 by wild-type and mutant follistatin. *Endocrinology* **149**, 4589–4595 (2008).

539. Asari, T. *et al.* Structural Basis for the Effective Myostatin Inhibition of the Mouse Myostatin Prodomain-Derived Minimum Peptide. *ACS Med Chem Lett* **8**, 113–117 (2016).

540. Cotton, T. R. *et al.* Structure of the human myostatin precursor and determinants of growth factor latency. *EMBO J* **37**, 367–383 (2018).

541. Yang, J. *et al.* Expression of myostatin pro domain results in muscular transgenic mice. *Mol Reprod Dev* **60**, 351–361 (2001).

542. Welsh, B. T. *et al.* Preclinical Safety Assessment and Toxicokinetics of Apitegromab, an Antibody Targeting Proforms of Myostatin for the Treatment of Muscle-Atrophying Disease. *Int J Toxicol* **40**, 322–336 (2021).

543. Mariot, V. *et al.* Downregulation of myostatin pathway in neuromuscular diseases may explain challenges of anti-myostatin therapeutic approaches. *Nature Communications* **8**, 1859 (2017).

544. Barrett, D. *et al.* A Randomized Phase 1 Safety, Pharmacokinetic and Pharmacodynamic Study of the Novel Myostatin Inhibitor Apitegromab (SRK-015): A Potential Treatment for Spinal Muscular Atrophy. *Adv Ther* (2021) doi:10.1007/s12325-021-01757-z.

545. Place, A. A Phase 2 Study to Evaluate the Efficacy and Safety of SRK-015 in Patients with Later-Onset Spinal Muscular Atrophy (TOPAZ): An Introduction (4534). *Neurology* **94**, (2020).

546. Hwee, D. T. *et al.* The Small-Molecule Fast Skeletal Troponin Activator, CK-2127107, Improves Exercise Tolerance in a Rat Model of Heart Failure. *J Pharmacol Exp Ther* **353**, 159–168 (2015).

547. Andrews, J. A. *et al.* CK-2127107 amplifies skeletal muscle response to nerve activation in humans. *Muscle Nerve* **57**, 729–734 (2018).

548. EBASHI, S. & KODAMA, A. A New Protein Factor Promoting Aggregation of Tropomyosin. *The Journal of Biochemistry* **58**, 107–108 (1965).

549. EBASHI, S. & KODAMA, A. Interaction of Troponin with F-Actin in the Presence of Tropomyosin. *The Journal of Biochemistry* **59**, 425–426 (1966).

550. Gomes, A. V., Potter, J. D. & Szczesna-Cordary, D. The Role of Troponins in Muscle Contraction. *IUBMB Life* **54**, 323–333 (2002).

551. Zierath, J. R. & Hawley, J. A. Skeletal Muscle Fiber Type: Influence on Contractile and Metabolic Properties. *PLoS Biol* **2**, (2004).

552. Yang, Z., Yamazaki, M., Shen, Q. W. & Swartz, D. R. Differences between Cardiac and Skeletal Troponin Interaction with the Thin Filament Probed by Troponin Exchange in Skeletal Myofibrils. *Biophys J* **97**, 183–194 (2009).

553. Sheng, J.-J. & Jin, J.-P. TNNI1, TNNI2 and TNNI3: Evolution, Regulation, and Protein Structure-Function Relationships. *Gene* **576**, 385–394 (2016).

554. Wei, B. & Jin, J.-P. TNNT1, TNNT2, and TNNT3: Isoform genes, regulation, and structure-function relationships. *Gene* **582**, 1–13 (2016).

555. Schreier, T., Kedes, L. & Gahlmann, R. Cloning, structural analysis, and expression of the human slow twitch skeletal muscle/cardiac troponin C gene. *J. Biol. Chem.* **265**, 21247–21253 (1990).

556. Gahlmann, R. & Kedes, L. Cloning, structural analysis, and expression of the human fast twitch skeletal muscle troponin C gene. *J. Biol. Chem.* **265**, 12520–12528 (1990).

557. Takeda, S., Yamashita, A., Maeda, K. & Maéda, Y. Structure of the core domain of human cardiac troponin in the Ca 2+ -saturated form. *Nature* **424**, 35–41 (2003).

558. Farah, C. S. *et al.* Structural and regulatory functions of the NH2- and COOH-terminal regions of skeletal muscle troponin I. *Journal of Biological Chemistry* **269**, 5230–5240 (1994).

559. Chen, Y.-C., Sumandea, M. P., Larsson, L., Moss, R. L. & Ge, Y. Dissecting Human Skeletal Muscle Troponin Proteoforms by Top-down Mass Spectrometry. *J Muscle Res Cell Motil* **36**, 169–181 (2015).

560. Farah, C. S. & Reinach, F. C. The troponin complex and regulation of muscle contraction. *The FASEB Journal* **9**, 755–767 (1995).

561. Malik, N. A., Anantharamaiah, G. M., Gawish, A. & Cheung, H. C. Structural and biological studies on synthetic peptide analogues of a low-affinity calcium-binding site of skeletal troponin C. *Biochim Biophys Acta* **911**, 221–230 (1987).

562. Szczesna, D. *et al.* The role of the four Ca2+ binding sites of troponin C in the regulation of skeletal muscle contraction. *J Biol Chem* **271**, 8381–8386 (1996).

563. Kischel, P., Bastide, B., Potter, J. D. & Mounier, Y. The role of the Ca2+ regulatory sites of skeletal troponin C in modulating muscle fibre reactivity to the Ca2+ sensitizer bepridil. *Br J Pharmacol* **131**, 1496–1502 (2000).

564. Zsolnay, V., Fill, M. & Gillespie, D. Sarcoplasmic Reticulum Ca2+ Release Uses a Cascading Network of Intra-SR and Channel Countercurrents. *Biophys J* **114**, 462–473 (2018).

565. Inui, M., Saito, A. & Fleischer, S. Purification of the ryanodine receptor and identity with feet structures of junctional terminal cisternae of sarcoplasmic reticulum from fast skeletal muscle. *Journal of Biological Chemistry* **262**, 1740–1747 (1987).

566. Gillespie, D. & Fill, M. Intracellular calcium release channels mediate their own countercurrent: the ryanodine receptor case study. *Biophys J* **95**, 3706–3714 (2008).

567. Chin, E. R. Intracellular Ca2+ signaling in skeletal muscle: decoding a complex message. *Exerc Sport Sci Rev* **38**, 76–85 (2010).

568. Pandey, R. *et al.* Central core myopathy with RYR1 mutation masks 5q spinal muscular atrophy. *Eur J Paediatr Neurol* **15**, 70–73 (2011).

569. Russell, A. J. *et al.* Activation of fast skeletal muscle troponin as a potential therapeutic approach for treating neuromuscular diseases. *Nat Med* **18**, 452–455 (2012).

570. Sanders, D. B., Rosenfeld, J., Dimachkie, M. M., Meng, L. & Malik, F. I. A Double-Blinded, Randomized, Placebo-Controlled Trial to Evaluate Efficacy, Safety, and Tolerability of Single Doses of Tirasemtiv in Patients with Acetylcholine Receptor-Binding Antibody-Positive Myasthenia Gravis. *Neurotherapeutics* **12**, 455–460 (2015).

571. Hwee, D. T. *et al.* Fast Skeletal Muscle Troponin Activator tirasemtiv Increases Muscle Function and Performance in the B6SJL-SOD1G93A ALS Mouse Model. *PLOS ONE* **9**, e96921 (2014).

572. Rudnicki, S. A. *et al.* Reldesemtiv in Patients with Spinal Muscular Atrophy: a Phase 2 Hypothesis-Generating Study. *Neurotherapeutics* (2021) doi:10.1007/s13311-020-01004-3.

573. Dickson, M. & Gagnon, J. P. The cost of new drug discovery and development. *Discov Med* **4**, 172–179 (2004).

574. McNamee, L. M., Walsh, M. J. & Ledley, F. D. Timelines of translational science: From technology initiation to FDA approval. *PLoS One* **12**, (2017).

575. Blin, O., Lefebvre, M.-N., Rascol, O. & Micallef, J. Orphan drug clinical development. *Therapies* **75**, 141–147 (2020).

576. Micallef, J. & Blin, O. Orphan drug designation in Europe: A booster for the research and development of drugs in rare diseases. *Therapies* **75**, 133–139 (2020).

577. Herder, M. What Is the Purpose of the Orphan Drug Act? *PLoS Med* **14**, (2017).

578. Clinical Trial Success Rates by Phase and Therapeutic Area. *American Council on Science and Health* https://www.acsh.org/news/2020/06/11/clinical-trial-success-rates-phase-and-therapeutic-area-14845 (2020).

579. Hay, M., Thomas, D. W., Craighead, J. L., Economides, C. & Rosenthal, J. Clinical development success rates for investigational drugs. *Nature Biotechnology* **32**, 40–51 (2014).

580. Hingorani, A. D. *et al.* Improving the odds of drug development success through human genomics: modelling study. *Scientific Reports* **9**, 18911 (2019).

581. Sunyach, C. *et al.* Olesoxime delays muscle denervation, astrogliosis, microglial activation and motoneuron death in an ALS mouse model. *Neuropharmacology* **62**, 2346–2352 (2012).

582. Bertini, E. *et al.* Safety and efficacy of olesoxime in patients with type 2 or non-ambulatory type 3 spinal muscular atrophy: a randomised, double-blind, placebo-controlled phase 2 trial. *Lancet Neurol* **16**, 513–522 (2017).

583. Muntoni, F. *et al.* Long-term follow-up of patients with type 2 and non-ambulant type 3 spinal muscular atrophy (SMA) treated with olesoxime in the OLEOS trial. *Neuromuscular Disorders* **30**, 959–969 (2020).

584. Angelis, A., Tordrup, D. & Kanavos, P. Socio-economic burden of rare diseases: A systematic review of cost of illness evidence. *Health Policy* **119**, 964–979 (2015).

585. Wouters, O. J., McKee, M. & Luyten, J. Estimated Research and Development Investment Needed to Bring a New Medicine to Market, 2009-2018. *JAMA* **323**, 844–853 (2020).

586. Rudrapal, M., Khairnar, S. J. & Jadhav, A. G. Drug Repurposing (DR): An Emerging Approach in Drug Discovery. *Drug Repurposing - Hypothesis, Molecular Aspects and Therapeutic Applications* (2020) doi:10.5772/intechopen.93193.

587. Talevi, A. & Bellera, C. L. Challenges and opportunities with drug repurposing: finding strategies to find alternative uses of therapeutics. *Expert Opinion on Drug Discovery* **15**, 397–401 (2020).

588. Menduti, G., Rasà, D. M., Stanga, S. & Boido, M. Drug Screening and Drug Repositioning as Promising Therapeutic Approaches for Spinal Muscular Atrophy Treatment. *Front. Pharmacol.* **11**, (2020).

589. Hoolachan, J. M., Sutton, E. R. & Bowerman, M. Teaching an old drug new tricks: repositioning strategies for spinal muscular atrophy. *Future Neurology* **14**, FNL25 (2019).

590. Ashburn, T. T. & Thor, K. B. Drug repositioning: identifying and developing new uses for existing drugs. *Nature Reviews Drug Discovery* **3**, 673–683 (2004).

591. Jin, G. & Wong, S. T. C. Toward better drug repositioning: prioritizing and integrating existing methods into efficient pipelines. *Drug Discov Today* **19**, 637–644 (2014).

592. Allarakhia, M. Open-source approaches for the repurposing of existing or failed candidate drugs: learning from and applying the lessons across diseases. *Drug Des Devel Ther* **7**, 753–766 (2013).

593. Cha, Y. *et al.* Drug repurposing from the perspective of pharmaceutical companies. *Br J Pharmacol* **175**, 168–180 (2018).

594. Mohseni, J., Zabidi-Hussin, Z. a. M. H. & Sasongko, T. H. Histone deacetylase inhibitors as potential treatment for spinal muscular atrophy. *Genet Mol Biol* **36**, 299–307 (2013).

595. Kernochan, L. E. *et al.* The role of histone acetylation in SMN gene expression. *Hum Mol Genet* **14**, 1171–1182 (2005).

596. Xu, W. S., Parmigiani, R. B. & Marks, P. A. Histone deacetylase inhibitors: molecular mechanisms of action. *Oncogene* **26**, 5541–5552 (2007).

597. Chang, J.-G. *et al.* Treatment of spinal muscular atrophy by sodium butyrate. *Proc Natl Acad Sci U S A* **98**, 9808–9813 (2001).

598. Andreassi, C. *et al.* Phenylbutyrate increases SMN expression in vitro: relevance for treatment of spinal muscular atrophy. *Eur J Hum Genet* **12**, 59–65 (2004).

599. Brichta, L. *et al.* Valproic acid increases the SMN2 protein level: a well-known drug as a potential therapy for spinal muscular atrophy. *Hum Mol Genet* **12**, 2481–2489 (2003).

600. Sumner, C. J. *et al.* Valproic acid increases SMN levels in spinal muscular atrophy patient cells. *Ann Neurol* **54**, 647–654 (2003).

601. Harahap, I. S. K. *et al.* Valproic acid increases SMN2 expression and modulates SF2/ASF and hnRNPA1 expression in SMA fibroblast cell lines. *Brain Dev* **34**, 213–222 (2012).

602. Hahnen, E. *et al.* In vitro and ex vivo evaluation of second-generation histone deacetylase inhibitors for the treatment of spinal muscular atrophy. *J Neurochem* **98**, 193–202 (2006).

603. Avila, A. M. *et al.* Trichostatin A increases SMN expression and survival in a mouse model of spinal muscular atrophy. *J Clin Invest* **117**, 659–671 (2007).

604. Narver, H. L. *et al.* Sustained improvement of spinal muscular atrophy mice treated with trichostatin A plus nutrition. *Ann Neurol* **64**, 465–470 (2008).

605. Liu, H., Yazdani, A., Murray, L. M., Beauvais, A. & Kothary, R. The Smn-Independent Beneficial Effects of Trichostatin A on an Intermediate Mouse Model of Spinal Muscular Atrophy. *PLoS One* **9**, (2014).

606. Tsai, L.-K., Tsai, M.-S., Ting, C.-H. & Li, H. Multiple therapeutic effects of valproic acid in spinal muscular atrophy model mice. *J Mol Med (Berl)* **86**, 1243–1254 (2008).

607. Mercuri, E. *et al.* Pilot trial of phenylbutyrate in spinal muscular atrophy. *Neuromuscul Disord* **14**, 130–135 (2004).

608. Rak, K. *et al.* Valproic acid blocks excitability in SMA type I mouse motor neurons. *Neurobiol Dis* **36**, 477–487 (2009).

609. Kissel, J. T. *et al.* SMA CARNI-VAL TRIAL PART II: A Prospective, Single-Armed Trial of L-Carnitine and Valproic Acid in Ambulatory Children with Spinal Muscular Atrophy. *PLoS One* **6**, (2011).

610. Krosschell, K. J. *et al.* Clinical trial of L-Carnitine and valproic acid in spinal muscular atrophy type I. *Muscle Nerve* **57**, 193–199 (2018).

611. Kissel, J. T. *et al.* SMA valiant trial: a prospective, double-blind, placebo-controlled trial of valproic acid in ambulatory adults with spinal muscular atrophy. *Muscle Nerve* **49**, 187–192 (2014).

612. Swoboda, K. J. *et al.* Phase II Open Label Study of Valproic Acid in Spinal Muscular Atrophy. *PLOS ONE* **4**, e5268 (2009).

613. Pagliarini, V., Guerra, M., Di Rosa, V., Compagnucci, C. & Sette, C. Combined treatment with the histone deacetylase inhibitor LBH589 and a splice-switch antisense oligonucleotide enhances SMN2 splicing and SMN expression in Spinal Muscular Atrophy cells. *J Neurochem* **153**, 264–275 (2020).

614. Gong, L. *et al.* Celecoxib pathways: pharmacokinetics and pharmacodynamics. *Pharmacogenet Genomics* **22**, 310–318 (2012).

615. Farooq, F. *et al.* Celecoxib increases SMN and survival in a severe spinal muscular atrophy mouse model via p38 pathway activation. *Hum. Mol. Genet.* **22**, 3415–3424 (2013).

616. Martinez, A., Alonso, M., Castro, A., Pérez, C. & Moreno, F. J. First non-ATP competitive glycogen synthase kinase 3 beta (GSK-3beta) inhibitors: thiadiazolidinones (TDZD) as potential drugs for the treatment of Alzheimer's disease. *J Med Chem* **45**, 1292–1299 (2002).

617. Ochalek, A. *et al.* Neurons derived from sporadic Alzheimer's disease iPSCs reveal elevated TAU hyperphosphorylation, increased amyloid levels, and GSK3B activation. *Alzheimers Res Ther* **9**, 90 (2017).

618. Lovestone, S. *et al.* A phase II trial of tideglusib in Alzheimer's disease. *J Alzheimers Dis* **45**, 75–88 (2015).

619. Jacobs, K. M. *et al.* GSK-3β: A Bifunctional Role in Cell Death Pathways. *Int J Cell Biol* **2012**, (2012).

620. Maurer, M. H. *et al.* Glycogen synthase kinase 3beta (GSK3beta) regulates differentiation and proliferation in neural stem cells from the rat subventricular zone. *J Proteome Res* **6**, 1198–1208 (2007).

621. Verhees, K. J. P. *et al.* Glycogen synthase kinase-3β is required for the induction of skeletal muscle atrophy. *Am J Physiol Cell Physiol* **301**, C995–C1007 (2011).

622. van der Velden, J. L. J. *et al.* Myogenic differentiation during regrowth of atrophied skeletal muscle is associated with inactivation of GSK-3beta. *Am J Physiol Cell Physiol* **292**, C1636-1644 (2007).

623. van der Velden, J. L. J. *et al.* Inhibition of glycogen synthase kinase-3beta activity is sufficient to stimulate myogenic differentiation. *Am J Physiol Cell Physiol* **290**, C453-462 (2006).

624. Horrigan, J. *et al.* A Phase 2 Study of AMO-02 (Tideglusib) in Congenital and Childhood-Onset Myotonic Dystrophy Type 1 (DM1). *Pediatr Neurol* **112**, 84–93 (2020).

625. Vandewalle, J., Luypaert, A., Bosscher, K. D. & Libert, C. Therapeutic Mechanisms of Glucocorticoids. *Trends in Endocrinology & Metabolism* **29**, 42–54 (2018).

626. Cruz-Topete, D. & Cidlowski, J. A. One Hormone Two Actions: Anti- and Pro-inflammatory Effects of Glucocorticoids. *Neuroimmunomodulation* **22**, 20–32 (2015).

627. Matthews, E., Brassington, R., Kuntzer, T., Jichi, F. & Manzur, A. Y. Corticosteroids for the treatment of Duchenne muscular dystrophy. *Cochrane Database of Systematic Reviews* **13**, (2016).

628. Oray, M., Abu Samra, K., Ebrahimiadib, N., Meese, H. & Foster, C. S. Long-term side effects of glucocorticoids. *Expert Opin Drug Saf* **15**, 457–465 (2016).

629. Ricotti, V. *et al.* Long-term benefits and adverse effects of intermittent versus daily glucocorticoids in boys with Duchenne muscular dystrophy. *J Neurol Neurosurg Psychiatry* **84**, 698–705 (2013).

630. Quattrocelli, M. *et al.* Intermittent glucocorticoid steroid dosing enhances muscle repair without eliciting muscle atrophy. *J Clin Invest* **127**, 2418–2432 (2017).

631. Bulfield, G., Siller, W. G., Wight, P. A. & Moore, K. J. X chromosome-linked muscular dystrophy (mdx) in the mouse. *Proc Natl Acad Sci U S A* **81**, 1189–1192 (1984).

632. Beenakker, E. A. C. *et al.* Intermittent Prednisone Therapy in Duchenne Muscular Dystrophy: A Randomized Controlled Trial. *Arch Neurol* **62**, 128–132 (2005).

633. McMillan, H. J. Intermittent glucocorticoid regimes for younger boys with duchenne muscular dystrophy: Balancing efficacy with side effects. *Muscle & Nerve* **59**, 638–639 (2019).

634. Mendell, J. R. *et al.* Randomized, Double-Blind Six-Month Trial of Prednisone in Duchenne's Muscular Dystrophy. *New England Journal of Medicine* **320**, 1592–1597 (1989).

635. Morrison-Nozik, A. *et al.* Glucocorticoids enhance muscle endurance and ameliorate Duchenne muscular dystrophy through a defined metabolic program. *Proc Natl Acad Sci U S A* **112**, E6780–E6789 (2015).

636. Quattrocelli, M. *et al.* Intermittent Glucocorticoid Dosing Improves Muscle Repair and Function in Mice with Limb-Girdle Muscular Dystrophy. *Am J Pathol* **187**, 2520–2535 (2017).

637. Baehr, L. M., Waddell, D. S., Yang, H. Y., Furlow, J. D. & Bodine, S. C. Upregulation of FOXO1 and FOXO3a Following Denervation and Dexamethasone Treatment. *The FASEB Journal* **21**, A1308–A1308 (2007).

638. Goecks, J., Nekrutenko, A., Taylor, J., & Galaxy Team. Galaxy: a comprehensive approach for supporting accessible, reproducible, and transparent computational research in the life sciences. *Genome Biol.* **11**, R86 (2010).

639. Afgan, E. *et al.* The Galaxy platform for accessible, reproducible and collaborative biomedical analyses: 2018 update. *Nucleic Acids Res* **46**, W537–W544 (2018).

640. Andrew, S. FastQC A Quality Control tool for High Throughput Sequence Data. *Babraham Bioinformatics* http://www.bioinformatics.babraham.ac.uk/projects/fastqc/.

641. Bolger, A. M., Lohse, M. & Usadel, B. Trimmomatic: a flexible trimmer for Illumina sequence data. *Bioinformatics* **30**, 2114–2120 (2014).

642. FASTX-Toolkit. http://hannonlab.cshl.edu/fastx_toolkit/.

643. Kim, D., Langmead, B. & Salzberg, S. L. HISAT: a fast spliced aligner with low memory requirements. *Nat Methods* **12**, 357–360 (2015).

644. Wang, L., Wang, S. & Li, W. RSeQC: quality control of RNA-seq experiments. *Bioinformatics* **28**, 2184–2185 (2012).

645. Ewels, P., Magnusson, M., Lundin, S. & Käller, M. MultiQC: summarize analysis results for multiple tools and samples in a single report. *Bioinformatics* **32**, 3047–3048 (2016).

646. Liao, Y., Smyth, G. K. & Shi, W. featureCounts: An efficient general-purpose program for assigning sequence reads to genomic features. *Bioinformatics* **30**, 923–930 (2014).

647. Love, M. I., Huber, W. & Anders, S. Moderated estimation of fold change and dispersion for RNA-seq data with DESeq2. *Genome Biology* **15**, 550 (2014).

648. Yu, D., Huber, W. & Vitek, O. Shrinkage estimation of dispersion in Negative Binomial models for RNA-seq experiments with small sample size. *Bioinformatics* **29**, 1275–1282 (2013).

649. Grubbs, F. E. Sample Criteria for Testing Outlying Observations. *Ann. Math. Statist.* **21**, 27–58 (1950).

650. Pagès, H., Carlson, M., Falcon, S. & Li, N. *AnnotationDbi: Manipulation of SQLite-based annotations in Bioconductor*. (Bioconductor version: Release (3.9), 2019). doi:10.18129/B9.bioc.AnnotationDbi.

651. Draghici, S. *et al.* A systems biology approach for pathway level analysis. *Genome Res* **17**, 1537–1545 (2007).

652. Donato, M. *et al.* Analysis and correction of crosstalk effects in pathway analysis. *Genome Res.* **23**, 1885–1893 (2013).

653. Tarca, A. L. *et al.* A novel signaling pathway impact analysis. *Bioinformatics* **25**, 75–82 (2009).

654. Ahsan, S. & Drăghici, S. Identifying Significantly Impacted Pathways and Putative Mechanisms with iPathwayGuide: iPathwayGuide. in *Current Protocols in Bioinformatics* (eds. Bateman, A., Pearson, W. R., Stein, L. D., Stormo, G. D. & Yates, J. R.) 7.15.1-7.15.30 (John Wiley & Sons, Inc., 2017). doi:10.1002/cpbi.24.

655. Kanehisa, M., Furumichi, M., Tanabe, M., Sato, Y. & Morishima, K. KEGG: new perspectives on genomes, pathways, diseases and drugs. *Nucleic Acids Res* **45**, D353–D361 (2017).

656. Ashburner, M. *et al.* Gene ontology: tool for the unification of biology. The Gene Ontology Consortium. *Nat. Genet.* **25**, 25–29 (2000).

657. The Gene Ontology Consortium. The Gene Ontology Resource: 20 years and still GOing strong. *Nucleic Acids Res.* **47**, D330–D338 (2019).

658. Drăghici, S., Khatri, P., Martins, R. P., Ostermeier, G. C. & Krawetz, S. A. Global functional profiling of gene expression☆☆This work was funded in part by a Sun Microsystems grant awarded to S.D., NIH Grant HD36512 to S.A.K., a Wayne State University SOM Dean's Post-Doctoral Fellowship, and an NICHD Contraception and Infertility Loan to G.C.O. Support from the WSU MCBI mode is gratefully appreciated. *Genomics* **81**, 98–104 (2003).

659. Cotto, K. C. *et al.* DGIdb 3.0: a redesign and expansion of the drug-gene interaction database. *Nucleic Acids Res.* **46**, D1068–D1073 (2018).

660. NCATS Inxight: Drugs. https://drugs.ncats.io/.

661. BNF: British National Formulary - NICE. https://bnf.nice.org.uk/.

662. Wishart, D. S. *et al.* DrugBank: a knowledgebase for drugs, drug actions and drug targets. *Nucleic Acids Res.* **36**, D901-906 (2008).

663. Wishart, D. S. *et al.* DrugBank 5.0: a major update to the DrugBank database for 2018. *Nucleic Acids Res* **46**, D1074–D1082 (2018).

664. Subramanian, A. *et al.* A Next Generation Connectivity Map: L1000 Platform and the First 1,000,000 Profiles. *Cell* **171**, 1437-1452.e17 (2017).

665. Yaffe, D. & Saxel, O. Serial passaging and differentiation of myogenic cells isolated from dystrophic mouse muscle. *Nature* **270**, 725 (1977).

666. McMahon, D. K. *et al.* C2C12 cells: biophysical, biochemical, and immunocytochemical properties. *Am. J. Physiol.* **266**, C1795-1802 (1994).

667. Mirza, K. A., Pereira, S. L., Edens, N. K. & Tisdale, M. J. Attenuation of muscle wasting in murine C2C12 myotubes by epigallocatechin-3-gallate. *J Cachexia Sarcopenia Muscle* **5**, 339–345 (2014).

668. Lei, S. *et al.* Expression patterns of regulatory lncRNAs and miRNAs in muscular atrophy models induced by starvation in vitro and in vivo. *Mol Med Rep* **20**, 4175–4185 (2019).

669. Simon, M. M. *et al.* A comparative phenotypic and genomic analysis of C57BL/6J and C57BL/6N mouse strains. *Genome Biology* **14**, R82 (2013).

670. Jablonka, S., Schrank, B., Kralewski, M., Rossoll, W. & Sendtner, M. Reduced survival motor neuron (Smn) gene dose in mice leads to motor neuron degeneration: an animal model for spinal muscular atrophy type III. *Hum Mol Genet* **9**, 341–346 (2000).

671. Hatzipetros, T. *et al.* A Quick Phenotypic Neurological Scoring System for Evaluating Disease Progression in the SOD1-G93A Mouse Model of ALS. *Journal of Visualized Experiments : JoVE* (2015) doi:10.3791/53257.

672. RNAprep - Trizol combined with Columns. http://www.molbi.de/protocols/rna_prep_comb_trizol_v1_0.htm.

673. Pfaffl, M. W. A new mathematical model for relative quantification in real-time RT–PCR. *Nucleic Acids Res* **29**, e45 (2001).

674. Reue, K. mRNA Quantitation Techniques: Considerations for Experimental Design and Application. *The Journal of Nutrition* **128**, 2038–2044 (1998).

675. Schena, M., Shalon, D., Davis, R. W. & Brown, P. O. Quantitative Monitoring of Gene Expression Patterns with a Complementary DNA Microarray. *Science* **270**, 467–470 (1995).

676. Wang, Z., Gerstein, M. & Snyder, M. RNA-Seq: a revolutionary tool for transcriptomics. *Nat Rev Genet* **10**, 57–63 (2009).

677. Stark, R., Grzelak, M. & Hadfield, J. RNA sequencing: the teenage years. *Nature Reviews Genetics* **20**, 631–656 (2019).

678. Russo, G., Zegar, C. & Giordano, A. Advantages and limitations of microarray technology in human cancer. *Oncogene* **22**, 6497–6507 (2003).

679. Boelens, M. C. *et al.* Microarray amplification bias: loss of 30% differentially expressed genes due to long probe – poly(A)-tail distances. *BMC Genomics* **8**, 277 (2007).

680. Weirick, T. *et al.* The identification and characterization of novel transcripts from RNA-seq data. *Brief Bioinform* **17**, 678–685 (2016).

681. Han, Y., Gao, S., Muegge, K., Zhang, W. & Zhou, B. Advanced Applications of RNA Sequencing and Challenges. *Bioinform Biol Insights* **9s1**, BBI.S28991 (2015).

682. Zhao, S., Zhang, Y., Gamini, R., Zhang, B. & von Schack, D. Evaluation of two main RNA-seq approaches for gene quantification in clinical RNA sequencing: polyA+ selection versus rRNA depletion. *Scientific Reports* **8**, 4781 (2018).

683. Tripathi, R., Chakraborty, P. & Varadwaj, P. K. Unraveling long non-coding RNAs through analysis of high-throughput RNA-sequencing data. *Non-coding RNA Research* **2**, 111–118 (2017).

684. Kukurba, K. R. & Montgomery, S. B. RNA Sequencing and Analysis. *Cold Spring Harb Protoc* **2015**, pdb.top084970 (2015).

685. Li, S. *et al.* Multi-platform assessment of transcriptome profiling using RNA-seq in the ABRF next-generation sequencing study. *Nature Biotechnology* **32**, 915–925 (2014).

686. Lahens, N. F. *et al.* A comparison of Illumina and Ion Torrent sequencing platforms in the context of differential gene expression. *BMC Genomics* **18**, 602 (2017).

687. Jeon, S. A. *et al.* Comparison of the MGISEQ-2000 and Illumina HiSeq 4000 sequencing platforms for RNA sequencing. *Genomics Inform* **17**, e32 (2019).

688. Kumar, R. *et al.* A High-Throughput Method for Illumina RNA-Seq Library Preparation. *Front. Plant Sci.* **3**, (2012).

689. Yang, X. *et al.* HTQC: a fast quality control toolkit for Illumina sequencing data. *BMC Bioinformatics* **14**, 33 (2013).

690. Trapnell, C. & Salzberg, S. L. How to map billions of short reads onto genomes. *Nat Biotechnol* **27**, 455–457 (2009).

691. Mortazavi, A., Williams, B. A., McCue, K., Schaeffer, L. & Wold, B. Mapping and quantifying mammalian transcriptomes by RNA-Seq. *Nature Methods* **5**, 621–628 (2008).

692. Kim, D. *et al.* TopHat2: accurate alignment of transcriptomes in the presence of insertions, deletions and gene fusions. *Genome Biology* **14**, R36 (2013).

693. Dobin, A. *et al.* STAR: ultrafast universal RNA-seq aligner. *Bioinformatics* **29**, 15–21 (2013).

694. Benoit-Pilven, C. *et al.* Complementarity of assembly-first and mapping-first approaches for alternative splicing annotation and differential analysis from RNAseq data. *Scientific Reports* **8**, 4307 (2018).

695. Transcript assembly and quantification by RNA-Seq reveals unannotated transcripts and isoform switching during cell differentiation | Nature Biotechnology. https://www.nature.com/articles/nbt.1621.

696. Pertea, M. *et al.* StringTie enables improved reconstruction of a transcriptome from RNA-seq reads. *Nature Biotechnology* **33**, 290–295 (2015).

697. Anders, S., Pyl, P. T. & Huber, W. HTSeq—a Python framework to work with high-throughput sequencing data. *Bioinformatics* **31**, 166–169 (2015).

698. Zhang, H. Overview of Sequence Data Formats. in *Statistical Genomics: Methods and Protocols* (eds. Mathé, E. & Davis, S.) 3–17 (Springer, 2016). doi:10.1007/978-1-4939-3578-9_1.

699. Tyner, C. *et al.* The UCSC Genome Browser database: 2017 update. *Nucleic Acids Res* **45**, D626–D634 (2017).

700. Maglott, D., Ostell, J., Pruitt, K. D. & Tatusova, T. Entrez Gene: gene-centered information at NCBI. *Nucleic Acids Res* **39**, D52–D57 (2011).

701. Kersey, P. J. *et al.* Ensembl Genomes 2018: an integrated omics infrastructure for non-vertebrate species. *Nucleic Acids Res* **46**, D802–D808 (2018).

702. An integrative method to normalize RNA-Seq data | BMC Bioinformatics | Full Text. https://bmcbioinformatics.biomedcentral.com/articles/10.1186/1471-2105-15-188.

703. Wagner, G. P., Kin, K. & Lynch, V. J. Measurement of mRNA abundance using RNA-seq data: RPKM measure is inconsistent among samples. *Theory Biosci.* **131**, 281–285 (2012).

704. Li, B. & Dewey, C. N. RSEM: accurate transcript quantification from RNA-Seq data with or without a reference genome. *BMC Bioinformatics* **12**, 323 (2011).

705. Robinson, M. D., McCarthy, D. J. & Smyth, G. K. edgeR: a Bioconductor package for differential expression analysis of digital gene expression data. *Bioinformatics* **26**, 139–140 (2010).

706. Robinson, M. D. & Oshlack, A. A scaling normalization method for differential expression analysis of RNA-seq data. *Genome Biology* **11**, R25 (2010).

707. Anders, S. & Huber, W. Differential expression analysis for sequence count data. *Genome Biology* **11**, R106 (2010).

708. Liu, H.-M. *et al.* Density distribution of gene expression profiles and evaluation of using maximal information coefficient to identify differentially expressed genes. *PLoS One* **14**, (2019).

709. Sun, S. *et al.* Differential expression analysis for RNAseq using Poisson mixed models. *Nucleic Acids Res* **45**, e106 (2017).

710. Ren, X. & Kuan, P.-F. Negative binomial additive model for RNA-Seq data analysis. *BMC Bioinformatics* **21**, 171 (2020).

711. Jiang, H. & Wong, W. H. Statistical inferences for isoform expression in RNA-Seq. *Bioinformatics* **25**, 1026–1032 (2009).

712. Comparative evaluation of gene set analysis approaches for RNA-Seq data | BMC Bioinformatics | Full Text. https://bmcbioinformatics.biomedcentral.com/articles/10.1186/s12859-014-0397-8.

713. Gene ontology analysis for RNA-seq: accounting for selection bias | Genome Biology | Full Text. https://genomebiology.biomedcentral.com/articles/10.1186/gb-2010-11-2-r14.

714. Yang, C.-W. *et al.* An Integrative Transcriptomic Analysis for Identifying Novel Target Genes Corresponding to Severity Spectrum in Spinal Muscular Atrophy. *PLoS One* **11**, (2016).

715. Ng, S.-Y. *et al.* Genome-wide RNA-Seq of Human Motor Neurons Implicates Selective ER Stress Activation in Spinal Muscular Atrophy. *Cell Stem Cell* **17**, 569–584 (2015).

716. Meijboom, K. E. *et al. Combining multi-omics and drug perturbation profiles to identify novel treatments that improve disease phenotypes in spinal muscular atrophy*. http://biorxiv.org/lookup/doi/10.1101/2019.12.17.879353 (2019) doi:10.1101/2019.12.17.879353.

717. Maeda, M. *et al.* Transcriptome Profiling of Spinal Muscular Atrophy Motor Neurons Derived from Mouse Embryonic Stem Cells. *PLoS One* **9**, (2014).

718. Saal, L., Briese, M., Kneitz, S., Glinka, M. & Sendtner, M. Subcellular transcriptome alterations in a cell culture model of spinal muscular atrophy point to widespread defects in axonal growth and presynaptic differentiation. *RNA* **20**, 1789–1802 (2014).

719. In Vitro Screening for Drug Repositioning - Graeme F. Wilkinson, Kevin Pritchard, 2015. https://journals.sagepub.com/doi/10.1177/1087057114563024.

720. Drug repurposing from the perspective of pharmaceutical companies. - Abstract - Europe PMC. https://europepmc.org/article/med/28369768.

721. Karaman, B. & Sippl, W. Computational Drug Repurposing: Current Trends. *Curr. Med. Chem.* **26**, 5389–5409 (2019).

722. Conesa, A. *et al.* A survey of best practices for RNA-seq data analysis. *Genome Biol* **17**, (2016).

723. Zhou, Q., Su, X., Jing, G., Chen, S. & Ning, K. RNA-QC-chain: comprehensive and fast quality control for RNA-Seq data. *BMC Genomics* **19**, 144 (2018).

724. Sheng, Q. *et al.* Multi-perspective quality control of Illumina RNA sequencing data analysis. *Brief Funct Genomics* **16**, 194–204 (2017).

725. Chhangawala, S., Rudy, G., Mason, C. E. & Rosenfeld, J. A. The impact of read length on quantification of differentially expressed genes and splice junction detection. *Genome Biol* **16**, 131 (2015).

726. Fu, Y., Wu, P.-H., Beane, T., Zamore, P. D. & Weng, Z. Elimination of PCR duplicates in RNA-seq and small RNA-seq using unique molecular identifiers. *BMC Genomics* **19**, 531 (2018).

727. Parekh, S., Ziegenhain, C., Vieth, B., Enard, W. & Hellmann, I. The impact of amplification on differential expression analyses by RNA-seq. *Sci Rep* **6**, 25533 (2016).

728. Sahraeian, S. M. E. *et al.* Gaining comprehensive biological insight into the transcriptome by performing a broad-spectrum RNA-seq analysis. *Nature Communications* **8**, 59 (2017).

729. Landau, W. M. & Liu, P. Dispersion Estimation and Its Effect on Test Performance in RNA-seq Data Analysis: A Simulation-Based Comparison of Methods. *PLOS ONE* **8**, e81415 (2013).

730. Summermatter, S. *et al.* Blockade of Metallothioneins 1 and 2 Increases Skeletal Muscle Mass and Strength. *Mol. Cell. Biol.* **37**, e00305-16, /mcb/37/5/e00305-16.atom (2017).

731. Lecker, S. H. *et al.* Multiple types of skeletal muscle atrophy involve a common program of changes in gene expression. *FASEB J.* **18**, 39–51 (2004).

732. Gueugneau, M. *et al.* Increased Serpina3n release into circulation during glucocorticoid-mediated muscle atrophy: Serpina3n secretion in muscle atrophy. *Journal of Cachexia, Sarcopenia and Muscle* **9**, 929–946 (2018).

733. Mei, Z. *et al.* FBXO32 Targets c-Myc for Proteasomal Degradation and Inhibits c-Myc Activity. *J. Biol. Chem.* **290**, 16202–16214 (2015).

734. Dang, K. *et al.* Stable atrogin-1 (Fbxo32) and MuRF1 (Trim63) gene expression is involved in the protective mechanism in soleus muscle of hibernating Daurian ground squirrels (Spermophilus dauricus). *Biol Open* **5**, 62–71 (2016).

735. Bodine, S. C. & Baehr, L. M. Skeletal muscle atrophy and the E3 ubiquitin ligases MuRF1 and MAFbx/atrogin-1. *Am. J. Physiol. Endocrinol. Metab.* **307**, E469-484 (2014).

736. Furlow, J. D. *et al.* Altered gene expression patterns in muscle ring finger 1 null mice during denervation- and dexamethasone-induced muscle atrophy. *Physiological Genomics* **45**, 1168–1185 (2013).

737. Gordon, B. S., Rossetti, M. L. & Eroshkin, A. M. Arrdc2 and Arrdc3 elicit divergent changes in gene expression in skeletal muscle following anabolic and catabolic stimuli. *Physiological Genomics* **51**, 208–217 (2019).

738. Caetano-Anollés, K., Mishra, S. & Rodriguez-Zas, S. L. Synergistic and Antagonistic Interplay between Myostatin Gene Expression and Physical Activity Levels on Gene Expression Patterns in Triceps Brachii Muscles of C57/BL6 Mice. *PLoS ONE* **10**, e0116828 (2015).

739. Balsevich, G. *et al.* Stress-responsive FKBP51 regulates AKT2-AS160 signaling and metabolic function. *Nat Commun* **8**, (2017).

740. Jean, E. *et al.* Aldehyde dehydrogenase activity promotes survival of human muscle precursor cells. *J. Cell. Mol. Med.* **15**, 119–133 (2011).

741. Sakakibara, I., Santolini, M., Ferry, A., Hakim, V. & Maire, P. Six Homeoproteins and a linc-RNA at the Fast MYH Locus Lock Fast Myofiber Terminal Phenotype. *PLoS Genet* **10**, e1004386 (2014).

742. Frier, B. C., Williams, D. B. & Wright, D. C. The effects of apelin treatment on skeletal muscle mitochondrial content. *Am. J. Physiol. Regul. Integr. Comp. Physiol.* **297**, R1761-1768 (2009).

743. Schurch, N. J. *et al.* How many biological replicates are needed in an RNA-seq experiment and which differential expression tool should you use? *RNA* **22**, 839–851 (2016).

744. Mugahid, D. A. *et al.* Proteomic and Transcriptomic Changes in Hibernating Grizzly Bears Reveal Metabolic and Signaling Pathways that Protect against Muscle Atrophy. *Sci Rep* **9**, 19976 (2019).

745. Yakabe, M. *et al.* Inhibition of interleukin-6 decreases atrogene expression and ameliorates tail suspension-induced skeletal muscle atrophy. *PLoS ONE* **13**, e0191318 (2018).

746. Shieh, J.-M., Tseng, H.-Y., Jung, F., Yang, S.-H. & Lin, J.-C. Elevation of IL-6 and IL-33 Levels in Serum Associated with Lung Fibrosis and Skeletal Muscle Wasting in a Bleomycin-Induced Lung Injury Mouse Model. *Mediators of Inflammation* **2019**, 1–12 (2019).

747. Wada, E. *et al.* Treatment with the anti-IL-6 receptor antibody attenuates muscular dystrophy via promoting skeletal muscle regeneration in dystrophin-/utrophin-deficient mice. *Skeletal Muscle* **7**, 23 (2017).

748. Britto, F. A. *et al.* REDD1 deletion prevents dexamethasone-induced skeletal muscle atrophy. *Am. J. Physiol. Endocrinol. Metab.* **307**, E983-993 (2014).

749. Wu, Y. *et al.* REDD1 Is a Major Target of Testosterone Action in Preventing Dexamethasone-Induced Muscle Loss. *Endocrinology* **151**, 1050–1059 (2010).

750. Bowen, T. S. *et al.* Small-molecule inhibition of MuRF1 attenuates skeletal muscle atrophy and dysfunction in cardiac cachexia. *J Cachexia Sarcopenia Muscle* **8**, 939–953 (2017).

751. Bricceno, K. V. *et al.* Histone deacetylase inhibition suppresses myogenin-dependent atrogene activation in spinal muscular atrophy mice. *Hum Mol Genet* **21**, 4448–4459 (2012).

752. Lei, H. *et al.* Fatigue-induced Orosomucoid 1 Acts on C-C Chemokine Receptor Type 5 to Enhance Muscle Endurance. *Sci Rep* **6**, 18839 (2016).

753. Mansilla, F. *et al.* Translation elongation factor eEF1A binds to a novel myosin binding protein-C-like protein. *J. Cell. Biochem.* **105**, 847–858 (2008).

754. Ebrahimzadeh-Vesal, R., Teymoori, A., Dourandish, A. M. & Azimi-Nezhad, M. Identification of a novel nonsense mutation in kyphoscoliosis peptidase gene in an Iranian patient with myofibrillar myopathy. *Genes & Diseases* **5**, 331–334 (2018).

755. Hedberg-Oldfors, C. *et al.* A new early-onset neuromuscular disorder associated with kyphoscoliosis peptidase (KY) deficiency. *Eur J Hum Genet* **24**, 1771–1777 (2016).

756. Kaminski, H. J. *et al.* Differential RNA Expression Profile of Skeletal Muscle Induced by Experimental Autoimmune Myasthenia Gravis in Rats. *Front. Physiol.* **7**, (2016).

757. Gordon, B. S., Steiner, J. L., Williamson, D. L., Lang, C. H. & Kimball, S. R. Emerging role for regulated in development and DNA damage 1 (REDD1) in the regulation of skeletal muscle metabolism. *Am J Physiol Endocrinol Metab* **311**, E157–E174 (2016).

758. Gordon, B. S. *et al.* REDD1 induction regulates the skeletal muscle gene expression signature following acute aerobic exercise. *American Journal of Physiology-Endocrinology and Metabolism* **313**, E737–E747 (2017).

759. Lipina, C. & Hundal, H. S. Is REDD1 a Metabolic Éminence Grise? *Trends in Endocrinology & Metabolism* **27**, 868–880 (2016).

760. Main, A. M. *et al.* DNA methylation and gene expression of HIF3A: cross-tissue validation and associations with BMI and insulin resistance. *Clin Epigenet* **8**, 89 (2016).

761. Kim, Y. I., Lee, F. N., Choi, W. S., Lee, S. & Youn, J. H. Insulin Regulation of Skeletal Muscle PDK4 mRNA Expression Is Impaired in Acute Insulin-Resistant States. *Diabetes* **55**, 2311–2317 (2006).

762. Zhang, W. *et al.* Comprehensive analysis of long non-coding RNAs and mRNAs in skeletal muscle of diabetic Goto-Kakizaki rats during the early stage of type 2 diabetes. *PeerJ* **8**, e8548 (2020).

763. Wynn, R. M. *et al.* Pyruvate Dehydrogenase Kinase-4 Structures Reveal a Metastable Open Conformation Fostering Robust Core-free Basal Activity. *J. Biol. Chem.* **283**, 25305–25315 (2008).

764. Nakao, R. *et al.* Atypical expression of circadian clock genes in denervated mouse skeletal muscle. *Chronobiology International* **32**, 486–496 (2015).

765. Ellis, J. M., Bowman, C. E. & Wolfgang, M. J. Metabolic and Tissue-Specific Regulation of Acyl-CoA Metabolism. *PLoS ONE* **10**, e0116587 (2015).

766. Stavreva, D. A. *et al.* Dynamics of chromatin accessibility and long-range interactions in response to glucocorticoid pulsing. *Genome Res.* **25**, 845–857 (2015).

767. Wan, B. *et al.* A severe mouse model of spinal muscular atrophy develops early systemic inflammation. *Hum. Mol. Genet.* **27**, 4061–4076 (2018).

768. Tanaka, T., Narazaki, M. & Kishimoto, T. IL-6 in Inflammation, Immunity, and Disease. *Cold Spring Harb Perspect Biol* **6**, (2014).

769. Kim, H.-J. *et al.* Differential Effects of Interleukin-6 and -10 on Skeletal Muscle and Liver Insulin Action In Vivo. *Diabetes* **53**, 1060–1067 (2004).

770. Manole, E., Ceafalan, L. C., Popescu, B. O., Dumitru, C. & Bastian, A. E. Myokines as Possible Therapeutic Targets in Cancer Cachexia. *Journal of Immunology Research* **2018**, 1–9 (2018).

771. Gaspar, J. M. & Velloso, L. A. Hypoxia Inducible Factor as a Central Regulator of Metabolism – Implications for the Development of Obesity. *Front. Neurosci.* **12**, (2018).

772. Sun, H. *et al.* Functional metabolomics discover pentose and glucuronate interconversion pathways as promising targets for Yang Huang syndrome treatment with Yinchenhao Tang. *RSC Advances* **8**, 36831–36839 (2018).

773. Lenzen, S. & Panten, U. 2-oxocarboxylic acids and function of pancreatic islets in obese-hyperglycaemic mice. Insulin secretion in relation to 45Ca uptake and metabolism. *Biochem. J.* **186**, 135–144 (1980).

774. Praissman, J. L. & Wells, L. Mammalian O-Mannosylation Pathway: Glycan Structures, Enzymes, and Protein Substrates. *Biochemistry* **53**, 3066–3078 (2014).

775. The Biology of Peroxisome Proliferator-Activated Receptors | Diabetes. https://diabetes.diabetesjournals.org/content/53/suppl_1/S43.

776. Andrews, J. L. *et al.* CLOCK and BMAL1 regulate MyoD and are necessary for maintenance of skeletal muscle phenotype and function. *Proc. Natl. Acad. Sci. U.S.A.* **107**, 19090–19095 (2010).

777. McCarthy, J. J. *et al.* Identification of the circadian transcriptome in adult mouse skeletal muscle. *Physiol. Genomics* **31**, 86–95 (2007).

778. Staff, T. P. B. Correction: Transcriptional programming of lipid and amino acid metabolism by the skeletal muscle circadian clock. *PLOS Biology* **16**, e3000035 (2018).

779. Simon, C. M. *et al.* Converging mechanisms of p53 activation drive motor neuron degeneration in spinal muscular atrophy. *Cell Rep* **21**, 3767–3780 (2017).

780. SMN deficiency in severe models of spinal muscular atrophy causes widespread intron retention and DNA damage | PNAS. https://www.pnas.org/content/114/12/E2347.

781. Ng, S. Y., Dial, A. G. & Ljubicic, V. Intracellular Signaling in Skeletal Muscle is Dysregulated in a Pre-Clinical Model of Spinal Muscular Atrophy. *The FASEB Journal* **31**, 1083.8-1083.8 (2017).

782. Cerveró, C. *et al.* Chronic Treatment with the AMPK Agonist AICAR Prevents Skeletal Muscle Pathology but Fails to Improve Clinical Outcome in a Mouse Model of Severe Spinal Muscular Atrophy. *Neurotherapeutics* **13**, 198–216 (2016).

783. Arumugam, S. A Study on the Role of NF-kB Signaling Pathway Members in Regulating Survival Motor Neuron Protein level and in the Pathogenesis of Spinal Muscular Atrophy. *TDX (Tesis Doctorals en Xarxa)* (Universitat de Lleida, 2017).

784. Hellbach, N. *et al.* Skeletal muscle dysfunction and mitochondrial deficits in spinal muscular atrophy (SMA). *Neuromuscular Disorders* **27**, S30 (2017).

785. Alzheimer's disease: the role of mitochondrial dysfunction and potential new therapies | Bioscience Horizons: The International Journal of Student Research | Oxford Academic. https://academic.oup.com/biohorizons/article/doi/10.1093/biohorizons/hzw014/2753980.

786. Saxton, R. A. & Sabatini, D. M. mTOR Signaling in Growth, Metabolism, and Disease. *Cell* **168**, 960–976 (2017).

787. Khatri, P., Draghici, S., Ostermeier, G. C. & Krawetz, S. A. Profiling gene expression using onto-express. *Genomics* **79**, 266–270 (2002).

788. Jantzen, S. G., Sutherland, B. J., Minkley, D. R. & Koop, B. F. GO Trimming: Systematically reducing redundancy in large Gene Ontology datasets. *BMC Res Notes* **4**, 267 (2011).

789. Alexa, A., Rahnenführer, J. & Lengauer, T. Improved scoring of functional groups from gene expression data by decorrelating GO graph structure. *Bioinformatics* **22**, 1600–1607 (2006).

790. Grossmann, S., Bauer, S., Robinson, P. N. & Vingron, M. Improved detection of overrepresentation of Gene-Ontology annotations with parent child analysis. *Bioinformatics* **23**, 3024–3031 (2007).

791. Richter, E. A. & Hargreaves, M. Exercise, GLUT4, and skeletal muscle glucose uptake. *Physiol. Rev.* **93**, 993–1017 (2013).

792. Treadway, J. L., James, D. E., Burcel, E. & Ruderman, N. B. Effect of exercise on insulin receptor binding and kinase activity in skeletal muscle. *Am. J. Physiol.* **256**, E138-144 (1989).

793. Muscat, G. E. O. *et al.* Regulation of cholesterol homeostasis and lipid metabolism in skeletal muscle by liver X receptors. *J. Biol. Chem.* **277**, 40722–40728 (2002).

794. Barrientos, G. *et al.* Cholesterol removal from adult skeletal muscle impairs excitation–contraction coupling and aging reduces caveolin-3 and alters the expression of other triadic proteins. *Front. Physiol.* **6**, (2015).

795. Shi, H. *et al.* Mitogen-activated protein kinase signaling is necessary for the maintenance of skeletal muscle mass. *Am. J. Physiol., Cell Physiol.* **296**, C1040-1048 (2009).

796. Wright, V. P., Reiser, P. J. & Clanton, T. L. Redox modulation of global phosphatase activity and protein phosphorylation in intact skeletal muscle. *J Physiol* **587**, 5767–5781 (2009).

797. Squire, J. M. Muscle contraction: Sliding filament history, sarcomere dynamics and the two Huxleys. *Glob Cardiol Sci Pract* **2016**,.

798. ICD-10 Version:2019. https://icd.who.int/browse10/2019/en.

799. Hanada, M. *et al.* Effect of long-term treatment with corticosteroids on skeletal muscle strength, functional exercise capacity and health status in patients with interstitial lung disease. *Respirology* **21**, 1088–1093 (2016).

800. Acute steroid myopathy: a highly overlooked entity | QJM: An International Journal of Medicine | Oxford Academic. https://academic.oup.com/qjmed/article/111/5/307/4862462.

801. Horber, F. F., Scheidegger, J. R., Grünig, B. E. & Frey, F. J. Evidence that prednisone-induced myopathy is reversed by physical training. *J. Clin. Endocrinol. Metab.* **61**, 83–88 (1985).

802. Chemotherapy-induced muscle wasting: an update. https://www.ncbi.nlm.nih.gov/pmc/articles/PMC6036312/.

803. Rana, K., Lee, N. K., Zajac, J. D. & MacLean, H. E. Expression of androgen receptor target genes in skeletal muscle. *Asian J Androl* **16**, 675–683 (2014).

804. Altuwaijri, S. *et al.* Androgen receptor regulates expression of skeletal muscle-specific proteins and muscle cell types. *Endocrine* **25**, 27–32 (2004).

805. Kim, J., Park, J., Kim, N., Park, H. & Lim, K. Inhibition of androgen receptor can decrease fat metabolism by decreasing carnitine palmitoyltransferase I levels in skeletal muscles of trained mice. *Nutrition & Metabolism* **16**, 82 (2019).

806. Petering, R. C. & Brooks, N. A. Testosterone Therapy: Review of Clinical Applications. *Am Fam Physician* **96**, 441–449 (2017).

807. Fonseca, G. W. P. da, Dworatzek, E., Ebner, N. & von Haehling, S. Selective androgen receptor modulators (SARMs) as pharmacological treatment for muscle wasting in ongoing clinical trials. *Expert Opinion on Investigational Drugs* 13543784.2020.1777275 (2020) doi:10.1080/13543784.2020.1777275.

808. Ronkainen, P. H. A. *et al.* Catechol-O-Methyltransferase Gene Polymorphism Is Associated with Skeletal Muscle Properties in Older Women Alone and Together with Physical Activity. *PLoS One* **3**, (2008).

809. Mack, S. G., Cook, D. J., Dhurjati, P. & Butchbach, M. E. R. Systems biology investigation of cAMP modulation to increase SMN levels for the treatment of spinal muscular atrophy. *PLoS ONE* **9**, e115473 (2014).

810. Lazarou, M. *et al.* The ubiquitin kinase PINK1 recruits autophagy receptors to induce mitophagy. *Nature* **524**, 309–314 (2015).

811. Jin, S. M. & Youle, R. J. PINK1- and Parkin-mediated mitophagy at a glance. *J Cell Sci* **125**, 795–799 (2012).

812. Jacobs, F. M. J. *et al.* FoxO6, a novel member of the FoxO class of transcription factors with distinct shuttling dynamics. *J. Biol. Chem.* **278**, 35959–35967 (2003).

813. Kaestner, K. H., Knöchel, W. & Martínez, D. E. Unified nomenclature for the winged helix/forkhead transcription factors. *Genes Dev.* **14**, 142–146 (2000).

814. Senf, S. M., Dodd, S. L. & Judge, A. R. FOXO signaling is required for disuse muscle atrophy and is directly regulated by Hsp70. *Am J Physiol Cell Physiol* **298**, C38–C45 (2010).

815. Reed, S. A., Sandesara, P. B., Senf, S. M. & Judge, A. R. Inhibition of FoxO transcriptional activity prevents muscle fiber atrophy during cachexia and induces hypertrophy. *FASEB J* **26**, 987–1000 (2012).

816. Crossland, H., Constantin-Teodosiu, D., Gardiner, S. M., Constantin, D. & Greenhaff, P. L. A potential role for Akt/FOXO signalling in both protein loss and the impairment of muscle carbohydrate oxidation during sepsis in rodent skeletal muscle. *J Physiol* **586**, 5589–5600 (2008).

817. O'Neill, B. T. *et al.* FoxO Transcription Factors Are Critical Regulators of Diabetes-Related Muscle Atrophy. *Diabetes* **68**, 556–570 (2019).

818. Coolican, S. A., Samuel, D. S., Ewton, D. Z., McWade, F. J. & Florini, J. R. The Mitogenic and Myogenic Actions of Insulin-like Growth Factors Utilize Distinct Signaling Pathways. *J. Biol. Chem.* **272**, 6653–6662 (1997).

819. Cuenda, A. & Cohen, P. Stress-activated Protein Kinase-2/p38 and a Rapamycin-sensitive Pathway Are Required for C2C12 Myogenesis. *J. Biol. Chem.* **274**, 4341–4346 (1999).

820. Erbay, E. & Chen, J. The Mammalian Target of Rapamycin Regulates C2C12 Myogenesis via a Kinase-independent Mechanism. *J. Biol. Chem.* **276**, 36079–36082 (2001).

821. R, C., C, de A., M, B., A, C. & M, L. Insulin restores differentiation of Ras-transformed C2C12 myoblasts by inducing NF-kappaB through an AKT/P70S6K/p38-MAPK pathway. *Oncogene* **21**, 3739–3753 (2002).

822. Bois, P. R. J. & Grosveld, G. C. FKHR (FOXO1a) is required for myotube fusion of primary mouse myoblasts. *The EMBO Journal* **22**, 1147–1157 (2003).

823. Bastie, C. C. *et al.* FoxO1 stimulates fatty acid uptake and oxidation in muscle cells through CD36-dependent and -independent mechanisms. *J. Biol. Chem.* **280**, 14222–14229 (2005).

824. Tsuchida, A. *et al.* Insulin/Foxo1 pathway regulates expression levels of adiponectin receptors and adiponectin sensitivity. *J. Biol. Chem.* **279**, 30817–30822 (2004).

825. Kamei, Y. *et al.* Skeletal muscle FOXO1 (FKHR) transgenic mice have less skeletal muscle mass, down-regulated Type I (slow twitch/red muscle) fiber genes, and impaired glycemic control. *J. Biol. Chem.* **279**, 41114–41123 (2004).

826. Kamei, Y. *et al.* A forkhead transcription factor FKHR up-regulates lipoprotein lipase expression in skeletal muscle. *FEBS Letters* **536**, 232–236 (2003).

827. Deguise, M., Repentigny, Y. D., Beauvais, A., Bowerman, M. & Kothary, R. Abnormal fatty acid metabolism is a feature of spinal muscular atrophy. *Neuromuscular Disorders* **27**, S132–S133 (2017).

828. Zolkipli, Z. *et al.* Abnormal fatty acid metabolism in spinal muscular atrophy may predispose to perioperative risks. *European Journal of Paediatric Neurology* **16**, 549–553 (2012).

829. Blanqué, R. *et al.* Characterization of GLPG0492, a selective androgen receptor modulator, in a mouse model of hindlimb immobilization. *BMC Musculoskeletal Disorders* **15**, 291 (2014).

830. Rojas, L. B. A. & Gomes, M. B. Metformin: an old but still the best treatment for type 2 diabetes. *Diabetology & Metabolic Syndrome* **5**, 6 (2013).

831. Riedl, I. *et al.* AMPKγ3 is dispensable for skeletal muscle hypertrophy induced by functional overload. *Am J Physiol Endocrinol Metab* **310**, E461–E472 (2016).

832. Birk, J. B. & Wojtaszewski, J. F. P. Predominant α2/β2/γ3 AMPK activation during exercise in human skeletal muscle. *J Physiol* **577**, 1021–1032 (2006).

833. Ludolph, A. C. *et al.* Safety and efficacy of rasagiline as an add-on therapy to riluzole in patients with amyotrophic lateral sclerosis: a randomised, double-blind, parallel-group, placebo-controlled, phase 2 trial. *Lancet Neurol* **17**, 681–688 (2018).

834. Balagopal, P. *et al.* Oxandrolone enhances skeletal muscle myosin synthesis and alters global gene expression profile in Duchenne muscular dystrophy. *Am. J. Physiol. Endocrinol. Metab.* **290**, E530-539 (2006).

835. Bianchi, V. & Marbini, A. Neuroregenerative Effect of Oxandrolone: A Case Report. *Am J Case Rep* **16**, 763–767 (2015).

836. Hart, D. W. *et al.* Anabolic Effects of Oxandrolone After Severe Burn. *Ann Surg* **233**, 556–564 (2001).

837. Orr, R. & Singh, M. F. The Anabolic Androgenic Steroid Oxandrolone in the Treatment of Wasting and Catabolic Disorders. *Drugs* **64**, 725–750 (2004).

838. Fox, M., Minot, A. S. & Liddle, G. W. Oxandrolone: A Potent Anabolic Steroid of Novel Chemical Configuration. *J Clin Endocrinol Metab* **22**, 921–924 (1962).

839. Ren, H., Yin, P. & Duan, C. IGFBP-5 regulates muscle cell differentiation by binding to IGF-II and switching on the IGF-II auto-regulation loop. *J Cell Biol* **182**, 979–991 (2008).

840. Lee, S.-W. *et al.* AKAP6 inhibition impairs myoblast differentiation and muscle regeneration: Positive loop between AKAP6 and myogenin. *Sci Rep* **5**, (2015).

841. Cai, D., Dhe-Paganon, S., Melendez, P. A., Lee, J. & Shoelson, S. E. Two new substrates in insulin signaling, IRS5/DOK4 and IRS6/DOK5. *J. Biol. Chem.* **278**, 25323–25330 (2003).

842. Lamarre, S. *et al.* Optimization of an RNA-Seq Differential Gene Expression Analysis Depending on Biological Replicate Number and Library Size. *Front. Plant Sci.* **9**, (2018).

843. Radhakrishnan, A. & Green, R. Connections Underlying Translation and mRNA Stability. *J. Mol. Biol.* **428**, 3558–3564 (2016).

844. Koussounadis, A., Langdon, S. P., Um, I. H., Harrison, D. J. & Smith, V. A. Relationship between differentially expressed mRNA and mRNA-protein correlations in a xenograft model system. *Scientific Reports* **5**, 10775 (2015).

845. Edfors, F. *et al.* Gene-specific correlation of RNA and protein levels in human cells and tissues. *Mol Syst Biol* **12**, (2016).

846. Liu, Y., Beyer, A. & Aebersold, R. On the Dependency of Cellular Protein Levels on mRNA Abundance. *Cell* **165**, 535–550 (2016).

847. Buccitelli, C. & Selbach, M. mRNAs, proteins and the emerging principles of gene expression control. *Nat Rev Genet* **21**, 630–644 (2020).

848. Knorre, D. G., Kudryashova, N. V. & Godovikova, T. S. Chemical and Functional Aspects of Posttranslational Modification of Proteins. *Acta Naturae* **1**, 29–51 (2009).

849. Houtman, J. C. D., Barda-Saad, M. & Samelson, L. E. Examining multiprotein signaling complexes from all angles. *FEBS J* **272**, 5426–5435 (2005).

850. Benesch, J. L. P. Collisional Activation of Protein Complexes: Picking Up the Pieces. *Journal of the American Society for Mass Spectrometry* **20**, 341–348 (2009).

851. Castets, P. *et al.* mTORC1 and PKB/Akt control the muscle response to denervation by regulating autophagy and HDAC4. *Nature Communications* **10**, 3187 (2019).

852. Risson, V. *et al.* Muscle inactivation of mTOR causes metabolic and dystrophin defects leading to severe myopathy. *J Cell Biol* **187**, 859–874 (2009).

853. Tsokanos, F. *et al.* eIF4A inactivates TORC1 in response to amino acid starvation. *EMBO J* **35**, 1058–1076 (2016).

854. Rosner, M., Siegel, N., Valli, A., Fuchs, C. & Hengstschläger, M. mTOR phosphorylated at S2448 binds to raptor and rictor. *Amino Acids* **38**, 223–228 (2010).

855. Bentzinger, C. F. *et al.* Differential response of skeletal muscles to mTORC1 signaling during atrophy and hypertrophy. *Skeletal Muscle* **3**, 6 (2013).

856. Gupta, A. & Kumar, A. Pros and cons of the proteomics. *Biomed J* **37**, 163–164 (2014).

857. Swaney, D. L. & Villén, J. Proteomic Analysis of Protein Posttranslational Modifications by Mass Spectrometry. *Cold Spring Harb Protoc* **2016**, pdb.top077743 (2016).

858. Bailey, C. J. Metformin: historical overview. *Diabetologia* **60**, 1566–1576 (2017).

859. Bailey, C. J. & Day, C. Metformin: its botanical background. *Practical Diabetes International* **21**, 115–117 (2004).

860. G, S. Biguanides. A review of history, pharmacodynamics and therapy. *Diabete Metab* **9**, 148–163 (1983).

861. LaMoia, T. E. & Shulman, G. I. Cellular and Molecular Mechanisms of Metformin Action. *Endocr Rev* doi:10.1210/endrev/bnaa023.

862. Owen, M. R., Doran, E. & Halestrap, A. P. Evidence that metformin exerts its anti-diabetic effects through inhibition of complex 1 of the mitochondrial respiratory chain. *Biochem J* **348 Pt 3**, 607–614 (2000).

863. Foretz, M., Guigas, B., Bertrand, L., Pollak, M. & Viollet, B. Metformin: From Mechanisms of Action to Therapies. *Cell Metabolism* **20**, 953–966 (2014).

864. El-Mir, M.-Y. *et al.* Dimethylbiguanide Inhibits Cell Respiration via an Indirect Effect Targeted on the Respiratory Chain Complex I. *J. Biol. Chem.* **275**, 223–228 (2000).

865. Stephenne, X. *et al.* Metformin activates AMP-activated protein kinase in primary human hepatocytes by decreasing cellular energy status. *Diabetologia* **54**, 3101–3110 (2011).

866. Sharma, L. K., Lu, J. & Bai, Y. Mitochondrial Respiratory Complex I: Structure, Function and Implication in Human Diseases. *Curr Med Chem* **16**, 1266–1277 (2009).

867. Batandier, C. *et al.* The ROS production induced by a reverse-electron flux at respiratory-chain complex 1 is hampered by metformin. *J Bioenerg Biomembr* **38**, 33–42 (2006).

868. Zhang, Y. *et al.* Metformin interacts with AMPK through binding to γ subunit. *Mol Cell Biochem* **368**, 69–76 (2012).

869. An, H. *et al.* The importance of the AMPK gamma 1 subunit in metformin suppression of liver glucose production. *Scientific Reports* **10**, 10482 (2020).

870. Meng, S. *et al.* Metformin Activates AMP-activated Protein Kinase by Promoting Formation of the αβγ Heterotrimeric Complex. *J Biol Chem* **290**, 3793–3802 (2015).

871. Carling, D. *et al.* Mammalian AMP-activated protein kinase is homologous to yeast and plant protein kinases involved in the regulation of carbon metabolism. *J Biol Chem* **269**, 11442–11448 (1994).

872. Mitchelhill, K. I. *et al.* Mammalian AMP-activated protein kinase shares structural and functional homology with the catalytic domain of yeast Snf1 protein kinase. *J Biol Chem* **269**, 2361–2364 (1994).

873. Woods, A. *et al.* Characterization of AMP-activated Protein Kinase and Subunits ASSEMBLY OF THE HETEROTRIMERIC COMPLEX IN VITRO. *J. Biol. Chem.* **271**, 10282–10290 (1996).

874. Stapleton, D. *et al.* Mammalian AMP-activated Protein Kinase Subfamily. *J. Biol. Chem.* **271**, 611–614 (1996).

875. Bolster, D. R., Crozier, S. J., Kimball, S. R. & Jefferson, L. S. AMP-activated protein kinase suppresses protein synthesis in rat skeletal muscle through down-regulated mammalian target of rapamycin (mTOR) signaling. *J Biol Chem* **277**, 23977–23980 (2002).

876. Sullivan, J. E. *et al.* Inhibition of lipolysis and lipogenesis in isolated rat adipocytes with AICAR, a cell-permeable activator of AMP-activated protein kinase. *FEBS Lett* **353**, 33–36 (1994).

877. Jing, Y. *et al.* Hepatic p38α regulates gluconeogenesis by suppressing AMPK. *Journal of Hepatology* **62**, 1319–1327 (2015).

878. McBride, A., Ghilagaber, S., Nikolaev, A. & Hardie, D. G. The Glycogen-Binding Domain on the AMPK β Subunit Allows the Kinase to Act as a Glycogen Sensor. *Cell Metab* **9**, 23–34 (2009).

879. Lee, W. J. *et al.* AMPK activation increases fatty acid oxidation in skeletal muscle by activating PPARalpha and PGC-1. *Biochem Biophys Res Commun* **340**, 291–295 (2006).

880. Kishton, R. J. *et al.* AMPK is essential to balance glycolysis and mitochondrial metabolism to control T-ALL cell stress and survival. *Cell Metab* **23**, 649–662 (2016).

881. Musi, N. & Goodyear, L. J. AMP-activated protein kinase and muscle glucose uptake. *Acta Physiol Scand* **178**, 337–345 (2003).

882. Kim, J., Kundu, M., Viollet, B. & Guan, K.-L. AMPK and mTOR regulate autophagy through direct phosphorylation of Ulk1. *Nature Cell Biology* **13**, 132–141 (2011).

883. Crute, B. E., Seefeld, K., Gamble, J., Kemp, B. E. & Witters, L. A. Functional domains of the alpha1 catalytic subunit of the AMP-activated protein kinase. *J Biol Chem* **273**, 35347–35354 (1998).

884. Xin, F.-J., Wang, J., Zhao, R.-Q., Wang, Z.-X. & Wu, J.-W. Coordinated regulation of AMPK activity by multiple elements in the α-subunit. *Cell Res* **23**, 1237–1240 (2013).

885. Hawley, S. A. *et al.* Characterization of the AMP-activated protein kinase kinase from rat liver and identification of threonine 172 as the major site at which it phosphorylates AMP-activated protein kinase. *J Biol Chem* **271**, 27879–27887 (1996).

886. Thornton, C., Snowden, M. A. & Carling, D. Identification of a novel AMP-activated protein kinase beta subunit isoform that is highly expressed in skeletal muscle. *J Biol Chem* **273**, 12443–12450 (1998).

887. Oakhill, J. S. *et al.* β-Subunit myristoylation is the gatekeeper for initiating metabolic stress sensing by AMP-activated protein kinase (AMPK). *PNAS* **107**, 19237–19241 (2010).

888. Iseli, T. J. *et al.* AMP-activated protein kinase beta subunit tethers alpha and gamma subunits via its C-terminal sequence (186-270). *J Biol Chem* **280**, 13395–13400 (2005).

889. Cheung, P. C., Salt, I. P., Davies, S. P., Hardie, D. G. & Carling, D. Characterization of AMP-activated protein kinase gamma-subunit isoforms and their role in AMP binding. *Biochem J* **346**, 659–669 (2000).

890. Willows, R., Navaratnam, N., Lima, A., Read, J. & Carling, D. Effect of different γ-subunit isoforms on the regulation of AMPK. *Biochem J* **474**, 1741–1754 (2017).

891. Pinter, K., Grignani, R. T., Watkins, H. & Redwood, C. Localisation of AMPK γ subunits in cardiac and skeletal muscles. *J Muscle Res Cell Motil* **34**, 369–378 (2013).

892. Kjøbsted, R. *et al.* AMPK in skeletal muscle function and metabolism. *FASEB J.* **32**, 1741–1777 (2018).

893. Wojtaszewski, J. F. P. *et al.* 5'AMP activated protein kinase expression in human skeletal muscle: effects of strength training and type 2 diabetes. *J Physiol* **564**, 563–573 (2005).

894. Treebak, J. T., Birk, J. B., Hansen, B. F., Olsen, G. S. & Wojtaszewski, J. F. P. A-769662 activates AMPK beta1-containing complexes but induces glucose uptake through a PI3-kinase-dependent pathway in mouse skeletal muscle. *Am J Physiol Cell Physiol* **297**, C1041-1052 (2009).

895. Kristensen, D. E. *et al.* Human muscle fibre type-specific regulation of AMPK and downstream targets by exercise. *J Physiol* **593**, 2053–2069 (2015).

896. Lee-Young, R. S., Canny, B. J., Myers, D. E. & McConell, G. K. AMPK activation is fiber type specific in human skeletal muscle: effects of exercise and short-term exercise training. *J Appl Physiol (1985)* **107**, 283–289 (2009).

897. Tobias, I. S. *et al.* Fiber type-specific analysis of AMPK isoforms in human skeletal muscle: advancement in methods via capillary nanoimmunoassay. *Journal of Applied Physiology* **124**, 840–849 (2017).

898. Hayashi, T., Hirshman, M. F., Kurth, E. J., Winder, W. W. & Goodyear, L. J. Evidence for 5' AMP-activated protein kinase mediation of the effect of muscle contraction on glucose transport. *Diabetes* **47**, 1369–1373 (1998).

899. Kjøbsted, R. *et al.* Enhanced Muscle Insulin Sensitivity After Contraction/Exercise Is Mediated by AMPK. *Diabetes* **66**, 598–612 (2017).

900. Wang, C. *et al.* Metformin suppresses lipid accumulation in skeletal muscle by promoting fatty acid oxidation. *Clin Lab* **60**, 887–896 (2014).

901. Zabielski, P. *et al.* Effect of metformin on bioactive lipid metabolism in insulin-resistant muscle. *Journal of Endocrinology* **233**, 329–340 (2017).

902. Jäger, S., Handschin, C., St.-Pierre, J. & Spiegelman, B. M. AMP-activated protein kinase (AMPK) action in skeletal muscle via direct phosphorylation of PGC-1α. *PNAS* **104**, 12017–12022 (2007).

903. Suwa, M., Nakano, H. & Kumagai, S. Effects of chronic AICAR treatment on fiber composition, enzyme activity, UCP3, and PGC-1 in rat muscles. *J Appl Physiol (1985)* **95**, 960–968 (2003).

904. Nikolić, N. *et al.* Overexpression of PGC-1α Increases Fatty Acid Oxidative Capacity of Human Skeletal Muscle Cells. *Biochemistry Research International* vol. 2012 e714074 https://www.hindawi.com/journals/bri/2012/714074/ (2011).

905. Summermatter, S. *et al.* PGC-1α Improves Glucose Homeostasis in Skeletal Muscle in an Activity-Dependent Manner. *Diabetes* **62**, 85–95 (2013).

906. Handschin, C. *et al.* PGC-1α regulates the neuromuscular junction program and ameliorates Duchenne muscular dystrophy. *Genes Dev* **21**, 770–783 (2007).

907. Arnold, A.-S. *et al.* Morphological and functional remodelling of the neuromuscular junction by skeletal muscle PGC-1α. *Nat Commun* **5**, 3569 (2014).

908. Dinulovic, I. *et al.* PGC-1α modulates necrosis, inflammatory response, and fibrotic tissue formation in injured skeletal muscle. *Skeletal Muscle* **6**, 38 (2016).

909. Sandri, M. *et al.* PGC-1α protects skeletal muscle from atrophy by suppressing FoxO3 action and atrophy-specific gene transcription. *PNAS* **103**, 16260–16265 (2006).

910. Wang, J. *et al.* PGC-1α over-expression suppresses the skeletal muscle atrophy and myofiber-type composition during hindlimb unloading. *Bioscience, Biotechnology, and Biochemistry* **81**, 500–513 (2017).

911. Oliveira, A. G. & Gomes-Marcondes, M. C. C. Metformin treatment modulates the tumour-induced wasting effects in muscle protein metabolism minimising the cachexia in tumour-bearing rats. *BMC Cancer* **16**, (2016).

912. Langone, F. *et al.* Metformin protects skeletal muscle from cardiotoxin induced degeneration. *PLoS One* **9**, e114018 (2014).

913. Yousuf, Y., Datu, A., Barnes, B., Amini-Nik, S. & Jeschke, M. G. Metformin alleviates muscle wasting post-thermal injury by increasing Pax7-positive muscle progenitor cells. *Stem Cell Research & Therapy* **11**, 18 (2020).

914. Hafner, P. *et al.* Effect of Combination Citrulline and Metformin Treatment on Motor Function in Patients With Duchenne Muscular Dystrophy: A Randomized Clinical Trial. *JAMA Netw Open* **2**, e1914171 (2019).

915. Fontes-Oliveira, C. C., M. Soares Oliveira, B., Körner, Z., M. Harandi, V. & Durbeej, M. Effects of metformin on congenital muscular dystrophy type 1A disease progression in mice: a gender impact study. *Scientific Reports* **8**, 16302 (2018).

916. Zhang, L. *et al.* Role and mechanism underlying FoxO6 in skeletal muscle in vitro and in vivo. *Int J Mol Med* **48**, (2021).

917. Sims, D., Sudbery, I., Ilott, N. E., Heger, A. & Ponting, C. P. Sequencing depth and coverage: key considerations in genomic analyses. *Nat Rev Genet* **15**, 121–132 (2014).

918. Spinazzola, J. M. & Gussoni, E. Isolation of Primary Human Skeletal Muscle Cells. *Bio-protocol* **7**, (2017).

919. Gong, L., Goswami, S., Giacomini, K. M., Altman, R. B. & Klein, T. E. Metformin pathways: pharmacokinetics and pharmacodynamics. *Pharmacogenet Genomics* **22**, 820–827 (2012).

920. Rivera, M. E., Lyon, E. S. & Vaughan, R. A. Effect of metformin on myotube BCAA catabolism. *Journal of Cellular Biochemistry* **121**, 816–827 (2020).

921. He, L. & Wondisford, F. E. Metformin Action: Concentrations Matter. *Cell Metabolism* **21**, 159–162 (2015).

922. Pavlidou, T. *et al.* Regulation of myoblast differentiation by metabolic perturbations induced by metformin. *PLoS One* **12**, (2017).

923. Kim, Y. D. *et al.* Metformin inhibits hepatic gluconeogenesis through AMP-activated protein kinase-dependent regulation of the orphan nuclear receptor SHP. *Diabetes* **57**, 306–314 (2008).

924. Granlund, A., Jensen-Waern, M. & Essén-Gustavsson, B. The influence of the PRKAG3 mutation on glycogen, enzyme activities and fibre types in different skeletal muscles of exercise trained pigs. *Acta Veterinaria Scandinavica* **53**, 20 (2011).

925. Calura, E. *et al.* Meta-analysis of expression signatures of muscle atrophy: gene interaction networks in early and late stages. *BMC Genomics* **9**, 630 (2008).

926. Saini, J. *et al.* Cross-talk between motor neurons and myotubes via endogenously secreted neural and muscular growth factors. *Physiol Rep* **9**, e14791 (2021).

927. Zhang, X., Ji, X., Wang, Q. & Li, J. Z. New insight into inter-organ crosstalk contributing to the pathogenesis of non-alcoholic fatty liver disease (NAFLD). *Protein Cell* **9**, 164–177 (2018).

928. Christensen, C. S. *et al.* Skeletal Muscle to Pancreatic β-Cell Cross-talk: The Effect of Humoral Mediators Liberated by Muscle Contraction and Acute Exercise on β-Cell Apoptosis. *J Clin Endocrinol Metab* **100**, E1289-1298 (2015).

929. Pierzchlewicz, K., Kępa, I., Podogrodzki, J. & Kotulska, K. Spinal Muscular Atrophy: The Use of Functional Motor Scales in the Era of Disease-Modifying Treatment. *Child Neurology Open* **8**, 2329048X211008725 (2021).

930. Walton, R. G. *et al.* Metformin blunts muscle hypertrophy in response to progressive resistance exercise training in older adults: A randomized, double-blind, placebo-controlled, multicenter trial: The MASTERS trial. *Aging Cell* **18**, e13039 (2019).

931. Galuska, D., Nolte, L. A., Zierath, J. R. & Wallberg-Henriksson, H. Effect of metformin on insulin-stimulated glucose transport in isolated skeletal muscle obtained from patients with NIDDM. *Diabetologia* **37**, 826–832 (1994).

932. Ni, Y. *et al.* Mutations in NDUFS1 Cause Metabolic Reprogramming and Disruption of the Electron Transfer. *Cells* **8**, (2019).

933. Lopez-Fabuel, I. *et al.* Complex I assembly into supercomplexes determines differential mitochondrial ROS production in neurons and astrocytes. *Proc Natl Acad Sci USA* **113**, 13063–13068 (2016).

934. Graham, G. G. *et al.* Clinical Pharmacokinetics of Metformin. *Clin Pharmacokinet* **50**, 81–98 (2011).

935. Liu, Y. *et al.* Metformin attenuates blood-brain barrier disruption in mice following middle cerebral artery occlusion. *Journal of Neuroinflammation* **11**, (2014).

936. Singh, J., Olle, B., Suhail, H., Felicella, M. M. & Giri, S. Metformin-induced mitochondrial function and ABCD2 up-regulation in X-linked adrenoleukodystrophy involves AMP-activated protein kinase. *Journal of Neurochemistry* **138**, 86–100 (2016).

937. Sansa, A. *et al.* Spinal Muscular Atrophy autophagy profile is tissue-dependent: differential regulation between muscle and motoneurons. *Acta Neuropathologica Communications* **9**, 122 (2021).

938. Nilsson, E. C. *et al.* Opposite transcriptional regulation in skeletal muscle of AMP-activated protein kinase gamma3 R225Q transgenic versus knock-out mice. *J Biol Chem* **281**, 7244–7252 (2006).

939. Barnes, B. R. *et al.* Changes in exercise-induced gene expression in 5'-AMP-activated protein kinase gamma3-null and gamma3 R225Q transgenic mice. *Diabetes* **54**, 3484–3489 (2005).

940. Bertoli, S. *et al.* Spinal Muscular Atrophy, types I and II: What are the differences in body composition and resting energy expenditure? *Clin Nutr* **36**, 1674–1680 (2017).

941. Ahlskog, N. *et al.* Muscle overexpression of Klf15 via an AAV8-Spc5-12 construct does not provide benefits in spinal muscular atrophy mice. *Gene Ther* **27**, 505–515 (2020).

942. Jensen, J., Rustad, P. I., Kolnes, A. J. & Lai, Y.-C. The Role of Skeletal Muscle Glycogen Breakdown for Regulation of Insulin Sensitivity by Exercise. *Frontiers in Physiology* **2**, (2011).

943. Kim, J., Yang, G., Kim, Y., Kim, J. & Ha, J. AMPK activators: mechanisms of action and physiological activities. *Exp Mol Med* **48**, e224 (2016).

944. Foretz, M. *et al.* Metformin inhibits hepatic gluconeogenesis in mice independently of the LKB1/AMPK pathway via a decrease in hepatic energy state. *J Clin Invest* **120**, 2355–2369 (2010).

945. Marangos, P. J. *et al.* Adenosinergic Modulation of Homocysteine-Induced Seizures in Mice. *Epilepsia* **31**, 239–246 (1990).

946. Lim, M. A. *et al.* Reduced Activity of AMP-Activated Protein Kinase Protects against Genetic Models of Motor Neuron Disease. *J. Neurosci.* **32**, 1123–1141 (2012).

947. Liu, Y.-J. *et al.* Activation of AMP-activated protein kinase α1 mediates mislocalization of TDP-43 in amyotrophic lateral sclerosis. *Human Molecular Genetics* **24**, 787–801 (2015).

948. Kaneb, H. M., Sharp, P. S., Rahmani-Kondori, N. & Wells, D. J. Metformin Treatment Has No Beneficial Effect in a Dose-Response Survival Study in the SOD1G93A Mouse Model of ALS and Is Harmful in Female Mice. *PLoS ONE* **6**, (2011).

949. Wessels, B., Ciapaite, J., van den Broek, N. M. A., Nicolay, K. & Prompers, J. J. Metformin impairs mitochondrial function in skeletal muscle of both lean and diabetic rats in a dose-dependent manner. *PLoS One* **9**, e100525 (2014).

950. Tan, S. Y. *et al.* Type 1 and 2 diabetes mellitus: A review on current treatment approach and gene therapy as potential intervention. *Diabetes & Metabolic Syndrome: Clinical Research & Reviews* **13**, 364–372 (2019).

951. Grokett, B. H., Ahmad, N. & Warren, D. W. The effects of an anabolic steroid (oxandrolone) on reproductive development in the male rat. *Acta Endocrinol (Copenh)* **126**, 173–178 (1992).

952. Davey, R. A. & Grossmann, M. Androgen Receptor Structure, Function and Biology: From Bench to Bedside. *Clin Biochem Rev* **37**, 3–15 (2016).

953. Denayer, S., Helsen, C., Thorrez, L., Haelens, A. & Claessens, F. The Rules of DNA Recognition by the Androgen Receptor. *Mol Endocrinol* **24**, 898–913 (2010).

954. Llewellyn, W. Anavar (oxandrolone). in *Anabolics* 581–594 (Molecular Nutrition, 2011).

955. Tan, R. S., Cook, K. R. & Reilly, W. G. High Estrogen in Men After Injectable Testosterone Therapy: The Low T Experience. *Am J Mens Health* **9**, 229–234 (2015).

956. MacLean, H. *et al.* Impaired skeletal muscle development and function in male, but not female, genomic androgen receptor knockout mice. *FASEB journal : official publication of the Federation of American Societies for Experimental Biology* **22**, 2676–2689 (2008).

957. Sinha-Hikim, I., Taylor, W. E., Gonzalez-Cadavid, N. F., Zheng, W. & Bhasin, S. Androgen receptor in human skeletal muscle and cultured muscle satellite cells: up-regulation by androgen treatment. *J Clin Endocrinol Metab* **89**, 5245–5255 (2004).

958. MacKrell, J. G. *et al.* Molecular targets of androgen signaling that characterize skeletal muscle recovery and regeneration. *Nucl Recept Signal* **13**, (2015).

959. YIN, L., LU, L., LIN, X. & WANG, X. Crucial role of androgen receptor in resistance and endurance trainings-induced muscle hypertrophy through IGF-1/IGF-1R- PI3K/Akt- mTOR pathway. *Nutrition & Metabolism* **17**, 26 (2020).

960. Havnes, I. A., Jørstad, M. L., Innerdal, I. & Bjørnebekk, A. Anabolic-androgenic steroid use among women – A qualitative study on experiences of masculinizing, gonadal and sexual effects. *International Journal of Drug Policy* 102876 (2020) doi:10.1016/j.drugpo.2020.102876.

961. Mavros, Y. *et al.* Oxandrolone Augmentation of Resistance Training in Older Women: A Randomized Trial. *Med Sci Sports Exerc* **47**, 2257–2267 (2015).

962. Sheffield-Moore, M. *et al.* Short-Term Oxandrolone Administration Stimulates Net Muscle Protein Synthesis in Young Men1. *The Journal of Clinical Endocrinology & Metabolism* **84**, 2705–2711 (1999).

963. Payne, A. H., Abbaszade, I. G., Clarke, T. R., Bain, P. A. & Park, C. H. The multiple murine 3 beta-hydroxysteroid dehydrogenase isoforms: structure, function, and tissue- and developmentally specific expression. *Steroids* **62**, 169–175 (1997).

964. Fenichel, G., Pestronk, A., Florence, J., Robison, V. & Hemelt, V. A beneficial effect of oxandrolone in the treatment of Duchenne muscular dystrophy: a pilot study. *Neurology* **48**, 1225–1226 (1997).

965. Zeman, R. J. *et al.* Improved functional recovery with oxandrolone after spinal cord injury in rats. *Neuroreport* **20**, 864–868 (2009).

966. Rosenfeld, J., King, R. M. & Smith, J. E. Oxandrolone in ALS: Preliminary analysis. *Amyotrophic Lateral Sclerosis and Other Motor Neuron Disorders* **1**, S21–S26 (2000).

967. Rutkove, S. B. *et al.* A pilot randomized trial of oxandrolone in inclusion body myositis. *Neurology* **58**, 1081–1087 (2002).

968. Grunfeld, C., Kotler, D. P., Dobs, A., Glesby, M. & Bhasin, S. Oxandrolone in the treatment of HIV-associated weight loss in men: a randomized, double-blind, placebo-controlled study. *J Acquir Immune Defic Syndr* **41**, 304–314 (2006).

969. Lesser, G. J. *et al.* A phase III randomized study comparing the effects of oxandrolone (Ox) and megestrol acetate (Meg) on lean body mass (LBM), weight (wt) and quality of life (QOL) in patients with solid tumors and weight loss receiving chemotherapy. *JCO* **26**, 9513–9513 (2008).

970. LDH-Glo™ Cytotoxicity Assay | LDH Assay | LDH Release | J2380 | Promega. https://www.promega.co.uk/products/cell-health-assays/cell-viability-and-cytotoxicity-assays/ldh-glo-cytotoxicity-assay/.

971. Smith, S. M., Wunder, M. B., Norris, D. A. & Shellman, Y. G. A Simple Protocol for Using a LDH-Based Cytotoxicity Assay to Assess the Effects of Death and Growth Inhibition at the Same Time. *PLoS ONE* **6**, (2011).

972. Spangenburg, E. E., Abraha, T., Childs, T. E., Pattison, J. S. & Booth, F. W. Skeletal muscle IGF-binding protein-3 and -5 expressions are age, muscle, and load dependent. *American Journal of Physiology-Endocrinology and Metabolism* **284**, E340–E350 (2003).

973. Ganassi, M., Badodi, S., Wanders, K., Zammit, P. S. & Hughes, S. M. Myogenin is an essential regulator of adult myofibre growth and muscle stem cell homeostasis. *eLife* **9**, e60445 (2020).

974. Nouvel, A. *et al.* Optimization of RNA extraction methods from human metabolic tissue samples of the COMET biobank. *Sci Rep* **11**, 20975 (2021).

975. Habets, P. E. M. H. *et al.* RNA Content Differs in Slow and Fast Muscle Fibers: Implications for Interpretation of Changes in Muscle Gene Expression. *J Histochem Cytochem.* **47**, 995–1004 (1999).

976. Versteyhe, S. *et al.* Insulin receptor substrates-5 and -6 are poor substrates for the insulin receptor. *Mol Med Rep* **3**, 189–193 (2010).

977. Diel, P., Baadners, D., Schlüpmann, K., Velders, M. & Schwarz, J. P. C2C12 myoblastoma cell differentiation and proliferation is stimulated by androgens and associated with a modulation of myostatin and Pax7 expression. *Journal of Molecular Endocrinology* **40**, 231–241 (2008).

978. Chen, Y., Lee, N. K. L., Zajac, J. D. & MacLean, H. E. Generation and analysis of an androgen-responsive myoblast cell line indicates that androgens regulate myotube protein accretion. *J Endocrinol Invest* **31**, 910–918 (2008).

979. Wannenes, F. *et al.* Androgen receptor expression during C2C12 skeletal muscle cell line differentiation. *Mol Cell Endocrinol* **292**, 11–19 (2008).

980. Lee, D. K. Androgen receptor enhances myogenin expression and accelerates differentiation. *Biochem Biophys Res Commun* **294**, 408–413 (2002).

981. Liu, X.-H. *et al.* Nandrolone, an anabolic steroid, stabilizes Numb protein through inhibition of mdm2 in C2C12 myoblasts. *J Androl* **33**, 1216–1223 (2012).

982. Kumar, P., Nagarajan, A. & Uchil, P. D. Analysis of Cell Viability by the Lactate Dehydrogenase Assay. *Cold Spring Harb Protoc* **2018**, (2018).

983. Stockert, J. C., Blázquez-Castro, A., Cañete, M., Horobin, R. W. & Villanueva, Á. MTT assay for cell viability: Intracellular localization of the formazan product is in lipid droplets. *Acta Histochemica* **114**, 785–796 (2012).

984. Rothaeusler, K. & Baumgarth, N. Assessment of cell proliferation by 5-bromodeoxyuridine (BrdU) labeling for multicolor flow cytometry. *Curr Protoc Cytom* **Chapter 7**, Unit7.31 (2007).

985. Schittler, D., Allgöwer, F. & De Boer, R. J. A new model to simulate and analyze proliferating cell populations in BrdU labeling experiments. *BMC Syst Biol* **7**, S4 (2013).

986. Ahmad, A., Herndon, D. N. & Szabo, C. Oxandrolone protects against the development of multiorgan failure, modulates the systemic inflammatory response and promotes wound healing during burn injury. *Burns* **45**, 671–681 (2019).

987. Chinenov, Y., Coppo, M., Gupte, R., Sacta, M. A. & Rogatsky, I. Glucocorticoid receptor coordinates transcription factor-dominated regulatory network in macrophages. *BMC Genomics* **15**, 656 (2014).

988. Bosch-Marcé, M. *et al.* Increased IGF-1 in muscle modulates the phenotype of severe SMA mice. *Hum Mol Genet* **20**, 1844–1853 (2011).

989. Tsai, L.-K. *et al.* Systemic Administration of a Recombinant AAV1 Vector Encoding IGF-1 Improves Disease Manifestations in SMA Mice. *Molecular Therapy* **22**, 1450–1459 (2014).

990. Soeters, M. R., Soeters, P. B., Schooneman, M. G., Houten, S. M. & Romijn, J. A. Adaptive reciprocity of lipid and glucose metabolism in human short-term starvation. *Am J Physiol Endocrinol Metab* **303**, E1397-1407 (2012).

991. Tsintzas, K. *et al.* Differential regulation of metabolic genes in skeletal muscle during starvation and refeeding in humans. *J Physiol* **575**, 291–303 (2006).

992. Dungan, C. M., Wright, D. C. & Williamson, D. L. Lack of REDD1 reduces whole body glucose and insulin tolerance, and impairs skeletal muscle insulin signaling. *Biochem Biophys Res Commun* **453**, 778–783 (2014).

993. Hsieh, S.-K. *et al.* Promotion of myotube differentiation and attenuation of muscle atrophy in murine C2C12 myoblast cells treated with teaghrelin. *Chemico-Biological Interactions* **315**, 108893 (2020).

994. Sawano, S. *et al.* A One-Step Immunostaining Method to Visualize Rodent Muscle Fiber Type within a Single Specimen. *PLoS ONE* **11**, (2016).

995. Wu, Y., Bauman, W. A., Blitzer, R. D. & Cardozo, C. Testosterone-induced hypertrophy of L6 myoblasts is dependent upon Erk and mTOR. *Biochemical and Biophysical Research Communications* **400**, 679–683 (2010).

996. Fu, S., Lin, X., Yin, L. & Wang, X. Androgen receptor regulates the proliferation of myoblasts under appropriate or excessive stretch through IGF-1 receptor mediated p38 and ERK1/2 pathways. *Nutrition & Metabolism* **18**, 85 (2021).

997. Hindi, L., McMillan, J. D., Afroze, D., Hindi, S. M. & Kumar, A. Isolation, Culturing, and Differentiation of Primary Myoblasts from Skeletal Muscle of Adult Mice. *Bio Protoc* **7**, e2248 (2017).

998. Mouly, V. *et al.* Myoblast transfer therapy: is there any light at the end of the tunnel? *Acta Myol* **24**, 128–133 (2005).

999. Webster, C. & Blau, H. M. Accelerated age-related decline in replicative life-span of Duchenne muscular dystrophy myoblasts: implications for cell and gene therapy. *Somat Cell Mol Genet* **16**, 557–565 (1990).

1000. Vitucci, D. *et al.* Serum from differently exercised subjects induces myogenic differentiation in LHCN-M2 human myoblasts. *J Sports Sci* **36**, 1630–1639 (2018).

1001. Yoshioka, M., Boivin, A., Bolduc, C. & St-Amand, J. Gender difference of androgen actions on skeletal muscle transcriptome. *Journal of Molecular Endocrinology* **39**, 119–133 (2007).

1002. Morton, R. W. *et al.* Muscle Androgen Receptor Content but Not Systemic Hormones Is Associated With Resistance Training-Induced Skeletal Muscle Hypertrophy in Healthy, Young Men. *Front. Physiol.* **0**, (2018).

1003. Singh, N. N., Hoffman, S., Reddi, P. P. & Singh, R. N. Spinal muscular atrophy: Broad disease spectrum and sex-specific phenotypes. *Biochimica et Biophysica Acta (BBA) - Molecular Basis of Disease* **1867**, 166063 (2021).

1004. LaBarge, S., McDonald, M., Smith-Powell, L., Auwerx, J. & Huss, J. M. Estrogen-related receptor-α (ERRα) deficiency in skeletal muscle impairs regeneration in response to injury. *FASEB J* **28**, 1082–1097 (2014).

1005. Collins, B. C. *et al.* Deletion of estrogen receptor α in skeletal muscle results in impaired contractility in female mice. *J Appl Physiol (1985)* **124**, 980–992 (2018).

1006. Tuvdendorj, D. *et al.* Long-term oxandrolone treatment increases muscle protein net deposition via improving amino acid utilization in pediatric patients 6 months after burn injury. *Surgery* **149**, 645–653 (2011).

1007. Jeschke, M. G. *et al.* The Effect of Oxandrolone on the Endocrinologic, Inflammatory, and Hypermetabolic Responses During the Acute Phase Postburn. *Ann Surg* **246**, 351–362 (2007).

1008. Hepatic effects of 17 alpha-alkylated anaboli-androgenic steroids. *HIV Hotline* **8**, 2–5 (1998).

1009. Brown, T. R. Nonsteroidal Selective Androgen Receptors Modulators (SARMs): Designer Androgens with Flexible Structures Provide Clinical Promise. *Endocrinology* **145**, 5417–5419 (2004).

1010. Ponnusamy, S. *et al.* Androgen receptor agonists increase lean mass, improve cardiopulmonary functions and extend survival in preclinical models of Duchenne muscular dystrophy. *Human Molecular Genetics* **26**, 2526–2540 (2017).

1011. Jones, A., Hwang, D.-J., Narayanan, R., Miller, D. D. & Dalton, J. T. Effects of a novel selective androgen receptor modulator on dexamethasone-induced and hypogonadism-induced muscle atrophy. *Endocrinology* **151**, 3706–3719 (2010).

1012. Brener, A. *et al.* The endocrine manifestations of spinal muscular atrophy, a real-life observational study. *Neuromuscular Disorders* **30**, 270–276 (2020).

1013. Burgos, S. A. *et al.* Insulin resistance of protein anabolism accompanies that of glucose metabolism in lean, glucose-tolerant offspring of persons with type 2 diabetes. *BMJ Open Diabetes Research and Care* **4**, e000312 (2016).

1014. Abdulla, H., Smith, K., Atherton, P. J. & Idris, I. Role of insulin in the regulation of human skeletal muscle protein synthesis and breakdown: a systematic review and meta-analysis. *Diabetologia* **59**, 44–55 (2016).

1015. Everman, S. *et al.* Insulin does not stimulate muscle protein synthesis during increased plasma branched-chain amino acids alone but still decreases whole body proteolysis in humans. *Am J Physiol Endocrinol Metab* **311**, E671–E677 (2016).

1016. Chow, L. S. *et al.* Mechanism of insulin's anabolic effect on muscle: measurements of muscle protein synthesis and breakdown using aminoacyl-tRNA and other surrogate measures. *American Journal of Physiology-Endocrinology and Metabolism* **291**, E729–E736 (2006).

1017. Pinheiro-Dardis, C. M. *et al.* Insulin treatment reverses the increase in atrogin-1 expression in atrophied skeletal muscles of diabetic rats with acute joint inflammation. *Ther Clin Risk Manag* **14**, 275–286 (2018).

1018. Timmerman, K. L. *et al.* Insulin Stimulates Human Skeletal Muscle Protein Synthesis via an Indirect Mechanism Involving Endothelial-Dependent Vasodilation and Mammalian Target of Rapamycin Complex 1 Signaling. *The Journal of Clinical Endocrinology & Metabolism* **95**, 3848–3857 (2010).

1019. Heller, S. R., Peyrot, M., Oates, S. K. & Taylor, A. D. Hypoglycemia in patient with type 2 diabetes treated with insulin: it can happen. *BMJ Open Diabetes Research and Care* **8**, e001194 (2020).

1020. Hauner, H. The mode of action of thiazolidinediones. *Diabetes Metab Res Rev* **18 Suppl 2**, S10-15 (2002).

1021. Manickam, R., Duszka, K. & Wahli, W. PPARs and Microbiota in Skeletal Muscle Health and Wasting. *Int J Mol Sci* **21**, E8056 (2020).

1022. Li, J. *et al.* Angiotensin II-induced muscle atrophy via PPARγ suppression is mediated by miR-29b. *Molecular Therapy - Nucleic Acids* **23**, 743–756 (2021).

1023. Trobec, K. *et al.* Rosiglitazone reduces body wasting and improves survival in a rat model of cancer cachexia. *Nutrition* **30**, 1069–1075 (2014).

1024. Moore-Carrasco, R. *et al.* Effects of the PPARgamma agonist GW1929 on muscle wasting in tumour-bearing mice. *Oncol Rep* **19**, 253–256 (2008).

1025. Benedusi, V., Martorana, F., Brambilla, L., Maggi, A. & Rossi, D. The Peroxisome Proliferator-activated Receptor γ (PPARγ) Controls Natural Protective Mechanisms against Lipid Peroxidation in Amyotrophic Lateral Sclerosis *. *Journal of Biological Chemistry* **287**, 35899–35911 (2012).

1026. Iida, M. *et al.* Pioglitazone suppresses neuronal and muscular degeneration caused by polyglutamine-expanded androgen receptors. *Human Molecular Genetics* **24**, 314–329 (2015).

1027. Kim, J. K. *et al.* Differential Effects of Rosiglitazone on Skeletal Muscle and Liver Insulin Resistance in A-ZIP/F-1 Fatless Mice. *Diabetes* **52**, 1311–1318 (2003).

1028. Floyd, J. S., Barbehenn, E., Lurie, P. & Wolfe, S. M. Case series of liver failure associated with rosiglitazone and pioglitazone. *Pharmacoepidemiol Drug Saf* **18**, 1238–1243 (2009).

1029. Sebba, A. Tocilizumab: The first interleukin-6-receptor inhibitor. *American Journal of Health-System Pharmacy* **65**, 1413–1418 (2008).

1030. Emery, P. *et al.* Safety and tolerability of subcutaneous sarilumab and intravenous tocilizumab in patients with rheumatoid arthritis. *Rheumatology* **58**, 849–858 (2019).

1031. McCarty, D. & Robinson, A. Efficacy and safety of sarilumab in patients with active rheumatoid arthritis. *Therapeutic Advances in Musculoskeletal* **10**, 61–67 (2018).

1032. Muñoz-Cánoves, P., Scheele, C., Pedersen, B. K. & Serrano, A. L. Interleukin-6 myokine signaling in skeletal muscle: a double-edged sword? *The Febs Journal* **280**, 4131 (2013).

1033. Serrano, A. L., Baeza-Raja, B., Perdiguero, E., Jardí, M. & Muñoz-Cánoves, P. Interleukin-6 is an essential regulator of satellite cell-mediated skeletal muscle hypertrophy. *Cell Metab* **7**, 33–44 (2008).

1034. Haddad, F., Zaldivar, F., Cooper, D. M. & Adams, G. R. IL-6-induced skeletal muscle atrophy. *Journal of Applied Physiology* **98**, 911–917 (2005).

1035. Madaro, L. *et al.* Denervation-activated STAT3-IL6 signaling in fibro-adipogenic progenitors promotes myofibers atrophy and fibrosis. *Nature cell biology* **20**, 917 (2018).

1036. Yu, D., Peng, Y., Ayaz-Guner, S., Gregorich, Z. R. & Ge, Y. Comprehensive Characterization of AMP-activated Protein Kinase Catalytic Domain by Top-down Mass Spectrometry. *J Am Soc Mass Spectrom* **27**, 220–232 (2016).

1037. Lee, S. Y. *et al.* A Proteotranscriptomic-Based Computational Drug-Repositioning Method for Alzheimer's Disease. *Front. Pharmacol.* **0**, (2020).

1038. Yu, L., Li, K. & Zhang, X. Next-generation metabolomics in lung cancer diagnosis, treatment and precision medicine: mini review. *Oncotarget* **8**, 115774–115786 (2017).

1039. Kessler, T. *et al.* Cerebrospinal fluid proteomic profiling in nusinersen-treated patients with spinal muscular atrophy. *J Neurochem* **153**, 650–661 (2020).

1040. Weckwerth, W. Metabolomics: an integral technique in systems biology. *Bioanalysis* **2**, 829–836 (2010).

1041. Weckwerth, W. Metabolomics in systems biology. *Annu Rev Plant Biol* **54**, 669–689 (2003).

1042. Dubuis, S., Ortmayr, K. & Zampieri, M. A framework for large-scale metabolome drug profiling links coenzyme A metabolism to the toxicity of anti-cancer drug dichloroacetate. *Commun Biol* **1**, 1–11 (2018).

1043. Wishart, D. S. Emerging applications of metabolomics in drug discovery and precision medicine. *Nat Rev Drug Discov* **15**, 473–484 (2016).

1044. Gardell, S. J., Zhang, X., Kapoor, N., Petucci, C. & Coen, P. M. Metabolomics Analyses of Muscle Atrophy Induced by Hind Limb Unloading. *Methods Mol Biol* **1996**, 297–309 (2019).

1045. Uchitomi, R. *et al.* Metabolomic Analysis of Skeletal Muscle in Aged Mice. *Sci Rep* **9**, 10425 (2019).

1046. Subramanian, I., Verma, S., Kumar, S., Jere, A. & Anamika, K. Multi-omics Data Integration, Interpretation, and Its Application. *Bioinformatics and Biology Insights* **14**, (2020).

1047. Pinu, F. R. *et al.* Systems Biology and Multi-Omics Integration: Viewpoints from the Metabolomics Research Community. *Metabolites* **9**, (2019).

1048. Cho, C. R., Labow, M., Reinhardt, M., van Oostrum, J. & Peitsch, M. C. The application of systems biology to drug discovery. *Curr Opin Chem Biol* **10**, 294–302 (2006).

1049. Xia, J., Psychogios, N., Young, N. & Wishart, D. S. MetaboAnalyst: a web server for metabolomic data analysis and interpretation. *Nucleic Acids Research* **37**, W652 (2009).

1050. Shannon, P. *et al.* Cytoscape: a software environment for integrated models of biomolecular interaction networks. *Genome Res* **13**, 2498–2504 (2003).

1051. Cottret, L. *et al.* MetExplore: a web server to link metabolomic experiments and genome-scale metabolic networks. *Nucleic Acids Res* **38**, W132-137 (2010).

1052. Berg, J. A. *et al.* Gazing into the Metaboverse: Automated exploration and contextualization of metabolic data. *bioRxiv* 2020.06.25.171850 (2020) doi:10.1101/2020.06.25.171850.

1053. Finkel, R. S. *et al.* Candidate Proteins, Metabolites and Transcripts in the Biomarkers for Spinal Muscular Atrophy (BforSMA) Clinical Study. *PLoS ONE* **7**, (2012).

1054. Advani, D. & Kumar, P. Therapeutic Targeting of Repurposed Anticancer Drugs in Alzheimer's Disease: Using the Multiomics Approach. *ACS Omega* **6**, 13870–13887 (2021).

1055. Zhang, M., Luo, H., Xi, Z. & Rogaeva, E. Drug Repositioning for Diabetes Based on 'Omics' Data Mining. *PLoS ONE* **10**, (2015).

1056. Khosravi, A., Jayaram, B., Goliaei, B. & Masoudi-Nejad, A. Active repurposing of drug candidates for melanoma based on GWAS, PheWAS and a wide range of omics data. *Mol Med* **25**, 30 (2019).

1057. Tomazou, M. *et al.* Multi-omics data integration and network-based analysis drives a multiplex drug repurposing approach to a shortlist of candidate drugs against COVID-19. *Briefings in Bioinformatics* (2021) doi:10.1093/bib/bbab114.

1058. Hochhaus, A. & Kantarjian, H. The development of dasatinib as a treatment for chronic myeloid leukemia (CML): from initial studies to application in newly diagnosed patients. *Journal of Cancer Research and Clinical Oncology* **139**, 1971 (2013).

1059. Ma, X. *et al.* Persistent Rheb-induced mTORC1 activation in spinal cord neurons induces hypersensitivity in neuropathic pain. *Cell Death Dis* **11**, 1–11 (2020).

1060. Bosland, M. C. & Mahmoud, A. M. Hormones and prostate carcinogenesis: Androgens and estrogens. *J Carcinog* **10**, 33 (2011).

1061. Little, D. *et al.* PTEN depletion decreases disease severity and modestly prolongs survival in a mouse model of spinal muscular atrophy. *Mol Ther* **23**, 270–277 (2015).

1062. Draghici, S. *et al.* COVID-19: disease pathways and gene expression changes predict methylprednisolone can improve outcome in severe cases. *Bioinformatics* (2021) doi:10.1093/bioinformatics/btab163.